# Prediction of DI-CI Engine Performance and Emission Characteristics of Varying Renewable Diesel Fuels with Experimental Results from Marine Diesel fuel

Lamin Jawara

Master's thesis

Norwegian University of Science and Technology

NTNU

Faculty of Engineering Science and Technology

Department of Marine Technology

Trondheim

6/20/2011

# Preface

This study is undertaken as a part of an MSc program in Marine Technology at the Norwegian University of Science and Technology (NTNU). The MSc thesis is done in collaboration with STATOIL as industry partners. It is part of STATOIL's research program to develop renewable fuels to meet the European Union climate package of 10% target for all fuels used in road transportation to be renewable by 2020. STATOIL has produced some renewable fuels on experimental basis in their laboratory in Norway and in other locations in Sweden.

It is the aim of this study to investigate the feasibility of these renewable fuels as a viable alternative fuel for compression ignition engines from a technical standpoint. This investigation is done by experimental methods using the Ricardo Hydra research engine provided by the fuel research department of STATOIL and installed in the NTNU's Marine Systems laboratory for this purpose. However, the standard hydra engine does not provide the level of technology and control required to make a detailed study of the combustion properties of the fuels and as a result a number of modifications have to be performed to bring the engine to an acceptable standard. Invariably, the conventional fuel injection system had to be replaced with a common rail system and this necessitated the replacement of the complete cylinder head. The control and combustion analysis system (CAS) had to be replaced with a modern system that allows independent control of the engine operating systems to enable us to study the effect of changing operations conditions on fuel combustion properties and engine exhaust emission.

The plan was to get the engine ready before the start of the MSc thesis work. However, a number of delays have been encountered before the engine was able to be stabilized for collection of usable data. A series of problems has been discovered during the preliminary experiments and upon analysis of the preliminary experimental results necessitating further corrective action to be taken on the engine. Upon a series of discussions with my supervisor in consultation with laboratory personnel, we came to an agreement that further experiment with the Ricardo hydra research engine be abandoned.

As a consequence a new approach has to be sought for the completion of the master's thesis within the limited time permissible. Since experiments has already been successfully carried out on the marine diesel fuel (MDO), it was found compelling to use the experimental results of the MDO to determine empirically the performance and emission characteristic of the renewable fuels. It became consequentially necessary to change the original topic from 'Performance and Emission characterization of Hydra Research Engine with Varying Renewable Fuels' to 'Prediction of DI-CI Performance and Emission characteristics of Varying Renewable Fuels using Experimental Results from Marine Diesel Fuel'.

# Acknowledgement

I wish to extend gratitude to my supervisor, Professor Harald Valland of Marine Technology department, NTNU for many interesting discussions and invaluable support. Much thanks to Statoil for providing the test engine and the research fuels and special thanks goes to Dr. Øyvind Buhaug, Principal Engineer at Statoil for providing valuable data and insight into leading researches in renewable fuels. Special thanks to Mr. Frode Gran for his help in setting up the experiment and its measurement and control system and Mr. Oddoar Paulsen and their team at the workshop. I am also indebted to Senior Engineer, Ingebrigt Valberg and Research Scientist, Jørgen Nielsen of the Norwegian Marine Technology Research Institute (Marintek-Sintef) and Sergey PhD candidate for their assistance during the experiment. I wish to thank my wife Zianab Gibba, my daughter, Fatoumatta Jawara and my two sons, Muhammad Lamin Jawara and Famalang Lamin Jawara for their understanding and patience throughout the period of the MSc program. Lastly I thank colleagues and coworkers at Gambia Ports Authority and family for their moral support.

**NTNU**
**The Norwegian University of Science and Technology**

**Faculty of Engineering Science and Technology**
**Department of Marine Technology**

**MASTER THESIS ASSIGNMENT**
**for**
**Stud.techn. Lamin Jawara**
**Spring semester 2011**

## Renewable Diesel Fuels

*Fornybare drivstoffer for dieselmotorer*

**Background**

Norwegian authorities require that a certain fraction of fuels sold in Norway must be renewable, and the fraction is expected to increase in the future. Similar requirements are also given in EU countries and some states in USA. The oil companies are free to choose renewable components and to select the products where they are been added. This freedom is in practice limited by product standards, etc.

Currently raps methyl ester (RME) is used as an additive. Even if this product functions well it has several drawbacks like storage stability and cold climate operation. It is therefore a considerable interest in renewable fuels with better properties.

STATOIL produces on experimental basis renewable diesel fuels and is interested in engine tests using these fuels. The engine tests will be carried out using a Ricardo Hydra Diesel research engine for fuel quality and combustion research which was recently installed in our Machinery Laboratory.

**Overall Aim and Focus**

The MSc assignment should study the combustion properties expressed by for example ROHR, thermal efficiency, fuel consumption, and exhaust emissions for several types of renewable diesel fuels by experiments using the Hydra Diesel engine.

A part of the assignment will deal with testing of the Hydra Diesel, its data monitoring system, analysis of measurements, and report generation.

**The assignment should be prepared based on following points:**

**Part 1**

- Provide documentation of the Ricardo Hydra Diesel research engine and its control and measurement system.
- Discuss typical measurement procedures suitable for fuel quality testing on the Ricardo Hydra Diesel research engine, including analysis of the raw measurement data. Establish suitable measurement protocols.
- Perform initial engine testing and assess the quality of measurement data, including repeatability.

1

**Part 2**

- Perform initial fuel tests using bio fuel samples provided by STATOIL and commercial auto diesel fuel.
- Based on the test results, identify measurement data and engine performance characteristics that are particularly relevant as measures of fuel quality.
- Carry out fuel testing with a wider selection of fuel samples.

*This assignment will be in cooperation with STATOIL , Principal Engineer Øyvind Buhaug*

The assignment text must be included as a part of the MSc-report.

The report should be written like a research report, with an abstract, conclusions, contents list, reference list, etc. During preparation of the report it is important that the candidate emphasizes easily understood and well written text. For ease of reading the report should contain adequate references at appropriate places to related text, tables and figures. On evaluation, a lot of weight is put on thorough preparation of results, their clear presentation in the form of tables and/or graphs, and on comprehensive discussion.
All used sources must be completely documented. For textbooks and periodicals, author, title, year, page number and eventually figure number must be specified.

It is assumed that the student should take initiative for establishing satisfactory contact with his teacher and eventual advisors.

In accordance with current regulations NTNU reserves the right to use any results from the project work in connection with teaching, research, publication, or other activities.

Two -2- copies of the report are required. A complete copy of all material on digital form on CD-ROM in Word-format or other relevant format should be handed in together with the written material.

The MSc-report must be delivered no later than June 14, 2011.

Department of Marine Technology, 2011-02-16

Harald Valland
professor

**NTNU**
**The Norwegian University of Science and Technology**

**Faculty of Engineering Science and Technology**
**Department of Marine Technology**

**REVISION OF**
**MASTER THESIS ASSIGNMENT**
**for**
**Stud.techn. Lamin Jawara**
**Spring semester 2011**

## Renewable Diesel Fuels

*Fornybare drivstoffer for dieselmotorer*

Due to unexpected problems with the Hydra Diesel Research Engine installation the MSc Assignment has to be revised and modified. These problems were totally out of the candidate's control. He had no responsibility for the occurrence of the problems, or for their correction.

The Hydra Diesel Engine has been available for the candidate only in short periods. The volume of test data has therefore been very much reduced compared to what was expected at the start of the work, when the assignment was defined.

It has not been possible to obtain stable and reliable operation of the engine system within the limited time available. Part 2 of the assignment concerning experimental testing of various bio-fuels could not be carried out because this would require the ability to identify small differences between different fuels.

Due to the problems described above, the assignment must be modified:

- The experimental section of Part 2 has to be abandoned.
- Sections concerning background, planning, and preparations for testing of bio-fuels should be included.

Introductory work carried out before the extent of the engine problems was fully understood represents a part of the work carried out and should be included in the report, even if it is not supported by experiments.

2011-06-15

This master's thesis is dedicated to The Gambia

# Abstract

This paper discusses finding of combustion research carried out using Ricardo hydra research diesel engine with varying renewable fuels. The primary fuel of investigation is rapeseed methyl ester (RME) and marine diesel fuel (MDO) was used as the primary reference fuel (PRF). The results of the PRF have been acquired by experiment and have been used to characterize the heat release rates, brake fuel conversion efficiency (BFCE), brake specific fuel consumption (BSFC), brake fuel energy consumption (BSEC), exhaust temperature; Oxides of nitrogen ($NO_x$), carbon monoxide (CO), carbon dioxide ($CO_2$) and hydrocarbon (HC) emissions have also been studied. Empirical correlations have been developed and used to predict the corresponding results with several blends of renewable fuels. The analysis of the results showed a good correlation between the results of the MDO and the blends of the renewable fuels. The results showed that the difference between mean BSFC of the MDO and the predicted values of the blend of the liquefied petroleum and 10% rapeseed (LGO-10) was only 0.82%. Predicted values for B20, B40 and B100 were 1.65%, 3.33% and 8.53% respectively. At maximum load the predicted lost in power for LGO-10 ranges from 0.88% at maximum speed to 0.85% at low speed. The predicted lost in power for B20, B40 and B100 were 1.61%, 3.21% and 7.86% respectively at maximum speed and 1.71%, 3.13% and 7.86% respectively at low speed range. The mean increase between the measured mean $NO_x$ emission from MDO and the LGO-10 was 0.98%, while CO and CO2 emissions fall by 6.35%. There was also a mean reduction of HC emission by 10.59%. Similar changes have been predicted in B20 and B40 emissions.

Petrol from plants: Genius or wishful thinking? – *The Economist*

# Table of Contents

Preface ... ii

Acknowledgement ... iv

Abstract ... ix

***List of figures*** ... xiv

***List of Tables*** ... xix

Nomenclature ... xx

Introduction ... 1

Part One ... 4

Chapter One: Background ... 4

1.1. Fundamental of renewable fuels ... 4

1.2. Literature Review ... 8

Chapter Two: Experimental Setup ... 14

2.1. Hydra single cylinder research engine ... 14

***2.2.1. Effect on Compression Ratio*** ... 19

***2.2.2. Effect on Clearance Volume*** ... 20

2.2. Emission Measurement and Analyzer ... 22

***2.3. Particle Emission Measurement*** ... 25

2.4. Measurements and Data Acquisition System ... 29

Chapter Three: Experimental Procedure ... 33

3.1. Planning of the experiment ... 33

3.2. Test modes ... 34

3.3. Establishing idling speed ... 35

3.4. Operating Conditions for preliminary testing ... 35

***6.1. Modified engine operating conditions*** ... 42

3.6. Hydra engine starting sequence ... 47

3.7. Test Sequence ... 48

3.8. Engine Performance Parameters ... 49

3.8.1. Brake fuel conversion efficiency ..... 52
3.8.2. Rate of Heat Released ..... 53
3.8.3. Dynamic Cylinder Pressure ..... 57
3.8.4. The cylinder volume function ..... 59
3.8.5. Exhaust emission measurement ..... 60
Chapter four: Statistical Analysis of preliminary data ..... 63
4.1. Analysis of Variance and Repeatability ..... 63
***4.2. Repeatability Analysis*** ..... 91
4.4. Assumptions made in the ANOVA ..... 99
Chapter Five: Experimental result ..... 100
***5.1. Effects of Atmospheric Pressure*** ..... 100
Figure 58 shows a cylinder pressure derivative developed from the experimental pressure data obtained during the experiment. ..... 103
***5.3. Rate of heat release*** ..... 104
Part Two ..... 124
Chapter six: Empirical Correlations ..... 124
6.1. Introduction ..... 124
6.2. Description of research fuels ..... 124
6.3. Empirical Correlations ..... 125
Chapter Six: Results and Discussion ..... 133
***6.1. Brake fuel conversion efficiency*** ..... 133
***6.2. Effect on brake specific fuel consumption*** ..... 136
***6.3. Effect on power and torque*** ..... 141
6.1. Exhaust emission characeristics ..... 143
Chapter Seven: Conclusion ..... 150
Bibliography ..... 154
Appendix A ..... 160
Appendix B ..... 171
Appendix C ..... 182

Appendix D ..... 184

Appendix E ..... 188

# *List of figures*

Figure 1: Typical transestrification reaction ..... 5
Figure 2: Schematic diagram of biodiesel production ..... 8
Figure 3: Photograph of test engine ..... 14
Figure 4: Photograph of cylinder head and injection system ..... 15
Figure 5: Experimental Setup ..... 16
Figure 6: Determining the compression ration ..... 21
Figure 7: Exhaust emission measurement equipments ..... 24
Figure 8: Schematic diagram of non-dispersive infrared measurement method. ..... 25
Figure 9: Experimental setup with particle sampling system ..... 26
Figure 10: Schematic diagram of ELPI particulate matter measurement system ..... 27
Figure 11: Photograph of particle measurement system ..... 28
Figure 12: Sample output data of PM measurement system ..... 29
Figure 13: Control room ..... 31
Figure 14: Flow chart of experimental methodology ..... 33
Figure 15: Percentage of full-load torque at each engine speed ..... 37
Figure 16: Dynamic in-cylinder pressure measurement trace ..... 38
Figure 17: smoke number vs. torque at 1188rpm ..... 40
Figure 18: smoke number vs. toque at 1800rpm ..... 40
Figure 19: smoke number as a function of torque at 3400 rpm ..... 41
Figure 20: Percentage of full-load torque at each engine speed ..... 44
Figure 21: Flow chart of experimental setup starting sequence ..... 48
Figure 22: Flow chart of test sequence ..... 49
Figure 23: Statistical analysis of torque measurement error at part load ..... 65
Figure 24: Statistical analysis of torque measurement error at full load ..... 66
Figure 25: Boxplot of torque for nine trials at part load ..... 67
Figure 26: Individual value plot of torque for nine trials at part load ..... 68
Figure 27: Boxplot of Torque for nine trials at full load ..... 69
Figure 28: Individual value plot of torque at full load ..... 70
Figure 29: Statistical analysis of the error in power measurement at part load ..... 71
Figure 30: Statistical analysis of the error in power measurement at full load ..... 71
Figure 31: Boxplot of power for nine different trials at part load ..... 72
Figure 32: Individual value plot of nine different trials at part load ..... 73
Figure 33: Boxplot of nine different trials at full load ..... 75
Figure 34: Individual value plot of nine different trials full load ..... 75

Figure 35: Residual plots of speed measurement for 12 different trials ..... 76
Figure 36: Boxplot of speed measurement for 12 trials ..... 77
Figure 37: Individual value plots of speed measurement with 12 different trials ..... 78
Figure 38: Residual plots of specific fuel consumption measurement of nine trials at full load ..... 79
Figure 39: Residual plots of specific fuel consumption measurement of nine trials at full load ..... 79
Figure 40: Boxplot of specific fuel consumption of nine trials at part load ..... 80
Figure 41: Individual value plot of nine trials of specific fuel consumption measurement at part load ..... 81
Figure 42: Boxplot of specific fuel consumption of nine trials at full load ..... 82
Figure 43: Individual value plots of nine trials at full load ..... 82
Figure 44: Residual plots of air consumption measurement of nine trials at part load ..... 83
Figure 45: Residual plots of air consumption measurement of nine trials at full load ..... 84
Figure 46: Box plot of air consumption of nice trials at part load ..... 85
Figure 47: Box plot of individual trials of air consumption of nine trials at full load ..... 85
Figure 48: Individual value plot of air consumption of nine trials at full load ..... 86
Figure 49: Individual value plot of air consumption of nine trials at full load ..... 87
Figure 50: Residual plot of exhaust temperature for nice trials at part load and 3000rpm ..... 88
Figure 51: Residual plot of exhaust temperature for nice trials at full load and 3000rpm ..... 88
Figure 52: Box plot of exhaust temperature for nice trials at full load and 3000rpm ..... 89
Figure 53: Box plot of exhaust temperature for nice trials at full load and 3000rpm ..... 89
Figure 54: Individual value plot of exhaust temperature for nice trials at full load and 3000rpm ..... 90
Figure 55: Individual value plot of exhaust temperature for nice trials at full load and 3000rpm ..... 91
Figure 56: Brake torque as a function of atmospheric pressure ..... 101
Figure 57: Brake torque as a function of atmospheric pressure ..... 102
Figure 58: Pressure derivation as a function of crank angle ..... 103
Figure 59: Heat release rate as a function of crank angle showing the different phases of combustion (source: (Patro, 1993)) ..... 104
Figure 60: Rate of heat release as a function of crank angle at part load and 1200 rpm ..... 105
Figure 61: Rate of heat release as a function of crank angle at part load and 1700 rpm ..... 106
Figure 62: Rate of heat release as a function of crank angle at part load and 3400 rpm ..... 106
Figure 63: Heat release rate curve as a function of crank angle at 1200 rpm with maximum load ..... 107

Figure 64: Heat release rate curve as a function of crank angle at 1700 rpm with maximum load ..... 108
Figure 65: Heat release rate curve as a function of crank angle at 3400 rpm with maximum load ..... 108
Figure 66: Characteristics of torque at various load points with varying speeds ..... 110
Figure 67: Characteristics of power at various load points with varying speeds ..... 111
Figure 68: Characteristics of BSFC at various load points with varying speeds ..... 112
Figure 69: Characteristics of fuel conversion efficiency at various load points ..... 112
Figure 70: Experimental brake fuel conversion efficiency as a function of fuel/air equivalent ratio ..... 114
Figure 71: Characteristics of air consumption at various loads with varying speeds ..... 115
Figure 72: Characteristic of injection duration at various load points ..... 115
Figure 73: Air/ Fuel ration as a function of engine load ..... 117
Figure 74: Torque as a function of injection duration with varying speeds ..... 117
Figure 75: Characteristics of exhaust temperature at various load points with varying speeds ..... 118
Figure 76: Oxides of nitrogen emission at different injection timing ..... 119
Figure 77: $NO_x$ emission at different mode points ..... 120
Figure 78: Hydrocarbon emission at different mode point ..... 120
Figure 79: Carbon dioxide emission at different mode points ..... 121
Figure 80: Carbon monoxide emission at different mode points ..... 122
Figure 81: Distribution of diesel particle number and mass distribution as a function of diameter (Source: Marintek-Sintef) ..... 122
Figure 82: Actual and estimated Brake fuel conversion efficiency with various renewable fuels and its blends ..... 133
Figure 83: Actual and estimated Brake fuel conversion efficiency with various renewable fuels and its blends ..... 134
Figure 84: Actual and predicted Brake fuel conversion efficiency with various renewable fuels and its blends ..... 134
Figure 85: Brake specific fuel consumption of diesel fuel and predicted values for biodiesel and its blends ..... 136
Figure 86: Brake specific fuel consumption of diesel fuel and predicted values for biodiesel and its blends ..... 137
Figure 87: Brake specific fuel consumption of diesel fuel and predicted values for biodiesel and its blends ..... 137
Figure 88: Brake specific energy consumption of diesel fuel and predicted values for biodiesel and its blends ..... 139

Figure 89: Brake specific energy consumption of diesel fuel and predicted values for biodiesel and its blends ..... 139
Figure 90: Brake specific energy consumption of diesel fuel and predicted values of various blends of biodiesel ..... 140
Figure 91: Actual and predicted power as a function of torque with various renewable fuels and its blends ..... 141
Figure 92: Actual and predicted power as a function of torque with various renewable fuels and its blends ..... 141
Figure 93: Actual and predicted power as a function of torque with various renewable fuels blends ..... 142
Figure 94: change in maximum brake power at various speeds ..... 142
Figure 95: Actual $NO_x$ emission from diesel and predicted emission from blends of biodiesel ..... 143
Figure 96: Actual $NO_x$ emission from diesel and predicted emission from biodiesel and its blends at 3400 rpm ..... 144
Figure 97: Carbon monoxide emission of marine diesel fuel with predicted values of renewable diesel blends ..... 146
Figure 98: Hydrocarbon emission of diesel fuel and predicted values for biodiesel and its blends ..... 147
Figure 99: Hydrocarbon emission of diesel fuel and predicted values for various blends of biodiesel ..... 147
Figure 100: actual and prediction values of $CO_2$ emission as a function of load ..... 148
Figure 101: Mode 8- Dynamic cylinder pressure as a function of crank angle for marine diesel fuel at idle speed ..... 172
Figure 102: Mode 7- Dynamic cylinder pressure as a function of crank angle for marine diesel fuel at 50% load and 2250 rpm ..... 172
Figure 103: Mode 6- Dynamic cylinder pressure as a function of crank angle for marine diesel fuel at 75% load and 2250 rpm ..... 173
Figure 104: Mode 5- Dynamic cylinder pressure as a function of crank angle for marine diesel fuel at 100% load and 2250 rpm ..... 173
Figure 105: Mode 4- Dynamic cylinder pressure as a function of crank angle for marine diesel fuel at 10% load and 3000 rpm ..... 174
Figure 106: Mode 3- Dynamic cylinder pressure as a function of crank angle for marine diesel fuel at 50% load and 3000 rpm ..... 174
Figure 107: Mode 2- Dynamic cylinder pressure as a function of crank angle for marine diesel fuel at 75% load and 3000 rpm ..... 175
Figure 108: Mode 1- Dynamic cylinder pressure as a function of crank angle for marine diesel fuel at 100% load and 3000 rpm ..... 175

Figure 109: Dynamic cylinder pressure vs. crank angle at (a) low load (b) medium load and (c) full load at 3000rpm for 12 different trials..... 177

# *List of Tables*

Table 1: Test engine specification ..... 18
Table 2: Exhaust emission measurement range and methods ..... 22
Table 3: ISO 8-point test mode ..... 34
Table 4: Experimental engine operating conditions at different test modes ..... 36
Table 5: FSN and load point definition ..... 41
Table 6: ISO Universal test cycle ..... 42
Table 7: Experimental engine operating conditions ..... 43
Table 8: Case 1 engine operating conditions ..... 45
Table 9: Case 2 engine operating conditions ..... 46
Table 10: Case 3 engine operating conditions ..... 46
Table 11: Factor of analysis for torque showing correlation with atmospheric pressure ..... 69
Table 12: Factor of analysis for power showing correlation with atmospheric pressure ..... 74
Table 13: Mean and standard deviation (in bracket) of part and full loads at 3000rpm ..... 93
Table 14: Mean and standard deviation (in bracket) of part and full loads at 2250rpm for 12 trials ..... 94
Table 15: Total mean and standard deviations ..... 96
Table 16: Measurement uncertainties at constant speed of 3000rpm ..... 97
Table 17: Measurement uncertainties at constant speed of 2250rpm for several trials ..... 98
Table 18: Mean atmospheric pressure data ..... 100
Table 19: Properties of test fuels ..... 125
Table 20: Coefficients for basic emission correlations (Source: (EPA, 2002)) ..... 130
Table 21: Mean values and % change in BSFC, BSEC and BFCE ..... 135
Table 22: Mean and predicted values of emissions ..... 145

# Nomenclature

## *Acronyms*

AC……Alternating Current
ANOVA……Analysis of Variance
AFR…… Air /Fuel Ratio
BDC……Bottom Dead Centre
BFCE……Brake fuel conversion effeciency
BSEC……Brake specific energy consumption
BSFC……Brake specific fuel consumption
B20……Blends of 20% biodiesel and 80% diesel fuel by volume
B40……Blends of 40% biodiesel and 60% diesel fuel by volume
B100……100% biodiesel fuel
CA……Crank angle
CAS……Combustion Analysis System
CAD……Crank Angle Degree
CI……Compression Ignition
CO……Carbon monoxide
$CO_2$……Carbon dioxide
CN……Cetane number
DC……Direct Current
ECU……Engine Control Unit
EGR……Exhaust Gas Recirculation
ELPI……ElectricLow Pressure Impactor
EVC…… Exhaust Valve Closing angle
FFA……Free Fatty Acid
HCCI……Homogenous Charge Compression Ignition
HP……High pressure
HRR……Heat Release Rate
ICE……Internal Combustion Engine
ID……Injection duration
LGO-10……Liquefied Gas oil with 10%Vol rapeseed oil
LHV……Lower Heating Value [MJ/kg]
LP……Low pressure
MDO……Marine diesel oil

MFB……..Mass Fraction Burnt
NO……..Nitric Oxide
$NO_x$ …….. Oxides of Nitrogen
$P_{bme}$……..Brake Mean Effective Pressure
$P_{me}$ ……..….Mean effective pressure
PM……..Particle emission
PRF……Primary Reference Fuel
PW……....Pulse Width [ms]
RME……..……Rapeseed Methyl Ester
RPM ……Revolutions Per Minute
ROHR……...Rate of Heat Release
SOC……...Start of Combustion
SR……Swirl ratio
TDC……..……Top Dead Centre
UHC……...Unburned Hydrocarbons

## *Symbols*

$a$……Crankshaft throw
$C_m$……mean piston speed
$\varphi$……Crankshaft angle [deg]
$\lambda$ ……Ratio of the connecting rod length to crank radius
$\rho$ ……Density [Kg/m$^3$]
$B$……Cylinder Bore
$V_c$……Cylinder clearance volume
$d$……differential of
$h$……Heating value of fuel
$P$……Power or Pressure depending on usage
$V$……Volume
$V_d$ ……Cylinder volume
T……Temperature
$T_b$ ……Brake Torque
$l$……length of connecting rode
$m$……mass
$N$……Engine speed [rpm]
$P_b$ ……Brake power [kW]
$Cp$……Specific heat at constant pressure
$\kappa$ *(kappa)*……Polytropic index
$m$……mass
$\dot{m}$ ……mass flow rate
$Q$……Heat
$R$……Ideal Gas Constant, 0.287[kJ/kgK]
$R_s$ ……Swirl ratio
S……Stroke
s……Distance between the crank axis and the piston pin axis
U……Internal energy
u……Uncertainty
V……Cylinder volume
$\varepsilon$……Compression ratio
$\omega$……angular velocity of crankshaft
$\sigma$ ……Standard deviation
$\eta$ ……efficiency
%B……Percentage of biodiesel content in the blend

## *Subscripts*

*a*.....Air
*b*.....at brake output of the engine
B.....Biodiesel fuel
c.....Clearance
ch.....Combustion
D.....Diesel fuel
*HT*.....Heat transfer
*n*.....Number
P.....piston
*x*.....*of* Oxides of nitrogen
*f*.....Of the fuel entering the engine cylinder
*d*.....of cylinder displacement volume
*v* .....volume

s.....of swirl in the cylinder

# Introduction

There has been an increasing interest in the development and research in renewable fuels worldwide. The reason for this renewed interest is as a result of several contributing factors; among them an increasing global energy consumption thus making the current energy use unsustainable and the harmful effect of exhaust emission from internal combustion engines. The need to reduce engine out emission is becoming more strigent and tighter control measures have been introduce worldwide. Engineers today therefore are required not only to make the existing designs and engine operation more efficient and reduce emissions to acceptable limits but to find sustainable forms of energy whose effect on the environment and human health will be minimal.

According to the European Environmental Agency (EEA); transport accounts for around a third of all final energy consumption in the EEA member countries and for more than a fifth of greenhouse gas emissions. Internal combustion engines (ICE) are known to contribute to greenhouse gases through emissions of mainly $CO_2$ and particle matter (PM). PM emissions from ICE can be oxidized and become strongly absorbing aerosols such as black carbon or soot with the capacity to strongly absorb solar radiation or become highly reflective micron-sized aerosols such as sulfates. Aerosols can lead to global warming by absorbing solar radiation depending on their absorption properties, geometry, reflectivity and size distribution. The effect of $CO_2$ as a greenhouse gas contributing to approximately 25% to global $CO_2$ emission is well documented in literature. (Thomas R. Karl et al, 2003).

Studies have confirmed that internal combustion engine are an important source of particle emissions, it is reported that between 0.2% and 0.5% of the fuel mass burned in diesel engines is emitted as particle matter (Heywood, 1998; N.K. Miller Jothia et al, 2006). Diesel particulate consists principally of carbonaceous material (soot) together with a range of organic compounds or aerosols, some of which are highly toxic and suspected or known carcinogens. Studies have shown that exposure to particle emission from diesel engines and other industrial sources can lead to serious health problems, including the incidence of cancers, heart disease and increased susceptibility to respiratory ailments such as pneumonia, bronchitis, and asthma (Anyon, 2008).

Engine manufacturers have however, made a series of improvements in engine design. Most of these improvements are geared to improving the combustion characteristics of the engine thereby reducing emission levels while avoid compromising the engine performance. As a result, newly built engine have their fuel injection system and combustion chambers redesigned. Improvements in sealing technology and piston rings have not only reduced engine oil consumption but reduce emissions of hydrocarbon (HC) and particle matter (PM). Nonetheless, as scientists are increasing understand the effects of these emissions on the environment and human health; the effort to further reduce these emissions is no longer left to the mercy of ingenuity of engineers but a matter of policy.

As a result legislative requirements have been developed by several nations, among them Norway, USA and other EU countries to find alternative fuels and reduce emission of harmful substances from transport vehicles. Recently developed legislations in these countries require that certain percentage of fuel is to be sold as

renewable fuels. The European Union climate package has set 10% target on the basis of energy content for all fuels used in road transportation to be renewable fuels by 2020. In the United Kingdom, the Renewable Transport Fuel obligation made it mandatory for all suppliers to sell 5% of all transport fuels as renewable by 2010. These and the aforementioned factor have renewed research in the field of renewable fuel technology.

As a result effords are being made to develop environmentally friendly biodegradable, non toxic alternative fuels that are sustainable in the long term. One renewable fuel that can be use in diesel engines without any substantial modification to the engine is biodiesel (Ardito et al, 1995). Biodiesel also referred to as fatty acid methyl ester (FAME) is a biodegradable fuel made from vegetable oils or animal fats and has properties similar to hydrocarbon diesel fuel (Jai-houng Leu, 2009) and (Yadav et al, 2010).

However, an important drawback to the commercial feasibility of biodiesel production is the high cost of lipid feedstock which made it not economically competitive with fossil fuel. This economic drawback can be overcome by using low grade lipid feedstock with high free fatty acid (FFA) content. A lot of waste cooking oil and seed oils has been found to contain a high FFA; tobacco seed oil with high FFA content can be used as substitute of conventional diesel (Yadav et al, 2010) Lipid feedstock which are non edible in nature like karanja oil and Mahua oil can also be used for production of biodiesel (Yadav et al, 2010). However, the limitation with the use of non edible feedstock is its low availability in commercial quantities

# Part One

## Chapter One: Background

### *1.1. Fundamental of renewable fuels*

Renewable fuel technology refers to the production of fuel from renewable resources; by renewable we mean it can be replenished by production of livestock or growing of plants. The fats of animal and plant are typically made of triglycerides which are esters containing three free fatty acids (FFA) and glycerol which is a trihydric alcohol. During the transesterification process (figure1), the triglycerides react with the alcohol in the presence of catalyst to produce mono-esters that are termed as biodiesel. Biodiesel is defined under the ASTM D6751 standard as the mono alkyl esters of long chain fatty acids derived from vegetable oils or animal fats and sometimes referred to as methyl and ethyl esters. Fatty acids (FA) are important sources of fuel because their metabolism yield large quantities of Adenosine-5'-triphosphate (ATP) which makes them a promising alternative fuel. Esters are formed by the reaction of an acid with an alcohol in which case water is also formed as a byproduct:

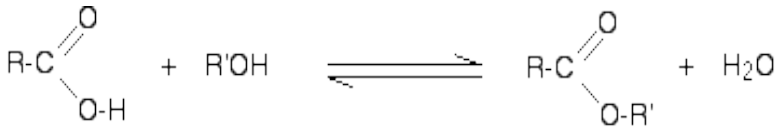


(1)

Where the Rs in the equation for the reaction between the acid RCOOH and an alcohol R'OH and the product RCOOR' are chains of carbon and hydrogen atoms.

When methanol is the alcohol used for the reaction, the ester formed is a methyl ester (ME), when ethanol is the alcohol used for the reaction, an ethyl ester (EE) is formed. A typical reaction that uses method for the reaction is shown in figure 1.

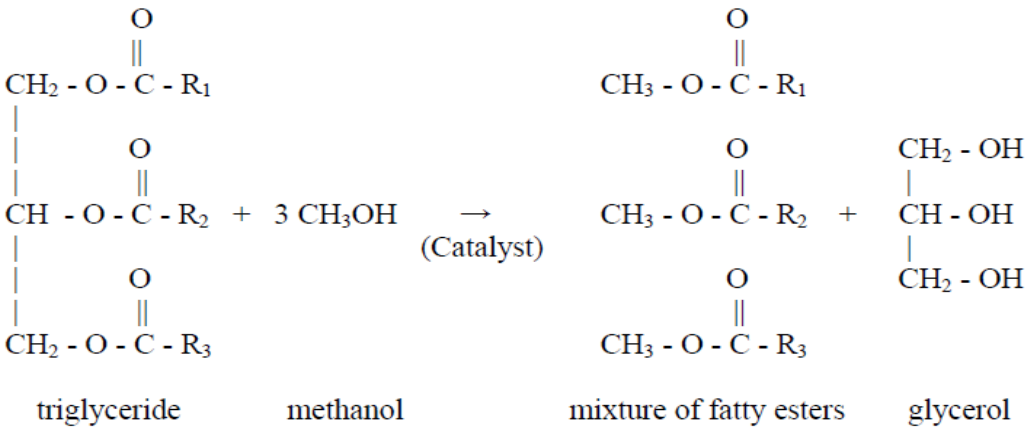


**Figure 1: Typical transestrification reaction**

Where $R_1$, $R_2$ and $R_3$ are FAs containing long chains of carbon and hydrogen atoms. The catalyst removes protons from the alcohol making it a stronger nucleophile to increase the rate of reaction. The triglyceride reacts with alcohol (methanol) to produce glycerol and MEs. Triglycerides are FAs occurring naturally from vegetable oils or animal fat. The FA profile depends on the source of the FA and determines the physical and chemical characteristics of the oil, fat and the esters derived from them.

The process of reducing the FA to FAME is a two step process; the first step is the reduction of the FFA content by esterification with alcohol in presence of acid catalyst. In the second step, the resulting triglyceride of the lipid reacts with methanol in presence of base catalyst to form ME and glycerol (Yadav et al, 2010).

The acid catalyst is generally sulfuric acid and the base catalyst is usually sodium or potassium hydroxide (F Halek et al, 2009) and (Yadav et al, 2010). Product from the reaction is separated into two phases under gravity. The FAME portion is washed with water and dried to meet the biodiesel fuel standards. The biodiesel produced from low grade lipid feedstock and its blends with fossil fuel can be used in diesel engines without any modifications of the engine

However, certain grades of biofuels commonly referred to as first generation (1G) biofuels made from sugar, starch and vegetable oil are mostly available today. These grades of biofuels pose a threat to food production in terms of land use and consumption. In order to avert this threat, a second grade of biofuels made from non-food crops such as stalks of wheat, corn, wood and inedible waste product are currently being developed as second generation (2G) biofuels. The main technical problem about the production of this grade of biofuels is breaking the cellulose material into glucose. Various experimental processes are being developed by using enzymes to break these organic materials into sugar which can eventually be fermented to produce biofuels. 1,5G biodiesel are recently being produced but not on large commercial scale. These are biodiesel from any vegetable oil which are non-edible. The productions of these biofuels are based on a refinery technology known as hydrotreating. This grade of biodiesel has a high diesel quality then the 1G biodiesel allowing higher blends. 2G bioethanol and biodiesel are from highly available cellulosic feedstock (e.g., straw, wood). The 3-4G biofuels are from micro and macro algae, $CO_2$ and bacteria.

Research conducted at Tu-Delf university in Netherlands by Jack Pronk at the department of Biotechnology have shown that ethanol can be produced from non-edible ground sources (e.g. straw) by incorporating a single bacteria gene in yeast. This modified yeast have been found to produces more ethanol and fewer by-products and it has since be licensed to Royal DSM N.V. who are using this technology to produce 2G biofuels from agricultural waste (M&C, 2011).

Another grade of biofuels known as Third Generation (3G) biofuels is also being developed. These are mainly from algae and bacteria and are referred to as Algae fuel or oilgae. Algae are low-input, high-yield feed stocks to produce biofuels. Based on laboratory experiments, it is claimed that algae can produce up to 30 times more energy per acre than land crops such as soybeans but these yields have yet to be produced commercially.

The biggest obstacle to the acceptance of biofuels is their production costs which make them more expensive than petroleum-based transportation fuels (DOE, 2000b). Additional obstacles for biodiesel include poor cold flow characteristics, engine startup and operability problems associated to low temperature. Biodiesel also has the tendency to degrade some types of elastomers and rubber compounds which can impact fuel hoses and fuel pump seals (Dunn, 2002). Another challenge facing wider use of biofuels is its energy content—only about two thirds the energy of an equal volume of gasoline (US Department of Energy). Several technologies for the production of these biofuels are still at a pilot/demonstration stage.

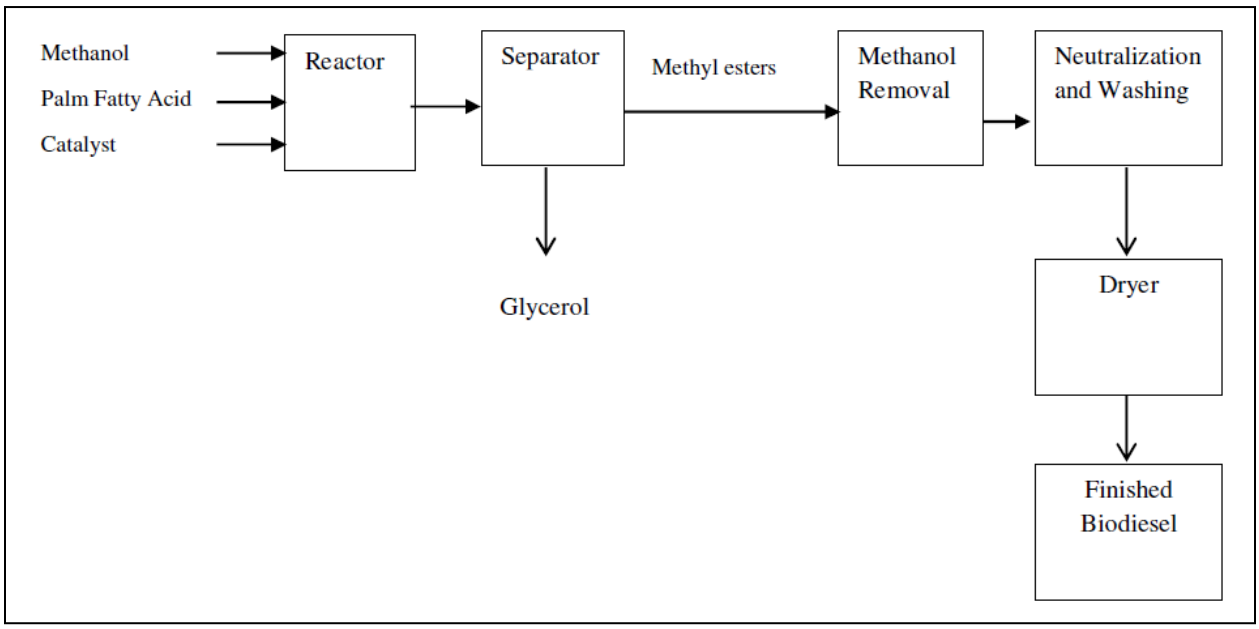


**Figure 2: Schematic diagram of biodiesel production**

## *1.2. Literature Review*

A lot of research has been done on the performance of biodiesel fuelled engines. Generally, the authors agreed that typical challenges are lower heating values resulting into less torque for any given injector pulse-width (Joshua A. Bittle et al, 2010). If torque is matched with longer pulsewidth by increasing injection duration (ID), then this will obviously translate to increased brake specific fuel consumption (Joshua A. Bittle at al, 2010) and (Yinnan YUAN et al, 2008). The lower heating value (LHV) of biodiesel has been generally attributed to the differing carbon, oxygen, hydrogen and sulphur contents (Bai-Fu Lin et al, 2008).

A pivotal issue in selecting fuel for use in compression ignition (CI) engines is its ignition quality. Ignition quality is usually quantified in terms of Cetane Number

(CN) which is a measure of the delay time between the time of injection and the start of combustion. In a study done by (Yinnan YUAN et al, 2008) using petroleum fuel and biodiesel B100, have shown that combustion timing occurs in advance, and the ignition delay decreases with biodiesel B100. They have demonstrated that at 50% and 100% load at a rated speed, the combustion occurs in advance by about 3ºCA.

The maximal heat release rates are reduced by 11.4% and 25.3%, respectively, and the related point occurs in advance by about 3ºCA. The diffuse combustion rate decreases, and the combustion durations are prolonged by 25ºCA and 13ºCA, respectively. This is a type of results we should expect because air pressure and temperature changes significantly at close to TDC. If the injection starts earlier the air temperature and pressure at that state are lower and the delay will increased accordingly.

The study performed by (Yinnan YUAN et al, 2008) have shown that the specific fuel consumption of biodiesel increased by 12% when compared with conventional diesel fuel for the same power output. When biodiesel is blend with petroleum diesel fuel, the brake specific fuel consumption (BSFC) has been found to increase. Similar results have been presented by (Bai-Fu Lin et al, 2008) in their experimental results with blends of palm kernel oil ester (PKOME) and petroleum oil. They have demonstrated that the BSFC increases as the percentage of PKOME in the blend increases, producing the same level of engine power as petroleum diesel fuel.

The ignition delay is affected both by physical factors and fuel properties. The physical factors that affect the fuel spray formation and charge air state (pressure, temperature and velocity) all have an impact on the ignition delay. These variables depend largely on the design of the combustion chamber, fuel inject system and engine operating conditions.

The ignition quality of the fuel, largely determined by the CN affects the ignition delay. The CN depends on the fuel molecular structure; straight-chain paraffinic compounds (normal alkanes) have the highest ignition quality which improves as the chain length increases. Aromatic compounds and alcohols have a poor ignition quality and hence the difficulty associated with the use of methanol and ethanol as possible alternative fuels (Heywood, 1998). (V. Nagaraju et al, 2008) have conducted a study on the effect of using B-20 (a blend of 20% soybean ME biodiesel and 80% ultra low sulfur diesel fuel) on auto ignition in high speed direct injection diesel engine equipped with a common rail injection system. The results showed that B20 did not contribute in the initial stages of fuel evaporation and the formation of an ignitable mixture resulting to an increased ignition delay.

An ignition delay of $3^0$ crank angles has been recorded by (Yinnan YUAN et al, 2008) in their comparison of diesel fuel and biodiesel B-100 at 100% and 50% engine loads. Similar results have been reported by (Joshua A. Bittle at al, 2010); in their reseach paper they reported that the start of combustion consistently occur earlier with biodiesel than with petroleum diesel. This has been associated with biodiesel's inherently shorter ignition dalay.

Swirl ratio $R_s$ is usually used to define swirl in the engine. It is defined as the angular velocity of a solid-body rotating flow $\omega_s$, which has equal angular momentum to the actual flow, divided by the crankshaft angular rotational speed (Heywood, 1998).

$$R_s = \frac{\omega_s}{2\pi N} \tag{2}$$

$$\omega_s = \frac{8}{B^2}\left(\int_{\varphi_1}^{\varphi_2} T d\varphi\right) \Big/ \left(\int_{\varphi_1}^{\varphi_2} \dot{m} d\varphi\right) \tag{3}$$

Studies have shown that swirl has an effect on the ignition delay period and consequently on engine emissions. (D.E Winterbone et al, 1994) performed an experiment to investigate the effect of swirl ratio on combustion using a Ricardo Hydra direct injection diesel engine. They have shown that too much swirl increases the ignition delay period and results in the amount of fuel burned in the pre-mixed mode thus resulting in an increase in the $NO_x$ emission but a reduction in the amount of soot formation. Similar results were presented by (Henein, 2006). Henein have also shown $NO_x$ emission increment by 50% as the swirl ratio was increased from 1.44 to 7.12 by using a single cylinder 4-valve direct injection diesel engine equipped with common rail injection system. This increased in $NO_x$ emission was attributed to the following factors: (1) Better fuel evaporation and mixing with the fresh charge, due to (a) the higher relative velocity and its effect on increasing the heat and mass transfer coefficients between the liquid phase and gas phase, (b) the spread of the spray over a wider angle, and the increase in the lean flame region downstream the swirl motion and (c) the increase in the wetted surface area of the wall after the spray impinges on the wall. All these factors contribute to the

increased in the volume of the premixed charge. (2) Higher swirl ratios increase turbulence and mixing and enhance the reaction rate, this Henein has demonstrated from the evidence of increased rate of heat release from premixed combustion fraction by 40%. This increase occurred, in spite of the increase in the cooling losses at the higher SR. (Henein, 2006) report also showed that the increased in the swirl ratio from 1.44 to 7.12 caused a drop of 2 bar in compression pressure and about 80ºC in the compression temperature.

The combustion process of a compression-ignition engine is defined by four phases according to the rate of heat released; ignition delay period, premixed combustion period, diffusion burning phase and oxidation phase (Heywood, 1998).

The rate of heat release is lower for biodiesel fuel than conventional petroleum fuel; this is mainly as a result of a low LHV of biodiesel. Yusuf Ali et al have carried out a series of tests on Cummins N14-140 Diesel engine to determine the rate of heat released using twelve fuels produced by blending methyl tallowate, methyl soyate and fuel ethanol with diesel fuel. They reported that the rate of heat released was reduced with increased amounts of methyl tallowate, methyl soyate and ethanol in the fuel blends. During premixed period the maximal heat release rate decreases. This is attributed to the presence of oxygen in biodiesel which makes the premixed combustion flame diffused making the peak heat released rate occur in advance (Yinnan YUAN et al, 2008). Additionally, alcohols such as methanol and ethanol are known to reduce the temperature of combustion, a condition that can decrease NO$x$, particulate matter, carbon dioxide, and smoke in exhaust emissions (Dunn, 2002).

Many researchers have reported different levels of Nitrogen Oxide ($NO_x$) emission from engines fuelled with biodiesel. (V. Nagaraju et al, 2008) have conducted an experiment on the effect of biodiesel B00 and B20 (a blend of 20% soybean methyl ester biodiesel and 80% ultra low sulphur diesel fuel) on engine out emission and have reported observations of generally lower $NO_x$ emission for B20 than for B00 except at high ignition pressures. At high ignition pressures, biodiesel evaporation is enhanced and its contribution to early stages of combustion is increased thus resulting in high $NO_x$ emission. Statistically, they have measured 4% decrease in $NO_x$ for B20 relative to B00. Similar studies has been performed by Fang et al (2008).

In general, the emission products, HC, CO and soot formed as a result of incomplete combustion are lower for B20 than B00 (V. Nagaraju et al, 2008). There are two main reason for this; the contribution of oxygen atoms present in biodiesel leading to complete combustion and the burning of the heavier masses of the biodiesel component which can progress down into the expansion stroke. Similar studies has recently been done by (Praveen K. et al, 2010) by using several blends of palm fatty acid biodiesel and diesel fuel. The results are presented in figures 6- 8.

# Chapter Two: Experimental Setup

## *2.1. Hydra single cylinder research engine*

The experimental engine is a single cylinder Ricardo hydra research fitted with a common rail direct injection system, shown in figure 3. The engine utilizes a toroidal bowl in the piston. The valves are operated through inverted bucket type tappets with pallets between the valve and tappet to set the tappet clearance. A high pressure pump supply fuel to the fuel injector at a pressure of 120 to 1400 bars.

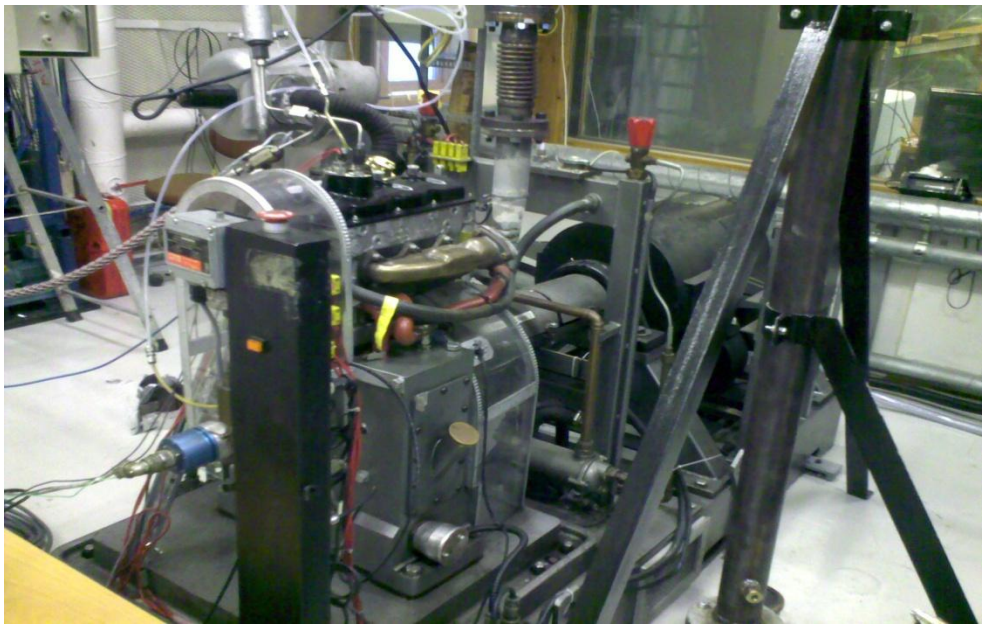

**Figure 3: Photograph of test engine**

A pulsation damper between the high pressure pump and the fuel injection valve maintains a constant flow of fuel into the cylinder. The engine has a solid skirt, two

compression rings and one oil ring and is cooled from below by an oil jet supplied from the lubrication system. The has been modified by replacing the cylinder head with that of one bank of an Audi V6 direct injection diesel engine shown in figure 4. The technical details for the Audi A8 engine are shown in appendix C.

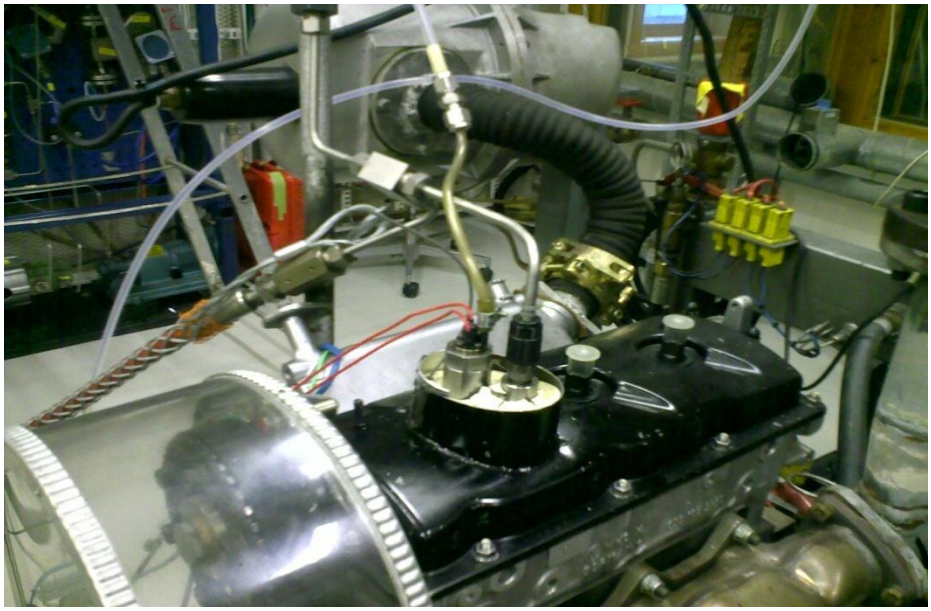

**Figure 4: Photograph of cylinder head and injection system**

The fuel injection system has also been replaced by a common rail fuel injection system with electronically controlled timing, duration and number of pulses. The injector is an electronically controlled version of the originally Audi (Bosch) injector. The modified test engine specification is shown in table 3:

The fuel injection system is divided into a low pressure and high pressure sides. In the low pressure side, fuel is supplied to the high pressure (HP) pump by the low

pressure (LP) pump from the fuel service tank through filters F1 and F2 via a flow meter. The output of the LP pump provides a slight positive inlet pressure of 0.15-0.8 bar for the HP pump inlet.

The output from the high pressure pump is supplied to the pulsation damper, which maintains a constant pressure supply to the fuel injector. During the experiment I have kept this pressure at 1200 bars. Fuel return from the injector pump is returned via a cooler to the tank/slope tank. The fuel temperature at the injector inlet is monitored on channel 2 of the multi-point temperature indicator at the control console and control by manual adjustment of the cooling water flow.

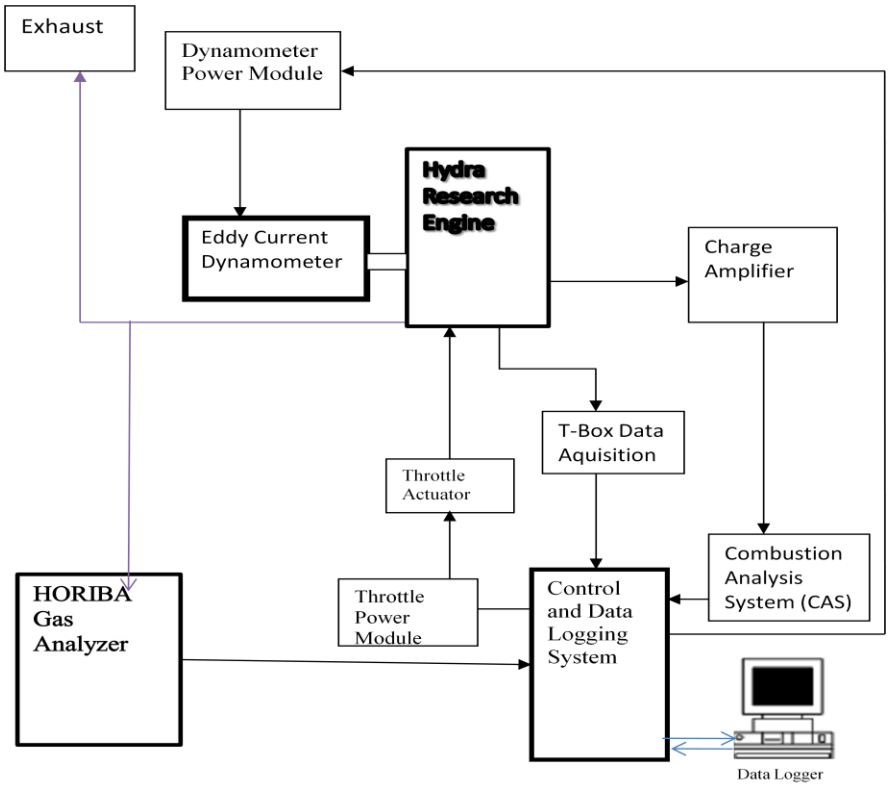


**Figure 5: Experimental Setup**

The Common Rail Injection System (CR) allows the fuel injection parameters; injection pressure, duration and start of injection to be selected independently from the operating speed and load. For this purpose the high pressure pump is driven independently by an electric motor. During operation the start of injection and duration are set manually by a means of closed loop pressure regulator system and an electronic control unit by feeding measured electric pulses to the injector's solenoid driver allowing delivery of specified fuel quantity into the cylinder.

The amount of fuel injected during each engine cycle is electronically controlled by the CAS. These variables are set by the user in the Lab view program. The actuator is operated by the throttle potentiometer on the control console which is usually set up so that 0 on the potentiometer corresponds to the fuel shut off position and 10 corresponds to the maximum fuel delivery position. Operation of the actuator is supervised by the Automatic Control Unit (ACU) so that in the event of any fault condition, the actuator is de-energized allowing the rack to close under the influence of its return spring. The fuel injection system is shown in appendix B

| | |
|---|---|
| Configuration | Four stroke, direct injection |
| Number of cylinders | 1 |
| Bore (mm) | 80.26 |
| Stroke (mm) | 88.90 |
| Displacement volume ($dm^3$) | 0.45 |
| Clearance volume ($dm^3$) | 0.043 |
| Maximum speed (rps) | 75 |
| Maximum power (KW) | 8 |
| Maximum cylinder pressure (bar) | 120 |
| Fuel injector | Bosch |
| Compression ratio | 19.5:1 |
| Valve timing | Valve timing is in accordance with table 2. |

**Table 1: Test engine specification**

The brake torque of the engine is measured with a regenerative dynamometer which is coupled to the engine. The dynamometer is an electric D.C. machine rated at 400 volts, 70 amps and has a continuous power rating of 30KW with a maximum speed of 100rev/s. The dynamometer can both load and motor the engine, a weight hanger is provided on each arm which allows the load to be calibrated for both clockwise and anticlockwise torque reactions. The dynamometer is operated through a KTK thyristor converter units so that it can act as a D.C. motor to drive the engine during starting and motoring operations, or as a D.C. generator when loading the engine. During loading the D.C. power from the dynamometer is converted to 3 phase A.C. by the converter unit and feed back into the mains

supply. A tachometer mounted on the dynamometer shaft provides a speed signal to the close loop speed control system so that the speed selected at the control console is maintained by automatic adjustments to the motoring or loading torque. The brake power of the engine is calculated from the bake torque and speed from the relation:

$$P_b = \frac{2\pi TN}{60} \tag{4}$$

From this relation, the Brake Mean Effective Pressure can be measured using power, speed and engine cylinder displacement as variables:

$$P_{bme} = \frac{2P_b}{V_d N / 60} \tag{5}$$

### *2.2.1. Effect on Compression Ratio*

Replacing the cylinder head with the Audi A6 head means that the compression ratio of the engine has been reduced from 20 to 19.5. The compression ratio largely depends on the design of the cylinder head, changing the compression ratio of the engine changes the cylinder pressure according to the formula below:

$$P = P_0 \times CR^{\gamma} \tag{6}$$

Where $P_0$ is the pressure when the piston is at TDC and $\gamma$ is the specific heat ratio of the fuel. This has repercussion on the performance of the engine in terms of specific fuel consumption (SFC). This effect has been documented in literature by

(H. Raheman et al, 2008) with a Ricardo E6 engine using biodiesel obtained from mahura oil (B100).

### *2.2.2. Effect on Clearance Volume*

Based on the new CR, the new clearance volume (CV) can be recalculated. The clearance volume is the volume of the cylinder when the piston is at TDC. Because of the irregularity in the shape of the combustion chamber, this measurement is done empirically by filling the combustion chamber with a known amount of fluid while the piston is at TDC. The result of the measurement and the calculated CV is shown below.

Measured piston bowl volume = 14.54 $cm^3$

Estimated valve cut out volume = 3.96 $cm^3$

Hence, total piston clearance volume = 18.50 $cm^3$

The compression ratio (CR) is found by taking the volume of the cylinder when the piston is at BDC and divide by the volume of the cylinder when the piston is at TDC (figure 6):

$$\varepsilon = \frac{V_{BDC}}{V_{TDC}} = \frac{V_d + V_c}{V_c}$$

$$\varepsilon = \frac{V_d + V_c}{V_c} = 19.5 \qquad (7)$$

It can be shown that the CV can be found by means of equation 8.

$$V_c = \frac{SV}{\varepsilon - 1} = \frac{449.77}{19.5 - 1} = 24.31 cm^3 \quad (8)$$

The displacement volume is calculated from the cylinder stroke and bore as the only variables. The stroke and the bore of the engine remains unchanged and therefore the displacement volume can be calculated from the well known formula below:

$$V_d = \frac{\pi d^2 . L}{4} \quad (9)$$

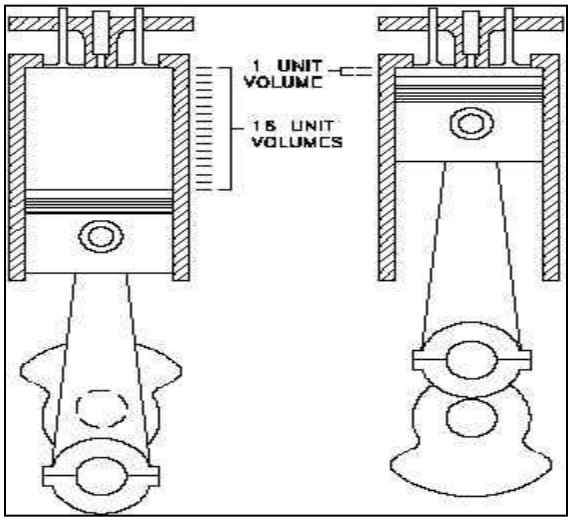


**Figure 6: Determining the compression ration**

## 2.2. Emission Measurement and Analyzer

The instrument used for measuring emission is the HORIBA PG-250. The instrument is able to measure five gas components simultaneously. The PG-250 uses non-dispersive infrared (NDIR) detection for CO, $SO_2$, and $CO_2$; chemiluminescence (CLD) cross-flow modulation for $NO_x$; and a galvanic cell or an optional zirconium oxide sensor for $O_2$ measurements. Samples of exhaust is connected through ducks in the exhaust manifold and sent to the Analyzer. The measurement results are displayed on a LCD display. The analyzer interfaces directly with the combustion analyzer computer through an RS-232C interface port that allows data transmission and for recording measured values. The instrument is always calibrated before measurements are being taken by connecting the calibration gases via the calibration inlet.

| Emission gas | Measurement range | Measurement method |
|---|---|---|
| $NO_x$ | 0-2500 ppm | Chemiluminescence |
| CO | 0-5000 ppm | Non-dispersive IR |
| $CO_2$ | 0-20 vol% | Non-dispersive IR |
| $O_2$ | 0-25 vol% | Galvanic cell |

**Table 2: Exhaust emission measurement range and methods**

The measurement of $NO_x$ is based on the principle of chemiluminescence. Fresh air is sucked through the air filter and cooled before being stored in a reaction chamber

to act as an ozone ($O_3$) supply. The $O_3$ is introduced to the exhaust sample; part of the nitrogen monoxide (NO) in the exhaust sample reacts with the $O_3$, oxidized and form nitrogen dioxide ($NO_2$). Part of this generated $NO_2$ is in an excited state ($NO_2$*) and when it returns to normal it emits light. This light is detected by photodiodes.

$$NO + O_3 \rightarrow NO_2 + O_2 \quad (10)$$

$$NO_2^* \rightarrow NO_2 + h\nu \quad (11)$$

The reaction time is extremely fast and only the NO present in the exhaust gas participates in the reaction and does not affect other components of the exhaust. The NO concentration is proportional to the light emitted. The sample exhaust gas is divided into two parts in the Analyzer; one part is deoxidized from $NO_2$ to NO by the $NO_x$ converter and is used for $NO_x$ ($NO_2$ + NO) concentration measurement. The other portion is used as is, as for measurement of NO.

The oxygen is measured by the well known Galvanic cell method. Gold is used as the anode and lead (Pb) is used for the cathode. Potassium hydroxide (KOH) is used as the electrolyte. A suitable load resistance is connected to the electrodes, exhaust gas passes through the permeable membrane and the $O_2$ inside is deoxidized by the anode as shown in the following equations:

(Anode) $$O_2 + 2H_2O + 4e^- \rightarrow 4OH^- \quad (12)$$

(Cathode) $$2Pb \rightarrow 2Pb^{2+} + 4e^- \quad (13)$$

The electromotive force generated by the electrochemical reaction is measured and calibrated to read the oxygen concentration.

**Figure 7: Exhaust emission measurement equipments**

The CO measurement is based on the non-dispersive infrared analysis method. By absorbing the infrared light beam the CO concentration in the exhaust gas is continuously measured. A schematic diagram of the Infrared analyzer is shown in figure x. Exhaust gas is introduced into the measurement cell where an infrared light beam is passed through and enters a detector cell that encloses a sample of CO gas at a steady state.

The splitter beam divides the infrared light for the measurement of a second gas component (not shown). The MAIN side reads the signal of the measured component gas of interest together with the interfering components and the COMP side reads the signal of the interfering component. These signals are then sent to a CPU where the two signals are compared and the interfering component's effects are eliminated

giving a precise measurement of CO. figure 8 shows the schematic diagram of this process

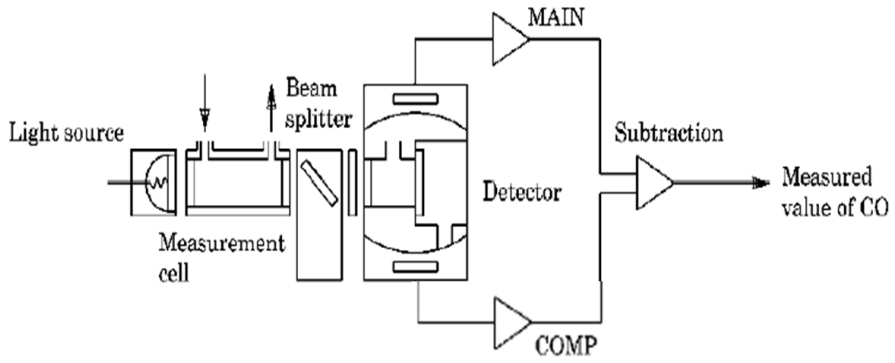


**Figure 8: Schematic diagram of non-dispersive infrared measurement method.**

## *2.3. Particle Emission Measurement*

Particulate emissions in the exhaust gas may originate from a number of sources; agglomeration of very small particles of partly burned fuel, partly burned lube oil, ash content of fuel oil and cylinder lube oil, sulphates and water. The size distribution of the aerosol is a function of the chemical and physical processes occurring between the point of aerosol generation and the point of aerosol collection. These processes, such as dilution, coagulation, condensation, homogeneous and heterogeneous nucleation, simultaneously affect the aerosol size distribution but are not well understood (David B. Kittelson et al, 1998). The formations of these compounds are affluence by fuel properties and combustion conditions.

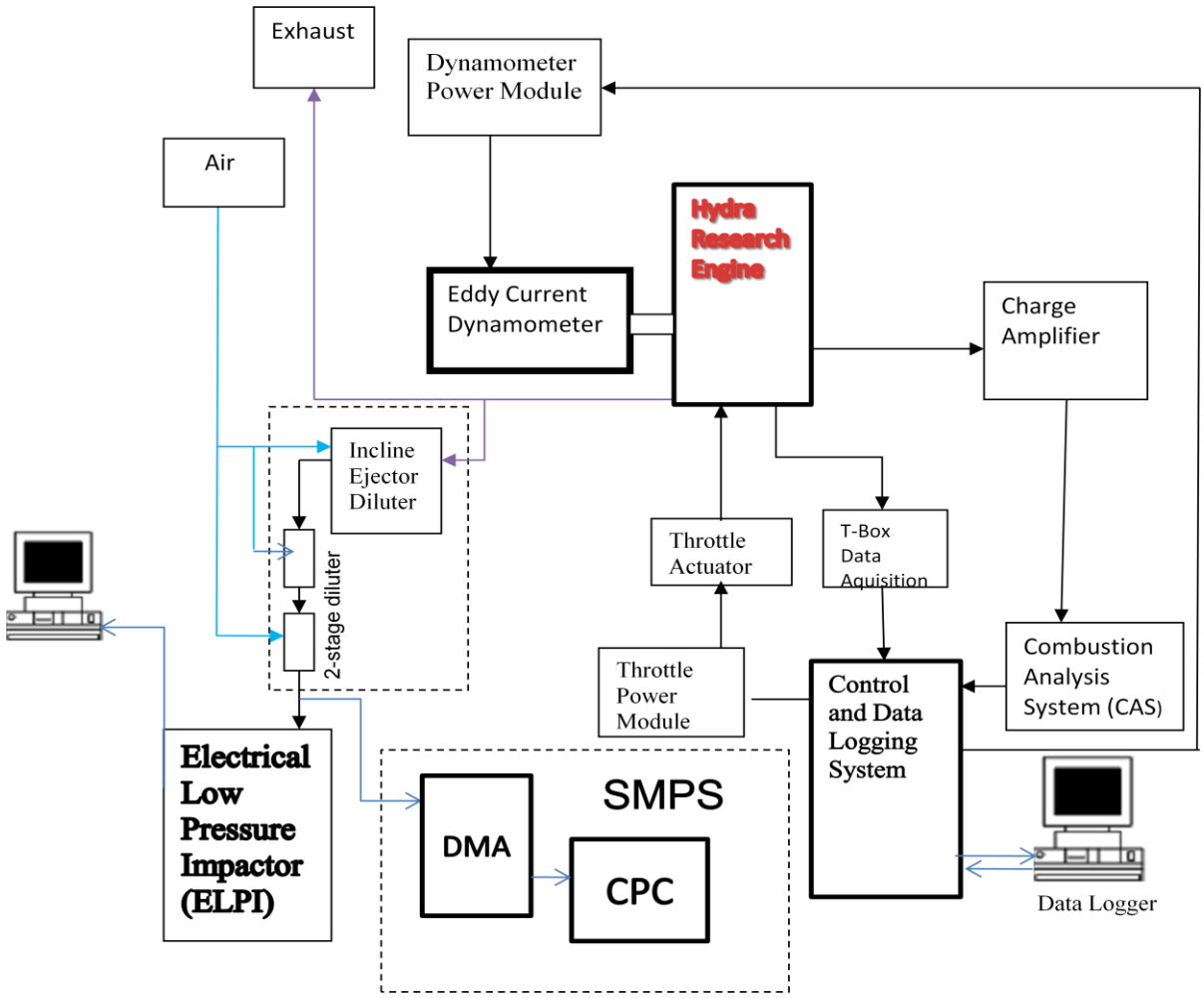


**Figure 9: Experimental setup with particle sampling system**

Figure 9 shows the experimental setup with the particle measurement system. In large direct injection engines, at temperatures above $500^0$C, individual particles of principally clusters of many small spheres or spherules of carbon of diameters of 15 to 30 nm (with a small amount of hydrogen) has been documented (Heywood, 1998). At low temperatures below $500^0$C, the particles tend to be coated with absorbed and

condensed high molecular weight organic compounds which include unburned hydrocarbons and oxygenated hydrocarbons (ketones, esters, ethers, organic acids and polynuclear aromatic hydrocarbons (Heywood, 1998). This is one key reason which makes the study of PM emission from biofuels an interesting issue.

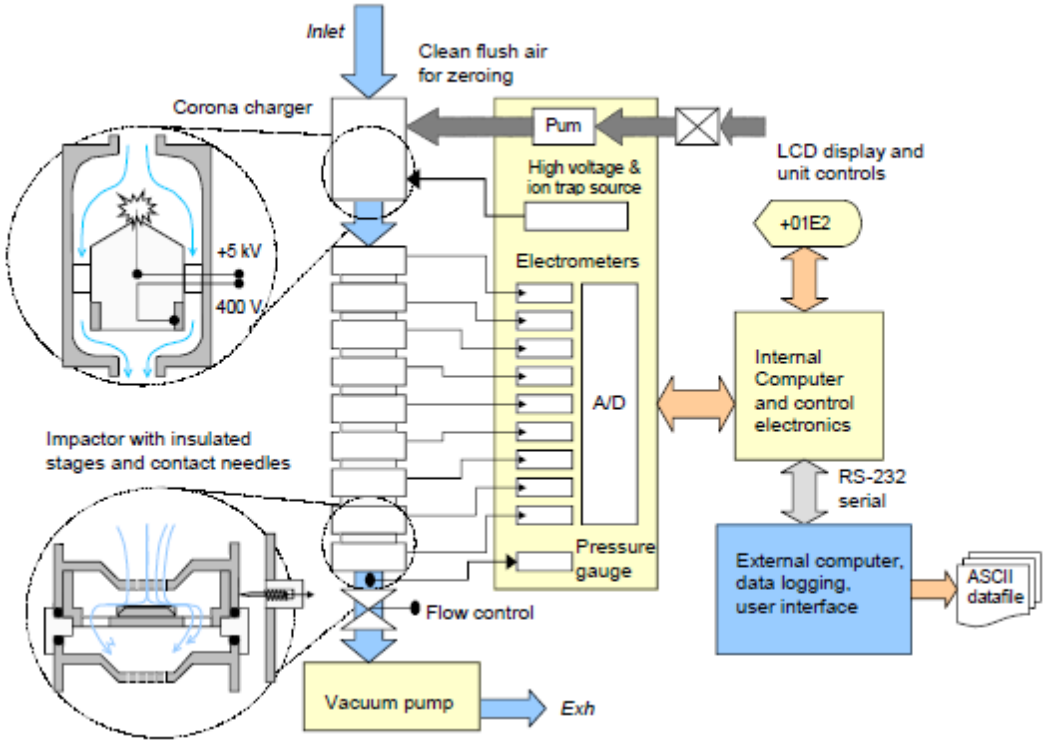


**Figure 10: Schematic diagram of ELPI particulate matter measurement system**

The instrument used for particle measurement in this study is ElectricLow Pressure Impactor (ELPI) (figure 10). This is a real-time particle size spectrometer designed at the Tampere University of Technology for real-time monitoring of aerosol particle size distribution. The ELPI measures airborne particle size distribution in the size range of 0.03µm to 10µm with 12 channels. With filter stage the size range can be extended down to 7 nm. The operating principle is based on

particle charging, inertial classification in a cascade impactor, and electricdetection of the aerosol particles. The main components of the instrument are a corona charger, low-pressure cascade impactor and multichannel electrometer.

**Figure 11: Photograph of particle measurement system**

In ELPI (photographic view shown in figure 11) the sample first passes through a unipolar positive polarity charger where the particles in the sample are charged electrically by small ions produced in a corona discharger. The charged particles are then classified into sizes in a low-pressure impactor. The impactor is an inertial device classifying the particles according to their aerodynamic diameter and not by their charge. The stages of the impactor are insulated electrically and each stage is connected individually to an electrometer current amplifier. The charged particles collected in a specific impactor stage produce an electric current, which is recorded by the respective electrometer channel. A larger charge correlates to a higher particle population.

The current value of each channel is proportional to the number of particles collected, and thus to the particle concentration in the particular size range. The current values are converted to a (aerodynamic) size distribution using particle size dependent relations describing the properties of the charger and the impactor stages. Figure 12 shows such a distribution during the experiment.


**Figure 12: Sample output data of PM measurement system**

## *2.4. Measurements and Data Acquisition System*

Dynamic cylinder pressure is measured using KISTLER sensor of type 6051B. It is capable of measuring cylinder pressures of between 0 to 250 bars at continuous operating temperatures of -50 to 350°C and at maximum short-time temperatures of 400°C. It operates on the principle of piezoelectric effect, the cylinder pressure acts on the diaphragm, which converts it into a proportional force. This force is transmitted onto the quartz, which under loading yields an electrostatic charge. An

electrode picks up this (negative) charge and takes it to the plug, after which the connected charge amplifier converts it into a (positive) voltage. The line powered charge amplifier is type 5011B which converts the signals from the piezoelectric measuring sensors into proportional signals. The microprocessor-controlled electronic circuitry allows continuous adjustment of the measuring range with simple controls on the front panel of the amplifier. This is feed to the computer system used for the analysis of the engine combustion which is connected to the measurement systems on the engine and dynamometer through the charge amplifier. Pressure readings are dynamic and are stored periodically by the user by taking a predefined average of four complete cylinder cycles for further analysis.

The measurement of the torque can be read both in analogue and digital and capable of measurements of 0- 50 Nm with a digital speed measurement system with a range of 0-120 rev/s. The injection timing can be adjusted from $0^0$ to $20^0$CA before TDC. The running hours for the duration of the test are digitally displayed on the control console with a range of 0- 999 hours. The injection timing control system has been designed to meet the requirement of a manual or computer controlled variable injection timing system.

**Figure 13: Control room**

The unit will provide an ignition drive pulse with a nominal dwell angle of 50 degrees, although this can be readily altered if required. The engine timing can be varied either by a 0 to 10 volts drive voltage or a manual control potentiometer, selection being made by an external control signal. The value of the injection timing can be read and adjusted in the Lab view program in the combustion analysis system (CAS) which is located in the control room (figure 13)

.

The injection control system accepts three external input signals; speed, crank angle reference and the injection reference. The signals are use to generate the relevant timing and gating pulses. The speed signal (about 100 pulses per revolution) is used to generate an analogue voltage level which is proportional to the engine speed. The speed and load meter display circuit receives the raw speed and pre-conditioned load signals plus a digital encoded barometer signal. The circuit conditions these in preparation for driving the front panel indicators and

displays. The circuit also outputs several digital status signals on the CAS status lines to indicate the speed and load levels.

# Chapter Three: Experimental Procedure

## *3.1. Planning of the experiment*

The applied test methodology is outlined in the following flow chart:

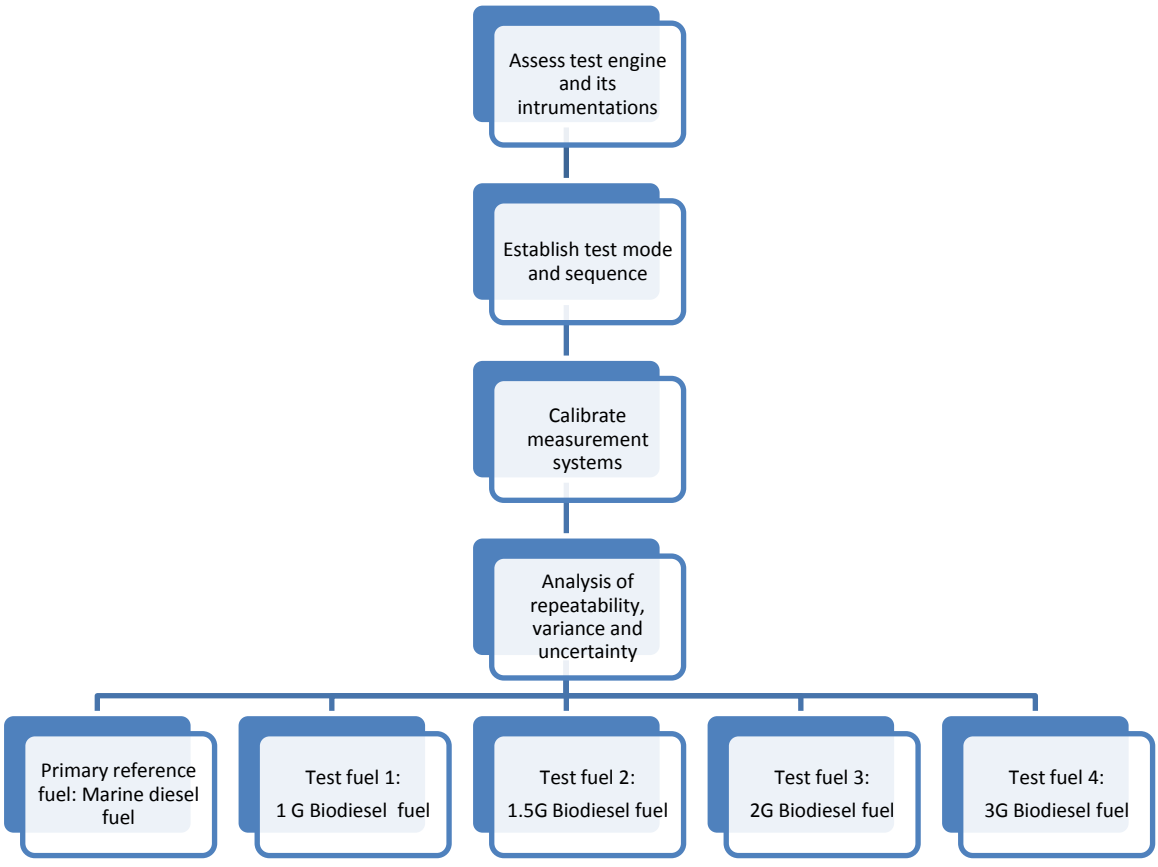


**Figure 14: Flow chart of experimental methodology**

## *3.2. Test modes*

The experimental procedure for the measurement of exhaust emission is based on 8 point test mode of the ISO 8178-4:2007. These 8 test points sufficiently define the power and torque curve from highest to the lowest speed range. The speed range also includes the maximum power and torque produce by the engine. The test cycles are performed in ascending order as shown in the table 3.

| Mode Number | 1 | 2 | 3 | 4 | 5 | 6 | 7 | 8 |
|---|---|---|---|---|---|---|---|---|
| Speed | Rated speed | | | | Intermediate speed | | | Low-idle speed |
| Torque (%) | 100 | 75 | 50 | 10 | 100 | 75 | 50 | 10 |
| Weighting factor | 0.15 | 0.15 | 0.15 | 0.1 | 0.1 | 0.1 | 0.1 | 0.15 |

**Table 3: ISO 8-point test mode**

The 8- modes are divided into three speed groups; modes 1-4 are based on the rated speed of the engine. the rated speed is defined as the speed at which the rated power is produced. Mode 5-7 are runned based on the intermediate speed of the engine and the 8$^{th}$ mode is based on the engine idle speed. The dynanometer loads based on the percentage maximum torque as indicated in table 3. Finally, a weight factor is assigned to each mode for the final analysis.

## 3.3. Establishing idling speed

The engine is coupled to a dynamometer with a continuous power rating of 30KW with a maximum speed of 100 rev/s. The dynamometer is an electric direct current machine rated at 400 volts, 70 amps. Since the dynamometer can both load and motor the engine, establishing the idle speed at an out power of zero from the engine is a trick business. However, using an injection timing of $9^0$ and ID of 0.31ms, an idle speed of 20rps established. The established idle speed will be eventually used for the $11^{th}$ mode of all the fuel test sequences.

## 3.4. Operating Conditions for preliminary testing

The test engine is naturally aspirated. The test is divided into 8 separate modes (table 4) and each mode defines a specific engine operating conditions. The operating conditions are defined by the load and speed. The injection timing and duration are selected for each mode to achieve the optimum operating conditions and are all within limits recommended by the research engine manufacturer.

| Mode | Injection timing (degrees) | Injection duration (milliseconds) | Load | speed |
|---|---|---|---|---|
| 8 | 9° | 0.31 | 0% | 20(Idle) |
| 7 | 12° | 0.5 | 50% | 37.5 |
| 6 | 13° | 0.75 | 75% | 37.5 |
| 5 | 13 | 1.23 | 100% | 37.5 |
| 4 | 19 | 0.34 | 10% | 50 |
| 3 | 18 | 0.45 | 50% | 50 |
| 2 | 17.5 | 0.54 | 75% | 50 |
| 1 | 18 | 0.75 | 100% | 50 |

**Table 4: Experimental engine operating conditions at different test modes**

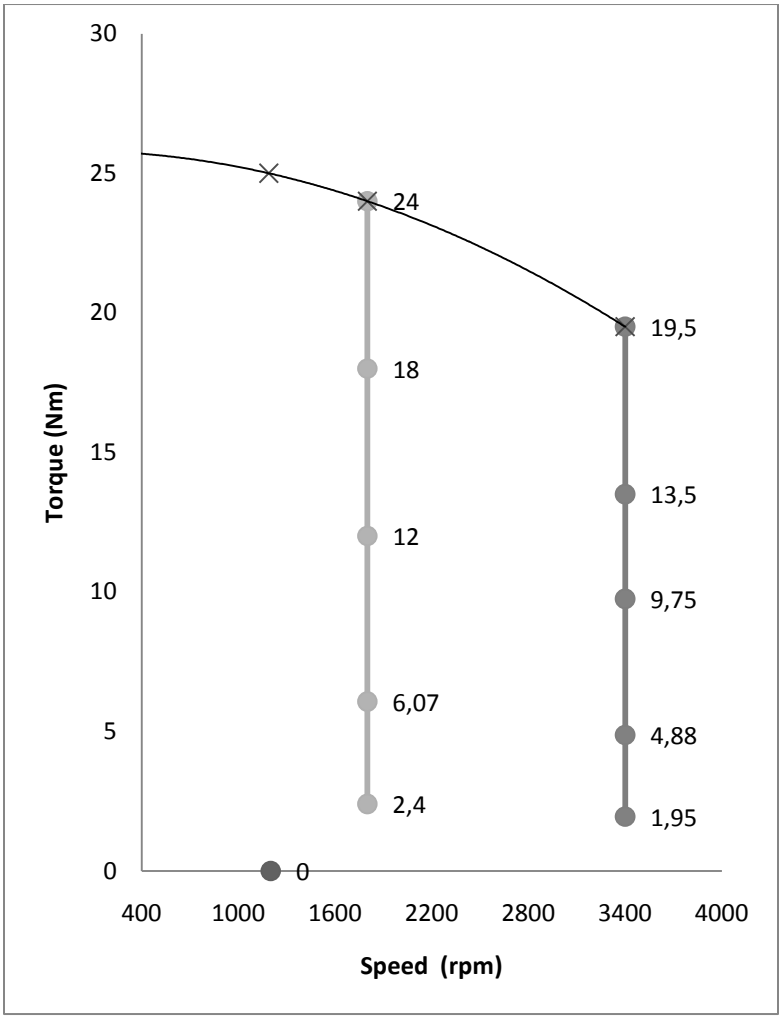


**Figure 15: Percentage of full-load torque at each engine speed**

The high pressure injection pump was set at 700 bars and the engine inlet air temperature is set at 50°. From these operating conditions the various load has been set as shown in figure 15. The variation in injection timing has an effect on $NO_x$ emission. By increasing the ignition delay substantial reduction in $NO_x$ emission can be achieved but with some penalty in SFC. Therefore in choosing the ignition timing, a compromised has been made towards BSFC and $NO_x$ emission.

HC are higher at low loads and can increase further with increased in ignition delay from the optimum. This phenomenon is even more pronounced at idle speed. At high loads, HC emissions are low but can also vary with ignition timing.

The goal of the initial testing is to assess the stability of the engine and its measurement systems. A series of measurement is performed to establish repeatability and further measurements are carried out for several days in order to incite understanding of the effect of atmospheric pressure on the performance of the test engine. To characterize the dynamic behavior of the engine, the dynamic in-cylinder pressure measurements (figure 16) is used.

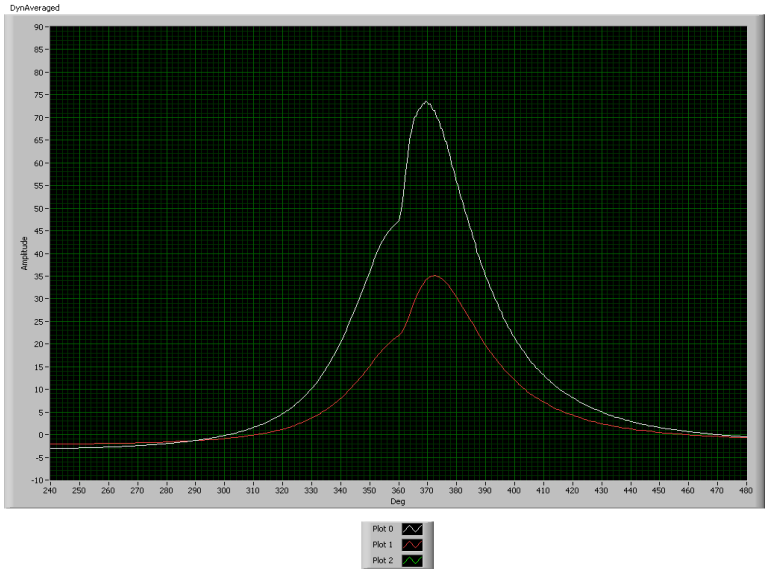


**Figure 16: Dynamic in-cylinder pressure measurement trace**

The cylinder pressure measurement profile is traced by taking the average of four complete cycles and displayed in real time in the combustion analyzer computer.

Pressure measurement is taken at every 0.5 crank angles culminating into 1440 data point for each complete cycle. The white line in figure 16 shows in-cylinder pressure trace while the red line traces the corresponding injection valve lift. Static measurements of power, torque, specific fuel consumption, air consumption, exhaust temperature are recorded at every 4 seconds interval and these data are use to characterize the steady state behavior of the engine. The uncertainty of measurement is analyzed by calculating the standard deviations and detail error analysis is done by using a known statistical method referred to as Analysis of Variance (ANOVA). The results for this analysis, methods used and presentation are explained in chapter five.

## *3.5. Maximum load and speed definition*

The maximum permissible speed and loads have been define using a Filter Smoke Number (FSN≤ 2.5) is in accordance with ISO 10054. This was achieved by drawing a known volume of exhaust gas at steady state to an AVL smoke meter through a paper filter. The FSN is determined by measuring the reflectance of the paper blacking by the exhaust gas. This is detected by photoelectric sensors and the results are calibrated to give the FSN.

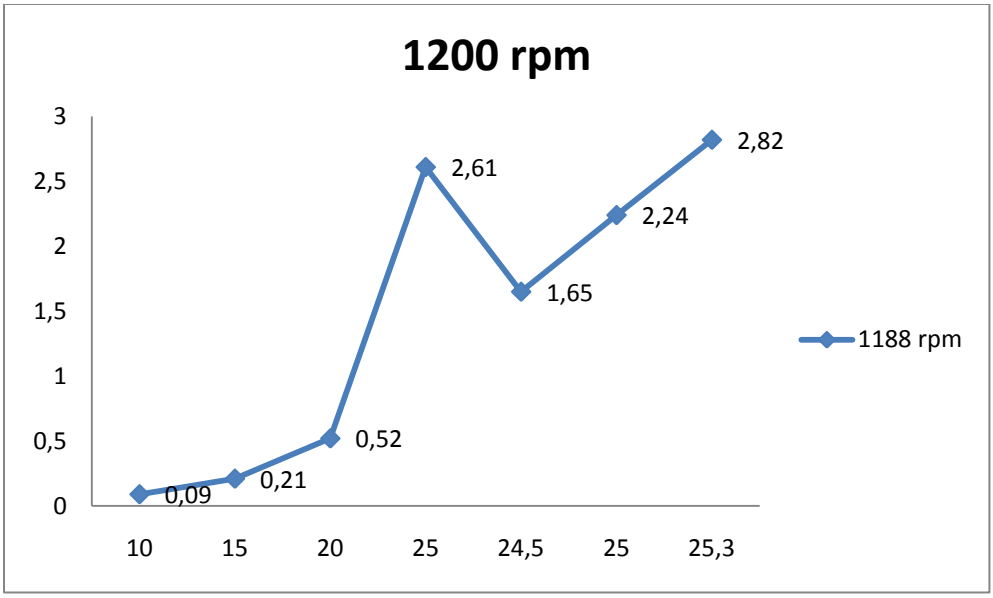


Figure 17: smoke number vs. torque at 1188rpm

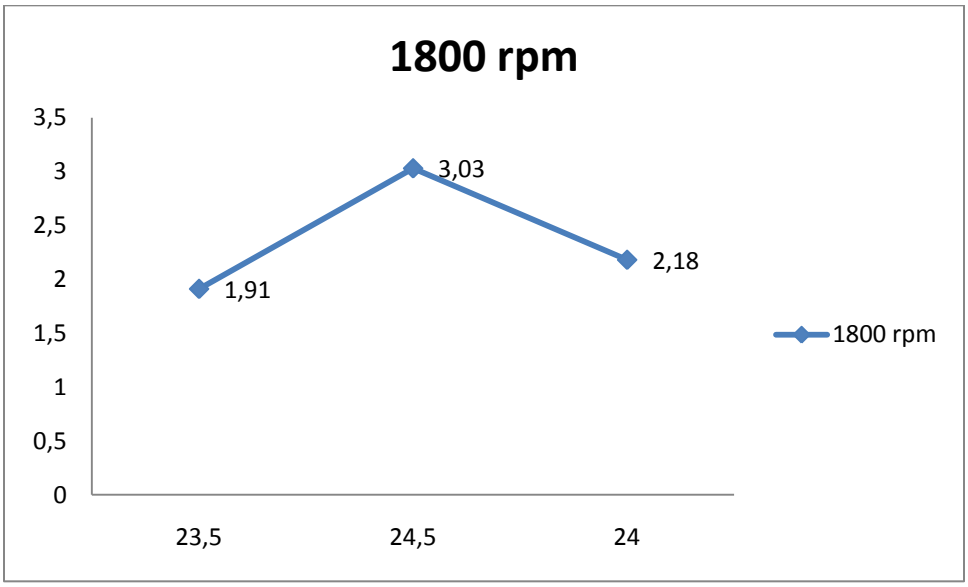


Figure 18: smoke number vs. toque at 1800rpm

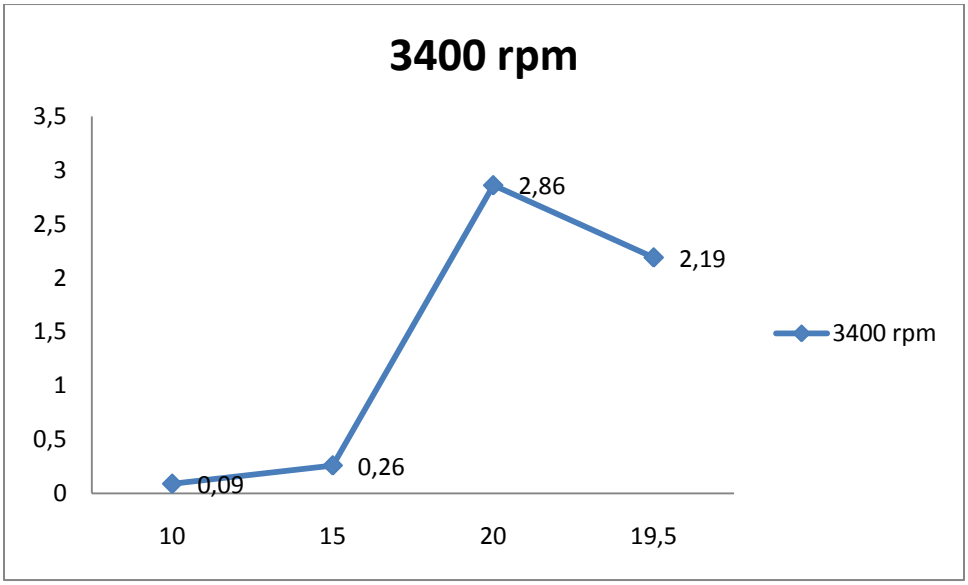


Figure 19: smoke number as a function of torque at 3400 rpm

| Speed (rpm) | Maximum load (Nm) | FSN |
|---|---|---|
| 1200 | 25 | 2.24 |
| 1800 | 24 | 2.18 |
| 3400 | 19.5 | 2.19 |

Table 5: FSN and load point definition

by varying the torque at each speed level and taking measurements of the FSN, the maximum permissible FSN for each speed level have been defined as shown in table 5.

## *6.1. Modified engine operating conditions*

Upon thorough analysis of the preliminary data and after making adjustments on the engines measurement and operating conditions, a new operation mode has been adopted based on the Universal test cycle of ISO 8178-4: 2007 as shown in table 6. This cycle is chosen because of its suitability for performance as well as emission measurement of test bench power plants. It is divided into three test cycles based on three constant speed ranges of the engine.map a wide range of loads

| Mode Number | 1 | 2 | 3 | 4 | 5 | 6 | 7 | 8 | 9 | 10 | 11 |
|---|---|---|---|---|---|---|---|---|---|---|---|
| Speed | Rated speed | | | | | Intermediate speed | | | | | Low-idle speed |
| Torque (%) | 100 | 75 | 50 | 25 | 10 | 100 | 75 | 50 | 25 | 10 | 0 |
| Weighting factor | | | | | | | | | | | |

**Table 6: ISO Universal test cycle**

The fuel injection pressure has been increased to 1200 bar and based on the measurement of the maximum permissible Filtered Smoke Number ((FSN) shown in table 5, suitable loads and speed matrix has been set for each operating mode.

| Mode | Injection timing (degrees) | Injection duration (ms) | Load (%) | Speed (rpm) |
|---|---|---|---|---|
| 1 | 17 | 0.53 | 100 | 3400 |
| 2 | 17 | 0.37 | 75 | 3400 |
| 3 | 17 | 0.34 | 50 | 3400 |
| 4 | 17 | 0.31 | 25 | 3400 |
| 5 | 17 | 0.30 | 10 | 3400 |
| 6 | 8.5 | 0.65 | 100 | 1700 |
| 7 | 8.5 | 0.52 | 75 | 1700 |
| 8 | 8.5 | 0.37 | 50 | 1700 |
| 9 | 8.5 | 0.35 | 25 | 1700 |
| 10 | 8.5 | 0.31 | 10 | 1700 |
| 11 | 9 | 0.31 | 0 | 1200 |

**Table 7: Experimental engine operating conditions**

The performance measurement modes are selected such that all engine operating conditions are simulated. Using the ISO test mode as a reference cycle, the test modes are based on 10%, 25%, 50%, 75% and 100% of maximum torque at three different speed levels. The mode points are defined by torque and speed as shown on figure 20.

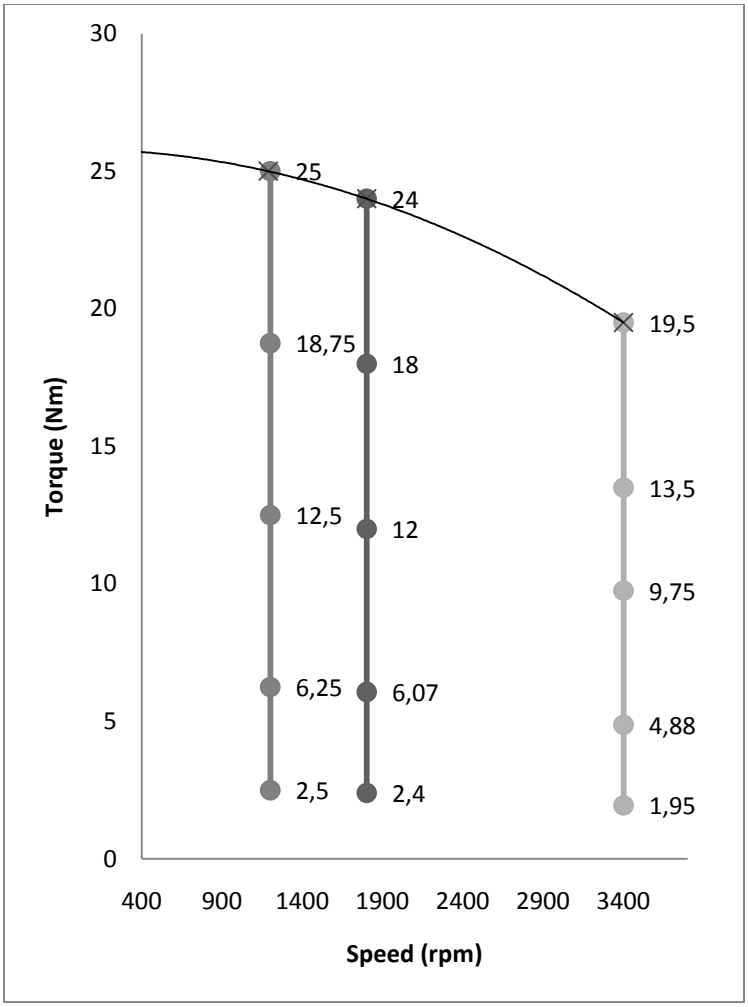


**Figure 20: Percentage of full-load torque at each engine speed**

The experiment is performed case by case basis by keeping the speed constant at three different speed levels and varying the torque as shown in tables 8-10.

*Case 1: 1200 rpm*

In case 1, the engine was maintained at a constant speed of 1200rpm and the load was varied as per table 9. The common rail pressure was set at 1200 bar. The injection time was also set at constant timing of 8.5° for all load points while the ID varies as in table 8.

| Injection duration (ms) | Torque (Nm) | Load (%) |
|---|---|---|
| 0.32 | 2.5 | 10 |
| 0.36 | 6.25 | 25 |
| 0.42 | 12.5 | 50 |
| 0.58 | 18.75 | 75 |
| 0.71 | 25 | 100 |

**Table 8: Case 1 engine operating conditions**

*Case 2: 1700 rpm*

The injection timing in case 2 was set at constant timing of 8.5° for all load points while the ID varies as in table 9. The engine was maintained at a constant speed of 1700rpm and the load was varied as described. The common rail pressure was set at 1200 bar.

| Injection duration (ms) | Torque (Nm) | Load (%) |
|---|---|---|
| 0.31 | 2.43 | 10 |
| 0.35 | 6.07 | 25 |
| 0.37 | 9.11 | 50 |
| 0.52 | 18.22 | 75 |
| 0.65 | 24.29 | 100 |

**Table 9: Case 2 engine operating conditions**

*Case 3: 3400 rpm*

In case 3, the engine was maintained at a constant speed of 3400rpm and the load was varied as described. The common rail pressure was set at 1200 bar. The injection time was also set at constant timing of 17° for all load points while the ID varies as in table 10.

| Injection duration (ms) | Torque (Nm) | Load (%) |
|---|---|---|
| 0.3 | 1.95 | 10 |
| 0.31 | 4.875 | 25 |
| 0.34 | 9.75 | 50 |
| 0.37 | 14.625 | 75 |
| 0.53 | 19.5 | 100 |

**Table 10: Case 3 engine operating conditions**

## *3.6. Hydra engine starting sequence*

The starting of the Ricardo research engine follows the same starting sequence as any normal diesel engine. As indicated in step 1, it is important to ascertain that the engine is moving freely without any obstruction. This can be verified by simply turning the output shaft twice. Check to ensure that oil level is between the minimum and maximum oil marks. There are two valves located in the engine room; one for cooling the engine and the other for cooling the fuel return from the engine, these should be opened before starting the engine and must be closed after the engine has been shutdown. The electronic injection system located in the engine room should be switched on; the fuse must be checked regularly and must be replaced when damaged. The cooling water pump and the dynamometer switches are located in the control room and these must be switched on at this stage.

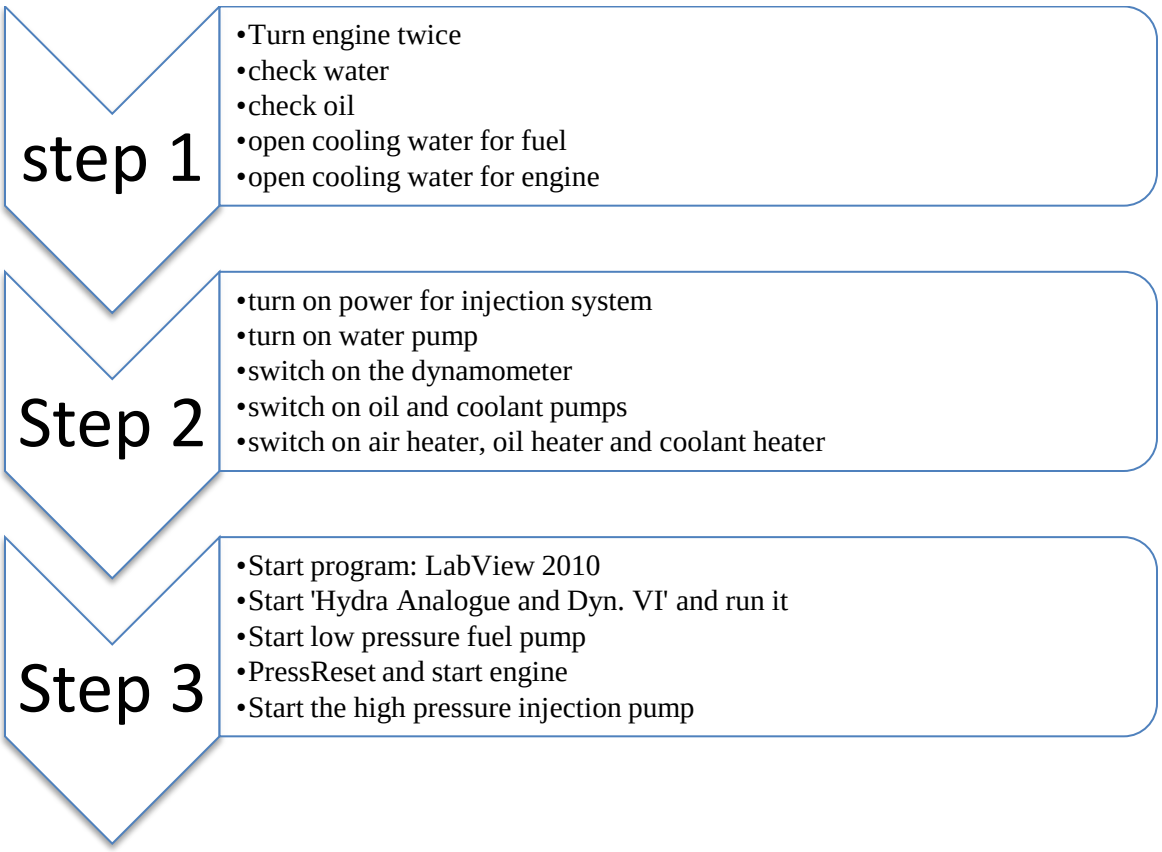


**Figure 21: Flow chart of experimental setup starting sequence**

## *3.7. Test Sequence*

The test sequence follows the ISO Universal test cycle (table 7). The sequence however starts with the eleventh mode descending down to mode one as shown in the flow chart at figure 22. Mode 11 is basically an idle mode set at a speed corresponding to zero power output from the engine. The details of this setting are explained in section 3.4.

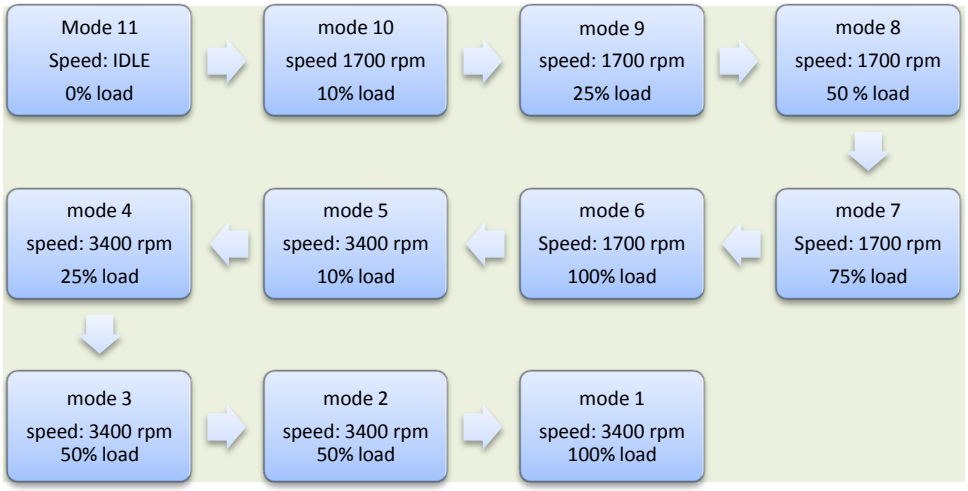


**Figure 22: Flow chart of test sequence**

The speed and loads are of those depicted in the flow chart. The combustion was however optimized for each mode by observing the dynamic pressure diagrams and making manual adjustments on the ignition timing and ID (table 4)

## *3.8. Engine Performance Parameters*

The development of models to study the behaviour of internal combustion engines has long been the focus of engineers. These models which have been developed over time have led to the improvement of performance and reduction of emission thus leading to a better engine design. The practical engine performance of interest are torque, power and specific fuel consumption. The torque depends on the engine's cylinder displacement volume and mean effective pressure which can be expressed as:

$$T = \frac{V_d P_{me}}{4\pi} \tag{14}$$

The power of the engine depends mainly on the effective piston area, mean effective pressure and mean piston speed. The power can be expressed as:

$$P = P_{me} A_p \frac{C_m}{4} \tag{15}$$

The brake mean effective pressure $P_{me}$ can be defined as the ratio of the brake work done ($W_b$) per cycle to the cylinder displacement volume.

$$P_{me} = \frac{W_b}{V_d} \tag{16}$$

Thus for an optimal design engine, the mean effective pressure and mean piston speed are limited by the cylinder inlet flow parameters; flow area limited by naturally aspirated engines and pressure limited by turbocharged engines due to stress limitations of the moving parts. The torque is therefore proportional to the displacement volume and the power to the piston area (Heywood, 1998).

During the experiment the engine speeds, torque, atmospheric pressure, air flow inside the clylinder and fuel consumption are measured. To show how these parameters effect the engine performance, an investigation into the relationship between the engine parameters is necessary. The following relation can be developed for power (Heywood, 1998):

$$P = \frac{\eta_f m_a N h_{LHV} (F/A)}{n_R} \tag{17}$$

For a four stroke engine, we can introduce the volumertic efficiency as follows:

$$P = \frac{\eta_f \eta_v N V_d h_{LHV} \rho_a (F/A)}{2} \tag{18}$$

By dividing the power above by the effective piston area the specific power can be shown for any engine regardless of cylinder size. This is the power per unit piston area shown as:

$$\frac{P}{A_p} = \frac{\eta_f \eta_v N S h_{LHV} \rho_a (F/A)}{2} \tag{19}$$

It is clear from the above equation that the specific power is proportional to the product of mean effective pressure and the mean piston speed as:

$$P_{me} = \eta_f \eta_v h_{LHV} \rho_a (F/A) \tag{20}$$

$$C_m = 2NS \tag{21}$$

The above relationships shows the importance of measuring the atmospheric pressure and engine speed. Parameters such as stroke and piston area are obtainable from the engine specification data while the lower heating values and fuel/air ratio can be extracted and calculated respectively from the fuel properties.

The volumetric efficiency $\eta_v$ of the engine is the ratio of the mass of air supplied through the intake valve during the intake stroke to the mass of air when perfectly filled by the displacement volume under standard atmospheric condition. The volumetric efficiency can be expressed as:

$$\eta_v = \frac{m_a}{\rho_a V_d} \tag{22}$$

Other important performance measurement parameters are explained in detail in section 3.5.1 to 3.5.5.

### *3.8.1. Brake fuel conversion efficiency*

The fuel conversion efficiency is an important criteria for determining how the energy content in the fuel in converted by the engine into useful work. The fuel conversion efficiency is calculated from the formula:

$$\eta_f = \frac{W_c}{m_f h_{LHV}} = \frac{P.n_R}{\left(\dot{m}_f n_R / N\right) h_{LHV}} = \frac{P}{\dot{m}_f h_{LHV}} \tag{23}$$

The work done by the engine in one cycle and absorbed by the dynamometer is the product of the power $P$ and number of crank revolution $n_R$ for each power stroke per cylinder (two for four stroke cycles and one for two stroke cycles).

The specific fuel consumption $(sfc)$, which is a measure of how efficiently the engine is using the fuel supplied to produce useful work, can be related to power as:

$$sfc = \frac{\dot{m}_f}{P} \tag{24}$$

Substituting in the above equation

$$\eta_f = \frac{1}{sfc.h_{LHV}} \tag{25}$$

$$\eta_f = \frac{3600}{sfc[g/KWh].h_{LHV}[MJ/kg]} \tag{26}$$

Since the lower heating value is a constant quantity for an specific fuel (typically between 42 to 44 MJ/kg for commercial hydrocarbon fuels). Thus the fuel conversion efficiency is determined by the specific fuel consumption. The specific fuel consumption is inversely proportional to fuel conversion efficiency, if the specific fuel consumption is high, we should expect lower fuel conversion efficiency. In comparing a number of different fuels with different lower heating values, we will also expect the lower heating value to have an effect on the fuel conversion efficiency.

### *3.8.2. Rate of Heat Released*

The equation of the heat flow can be derived from the first law of thermodynamic

$$dU = mc_v dT = dQ - pdV \tag{27}$$

The gas equation can be written as:

$$\frac{dP}{P}+\frac{dV}{V}=\frac{dT}{T} \tag{28}$$

The differential of temperature can be eliminated by substituting equation 29 into 28 and assuming that the internal energy,

$$U = mc_v T \tag{29}$$

Also considering that:

$$R = C_p - C_v \tag{30}$$

And

$$PV = mRT \tag{31}$$

In developing the heat release model, a single zone combustion defined by the ratios of specific heat of adiabatic index k in equation (32) is usually assumed.

$$\kappa = \frac{C_p}{C_v} \tag{32}$$

In reality, both $C_p$ and $C_v$ are functions of temperature and pressure. However, the values can remain fairly constant with little variations in temperature. Based on this argument, the HRR cure can be divided into three zones. These zones can be referred to as compression, combustion and expansion zones. In the compression zone, κ can be assigned values appropriate to air at the end of air compression

stroke before the onset of combustion; a value of approximately 1.35 has been suggested by (Heywood, 1998). In the combustion zone the most accurate value of κ for analysis rate of heat release analysis which occurs during combustion is not well defined. An estimate of 1.26- 1.3 at an equivalent ratio immediately after combustion has been estimated by (Heywood, 1998). However, for simplicity a uniform zone combustion model can be derived by solving for the differential of the heat Q which yields:

$$dQ = \frac{1}{\kappa - 1}\left[VdP + \kappa PdV\right] \tag{33}$$

Differentiating with respect to the crank angle yields:

$$\frac{dQ}{d\varphi} = \frac{1}{\kappa - 1}\left[V\frac{dP}{d\varphi} + \kappa P\frac{dV}{d\varphi}\right] \tag{34}$$

Knowing the volume function $V = V(\varphi)$ and the pressure function $P = P(\varphi)$ equation (34) defines the net heat flow entering the cylinder. During compression and expansion stroke the heat flow is entirely due to heat transfer, whereas during combustion the net heat flow is the difference between the net energy released by combustion and the heat loss due to heat transfer.

$$\frac{dQ}{d\varphi} = \frac{dQ_{ch}}{d\varphi} - \frac{dQ_{HT}}{d\varphi} \tag{35}$$

The first term on the right hand side is usually called the rate of heat release ROHR. Equation (36) can be used to determine the heat flow during compression

and expansion directly. Basically the gas composition is constant during these events. The composition however, changes during combustion and is different during expansion compared to compression.

Even if the assumption of constant gas composition is violated during combustion, equation (35) is often used for determining the Rate of Heat Release ROHR. The pattern of the ROHR-curve determined by this method will be approximately correct, giving the basis for comparing ROHR-curves of different fuels.

The total heat transferred can be determined by integration of equation (33):

$$Q = \int_{\varphi_0}^{\varphi_1} \frac{dQ}{d\varphi} d\varphi \tag{36}$$

When $\frac{dQ}{d\varphi}$ represent ROHR the total heat transferred corresponds to the total energy released by combustion, which again can be related to the fuel consumption:

$$Q = m_f h_{LHV} \eta_c \tag{37}$$

In diesel engines the combustion efficiency $\eta_c$ is very close to unity. However, accurate values of fuel consumption can be obtained only if accurate value of heat loss is available.

$$m_f = \frac{Q}{h_{LHV} \eta_c} \tag{38}$$

### *3.8.3. Dynamic Cylinder Pressure*

If the rate of heat released and the heat lost are known, the differential of the pressure can be determined from equations (27) and (28) as in the previous section:

$$dP = (\kappa - 1)\frac{1}{V}dQ - \kappa\frac{P}{V}dV \tag{39}$$

Differentiation with respect to crank angle:

$$\frac{dP}{d\varphi} = (\kappa - 1)\frac{1}{V}\frac{dQ}{d\varphi} - \kappa\frac{P}{V}\frac{dV}{d\varphi} \tag{40}$$

This differential equation determines the pressure function $P = P(\varphi)$ when the net heat $Q = Q(\varphi)$ and the volume function $V = V(\varphi)$ are known along with their derivatives. The solution can be found by numerical integration, step by step, starting from an assumed initial state, for example at the beginning of compression.

Equation (40) determines the pressure when the ROHR and the heat loss are known. The solution will depend on, among other parameters, the timing of ignition (start of combustion), the shape of the ROHR function, the duration of combustion, and the total energy released during combustion. Variation of these factors will

have impact on cylinder pressure and thereby also on indicated work and thermal efficiency.

Based on computed cylinder pressure the temperature can be found using the gas equation. If needed, the derivative of temperature may be determined by means of equation (28).

The equations defining the net heat flow, equation (34) and the cylinder pressure, equation (40) are both based on the assumption that the combustion gases have ideal gas properties and the heat capacities may be a function of temperature:

$$C_p = C_p(T) \tag{41}$$

$$C_v = C_v(T) \tag{42}$$

When using ideal gas properties the corresponding values of pressure, temperature and volume will be realistic, and far better than for computations based on perfect gas data.

The main limitations of the closed system dynamic state equations are related to the assumption of fixed gas composition. These limitations can be lifted by taking mass flow into and out of the system into account, and allowing the gas composition to change during combustion and during the gas exchange process.

### 3.8.4. The cylinder volume function

The compression ratio is defined by equation 7.

The connecting rod to crank ratio is defined by:

$$\lambda = \frac{l}{a} \tag{43}$$

The relation between the piston stroke and the crank angle is defined by equation 43.

$$S = 2a \tag{44}$$

The cylinder volume (Heywood, 1998) at any crank angle is given by

$$V_d = V_c + \frac{\pi B^2}{4}\left[l + a - s\right] \tag{45}$$

Where s is the intanteneous distance between the crank axis and the piston pin axis which can be further expresssed by

$$s = a\cos\varphi + \sqrt{\left[l^2 - a^2\sin^2\varphi\right]} \tag{46}$$

Combining equations (45) and (46) the cylinder volume can be computed as a function of crank angle from the equation (47) provided that the crank mechanism is rigid.

$$V_c(\varphi) = V_d \left\{ \frac{1}{\varepsilon - 1} + \frac{1}{2}\left[ 1 - \cos\varphi + \left( 1/\lambda \right)\left( 1 - \sqrt{1 - (\lambda \sin\varphi)^2} \right) \right] \right\} \quad (47)$$

This equation defines the clearance volume at any crank angle. This variation for a four stroke engine as the it goes through its two cycles is shown in appendix D.

The derivative of the volume with respect to crank angle $\frac{dV}{d\varphi}$ is found by differentiating the clearance volume function. The resulting differentiating equation shown below defines the rate of change of cylinder volume with respect to crank angle.

$$\frac{dV_c}{d\varphi} = \frac{V_d}{2}\left[ \sin\varphi + \frac{\lambda \sin 2\varphi}{2\sqrt{1 - (\lambda \sin\varphi)^2}} \right] \quad (48)$$

### *3.8.5. Exhaust emission measurement*

The formation of $NO_x$ in internal combustion engines is well documented in literature. Nitric oxide (NO) and nitrogen dioxide are collectively referred to as oxides of nitrogen ($NO_x$). NO, however, is predominantly produced in the cylinder of internal combustion engines. The main source of NO is the oxidation of nitrogen present in the atmosphere and combustion fuels where the fuel contains a significant amount of nitrogen. The formation rate is primarily a function of temperature and residence time at that temperature during the combustion process. At high temperatures, usually above 1600°C, nitrogen ($N_2$) and oxygen ($O_2$) in the combustion air disassociate into their atomic states and participate in a series of

reactions forming $NO$. It is accepted this formation is through the extended Zeldovich mechanism:

$$N_2 + O \rightarrow NO + N \quad (49)$$

$$N + O_2 \rightarrow NO + O \quad (50)$$

$$N + OH \rightarrow NO + H \quad (51)$$

(Heywood, 1998) Has shown that the initial NO formation rate can be formulated as shown in the equation below. This initial formation rate reaches its maximum at stoichiometric fuel/air equivalent ratio and decreases rapidly as the fuel/air equivalent ratio becomes richer or leaner.

$$\frac{d[NO]}{dt} = \frac{6\times10^{16}}{T^{1/2}} \exp\left(-\frac{69.090}{T}\right)[O_2]_e^{1/2}[N_2]_e \quad (52)$$

Where d[NO]/dt is the rate of NO formation, T is the temperature at which NO formation occurs, $[O]_e$ and $[N_2]_e$ are the equilibrium concentrations of oxygen and nitrogen dioxide. It is evident from the above equation that the formation rate is strongly dependent on the exponential term. High combustion temperature and high oxygen concentrations will yield high rate of NO formation. The rate of NO formation has been found to occur during the ignition delay period. During this time period, the fuel vaporizes, mixes with hot air which causes additional heating at stoichiometric conditions. During this evolution, the only area of sufficient

temperature and oxygen availability necessary for substantial kinetic NO formation is found at the flame front (DJ Timoney et al, 2005).

The characteristic time for this process can be written as

$$\tau_{NO}^{-1} = \frac{1}{[NO]_e}\frac{d[NO]}{dt} \tag{53}$$

From the reaction of oxygen ($O_2$) and nitrogen ($N_2$)

$$O_2 + N_2 \rightarrow 2NO \tag{54}$$

And considering the NO equilibrium concentration $[NO]_e$,

$$[NO]_e = (K_{NO}[O_2]_e[N_2]_e)^{1/2} \tag{55}$$

$$K_{NO} = 20.3 \times e^{-\left(\frac{21{,}650}{T}\right)} \tag{56}$$

The characteristic time for NO formation can be written as

$$\tau_{NO} = \frac{8\times10^{-16} T \exp\left(58{,}300/T\right)}{P^{1/2}} \tag{57}$$

Where the unit of $\tau_{NO}$ is given in seconds, T is given in Kelvin and P is given in atmospheres.

# Chapter four: Statistical Analysis of preliminary data

## *4.1. Analysis of Variance and Repeatability*

The quality of data is assessed by Analysis of Variance (ANOVA) which is a known statistical method. This is a good method for determining if there are significant differences for the twelve different trials of the in-cylinder pressures and performance data of the nine trials. The name "analysis of variance" is based on the manner in which the procedure uses variances to determine whether the means are significantly different. The procedure works by comparing the variance between group means versus the variance within groups as a method of determining whether the groups are all part of one larger population or separate populations with different characteristics. To use this method of analysis, we must set up two hypotheses; a null hypothesis which states that all population means (factor level means) are equal while the alternative hypothesis states that at least one is different:

$H_0 : \mu_1 = \mu_2 = ..... = \mu_k;$

$H\backslash$: At least two of the means are not equal.

$\alpha = 0.05$

Using these two hypotheses, we can model the correlation between the response variables and the different independent variables to be investigated. During the analysis in MINITAB the different measured data are entered in different columns

(unstacked). MINITAB allows multiple comparison methods for the mean and different error rates such as the Fisher's method and Turkey's method. However, during this analysis emphasis was put on the Turkey's method because this allows us to use family error rates (experiment wise) instead of individual error rates. The Turkey's family error rate is usually estimated between 0.001 and 0.5. The error rate used for this analysis is 0.05 and based on this error rate we can determine from the resulting p-value if our result is significantly different from the one observed. If the p-value is less than the confidence level, then it can be concluded that at least one measured data value mean is different.

Hsu's MCB, family error rate estimates confidence interval for the difference between each level mean and the best of the other level means. This method uses a family error rate sometimes referred to as family wise error rate to control what is referred to as "type 1" error, which basically means assuming a difference exist when it does not in fact exist. Confidence intervals which usually lie between a family error rate of 0.001 and 0.5 are usually used to assess if the means are different. For this analysis an error rate of 0.05 was used. If an interval has zero as an end point, it can be concluded that there is a statistically significant difference between the corresponding means. If on the other hand the interval does not have zero as an end point, the difference between means is not statistically significant.

The individual value plot and boxplot helps to visualize the central tendency, variation, and distribution of data. The residual plots give important information by which we can check the reliability of the test's assumptions. The plots tell us at a glance if we can trust the test results.

The three-in-one residual plot displays three different residual plots together in one graph window. This layout is very useful for comparing the plots to determine whether the model meets the assumptions of the analysis. The residual plots in the graph include:

- Histogram tells us the number of times a certain value occurs in the distribution. It therefore gives a good indicates whether the data are skewed or outliers exist in the data.
- Normal probability plot indicates whether the data are normally distributed, other variables are influencing the response, or outliers exist in the data
- Residuals versus fitted values indicates whether the variance is constant, a nonlinear relationship exists, or outliers exist in the data

The results of the ANOVA are shown as follows:

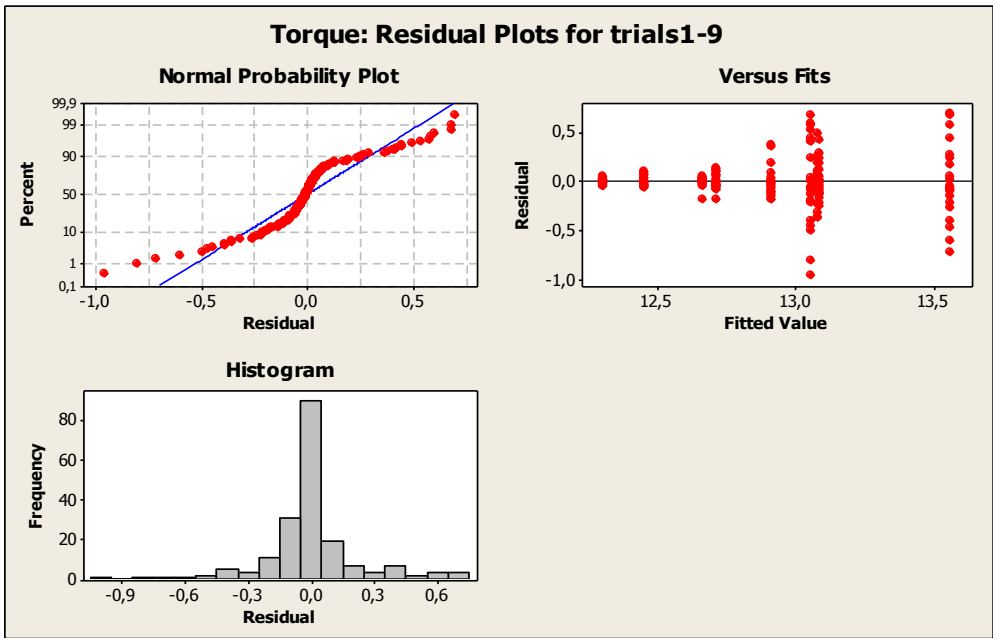


Figure 23: Statistical analysis of torque measurement error at part load

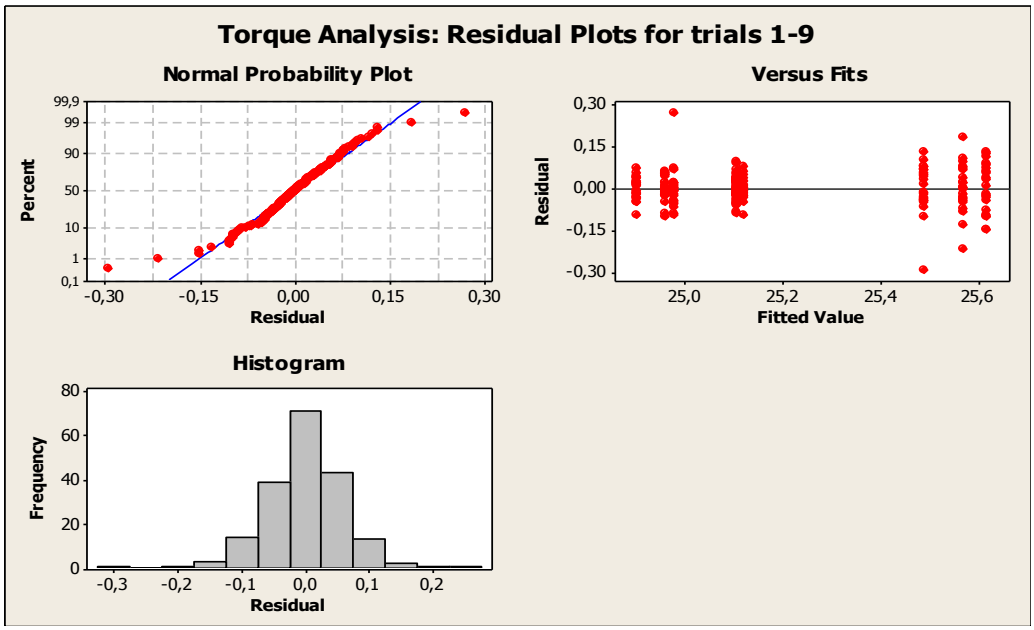


Figure 24: Statistical analysis of torque measurement error at full load

From figure 24 it is evident that the engine more stable at high load than at part load. The torque measurement at full load follows a fairly straight line in the normal probability plot with only a few outliers while exhibiting more deviations at part load (figure 23). In the residuals versus the fitted value plots, the errors have a constant variance at full load while the residuals increases with the fitted values indicating that the errors may not have a constant variance. Also in the frequency versus the residual at full load the errors are equally distributed at either sides of the histogram showing a fairly good stability while at low load they seems to be randomly distributed between -0.9 to 0.6 Nm. Though this variation is between 5 to 7% of the mean value but it is a clear indication of the instability of the engine at

part load. At full load the error ranges from -0.3 to 0.2 Nm with a mean torque of 25.2 Nm with a standard deviation of 0.28 Nm (figure 13).

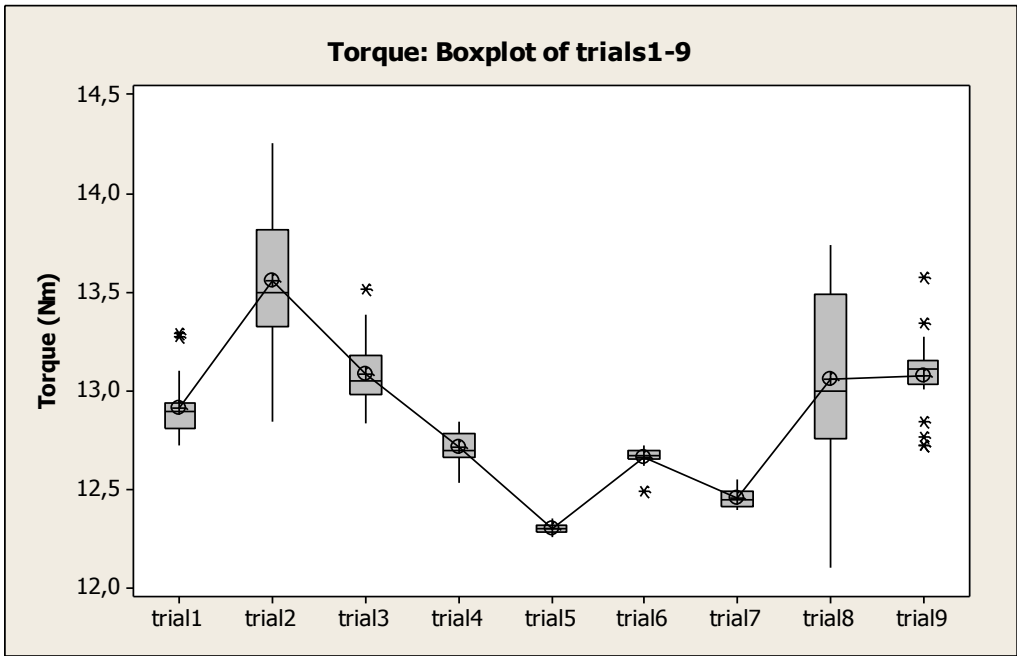


Figure 25: Boxplot of torque for nine trials at part load

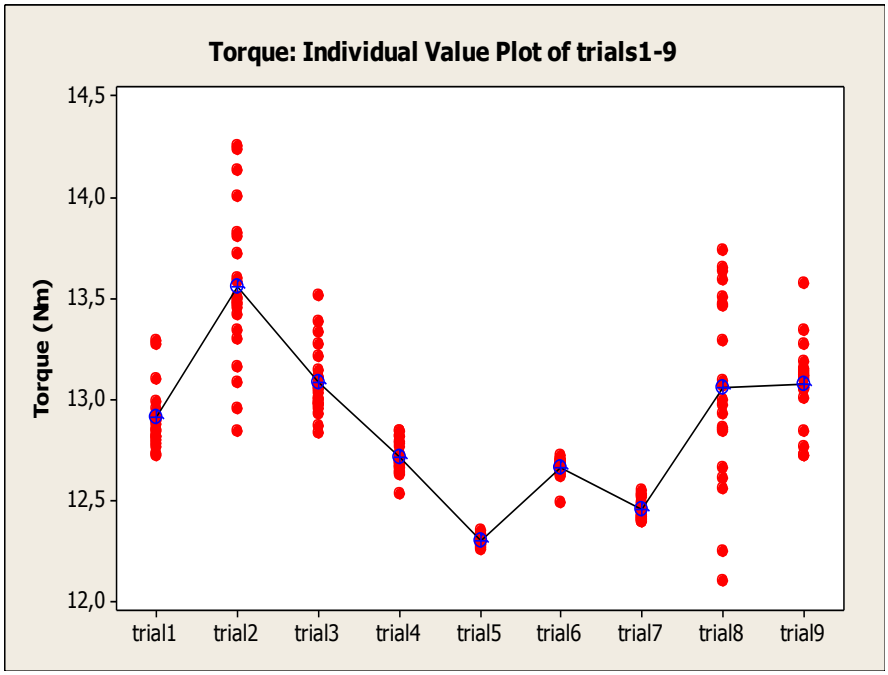


**Figure 26: Individual value plot of torque for nine trials at part load**

The boxplot (figure 25) and the individual value plot (figure 26) of torque at part load reveal a very disturbing data. The variations of the set of data do not follow any pattern. Trial 2 and 8 exhibits a larger variability than the rest of the trials but contain no outliers. However, the position of the median is significantly different from the mean and suggests that the data is skewed. This suggests that the variance in the errors term is not constant and therefore the measurement is not reliable. Furthermore, the evidence of outliers and skewness of the data suggest instability of the engine at part load or inconsistency in the measurement system.

| Trials | Mean Torque | Mean Atmospheric pressure |
|---|---|---|
| Trial 1-3 | 13,19 | 1.01227 |
| Trial 4-6 | 12,56 | 0.99089 |
| Trial 7-9 | 12,86 | 0.99731 |

**Table 11: Factor of analysis for torque showing correlation with atmospheric pressure**

The effect of atmospheric pressure on the brake torque of the engine is not readily apparent. By performing a factor of analysis as outlined in table 11, the mean torque is found to vary with atmospheric pressure according to table 11.

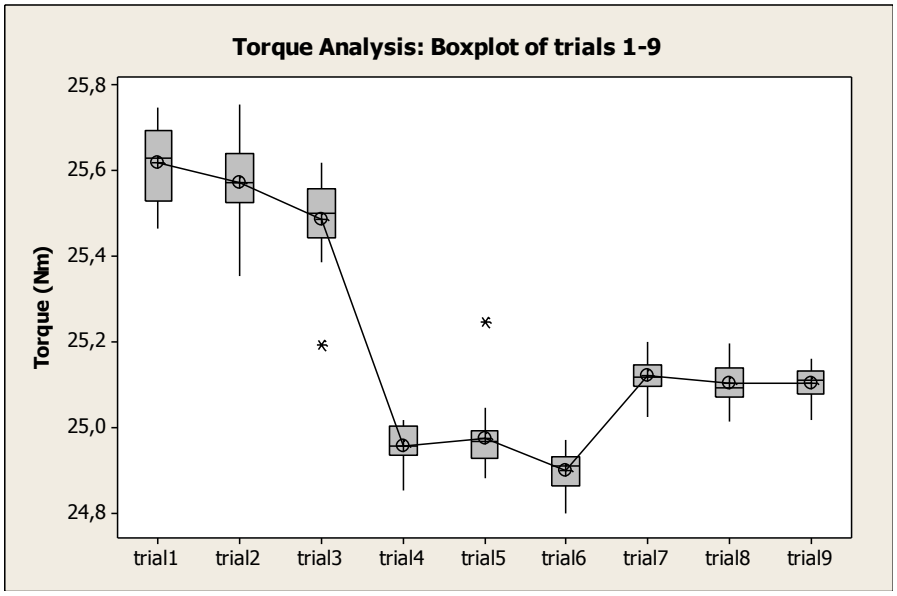


**Figure 27: Boxplot of Torque for nine trials at full load**

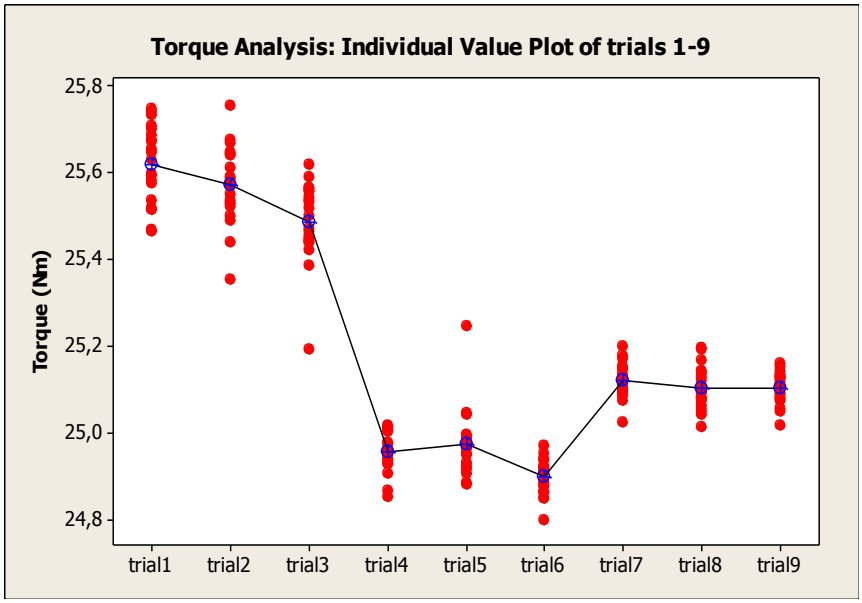


**Figure 28: Individual value plot of torque at full load**

Figure 28 and 29 shows the boxplot and the individual value plot of torque measurement at full. It is readily evident in the two figures that the variations of the set of data follow some specific pattern. All the individual data set seems to exhibit very small variances and the majority of the individual data set contain no outliers except data set in trials 3 and 5 each of which contain only a single outlier. From the Boxplot, the position of the median is not significantly different from the mean suggesting equal distribution of the error term on either side of the mean. Based on this plot, in seven out of the nine trials the residuals appear to be randomly scattered about zero. No evidence of non-constant variance, missing terms, or outliers exists in the majority of the data. By performing a factor of analysis; it is evident from the two plots that the variation of the data set is mainly as a result of effect of variation in atmospheric pressure.

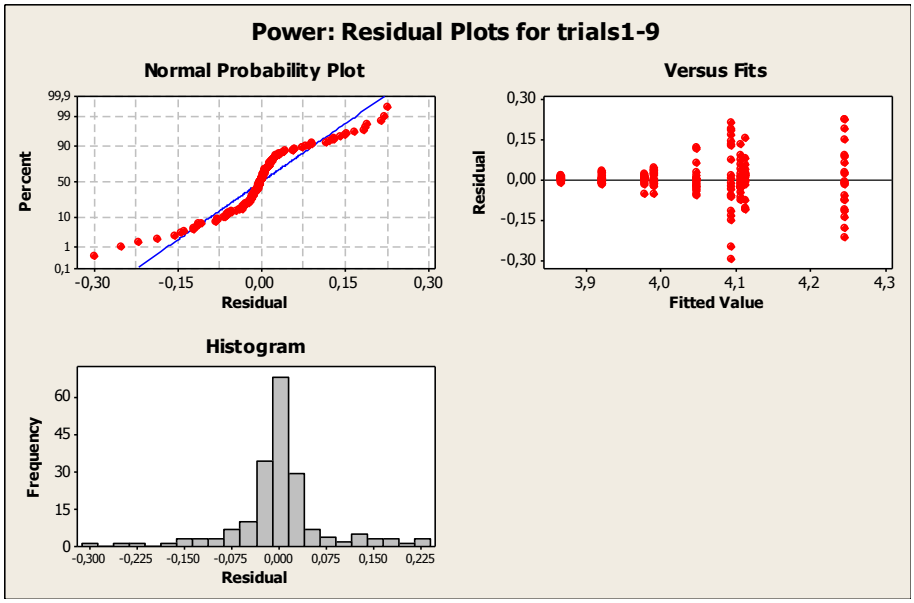


Figure 29: Statistical analysis of the error in power measurement at part load

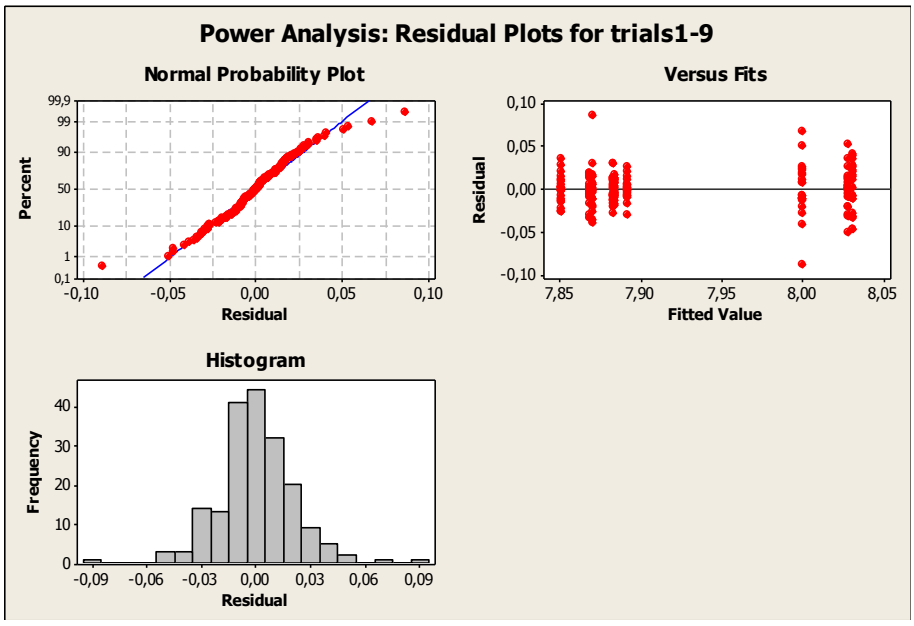


Figure 30: Statistical analysis of the error in power measurement at full load

The error analysis of power measurement seems to follow the same trend as the torque measurement with the error ranging from -0.3 to 0.225 at part load (figure 30) and -0.09 to 0.09 at full load (figure 31). The mean measured power at part load is 4.04KW with a standard deviation of 0.13 and 7.92KW with a standard deviation of 0.08 (table 13).

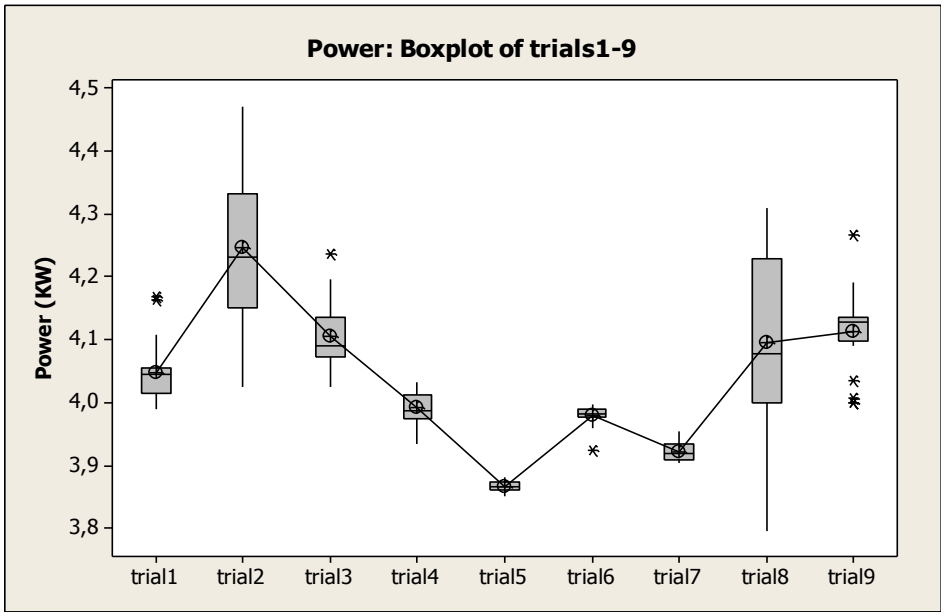


**Figure 31: Boxplot of power for nine different trials at part load**

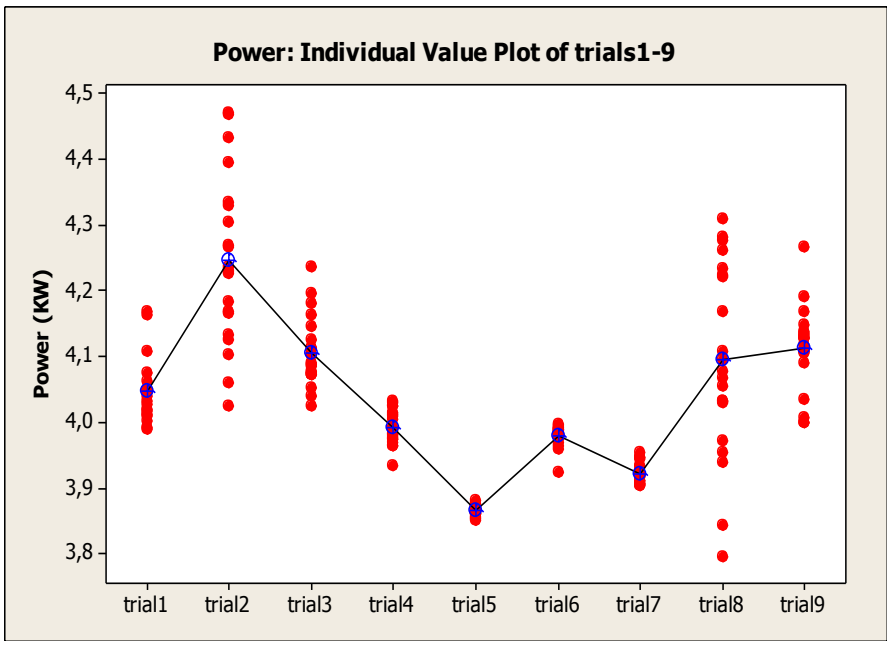


**Figure 32: Individual value plot of nine different trials at part load**

The boxplot (figure 32) and the individual value plot (figure 33) of power at part load also reveal a very inconsistent data. The variations of the set of data do not follow any pattern. The presence of a number of outliers in trials 1, 3, 6 and 9 suggest inconsistency in the data set. Trial 2 and 8 exhibits a larger variability than the rest of the trials but contain no outliers. However, the position of the median is significantly different from the mean and suggests that the data is skewed. This suggests that the variance in the errors term is not constant and therefore the measurement is not reliable. Furthermore, the evidence of outliers and skewness of the data suggest instability of the engine at part load of inconsistency in the measurement system.

| Trials | Mean Power | Mean Atmospheric pressure |
|---|---|---|
| Trial 1-3 | 13,19 | 1.01227 |
| Trial 4-6 | 12,56 | 0.99089 |
| Trial 7-9 | 12,86 | 0.99731 |

**Table 12: Factor of analysis for power showing correlation with atmospheric pressure**

The effect of atmospheric pressure on the brake power of the engine is not readily apparent. By performing a factor of analysis as outlined in table 12, the mean power is found to vary with atmospheric pressure according to table 12. This seems to suggest that the random nature data set are not only affected by the inconsistency in the measurement but also are affected by the atmospheric conditions.

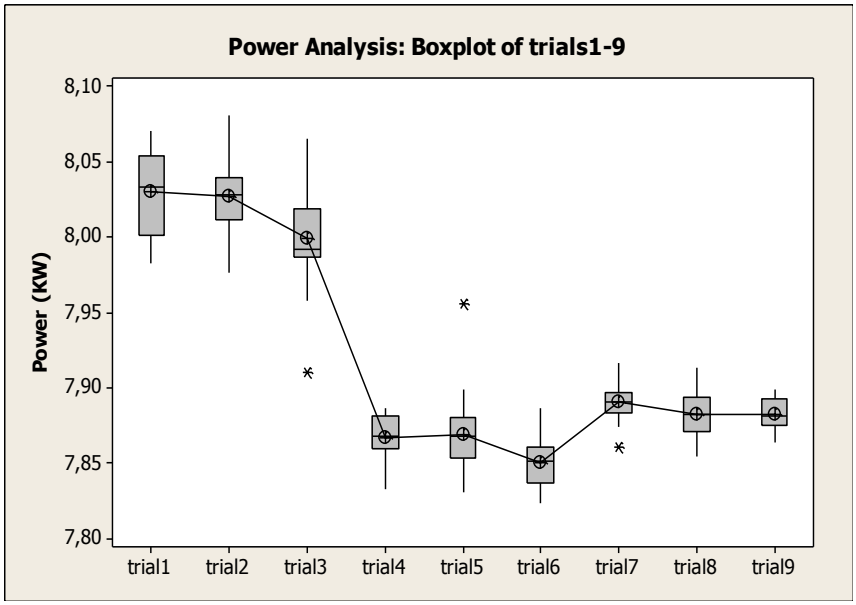


Figure 33: Boxplot of nine different trials at full load

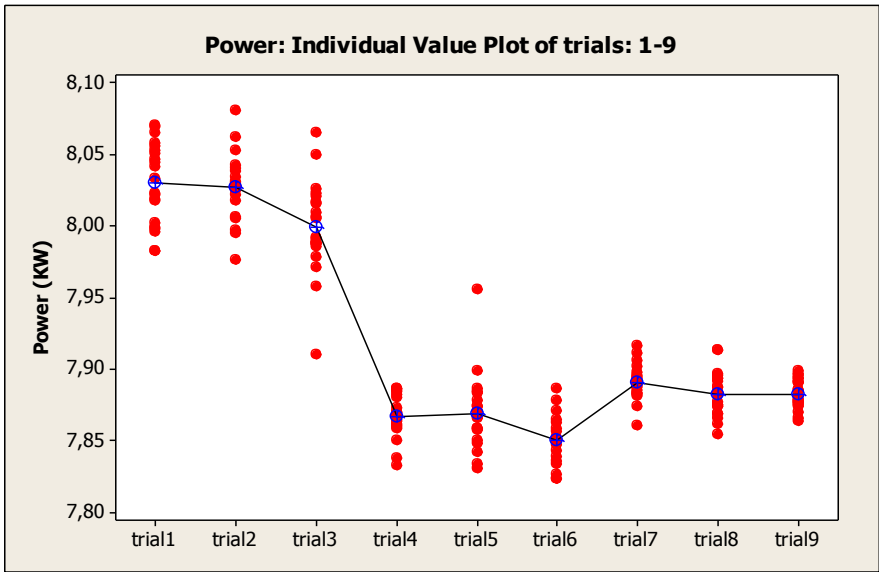


Figure 34: Individual value plot of nine different trials full load

Figure 33 and 34 shows the boxplot and the individual value plot of power measurement at maximum load. It is readily evident in the two figures that the variations of the set of data follow some specific pattern. All the individual data set seems to exhibit very small variances and the majority of the individual data set contain no outliers except data sets in trials 3, 5 and 7 each of which contain only a single outlier. From the Boxplot, the position of the median is not significantly different from the mean suggesting equal distribution of the error term on either side of the mean. Based on this plot, in seven out of the nine trials the residuals appear to be randomly scattered about zero. No evidence of non-constant variance, missing terms, or outliers exists in the majority of the data. By performing a factor of analysis; it is evident from the two plots that the variation of the data set is mainly as a result of effect of variation in atmospheric pressure.

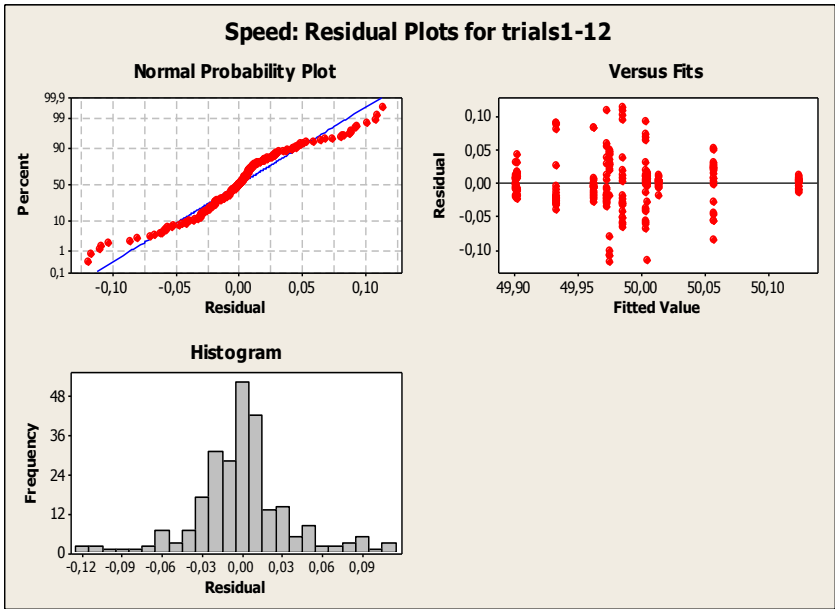


**Figure 35: Residual plots of speed measurement for 12 different trials**

Figure 35 shows the residual plots of speed measurement taken at 12 different engine trials. The analysis showed the error ranging from -0.12 to 0.9 with a mean speed of 2999 rpm and a standard deviation of 0.07 rpm.

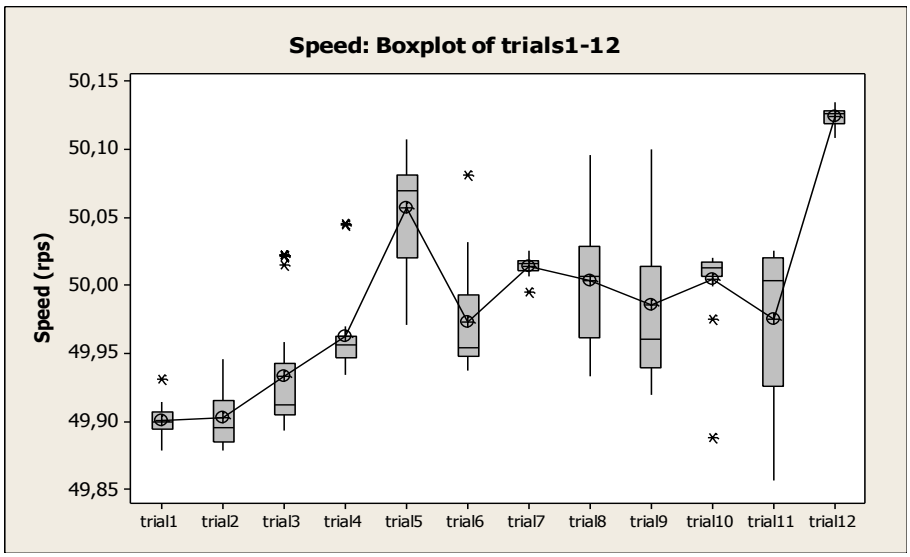


**Figure 36: Boxplot of speed measurement for 12 trials**

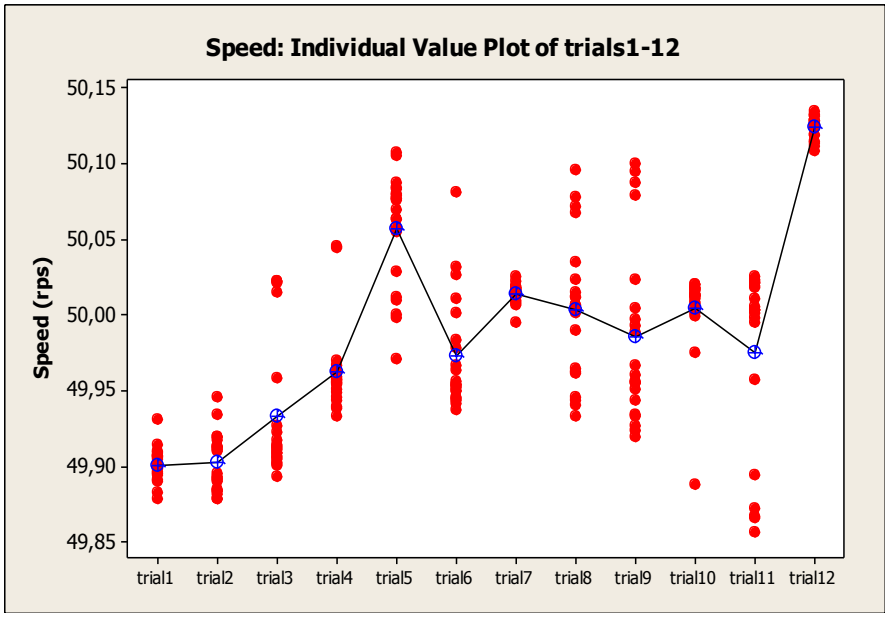


**Figure 37: Individual value plots of speed measurement with 12 different trials**

Figure 36 and 37 show box plot and individual value plots of speed measurement respective. The box shows limited spread in the data but also highlighted evidence of the existence of outliers in the data. The existences of outliers are also evident in the individual value plots with trial 12 exhibiting a higher precision than the rest of the data sets. There is also less spread in trials 2, 7 and 10 but all show some evidence of the existence of outliers. This can be as a result of transient behavior of the engine especially during load change.

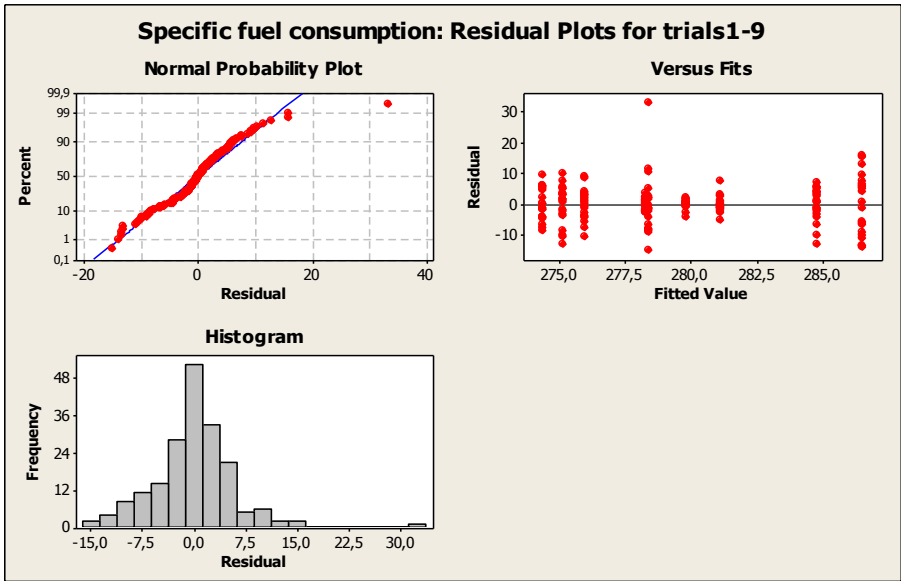


Figure 38: Residual plots of specific fuel consumption measurement of nine trials at full load

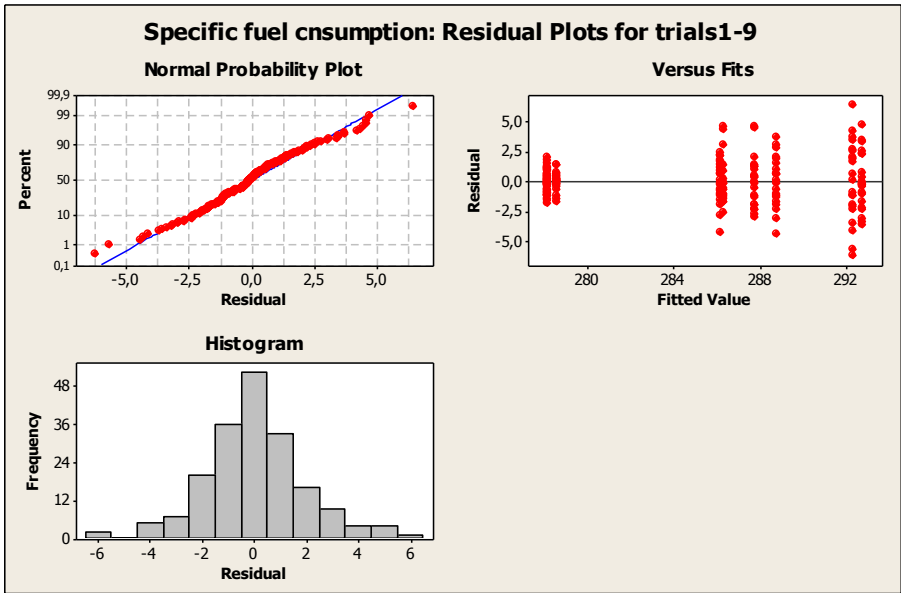


Figure 39: Residual plots of specific fuel consumption measurement of nine trials at full load

The normal probability plots of specific fuel consumption measurements at full as well as part load follows a fairly straight line apart from a single outlier in part load (figure 38) and a few outliers in the full load (figure 39). These outliers in the part load measurement could be as a result of surge during load changes. In the residuals versus the fitted value plots, the residuals are more randomly scattered about zero for the part load then the full load. In the full load the residuals seems to be increasing with the values and as a results the errors may not have a constant variance. However, in the frequency versus the residual at full load the errors are equally distributed at either sides of the histogram showing despite the errors in the measurement, the engine still sustain a good stability characteristics at full load. At part load there seems to be a good stability with the error ranging from -0.15 to 0.15 g/KWh with a mean BSFC of 279.39 g/KWh and a standard deviation of 6.76 g/KWh. The fuel consumption may not be stable in the part load but the variations in measurements from the mean are less than the full load.

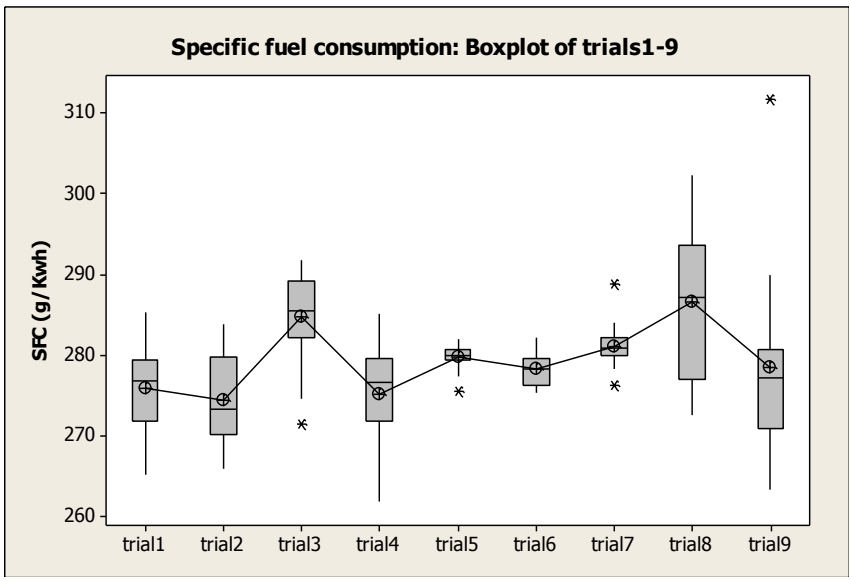


**Figure 40: Boxplot of specific fuel consumption of nine trials at part load**

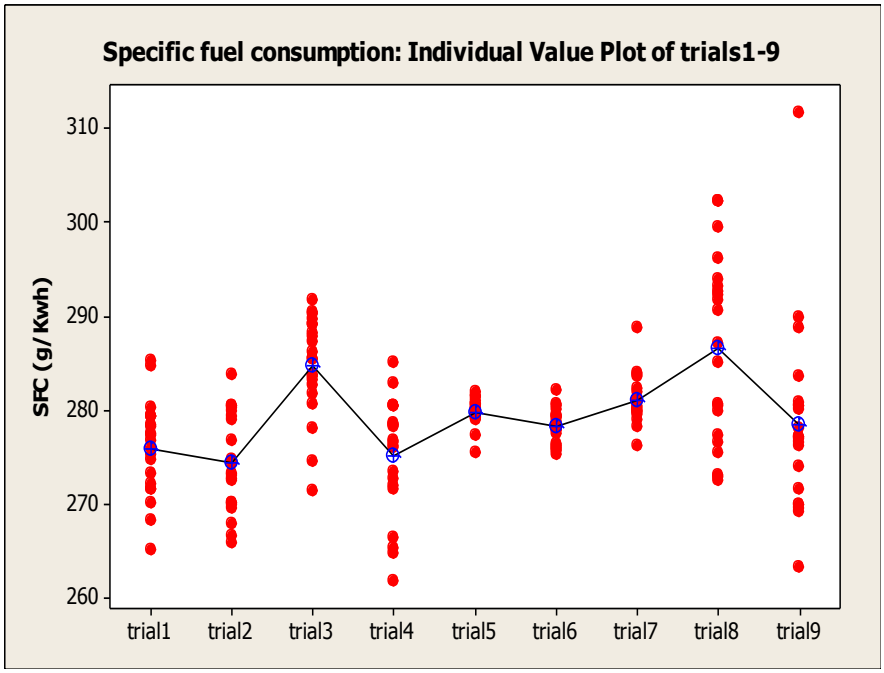


**Figure 41: Individual value plot of nine trials of specific fuel consumption measurement at part load**

Figures 40 and 41 show the Boxplot and individual value plot of nine trials of measurement of specific fuel consumption at part load. The variations of the individual data set do not follow any specific pattern. All the data set exhibit large variability except trials 5, 6 and 7 which are seems to be within acceptable limits. Outliers are found in trials 3, 5, 7 and 9. The offset of the outlier in data set 9 indicates that it may be an unidentified variable. The position of the median is significantly different from the mean in some of the data sets suggesting that some of the data sets are skewed. This suggests that the variances in the errors terms are not constant and this is an evidence of inconsistent measurement and cannot be relied upon. Furthermore, the evidence of outliers and skewness of the data suggest instability of the fuel consumption at part load or inconsistency in the fuel

measurement system. I will therefore conclude that the full consumption on part load cannot be relied upon.

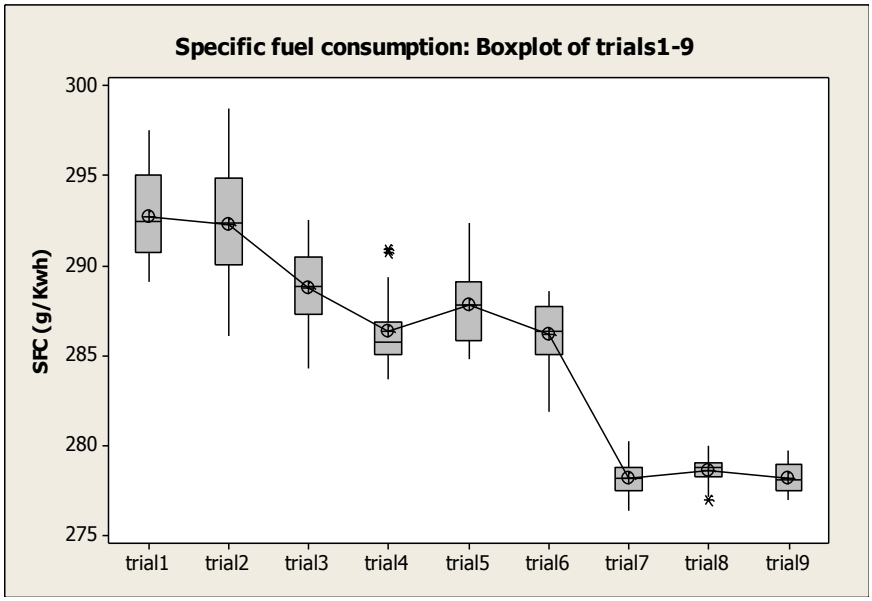


Figure 42: Boxplot of specific fuel consumption of nine trials at full load

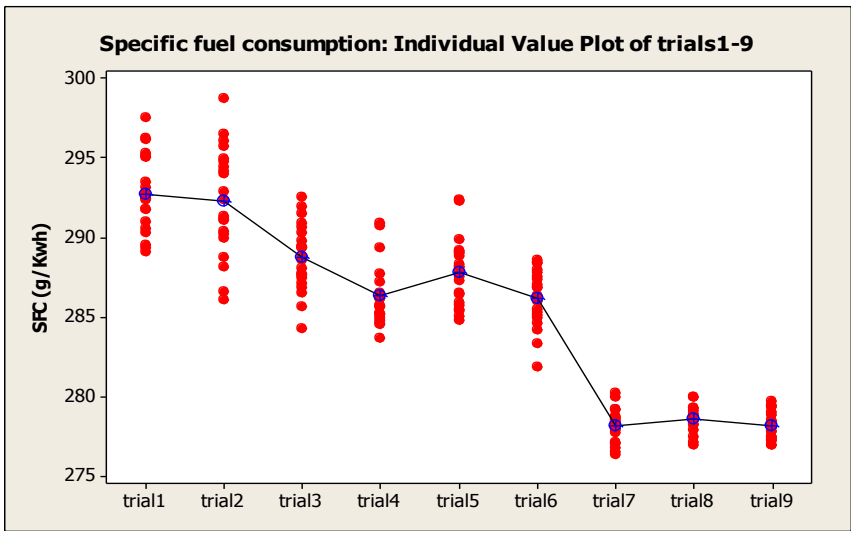


Figure 43: Individual value plots of nine trials at full load

Figure 42 and 43 shows the boxplot and the individual value plot of power measurement at maximum load. It is readily evident in the two figures that the variations of the set of data follow some specific pattern. All the individual data set seems to exhibit very small variances and the majority of the individual data set contain no outliers except data sets in trials 3, 5 and 7 each of which contain only a single outlier. From the Boxplot, the position of the median is not significantly different from the mean suggesting equal distribution of the error term on either side of the mean. Based on this plot, in seven out of the nine trials the residuals appear to be randomly scattered about zero. No evidence of non-constant variance, missing terms, or outliers exists in the majority of the data. By performing a factor of analysis; it is evident from the two plots that the variation of the data set is mainly as a result of effect of variation in atmospheric pressure.

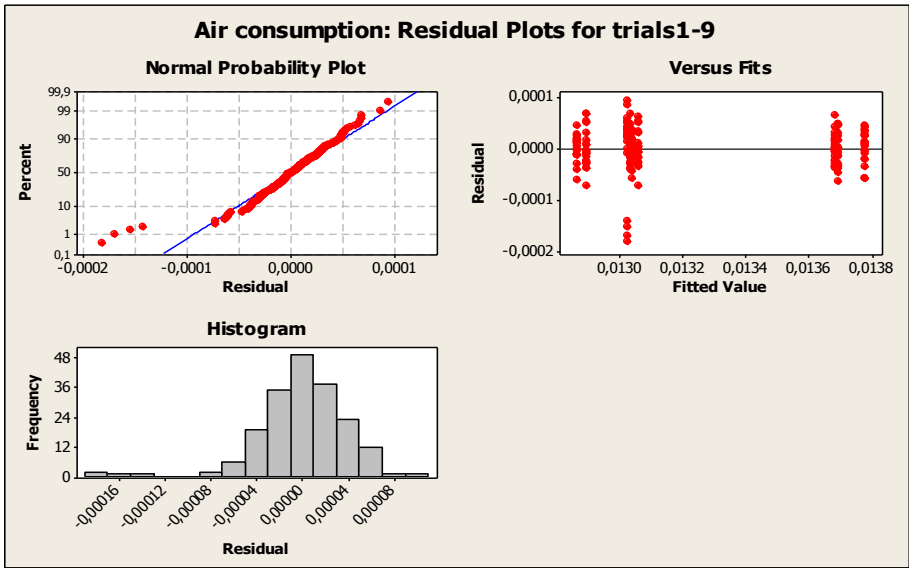


**Figure 44: Residual plots of air consumption measurement of nine trials at part load**

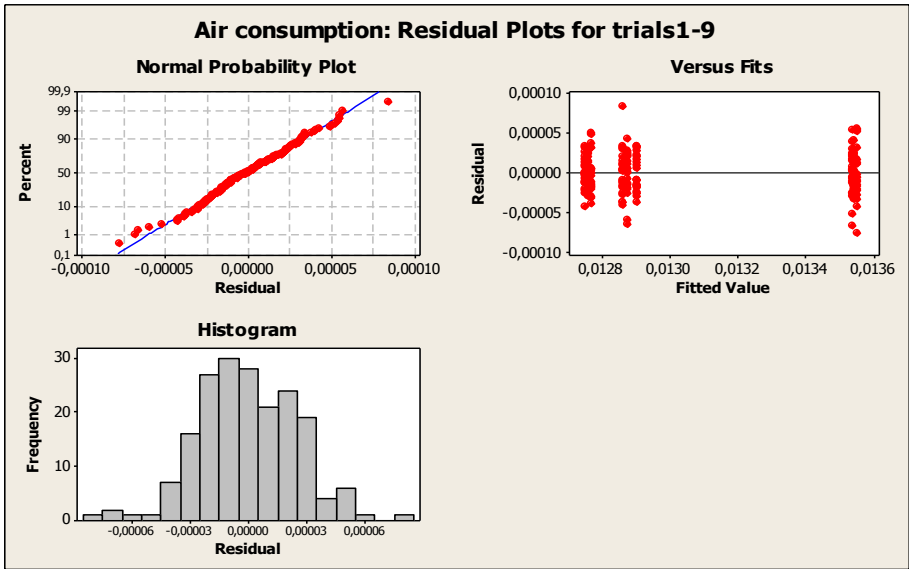


Figure 45: Residual plots of air consumption measurement of nine trials at full load

The normal probability plots of air consumption measurements at part load as well as full load follow a fairly straight line. However, the measurements at part load (figure 44) seem to exhibit some serious outliers which also seem to show at full load (figure 45) but with a less pronounced scale. This seems to suggest that the indicated error is an inherent one and the source of the error may come from the measurement system. However, I cannot make this conclusion base on this initial experiment; a more detailed investigation will be required. In the residuals versus the fitted value plots, the residuals are randomly scattered about zero for both the part load then the full load. In the frequency versus the residual at full load the errors are equally distributed at either sides of the histogram showing despite the errors in the measurement, the engine still sustain a good stability characteristics at both full load and part load. At part load there seems to be a good stability with the error ranging from -0.00008 to 0.00008 kg/s but also exhibits some evidence of

skewness. The histogram of the residual at full load indicates variable air flow and lack of stability in air consumption at full load

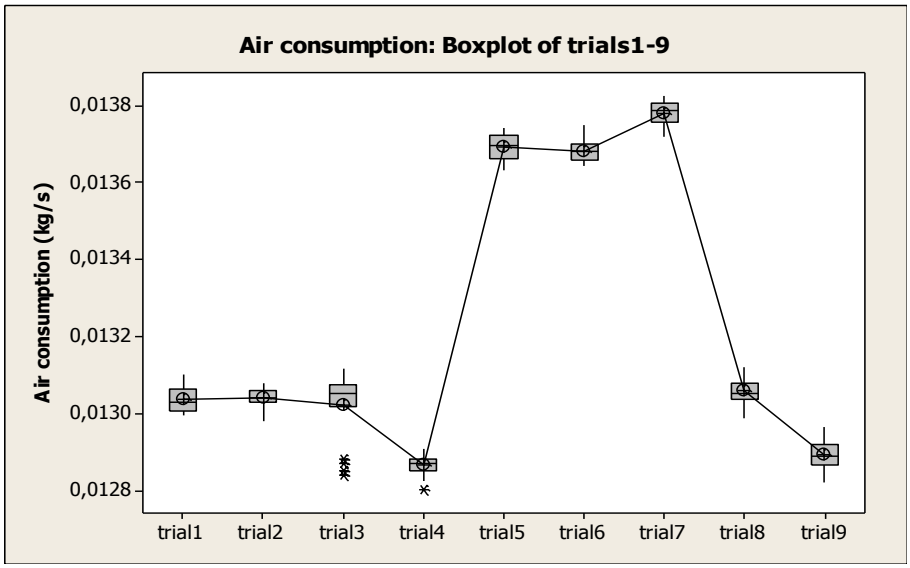


Figure 46: Box plot of air consumption of nice trials at part load

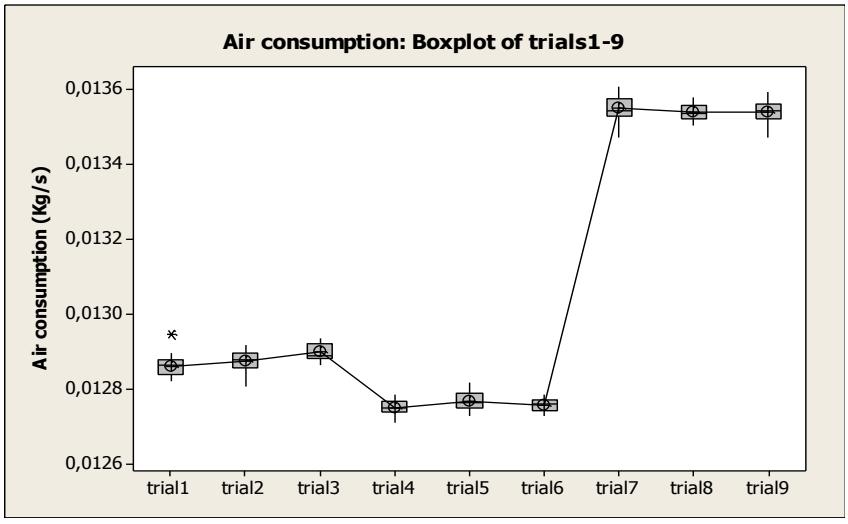


Figure 47: Box plot of individual trials of air consumption of nine trials at full load

Figure 46 and 47 shows the Boxplot of air consumption at part load and full load respectively. From both boxplots it is evident the air consumption is stable at both part and full load. The effect of atmospheric pressure on the both curves is apparent. The air is determined by the volumetric efficiency of the engine. the volumetric efficiency increases with the engine speed and as a result it is more stable at full load then at part load. Few outliers exist in the trial 3 of part load and trial 1 of full load. The variances are small in both cases showing evidence of precision of measurements.

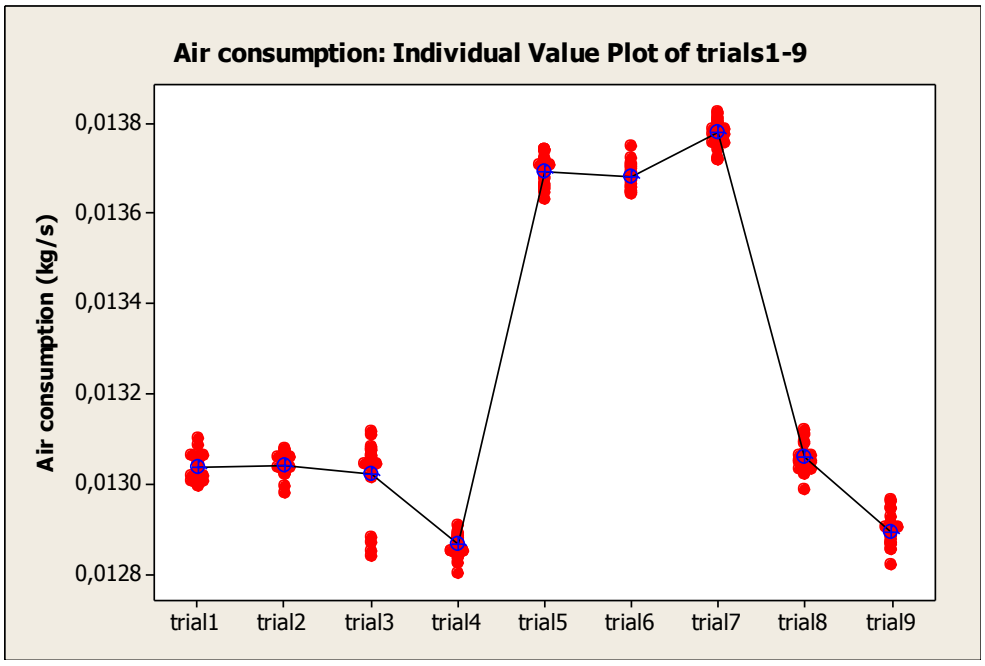


**Figure 48: Individual value plot of air consumption of nine trials at full load**

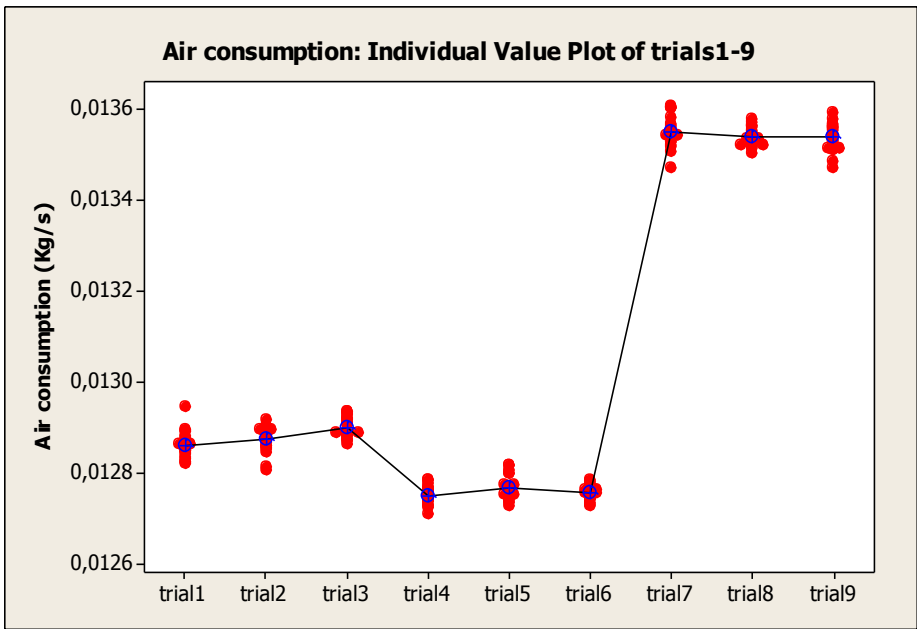


**Figure 49: Individual value plot of air consumption of nine trials at full load**

Figure 48 and 49 shows the individual value plot of air consumption at part load and full load respectively. From both plots it became evident that the air consumption is stable at both part and full load. The effect of atmospheric pressure on the both curves is apparent. The individual value plots show little variations with the data set of each trial showing evidence of consistency of measurement. By performing a factor of analysis, the variation can further be reduced.

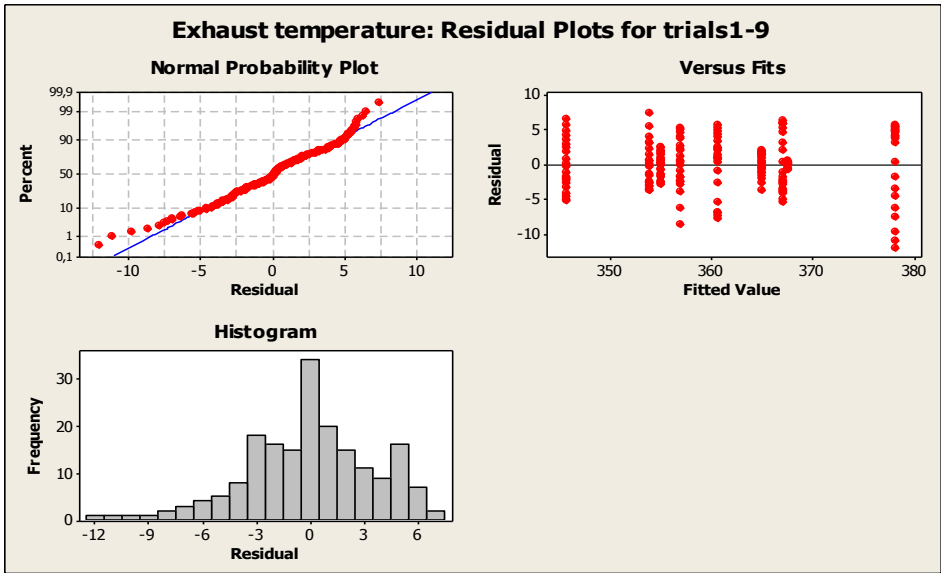


Figure 50: Residual plot of exhaust temperature for nice trials at part load and 3000rpm

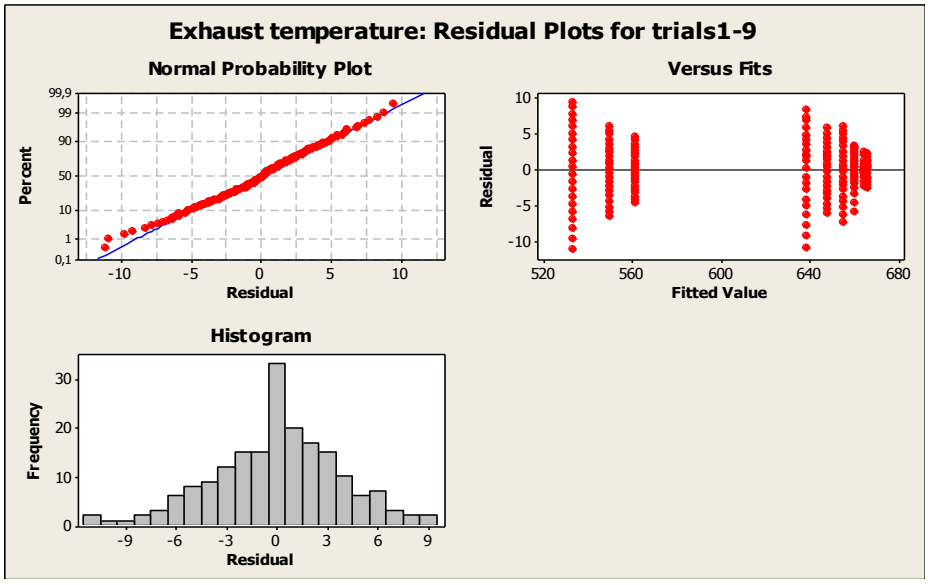


Figure 51: Residual plot of exhaust temperature for nice trials at full load and 3000rpm

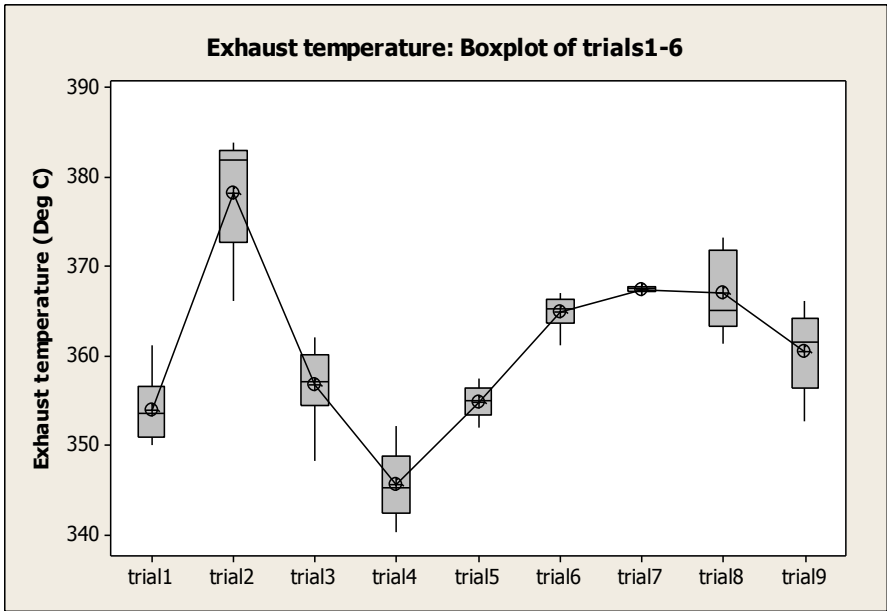


Figure 52: Box plot of exhaust temperature for nice trials at full load and 3000rpm

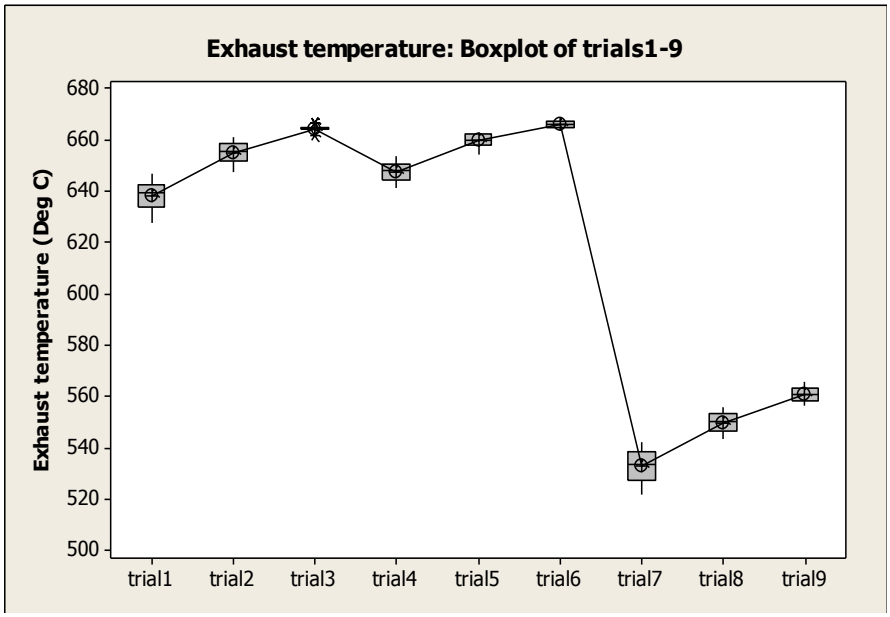


Figure 53: Box plot of exhaust temperature for nice trials at full load and 3000rpm

Figure 52 and 53 the boxplots show the of exhaust temperature at part load (figure 52) and full load (figure 53) for several trails. The measurements at full load exhibit a more consistent data with less variation. The part plot exhibit more variations and does not seems to follow any particular pattern.

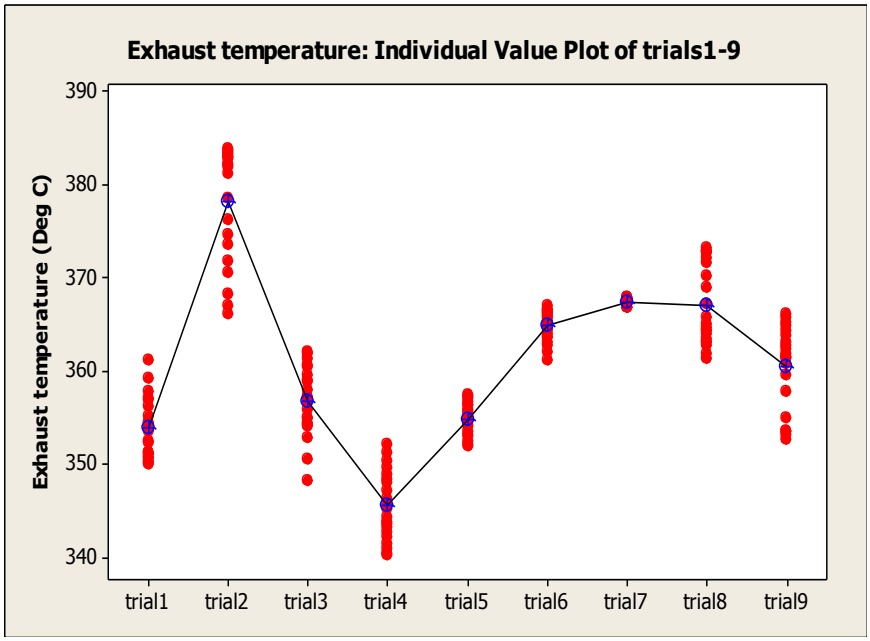


**Figure 54: Individual value plot of exhaust temperature for nice trials at full load and 3000rpm**

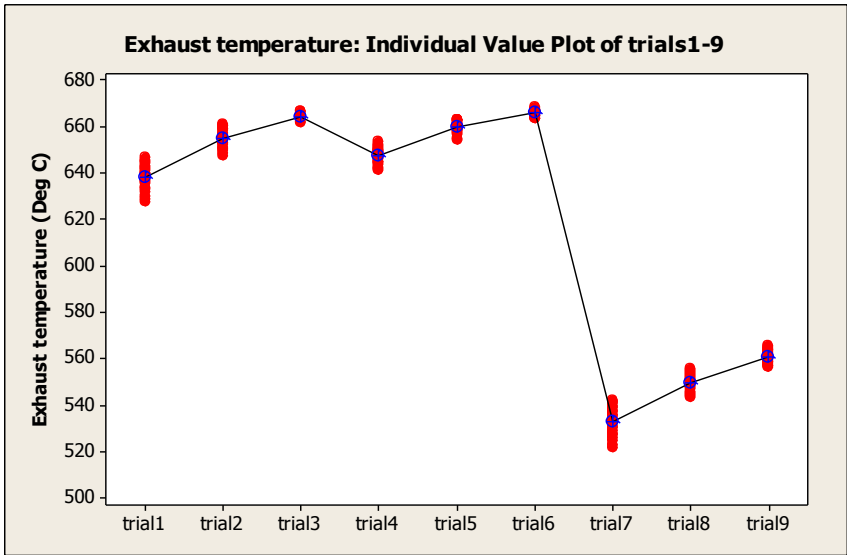


**Figure 55: Individual value plot of exhaust temperature for nice trials at full load and 3000rpm**

## *4.2. Repeatability Analysis*

Repeatability is based on performing the 8- point test mode as in table 4 at least three times for three days depicting different standard ambient atmospheric condition. The calculated standard deviations for all performance parameters at part load and full load at two constant speed levels are shown in tables 13 and 14

The pressure data are transient values measured at every one-half crank angle giving a total of 1440 data points for each complete cycle. The Lab View CAS takes the average of transient values at every four engine complete cycles. These pressure data are taken at specific intervals during the experiment over a period of several days. The values are based on operating conditions specified in table 4. The statistical analysis is based on the outcome of a total of 12 trials for pressure and nine trials for other performance parameters. To assess the repeatability of the

data acquired at different periods of the day and over several days, we start by assessing the mean of the measured in-cylinder transient pressures. These are calculated by measuring the in- cylinder pressure at each crank angle by the well known statistical formula:

$$\bar{\chi} = \frac{1}{n}\sum_{j=1}^{n}\chi_j = \frac{1}{n}\left(\chi_1 + \chi_2 + ..... + \chi_n\right) \tag{58}$$

Every data value taken at each $^{1}/_{2}^{o}$ crank angle will contribute to the mean and changing one of them will change the mean. The same procedure is use for the assessment of the performance data, the performance data is measured at every 4 second interval.

Similarly, the spread (variability) of the data values are also calculated by using the variance from which the standard deviations $\sigma$ are computed:

$$\sigma^2 = \frac{1}{n-1}\sum_{j=1}^{n}\left(\chi_j - \bar{\chi}\right)^2 = \frac{1}{n-1}\left[\left(\chi_1 - \bar{\chi}\right)^2 + ..... + \left(\chi_n - \bar{\chi}\right)^2\right] \tag{59}$$

The relative standard deviation (RSD) however, gives a more vivid picture of the deviations in the measurement and maybe more convenient to use. It is expressed in percent terms and is computed but finding the product of the SD and 100 and hence dividing this product by the mean.

$$RSE = \frac{100\sigma}{\bar{\chi}} \tag{60}$$

The calculated mean values and the standard deviation (in bracket) with the RSD for 50% and 100% loads at 3000 rpm are shown in table 13.

| Parameter | Load (50%) | | Load (100%) | |
|---|---|---|---|---|
| | Mean (SD) | RSD (%) | Mean (SD) | RSD (%) |
| $P_{max}$[bar] | 76.33(0.57) | 1.49 | 77.31(1.16) | 3.0 |
| $P_{me}$[bar] | 6.51(0.07) | 2.15 | 7.49(0.1) | 2.6 |
| BSFC[g/KWh] | 279.39(6.76) | 4.84 | 285.45(6.10) | 4.2 |
| Air consumption[g/s] | 13.23(0.37) | 5.6 | 13.06(0.37) | 5.6 |
| Exhaust temp [$^0$C] | 361.09(9.77) | 5.4 | 619.54(54.79) | 17.6 |
| Torque | 12.87(0.44) | 6.8 | 25,20(0.28) | 2.2 |
| Power[KW] | 4.04(0.13) | 6.4 | 7.92(0.08) | 2.0 |
| Speed[RPM] | 2999.18(0.07) | 0.004 | 2999.18(0.07) | 0.004 |
| $NO_x$[ppm | 385.94(1.03) | 0.6 | 340.58(0.84) | 0.6 |
| CO[ppm] | 141.59(0.44) | 0.6 | 2000(0.00) | 0 |
| $CO_2$[%] | 2.42(0.004) | 0.4 | 4.75(0.01) | 0.4 |
| $O_2$[%] | 17.68(0.01) | 0.12 | 14.25(0.02) | 0.2 |
| HC[ppm] | 32.14(0.01) | 0.06 | 28.71(1.00) | 7.0 |

**Table 13: Mean and standard deviation (in bracket) of part and full loads at 3000rpm**

Table 13 report the best estimate (mean) of the measured values and the variations (standard deviation) at part load and full load. The RSD have also been calculated based on p- value of 0.05 or at a significant level of 0.95. From the RSD it can be

seen that all the measurement are within the permissible standard deviations stipulated in table 4 of ISO 15550:2002(E) with the exception of the BSFC. The permissible standard deviation according to this ISO requirement is ±25ºC for exhaust temperature and ±3% for BSFC (15550, 2002).

| Parameter | Load (50%) | | Load (100%) | |
|---|---|---|---|---|
| | Mean (SD) | RSD (%) | Mean (SD) | RSD (%) |
| $P_{max}$[bar] | 77.08(0.41) | 0,53 | 81.58(0.68) | 0,83 |
| $P_{me}$[bar] | 6.71(0.11) | 1,64 | 6.87(0.73) | 10,63 |
| BSFC[g/Kwh] | 401.46(7.42) | 1,85 | 232.38(54.28) | 23,36 |
| Air consumption[g/s] | 10.03 (0.3) | 2,99 | 10.19 (0.32) | 3,14 |
| Exhaust temp [$^0$C] | 540(6.32) | 1,17 | 377(15.18) | 4,03 |
| Torque | 28.28(0.37) | 1,31 | 17.56(1.02) | 0,06 |
| Power[KW] | 6.67(0.09) | 1,35 | 4.14(0.24) | 5,80 |
| Speed[RPM] | 37.52(0.03) | 0,08 | 37.52(0.03) | 0,08 |
| $NO_x$[ppm | 784.78(5.8) | 0,74 | 294.21(20.06) | 6,82 |
| CO[ppm] | 161.83(0.68) | 0,42 | 2000(0.00) | 0,00 |
| $CO_2$[%] | 4.54(0.05) | 1,10 | 4.05(0.03) | 0,74 |
| $O_2$[%] | 14.73(0.07) | 0,48 | 14.99(0.08) | 0,53 |
| HC[ppm] | 29.23(0.09) | 0,31 | 29.5(0.1) | 0,34 |

**Table 14: Mean and standard deviation (in bracket) of part and full loads at 2250rpm for 12 trials**

Table 14 report the best estimate (mean) of the measured values and the variations (standard deviation) at part load and full load at 2250 rpm. The RSD have also been calculated based on p- value of 0.05 or at a significant level of 0.95. From the RSD it can be seen that all the measurement are within the permissible standard deviations stipulated in table 4 of ISO 15550:2002(E) with the exception of the brake power and BSFC at 100% load which were calculated to be 5.8% and 23.36% respectively. The permissible standard deviation according to this ISO requirement is ±3% for both brake power and BSFC (15550, 2002).

| Parameter | Mean standard deviation | Maximum standard deviation |
|---|---|---|
| $P_{max}$[bar] | 0.79 | 1.16 |
| $P_{ime}$[bar] | 0.37 | 0.73 |
| BSFC[g/KWh] | 30.19 | 54.28 |
| Air consumption[g/s] | 0.34 | 0.37 |
| Exhaust temp [$^0$C] | 30.56 | 54.79 |
| Torque [Nm] | 0.65 | 1.02 |
| Power[KW] | 0.16 | 0.24 |
| Speed[RPM] | 0.05 | 0.07 |
| $NO_x$[ppm] | 12.13 | 20.06 |
| CO[ppm] | 1.045 | 2.09 |
| $CO_2$[%] | 0.035 | 0.05 |
| $O_2$[%] | 0.045 | 0.08 |
| HC[ppm] | 0.53 | 1.0 |

**Table 15: Total mean and standard deviations**

Table 15 summarizes the mean deviations in all the measurements. It can be observed that the mean standard deviation in the measurements ranges from 0.05 rpm for speed to a maximum of 30.54°C representing deviations in the exhaust measurement. The maximum standard deviations ranges from a minimum of 0.05% representing deviations in the $CO_2$ emission to a maximum of 54.79 °C representing exhaust emission. It is worth noting that both the mean and maximum standard deviations of the BSFC are very high, exhibiting a mean SD of 30.19 g/KWh and a maximum of 54.28 g/KWh.

## *4.3. Uncertainty Analysis*

The uncertainty of measurement tells us about the quality of the measured data. The estimated uncertainties of the means are calculated from the equations:

$$u = \frac{\sigma}{\sqrt{n}} \tag{61}$$

Where n is the number of measurements in the set and $\sigma$ is the estimated standard deviation. The reported expanded uncertainty is based on a standard uncertainty multiplied by a coverage factor $k$ = 2, providing a level of confidence of approximately 95%.

| Parameter | Estimated uncertainty at part load | Estimated uncertainty at full load | No. of measurements |
|---|---|---|---|
| $P_{max}$[bar] | 0,33 | 0,67 | 12 |
| $P_{me}$[bar] | 0,001 | 0,002 | 1440 x12 =17280 |
| BSFC[g/KWh] | 1.0 | 0.9 | 21x9=189 |
| Air consumption[g/KWh] | 0,05 | 0,05 | |
| Exhaust temp [$^0$C] | 1,4 | 7,97 | |
| Torque | 0,06 | 0,04 | |
| Power[KW] | 0,018 | 0,01 | |
| Speed[RPM] | 0,01 | 0,01 | |
| $NO_x$[ppm | 0,36 | 0,3 | 33 |
| CO[ppm] | 0,15 | 0 | |
| $CO_2$[%] | 0,001 | 0,004 | |
| $O_2$[%] | 0,004 | 0,01 | |
| HC[ppm] | 0,004 | 0,01 | |

**Table 16: Measurement uncertainties at constant speed of 3000rpm**

Table 16 shows the uncertainties in the measured parameters at a constant speed of 3000 rpm both at part load and full load. All the uncertainties have been calculated to 95% confidence level. We can therefore say that we are 95% that the reported measurement values are accurate within the deviations shown in table 16. From the table, the level of uncertainties seems to be generally low with the exception of exhaust temperature measurement at full load. The measurement of CO seems not to exhibit any uncertainty at full load which practically seems unrealistic.

| Parameter | Estimated uncertainty at part load | Estimated uncertainty at full load | No. of measurements |
|---|---|---|---|
| $P_{max}$[bar] | 0.24 | 0.4 | 12 |
| $P_{me}$[bar] | 0.002 | 0.01 | 1440 x12 =17280 |
| BSFC[g/KWh] | 1.08 | 7.9 | 21x9=189 |
| Air consumption[g/KWh] | 0.04 | 0.04 | |
| Exhaust temp [$^0$C] | 0.92 | 2.2 | |
| Torque | 0.06 | 0.14 | |
| Power[KW] | 0.014 | 0.04 | |
| Speed[RPM] | 0.004 | 0.004 | |
| $NO_x$[ppm | 2.02 | 7.0 | 33 |
| CO[ppm] | 0.24 | 0 | |
| $CO_2$[%] | 0.02 | 0.01 | |
| $O_2$[%] | 0.02 | 0.02 | |
| HC[ppm] | 0.04 | 0.04 | |

**Table 17: Measurement uncertainties at constant speed of 2250rpm for several trials**

Table 17 shows the uncertainties in the measured parameters at a constant speed of 2250 rpm both at part load and full load. All the uncertainties have been calculated to 95% confidence level. We can therefore say that we are 95% that the reported measurement values are accurate within the deviations shown in table 17. From the table, the level of uncertainties seems to be generally low with the exception of BSFC and $NO_x$ measurement at full load. The measurement of CO seems not to exhibit any uncertainty at full load which practically seems NOT realistic.

## *4.4. Assumptions made in the ANOVA*

Some assumptions have been taken in carrying out the analysis of variance. Some of which are inherent with ANOVA.

- The dependent variables such as CA interval in pressure measurement and time interval in other performance measurement parameters are considered to be measured at equal intervals and normally distributed.
- The variances are considered to be homogenous.
- Random and systematic errors in the measurement instruments have not been considered.

# Chapter Five: Experimental result

## *5.1. Effects of Atmospheric Pressure*

The variation in the atmospheric pressure on different days is evident in table 18. The effect of this on the performance characteristic of the engine is clearly demonstrated in the Boxplots and individual value plots shown for each performance analysis. By performing a factor of analysis (FOA) on the sets of trial data, the effect of atmospheric pressure on the performance measurements can be studied in detail. By recording the atmospheric pressure which varies on different days, the nine trial data can be reduced to three data sets representing three days of trials as shown in figure 18.

| Trials | Mean Atmospheric pressure |
|---|---|
| 1-3 | 1.01227 |
| 4-6 | 0.99089 |
| 7-9 | 0.99731 |

**Table 18: Mean atmospheric pressure data**

Figure 32 and 33 shows characteristic of brake torque as a function of atmospheric pressure. The relationship between change in atmosphere pressure and the change in brake torque seems to follow an exponential function at part load and a linear

function at full load. This assertion is validated by the square of the Pearson product moment correlation coefficients which is a dimensionless index that ranges from -1.0 to 1.0 inclusive and reflects the extent of a linear relationship between two data sets. These indices are calculated to be unity for exponential function in part load and linear function in full load.

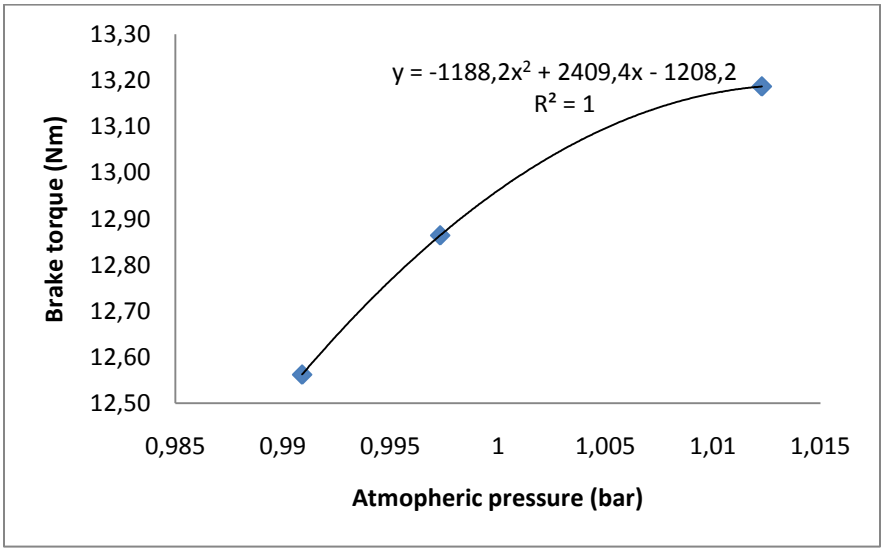


**Figure 56: Brake torque as a function of atmospheric pressure**

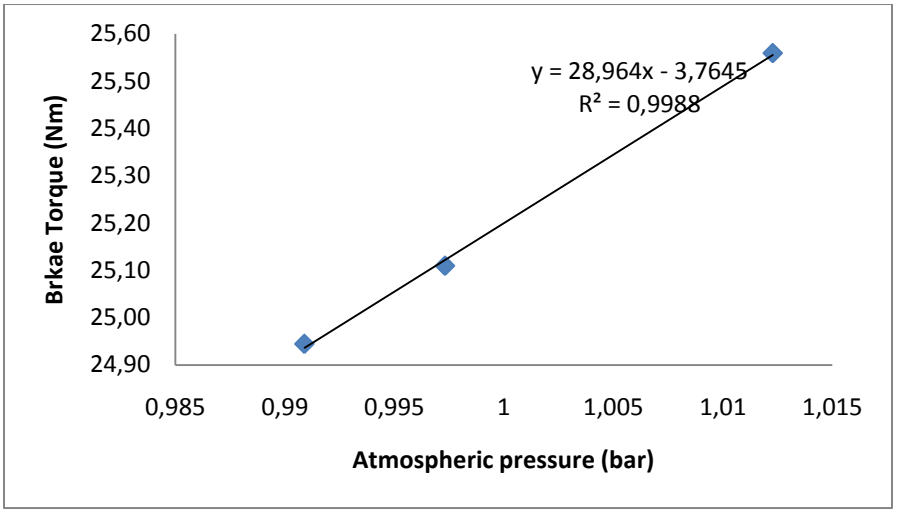


**Figure 57: B**rake torque as a function of atmospheric pressure

A percentage increase of 0.64% in atmospheric pressure has resulted to a percentage increase of 2.34% in torque at part load and 0.66% at full load. A further increase of 0.99731 to 1.01227 bar in atmospheric pressure has revealed a staggering increase of 0.45 Nm of torque at full load and 0.32 Nm of torque at part load. Measurement of maximum torque shows an increment of 0.66% in torque with a 0.64% increment in atmospheric pressure and a 1.48% increase in atmospheric pressure resulting to a 1.76% increase in torque.

## 5.2. *Analysis of cylinder pressure derivative*

The cylinder pressure derivative is an important component of combustion and rate of heat released analysis. The time required for combustion can be accurately calculated from the cylinder pressure derivative by measuring the instant of sudden increase in pressure gradient and the point of drop and then dividing by the angular velocity of the engine.

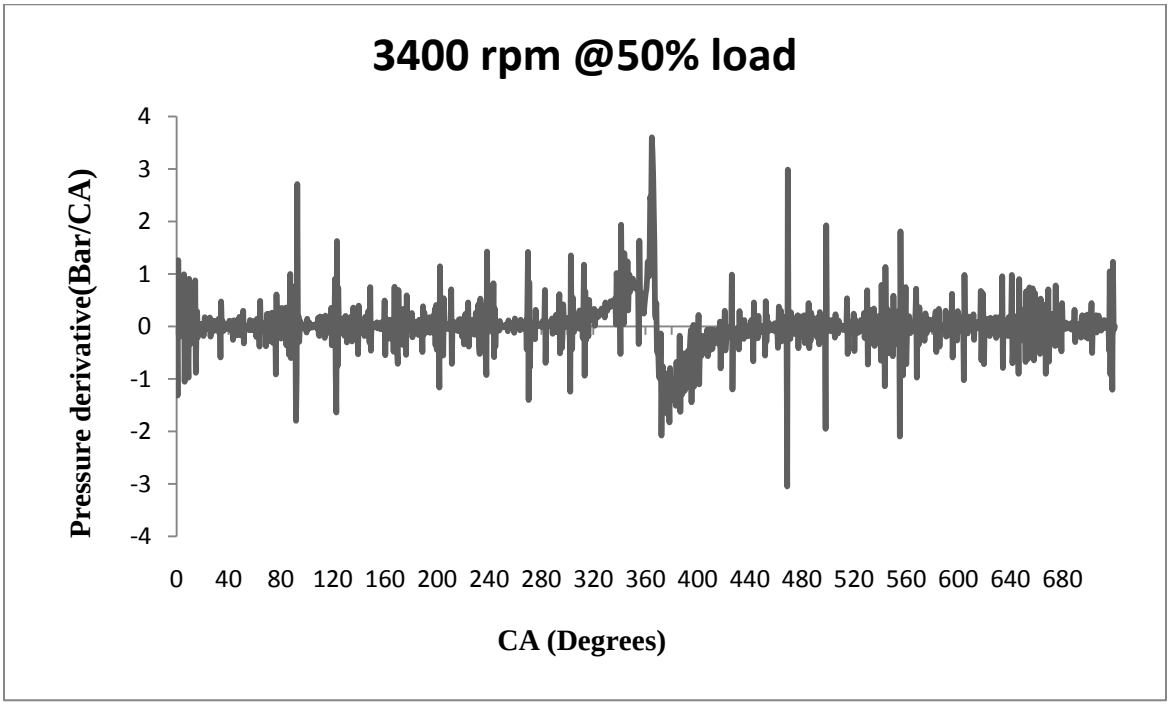


**Figure 58: Pressure derivation as a function of crank angle**

Figure 58 shows a cylinder pressure derivative developed from the experimental pressure data obtained during the experiment.

## *5.3. Rate of heat release*

The analysis and understanding of heat release in the cylinder during the combustion process is central to accurate characterization of the engine. The apparent heat release rate and the combustion reaction are the most useful information derived from the cylinder pressure measurement. The apparent heat release rate is computed by modeling the amount of fuel energy release during combustion necessary to produce variations observed during experiments. The reliability of the rate of heat release (ROHR) analysis results is generally dependent on the accuracy of the engine in-cylinder measurement trace measured by piezoelectric transducer conditioned by a charge amplifier. (Andre Valente Bueno et al, 2009). The ROHR is further affected by the accuracy of the cylinder pressure derivative. The pressure derivative is calculated by numerical differentiation of the measured dynamic cylinder pressure trace.

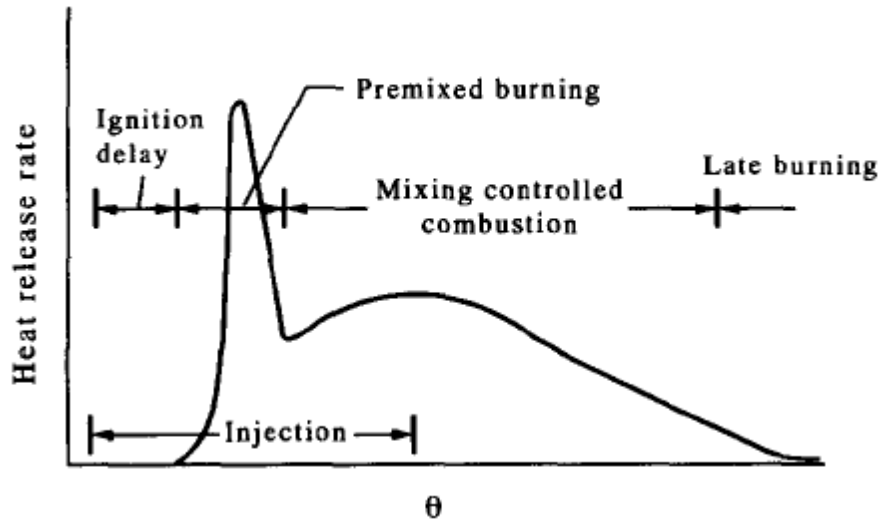


**Figure 59: Heat release rate as a function of crank angle showing the different phases of combustion (source: (Patro, 1993))**

Figure 59 shows an experimental heat release curve of a direct injection diesel engine showing the different stages of combustion. (Heywood, 1998) explains the various stages of this process identified by identifying the phases on a typical heat release rate diagram for a DI diesel engine as shown in figure 59. The heat release rate on the figure expresses the sum of the change of sensible internal energy of the cylinder gases and the work done on the piston.

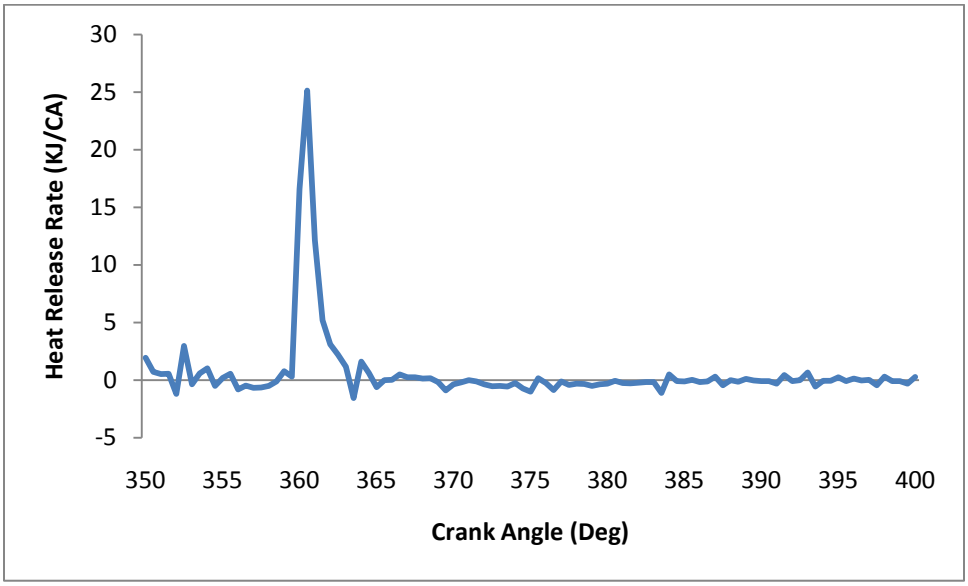


**Figure 60: Rate of heat release as a function of crank angle at part load and 1200 rpm**

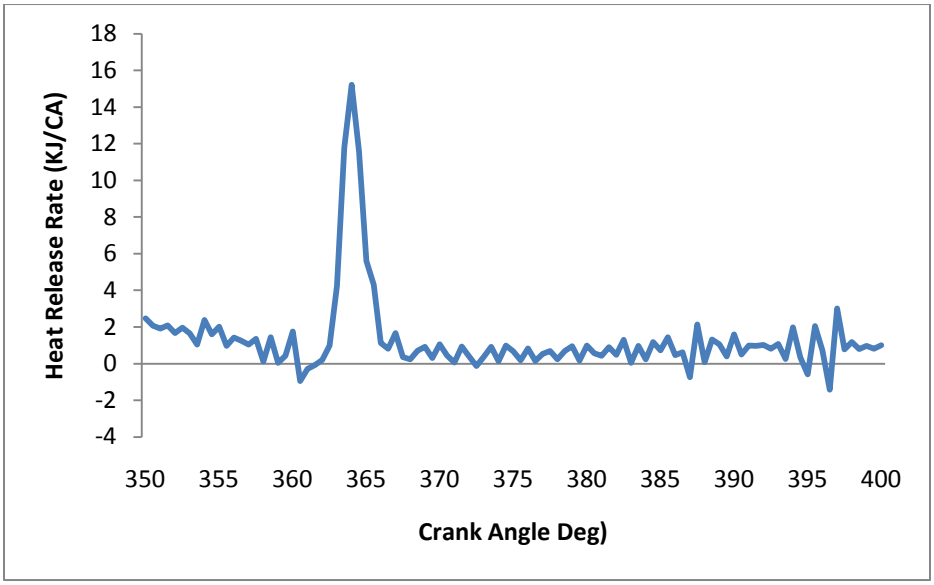


Figure 61: Rate of heat release as a function of crank angle at part load and 1700 rpm

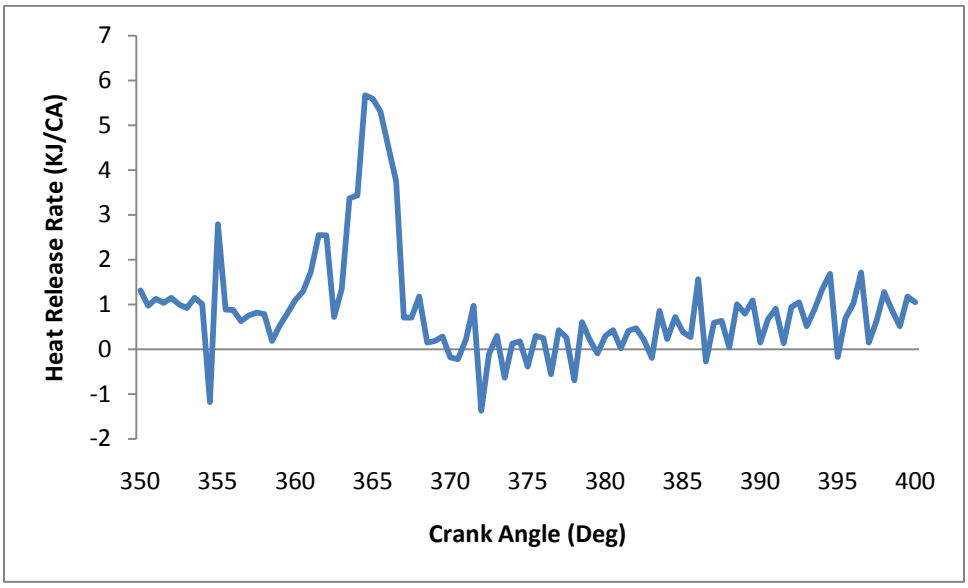


Figure 62: Rate of heat release as a function of crank angle at part load and 3400 rpm

Figures 60-62 show the heat release rate as a function of crank angle at part load near the combustion region at 1200 rpm, 1700 rpm and 3400 rpm respectively. Premixed or rapid combustion phase of 4 degree angle (CA) can be observed from figure 60, while figure 61 and 62 showed premixed phases of 5 degree CA and 7 degree CA respectively.

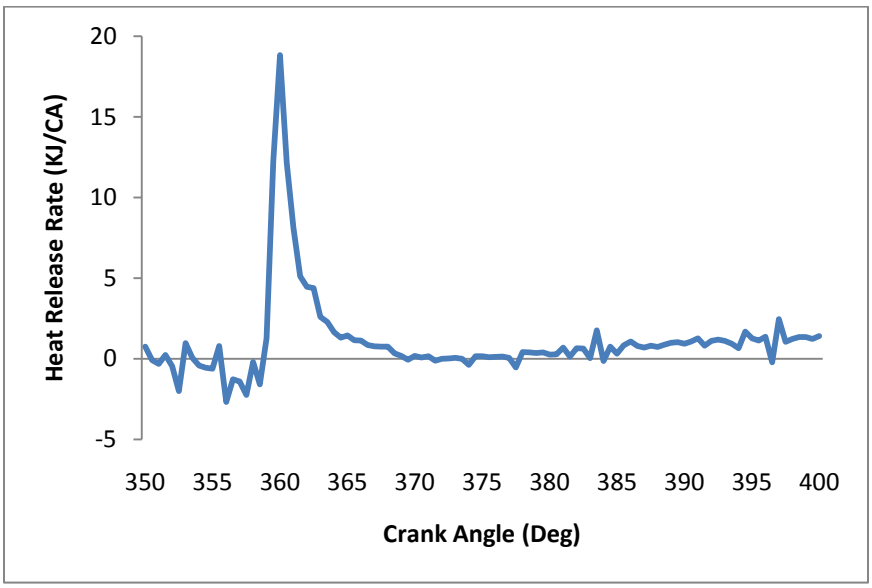


**Figure 63: Heat release rate curve as a function of crank angle at 1200 rpm with maximum load**

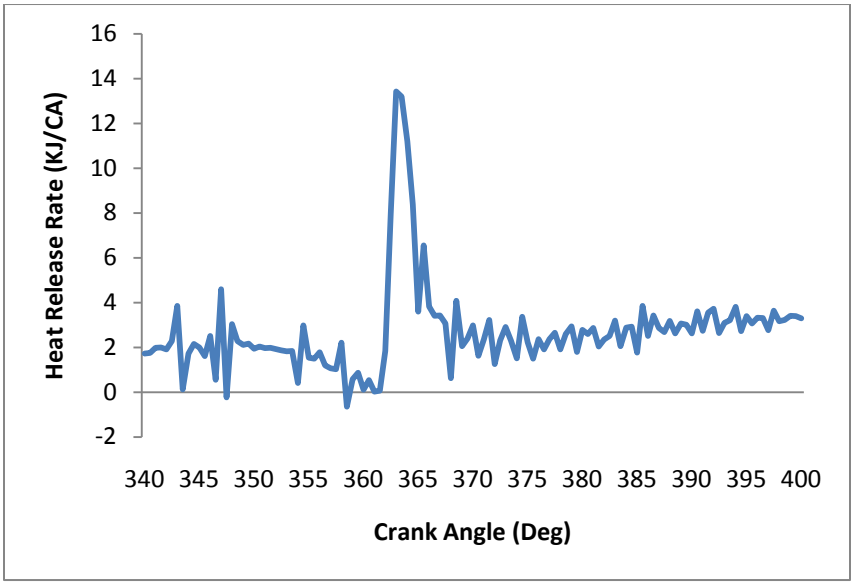


Figure 64: Heat release rate curve as a function of crank angle at 1700 rpm with maximum load

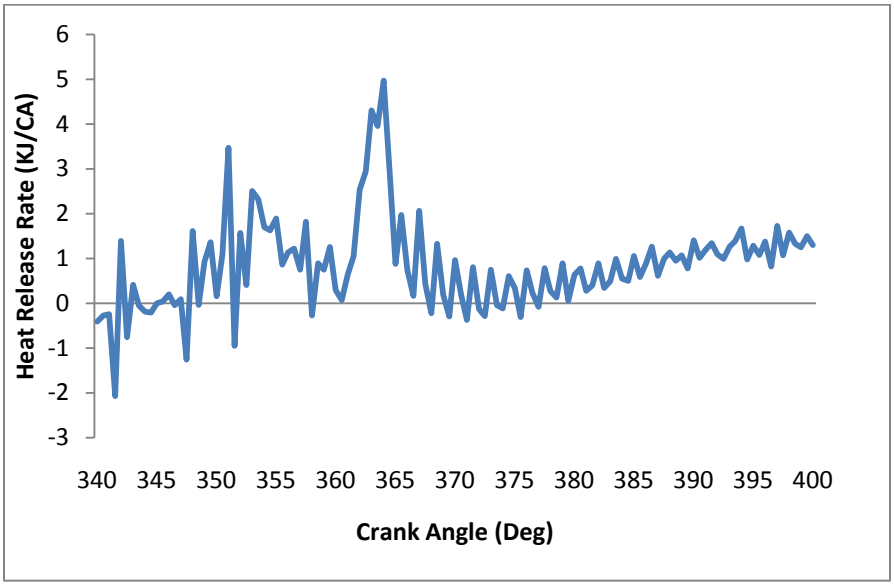


Figure 65: Heat release rate curve as a function of crank angle at 3400 rpm with maximum load

From figure 59, the fuel injection is followed by an ignition delay period before the start of combustion. The rapid or premixed combustion phase occurs within few CA intervals and this can be visualized in the HRR diagrams as ranging between 5 to 7.5 CA degrees. This flame propagation in this phase has been characterized by some researchers as being nearly non- luminous flame (Patro, 1993). It is also characterized by a very high ROHR. The premised combustion phase is followed by a mixed controlled phase which is largely characterized by a low combustible mixture and the HRR in this phase is dependent on the availability of residual combustibles fuel/air (F/A) mixture. At low load (figure 63) this phase is almost non-existence but is quite visible in figures 61-65. During this phase the flame is luminous and diffusive (Patro, 1993)

The final phase in the combustion process is the late combustion phase where the HRR propagation continues at a much lower rate and can be extended right into the expansion stroke. The flame propagation in this phase is essentially sustained by the unburned mass fraction of the fuel and energy release from soot and unburned carbons.

## 5.4. *Effect on Power and Torque*

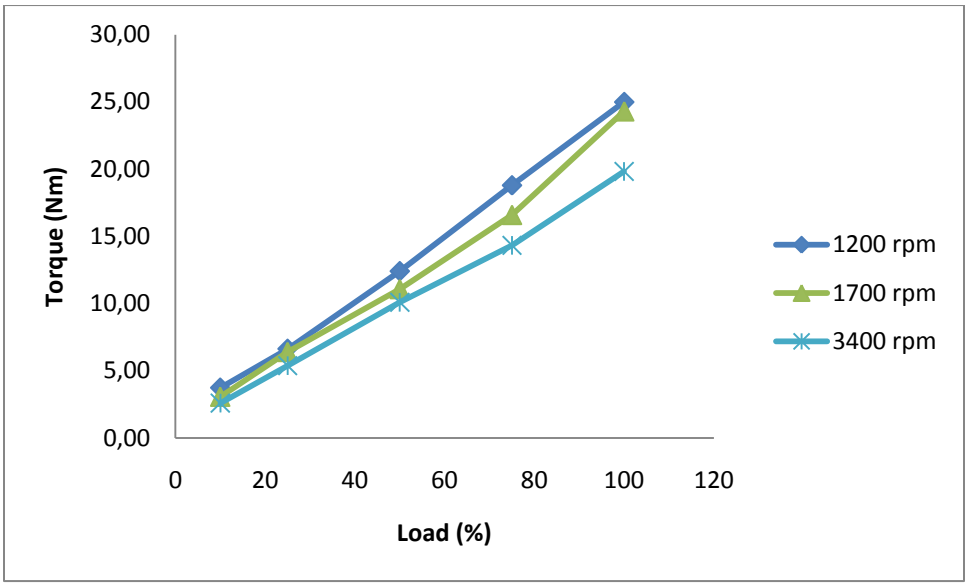


**Figure 66: Characteristics of torque at various load points with varying speeds**

The characteristic of torque at various load points is shown in figure 66. It is observed that as the load increases, the torque increases. This relationship is close to being linear for low speed of 1200 rpm. Since the load is a function of speed and torque, by keeping the speed constant a linear relationship is expected. The torque is a measure of the engine's ability to do work

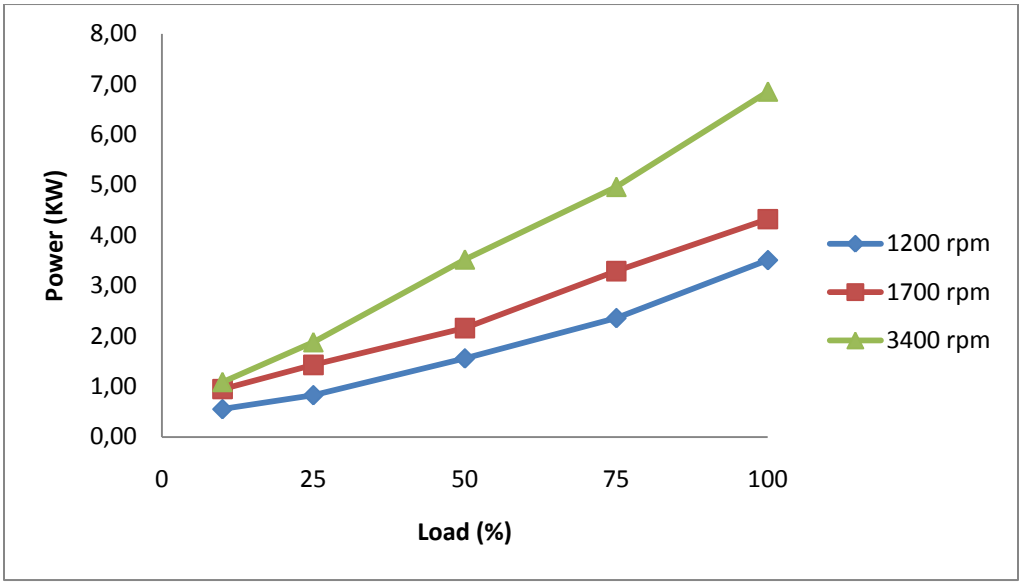


**Figure 67: Characteristics of power at various load points with varying speeds**

The variation of brake power output and load for different for three speed levels of 1200, 1700 and 3400 rpm is depicted in Figure 67. It is observed that for all speed levels the brake power increases as the engine load increases. The brake power increase as the engine speed increased. This is anticipated as the power is proportional to the angular speed of the engine.

## 5.5. *Effect on Brake Specific Fuel Consumption*

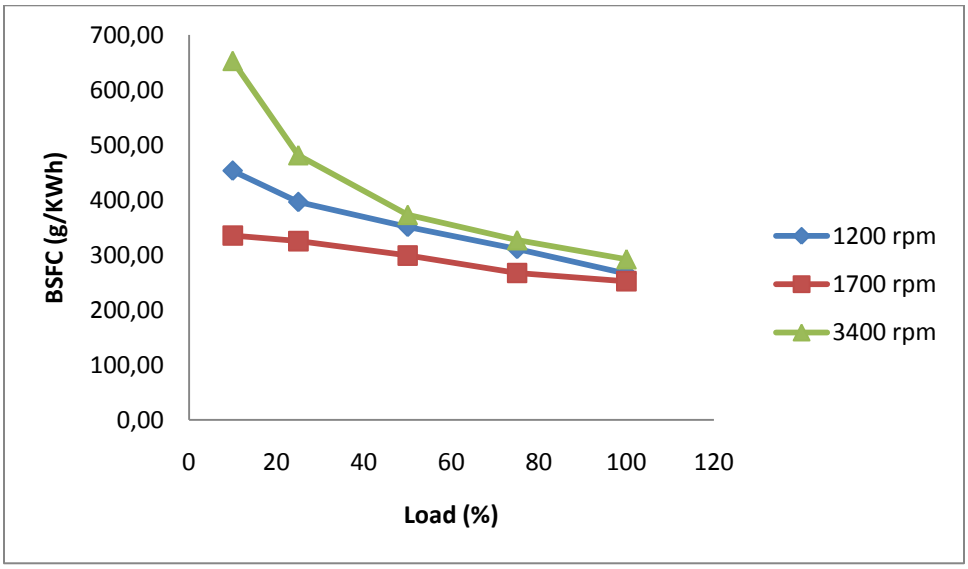


Figure 68: Characteristics of BSFC at various load points with varying speeds

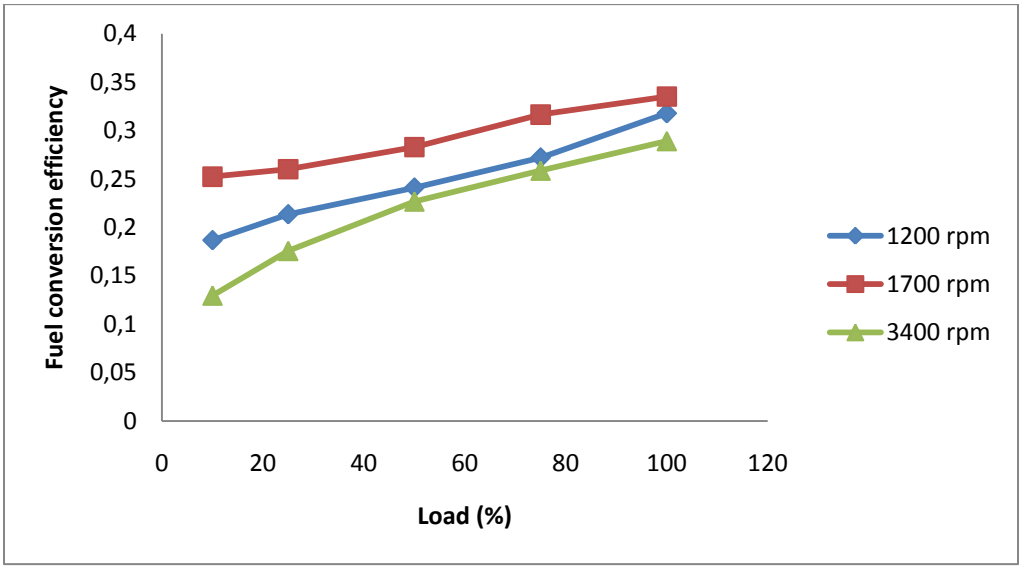


Figure 69: Characteristics of fuel conversion efficiency at various load points

Figure 69 shows the fuel conversion efficiency as a function of load and speed. The fuel conversion efficiency is a useful criterion for understanding the engine's operating condition. The fuel conversion efficiency depends on the specific fuel consumption and the lower heating value (LHV) of the fuel. Since the LHV is constant for most hydrocarbon fuels, thus the fuel conversion efficiency is inversely proportional to the specific fuel consumption. With the presence of sufficient oxygen, hydrocarbon fuels can be completely oxidized. This is usually referred to as the stoichiometric fuel/air or air/fuel ratios which depend largely on the composition of the fuel. At high engine speed of 3400 rpm, the fuel conversion efficiency increases with engine load. At medium speed of 1700 rpm, the increase in load results in increase in fuel conversion efficiency at low and part load conditions. But as the load increases from 50 to 75% the fuel conversion efficiency increases rapidly to a maximum of 0.59. This point can be regarded as the optimum utilization of the combustion energy where much of the fuel is oxidized. Fuel conversion efficiency is largely affected by compression ratio and air equivalent ratio. The effect of other variables has little effect and can sometimes be even negligible.

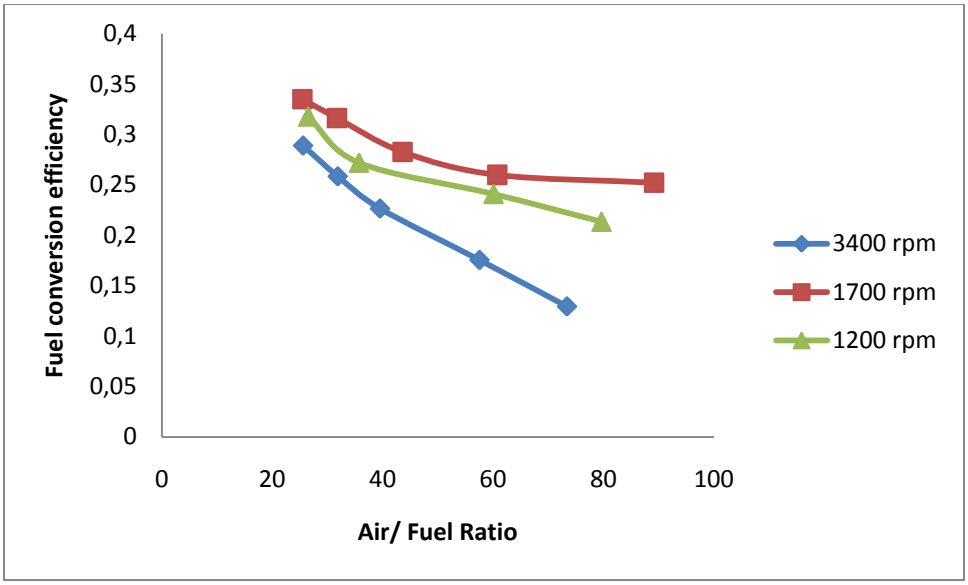


**Figure 70: Experimental brake fuel conversion efficiency as a function of fuel/air equivalent ratio**

The air equivalent ratio has everything to do with the ID vis-à-vis specific fuel consumption and the mass of air used. Decrease of air equivalent ratio below the stoichiometric air/fuel equivalent ratio results to an increase in efficiency. This occurs because the temperature of the burnt gases decreases after combustion resulting to a reduction in the specific heat of the burnt gases. As a result, the effective value of the ratio of the specific heats is increased over the expansion stroke. The efficiency increase is as a result of the expansion of the burn gases through a larger temperature ratio for a given volume expansion ratio prior to the expansion phase. Therefore the expansion stroke work is increased per mass fraction of fuel burnt.

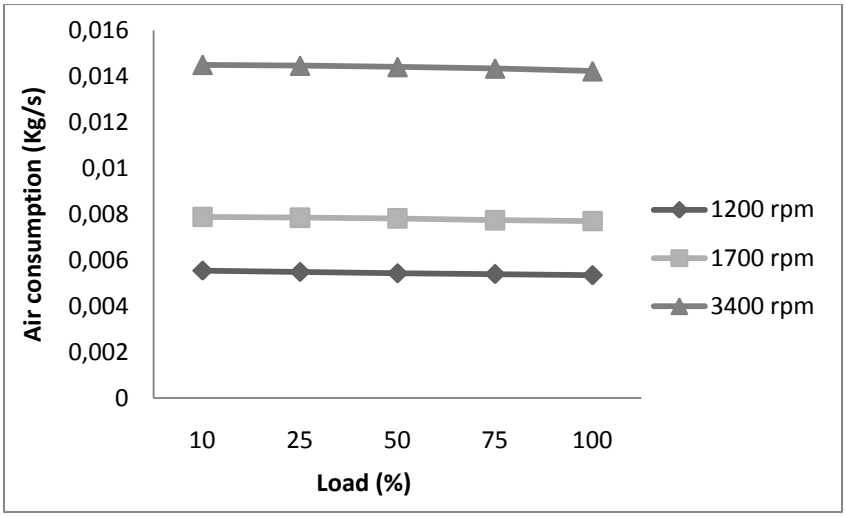


Figure 71: Characteristics of air consumption at various loads with varying speeds

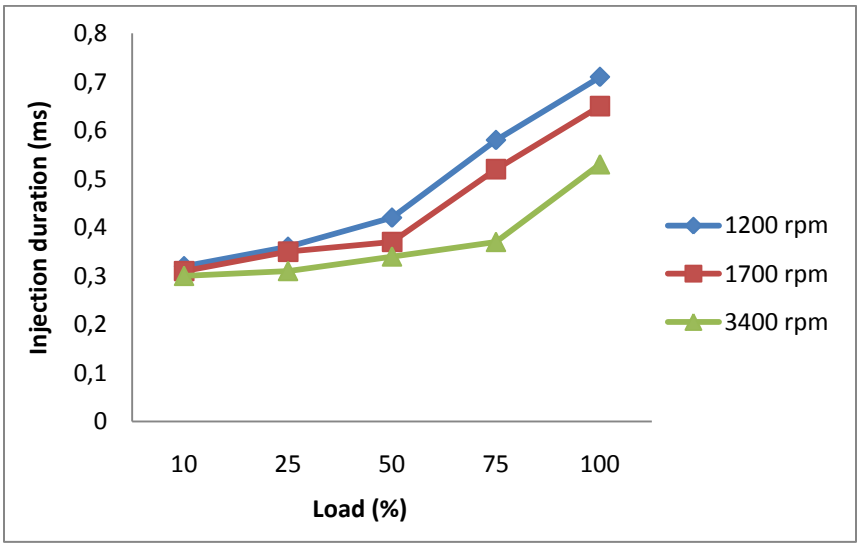


Figure 72: Characteristic of injection duration at various load points

Figure 72 gives the fuel ID as a function of load. Increases in ID result in an increase in engine torque. At part load and low loads only moderate increments in

ID are required for significant increment in load. But from 50 to 100% loads, significant amount of ID change ranging from 0.42 to 0.71 ms at low speed and 0.37 to 0.65 ms at mid speed range resulting to 41% and 43% respectively are required to attain full load conditions. However, at high engine speeds, only minimal change of 19% in ID results to an engine load change from 10% to 75% load while a 30% increment in ID is required to attain the final 25% load. At a maximum speed of 3400 rpm the change in ID required to change the engine load from 10% to 50% was only 12%.

The reason for this seemingly abnormal operating condition is because for the engine to produce sufficient power to attain the required torque, sufficient air must be available inside the cylinder for combustion. Since the experimental engine is a naturally aspirated engine enough air is not available at high load and therefore the engine depends mostly on the conversion of the chemical energy in the fuel to attain the required power. As a result the ID must be increased proportionately to increase fuel injection higher at high load conditions in order to attain the required toque at high load. This phenomenon can be easily understood if we link figure 72 to the air/ fuel ratio diagram as a function of engine load in figure 73.

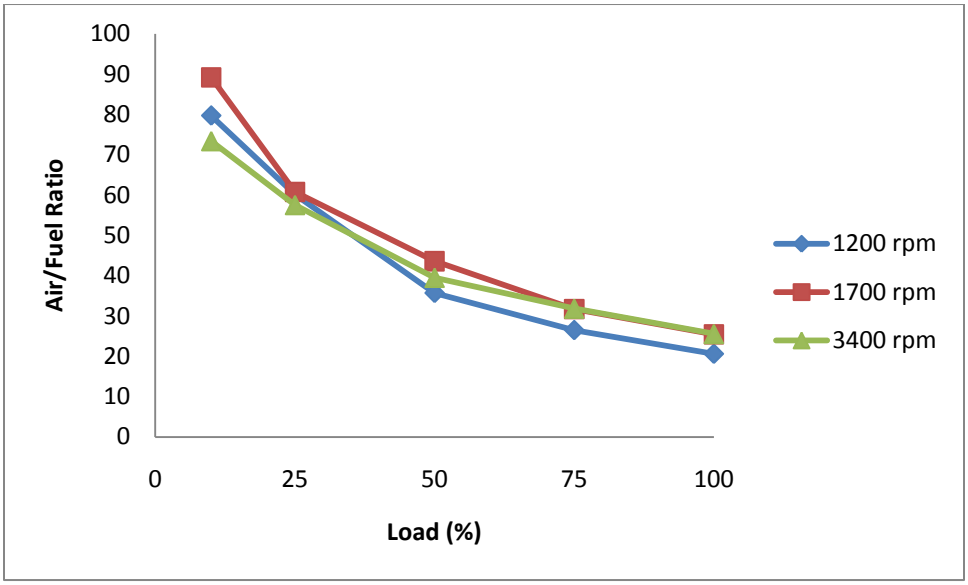


Figure 73: Air/ Fuel ration as a function of engine load

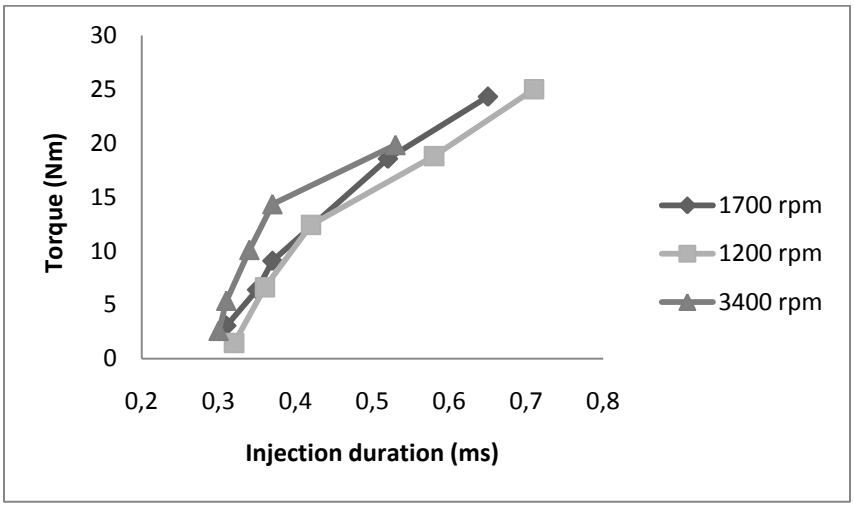


Figure 74: Torque as a function of injection duration with varying speeds

The variation of brake torque as a function of ID for three speed levels of 1200, 1700 and 3400 rpm is depicted in Figure 74. It is observed that for all speed levels the

brake toque increases as the ID increases. The brake power increase as the engine speed increase. This is anticipated as the power is proportional to the angular speed of the engine.

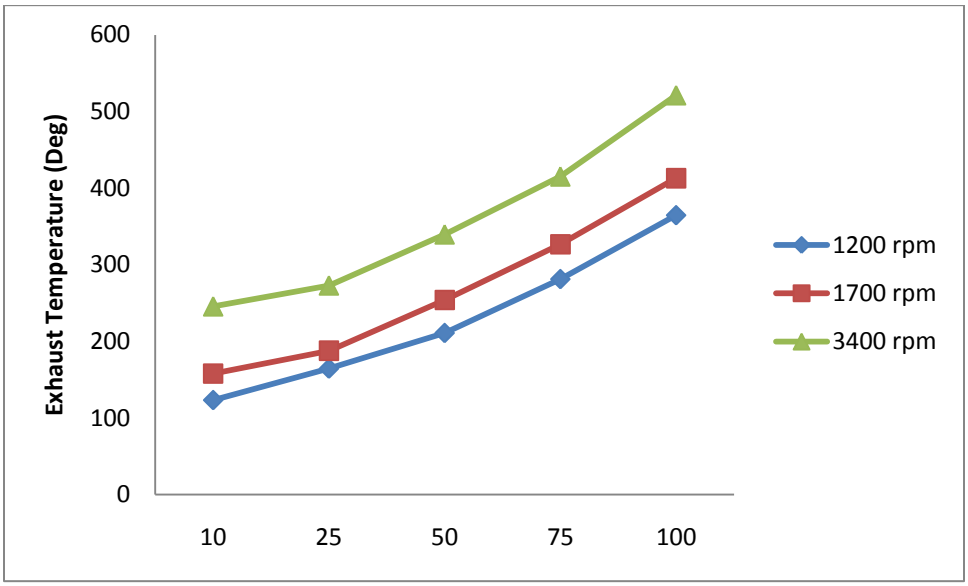


**Figure 75: Characteristics of exhaust temperature at various load points with varying speeds**

Figure 75 shows exhaust temperature as a function of load for the three constant speed levels used in the experiment. It can be observed that the exhaust temperature increases as the load increases for all the three speed levels. This is expected because as the load increases more fuel is burnt and as a result more heat is released during the combustion. It can further be observed from the curves that the exhaust temperature increases as the engine speed increases. This is because the torque is inversely proportional to the angular velocity of the engine. Therefore the torque developed decreases as the engine speed is increased. As a result more

fuel is burnt at higher engine speed to develop higher torque. Consequently the ROHR increases producing higher exhaust temperatures.

## *5.6. Exhaust emission*

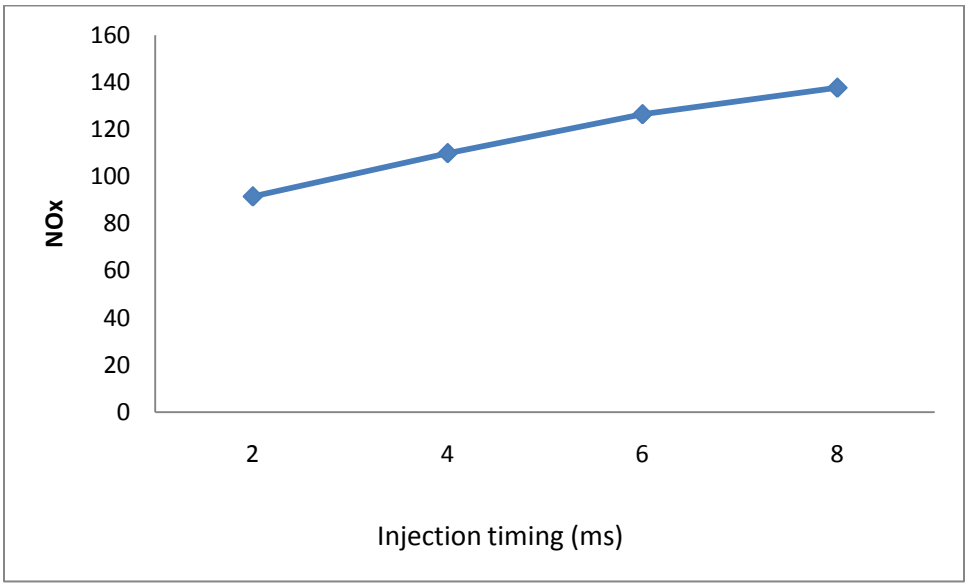


**Figure 76: Oxides of nitrogen emission at different injection timing**

Figure 76 shows a variation of $NO_x$ emission as a function of injection timing. The results show that as injection timing increases $NO_x$ emission increases. This is because $NO_x$ emission depends on the temperature and pressures in the cylinder. As the

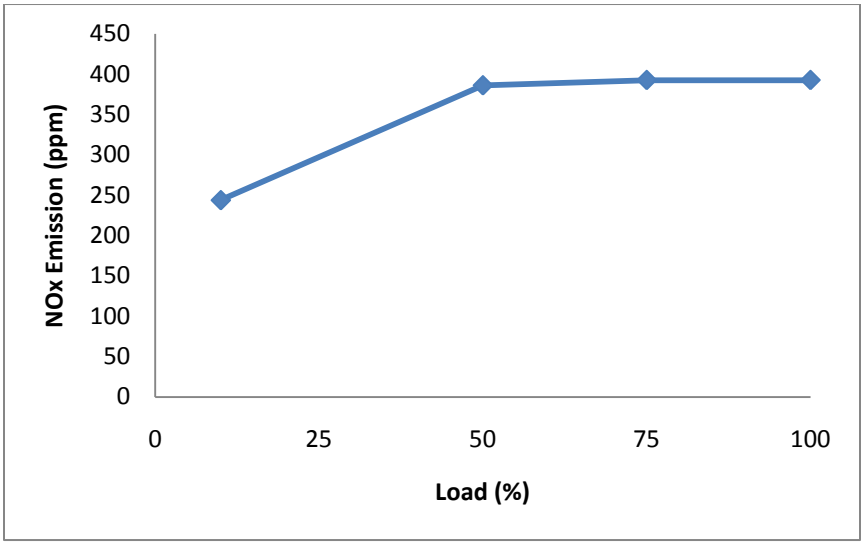


Figure 77: $NO_x$ emission at different mode points

Figure 77 shows $NO_x$ emission as a function of engine load. The graphical presentation shows that the variation in $NO_x$ emission at high load seems to be very small. Rapid increases in $NO_x$ emission occur during part and low load regions.

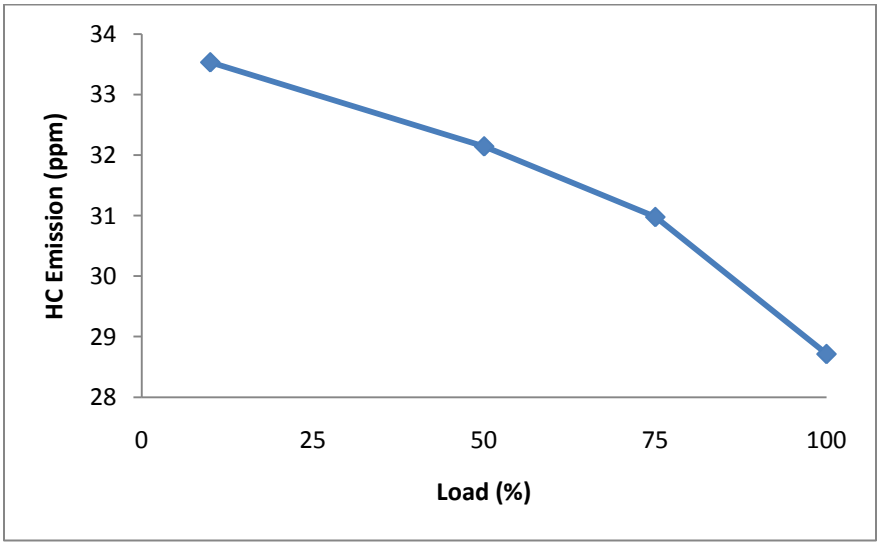


Figure 78: Hydrocarbon emission at different mode point

Figure 78 shows HC emission as a function of engine load. From the graphical presentation it can be shown that HC decreases as the load increases. For combustion to be efficient, proper atomization, mixing and ignition of the fuel is a prerequisite. Atomization and mixing of fuel however, largely depend on the physical properties of the fuel. Fuel viscosity and surface tension affects the penetration rate, maximum penetration and droplet size which in turn affects the mixing of fuel and air (Sakumar Puhan et al, 2004). Diesel engines are more efficient at high loads which are characterized by lean combustion. As a result less HC are produces as the load increases.

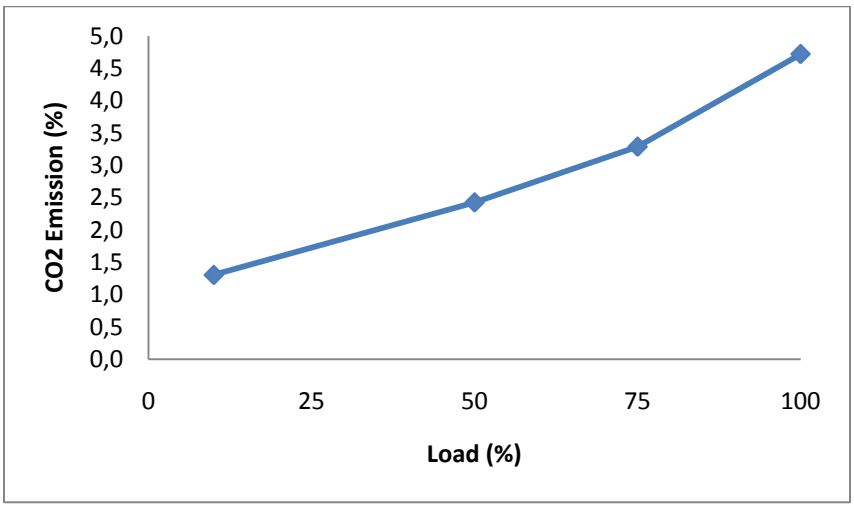


**Figure 79: Carbon dioxide emission at different mode points**

Figure 79 shows $CO_2$ emission as a function of engine load. The figure shows that $CO_2$ emission increases as the load increases. $CO_2$ emission from a CI engine is an indication of how efficiently the fuel is burnt inside the cylinder.

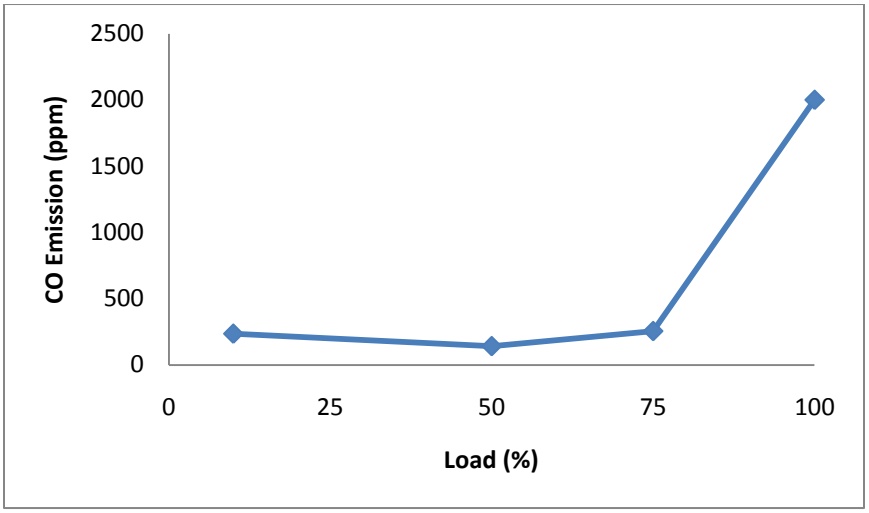


Figure 80: Carbon monoxide emission at different mode points

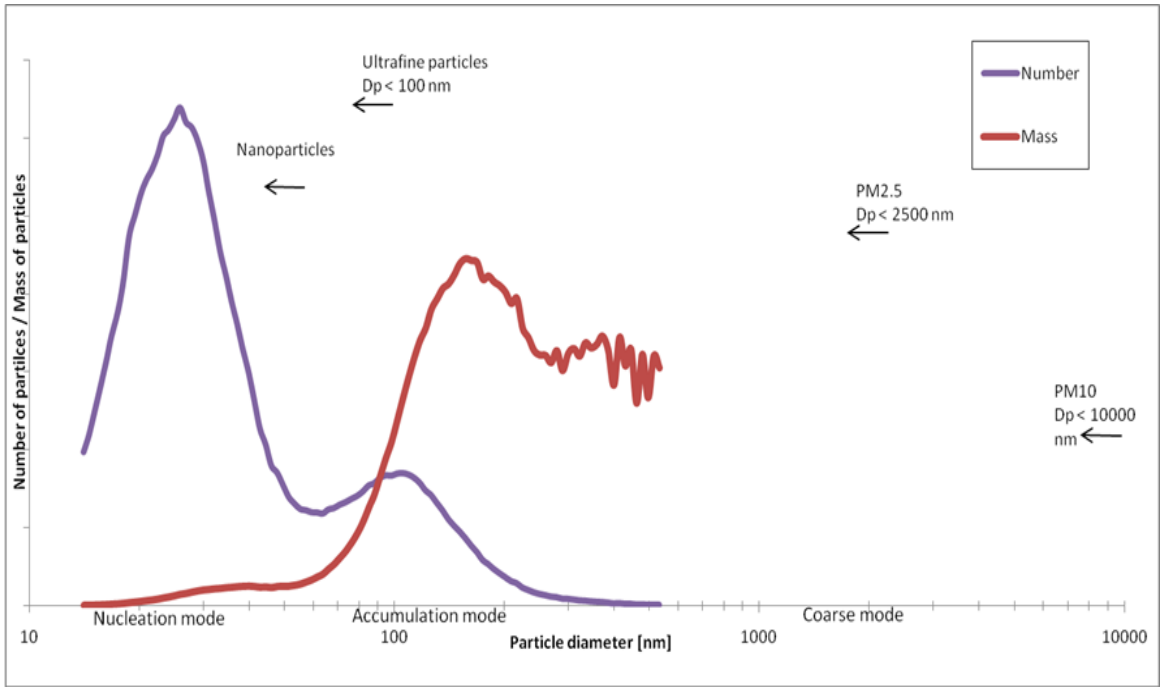


Figure 81: Distribution of diesel particle number and mass distribution as a function of diameter (Source: Marintek-Sintef)

Figure 81 shows an idealized diesel PM number and mass distributions measured by Marintek-Sintef using the MDO. It can be seen that a greater number of the particles are ultrafine or nanoparticles ($D_p$<100 nm) reside in the nucleation mode which ranges from 5 to 50 nm. This is where most of the carbonaceous agglomerates and associated adsorbed materials are deposited. The bulk of the heavier particles are concentrated in the accumulation mode which is characterized by particle sizes ranging from 50 to 150 nm. This mode usually consists of volatile organic and sulfur compounds that form during exhaust dilution and cooling, and may also contain solid carbon and metal compounds (David B. Kittelson, 1999)

# Part Two

## Chapter six: Empirical Correlations

### *6.1. Introduction*

Hydrocarbon diesel fuel is used as test fuel in the initial test using an eight mode test points shown in table 4. The original plan of the experiment is to conduct similar tests on a series of renewable fuels using the same test matrix. It is expected that since the test matrix is used, variations in the engine behavior will be as a result of physical and chemical properties of the experimental fuels. Since the condition of the engine did not allow for testing of the renewable diesel fuel within the limited time permissible for the completion of the master's thesis, I had little choice but to use the experimental results of the PRF to determine empirically the performance and emission characteristic of renewable fuels.

### *6.2. Description of research fuels*

In this study rape seed methyl ester was used as biodiesel and a marine diesel fuel with no oxygenated additive was used as the primary reference fuel (PRF). The renewable fuel and its blends were obtained from STATOIL and the PRF was obtained from the marine systems laboratory of department of Marine Technology also supplied by STATOIL. The lower heating value of LGO-10 was calculated

according to ASTM D-4868/90 based on density, sulfur and water contents. The properties of the research fuels are shown in table 19.

**Table 19: Properties of test fuels**

| Fuel | Units | Marine diesel fuel | LGO+ 10% Rapeseed | Rape seed methyl ester* |
|---|---|---|---|---|
| Density | $Kg/m^3$ | 820-860 | 844 | 883.7 |
| Cetane number (CN) | - | 47 | 57.9 | 54.7 |
| CN improvement | - | - | 5.8 | - |
| Cloud point | $^oC$ | 0 | -5 | |
| Lower heating value | MJ/kg | 42.6 | 42.84 | 39.0 |
| Nitrogen | ppm | - | 0.7 | |
| Sulphur | ppm | 500 | 9.9 | 5 |

***Source: (Sathaporn Chuepeng et al, 2010)**

From table 19, the main differences between MDO, LGO-10 and RME are

- An increase in Cetane number by 23.2% for LGO-10 and 16.4% for RME,
- An increase in density by 0.5% for LGO-10 and 5.2% for RME
- An increase in LHV of 0.6% LGO-10 and a reduction of 8.5% for RME.
- A large reduction in sulfur content of 4950% for LGO-10 and 5000% for RME.

## *6.3. Empirical Correlations*

When comparing two or more different test fuels on an engine test bench, equivalent performance requires attaining the same load conditions. Irrespective of the fuel used, the same torque and speed must be measured. Since the physical and chemical properties of the test fuels are different, it can be anticipated that the fuel

consumption, combustion characteristics, ignition delay and characteristics of the combustion gases will be different. The performance of the engine and exhaust emission are affected by properties of the fuel as the lower heating value (LHV), CN, density, isothermal compressibility and viscosity of the fuel. The kinematic viscosity has an effect on the injection line pressure and fiction of the moving parts in the fuel pump and the injector. (Koji Yamane et al, 2001) Carried out an experiment using a single cylinder direct inject engine fitted with a high-pressure injection system named KD-3, fitted with an automatic injector that allows the injection timing to be independent of the engine speed. They reported that the effect of kinematic viscosity on injection pressure and timing for diesel fuel and biodiesel was slight at 353K but significantly different at lower temperatures of 293k and 313k with the injection pressure of biodiesel rising earlier than diesel fuel. This has been attributed to the fact that at lower liquid pressures the bulk modulus of biodiesel is higher than diesel fuel. Therefore the rate of pressure rise accelerates and the injection timing is advanced. The ignition delay has an influence on the temperature and pressure inside the cylinder and therefore influences the formation of certain combustion gases. Figure 77 showed this effect on $NO_x$ formation.

Biodiesel has heating value approximately 9% and 14% less than conventional diesel fuel (Magin Lapuerta et al, 2008), and (Magin Lapuerta et al, 2008). Therefore if the engine efficiency remains the same, then we should expect higher fuel consumption proportionately to compensate for the lost in heating value by mass. Many researchers have reported that there is no significant difference at which the engine converts the chemical energy of the fuel to mechanical energy, be it diesel fuel or biodiesel (Canakci, 2005), (Magin Lapuerta et al, 2008), (Michael S. Graboski et al, 1999). The brake specific fuel consumption (BSFC) is defined by

equation 25. It is inversely proportional to the fuel conversion efficiency. If the LHV of the fuel is constant, the BSFC varies inversely as the fuel conversion efficiency. Base on the review of 217 fuel consumption observations, the following correlations has been developed (EPA, 2002)

$$BSFC_B = BSFC_D e^{0.0008189.\%B} \tag{62}$$

The BSFC of the marine diesel fuel (MDO) and the different blends of biodiesel can be related to volume through its density. However, we are more interested in the energy per volume which can be related through the following equation.

$$Energy/Volume\left[MJ/m^3\right] = h_{LHV}\left[MJ/Kg\right].\rho\left[Kg/m^3\right] \tag{63}$$

Since common rail pressure is kept at a constant pressure of 1200 bar, the mass flow rate is also expected to be the same during experiments on the different fuels.

$$\dot{m}_{fD} = \dot{m}_{fB} \tag{64}$$

Therefore for the purpose of comparison a more realistic method will be comparing the brake specific energy consumption (BSEC). The BSEC is a product of the BSFC and the LHV of the fuel as shown in the equations below:

$$BSEC\left[MJ/KWh\right] = BSFC\left[kg/KWh\right].h_{LHV}\left[MJ/Kg\right] \tag{65}$$

From the experimental results of fuel consumption on the MDO, the BSEC of biodiesel ($BSEC_B$) can be related to the BSEC of diesel fuel through the following equation.

$$BSEC_B = BSFC_B.h_{LHV_B} \tag{66}$$

By using equation 66, the $BSEC_B$ can be shown to relate to the LHV of the fuel, the BSFC of the MDO and the percentage by volume of the biodiesel content in the blend (%B).

$$BSEC_B = BSFC_D e^{0.0008189\%B}.h_{LHV_B} \tag{67}$$

The brake power of the engine has been measured experimentally using the MDO. Brake power is related to the BSFC through the following equation:

$$P_D = \frac{\dot{m}_f}{BSFC_D} \tag{68}$$

In the same way, brake power of the engine using biodiesel fuel can be predicted by the following equation:

$$P_B = \frac{\dot{m}_f}{BSFC_B} \tag{69}$$

From equation 69, it be seen that the mass flow rate during the experiment will remain the same irrespective of the fuel used. Therefore the brake power of the engine using biodiesel can be expected to be influenced by only the BSFC. The brake power developed by the engine using biodiesel can therefore be predicted by the following equations:

$$P_B = P_D . \frac{BSFC_D}{BSFC_B} \tag{70}$$

$$P_B = P_D e^{-0.0008189\%B} \tag{71}$$

The brake fuel conversion efficiency (BFCE) is the ratio of the brake power to the fuel energy introduced into the combustions chamber otherwise referred to as Brake Specific Energy Consumption (BSEC). The BSEC is the product of the BSFC and the LHV of the fuel. It is acceptable to use brake power to determine the BSCE in experimental engine studies (Magin Lapuerta et al, 2008). The efficiency obtained can therefore be conveniently referred to as the brake specific efficiency. The BFCE using hydrocarbon diesel fuel is given in equation 25. Similarly, the BFCE for any renewable fuel and its blends can be represented by equation 72, provided a correction factor is applied to the LHV of the blends.

$$\eta_B = \frac{1}{BSFC_B . h_{LHV_B}} \tag{72}$$

Using similar arguments as in the prediction of the BSEC of biodiesel, the BFCE of biodiesel can be represented by equation 73.

$$\eta_B = \frac{1}{BSFC_D.e^{0.0008189\%B}.h_{LHV_B}} \quad (73)$$

The correlations for the prediction of the exhaust gas emission are based on empirical formulas developed by EPA. In their analysis to investigate the effect of biodiesel on $NO_x$, PM, CO and HC, (EPA, 2002) developed a basic correlation between biodiesel concentration in hydrocarbon diesel fuel and percentage change in emission:

$$\% \text{ change in emissions} = e^{(a*vol\%biodiesel)}*100\% \quad (74)$$

Where 'a' is a coefficient for each of the four exhaust emission gases. These coefficients are shown in table 20 and were found to be statistically significant at p = 0.05 level.

| Emission gas | Coefficient 'a' |
|---|---|
| $NO_x$ | 0.0009794 |
| PM | -0.006384 |
| HC | -0.011195 |
| CO | -0.006561 |

**Table 20: Coefficients for basic emission correlations (Source: (EPA, 2002))**

Although several researchers have reported increases in $NO_x$ emission (Canakci, 2005) and (Mohon, 2011), many others have showed varied results. These results varied from no changes to $NO_x$ emission in comparison to hydrocarbon diesel to slight decreases. This can generally be attributed to the type of engines used, the test modes adopted, the properties and source of the biodiesel and several other factors. These factors made the development of an accurate correlation of $NO_x$ emission between biodiesel and hydrocarbon diesel particular challenging. However, the correlation adopted by EPA (equation 75) has been found to be accurate at a significant level of 0.95. In reviewing observations on which the $NO_X$ correlation were based on, it was noted that 75% of the observations are soy-based and 13% RME with an average CN of 49.

$$NO_{x_B} = NO_{x_D} e^{0.0009794\%B} \tag{75}$$

Most researchers have found a reduction in HC emission as compared t hydrocarbon diesel fuel. The correlation shown in equation 76 has been found by some authors to result to as much as 70% mean reduction in HC emission as compared to emissions from hydrocarbon diesel fuel (Magin Lapuerta et al, 2008).

$$HC_B = HC_D e^{-0.011195\%B} \tag{76}$$

However, some researchers found no significant changes in HC emission from biodiesel as compared to hydrocarbon diesel (Slavinska, 2006). However, equation

76 seems to give a more generally realistic result and has been found to be accurate with a significant level of 0.95. Based on the arguments stated above the correlation of both CO and CO can be shown by equations 77 and 78 respectively.

$$CO_B = CO_D e^{-006561\%B} \tag{77}$$

$$CO_{2B} = CO_{2D} e^{0.0000177\%B} \tag{78}$$

# Chapter Six: Results and Discussion

## *6.1. Brake fuel conversion efficiency*

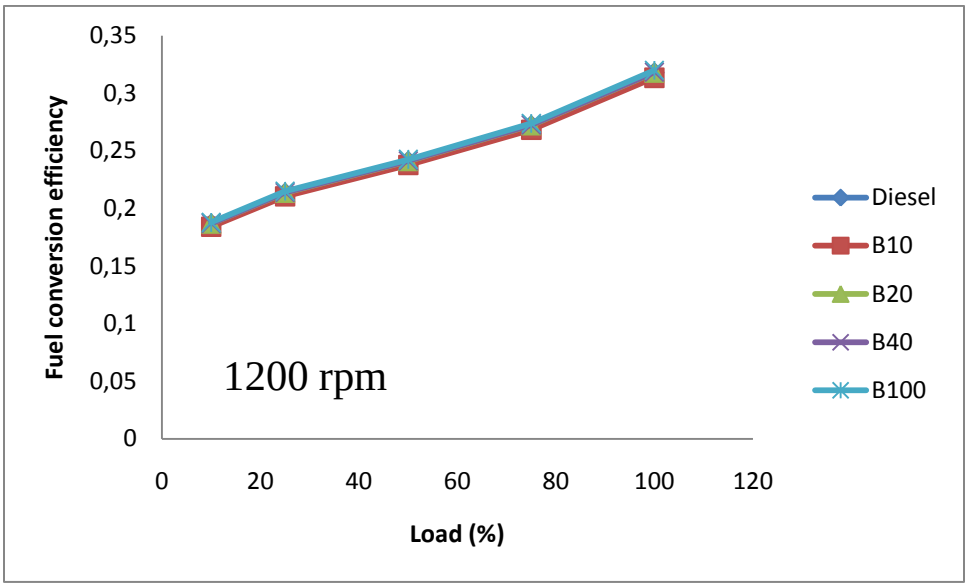


**Figure 82: Actual and estimated Brake fuel conversion efficiency with various renewable fuels and its blends**

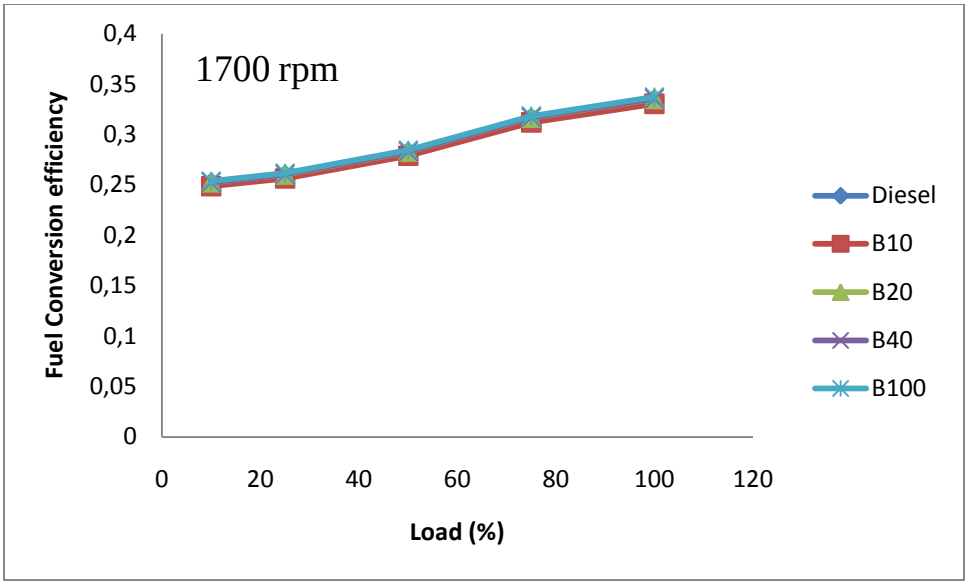


**Figure 83: Actual and estimated Brake fuel conversion efficiency with various renewable fuels and its blends**

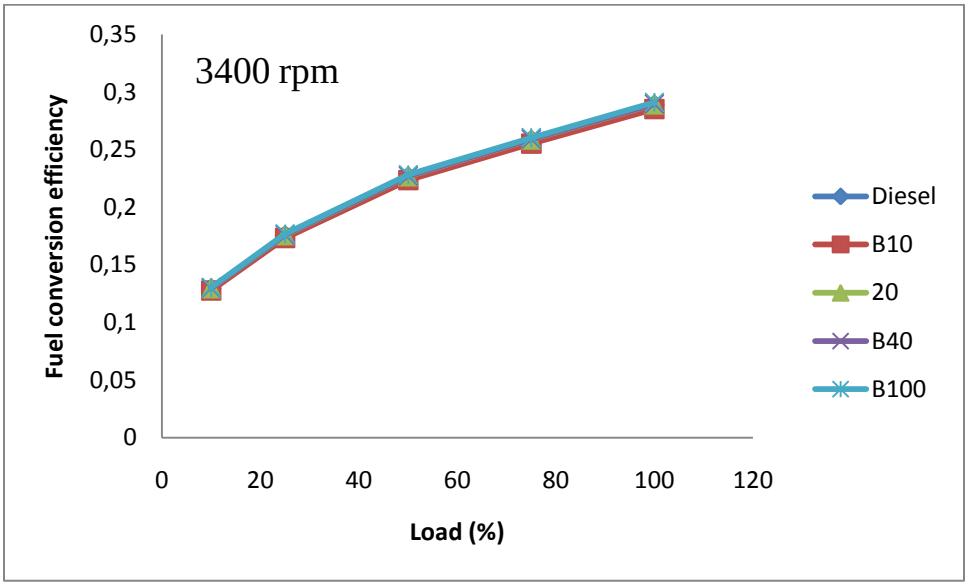


**Figure 84: Actual and predicted Brake fuel conversion efficiency with various renewable fuels and its blends**

Figures 83-84 depict the relationship between the fuel conversion efficiency and torque for three different speed levels. From the graphical presentations it can be observed that there are no significant changes in BFCE between the MDO and various blends of biodiesel. However, some increase can be observed in mean BFCE reported in table 21. The mean BFCE measured for the MDO during the experiment was 29.87% and the predicted mean values for B20 and B40 are 29.89% and 29.92% respectively. Similar results have been documented by some researchers. (Sakumar Puhan et al, 2004) reported measuring BFCE of 26.36% for hydrocarbon diesel fuel as compared to 26.42% for ethyle ester from mahua oil. (Rizalman Mamat et al, 2009) have measured Engine efficiency with Rape seed ME and ultra low sulfur diesel (ULSD) and they report that the engine efficiency of biodiesel to be 1.2%- 2% lower than ULSD. However, most authors, already cited in chapter five, have agreed that there are no significant change in the BFCE between hydrocarbon carbon diesel fuel and biodiesel with its blends.

| fuel type | BSFC (g/KWh) | %change in BSFC | BFCE | % change in BFCE | BSEC (KJ/KWh) | % change in BSEC |
|---|---|---|---|---|---|---|
| Diesel | 351,94 | - | 0,2550 | - | 14542 | - |
| LGO-10 | 381,97 | 0,82 | 0,2515 | -1,37 | 14745 | 1,39 |
| B20 | 357,75 | 1,65 | 0,2552 | 0,07 | 14194 | -1,16 |
| B40 | 363,66 | 3,33 | 0,2554 | 0,16 | 15061 | -2,34 |
| B100 | 354,83 | 8.53 | 0.2566 | 0.64 | 14897 | -0.64 |

**Table 21: Mean values and % change in BSFC, BSEC and BFCE**

Referring to table 21, it can be observed that the predicted mean BFCE for LGO-10 is 1.37% less than that of MDO. The main reason for this is because of differences between the base fuel of the LGO-10 and the MDO. The increase in BFCE of LGO-10 over the MDO can be attributed to a slight higher LHV of the LGO-10 than the latter. For the rest of the renewable fuels, the predicted results showed no significant difference in the BFCE.

## *6.2. Effect on brake specific fuel consumption*

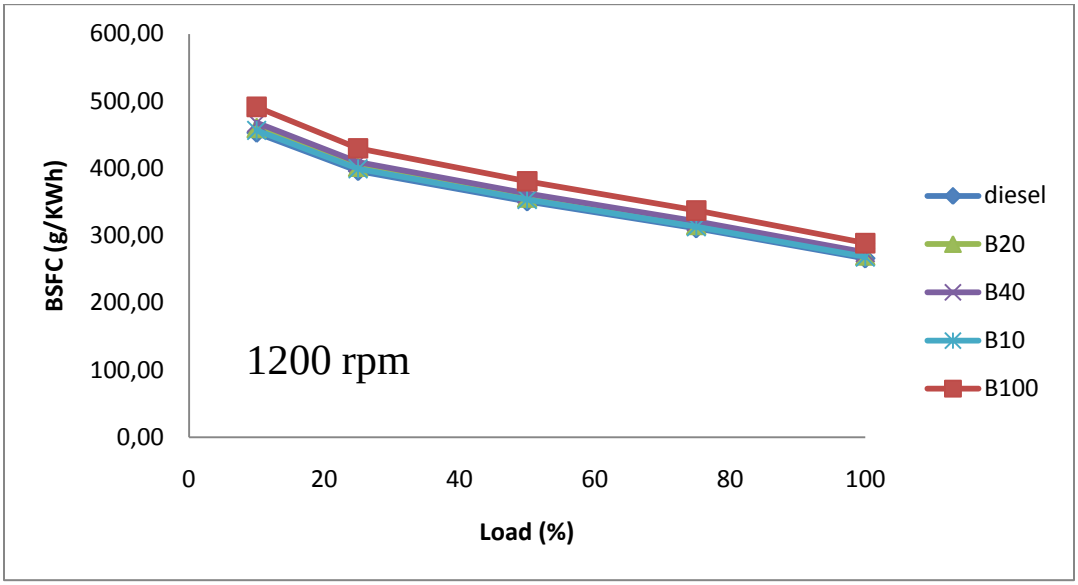


**Figure 85: Brake specific fuel consumption of diesel fuel and predicted values for biodiesel and its blends**

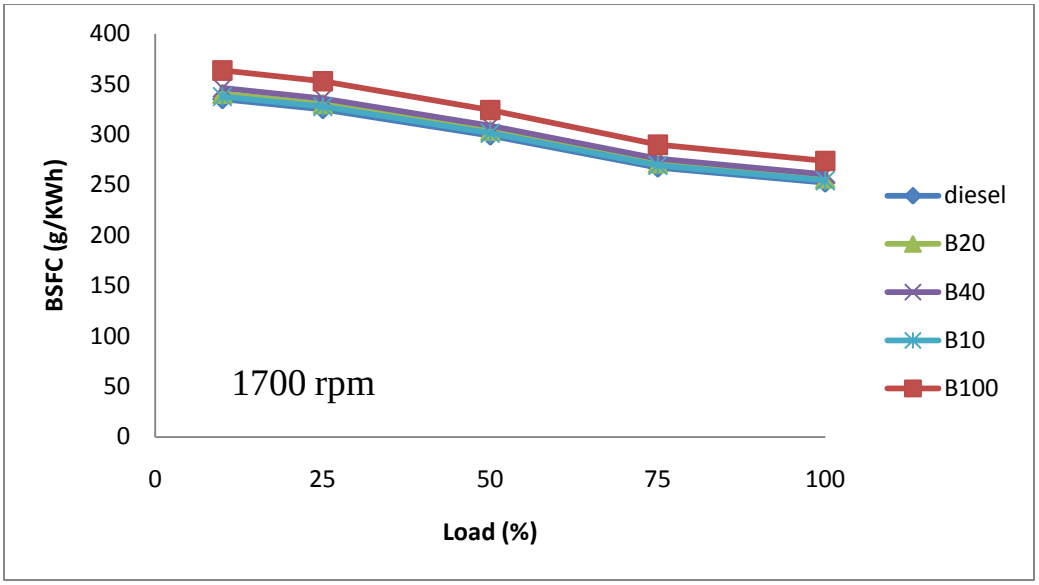


Figure 86: Brake specific fuel consumption of diesel fuel and predicted values for biodiesel and its blends

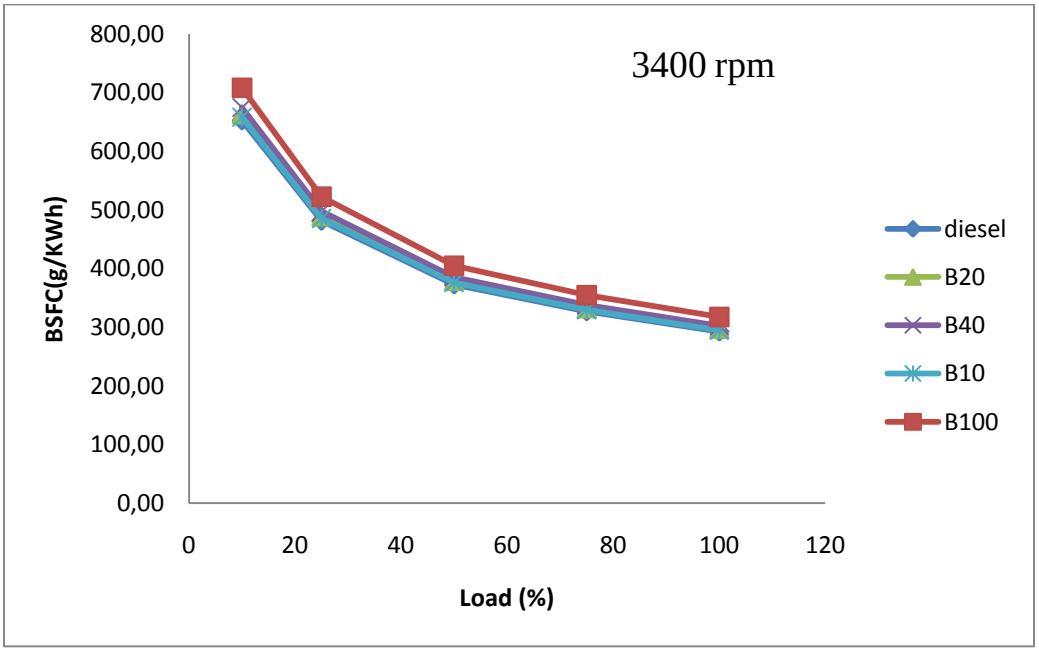


Figure 87: Brake specific fuel consumption of diesel fuel and predicted values for biodiesel and its blends

Figure 85-87 compare brake specific fuel consumption (BSFC) of MDO, LGO-10 and blends of various proportions by volume of rapeseed ME. The BSFC has been found to generally decrease sharply for all fuels at higher loads. This phenomenon is even more pronounced at medium and high speed conditions. This is understandable since there is relatively less proportion of heat loss around the cylinder walls at higher loads than lower loads. Therefore proportionately, less fuel is needed to attain a certain brake power at higher loads than at lower loads. This is also an indication that compression ignition engines run more efficiently at higher loads than at lower loads. At 1700 rpm the BSFC for diesel fuel decreases from 335 g/KWh at low load to 252 g/KWh at full load and for LGO-10, the BSFC decreases from 338 g/KWh at low load to 254 g/KWh at full load condition.

The BSFC is observed to increase as the proportion of the biodiesel fuel in the blend increases. The average BSFC of 351.94 g/KWh has been measured for the MDO during the experiment. The predicted mean BSFC of LGO-10 is 381.97 g/KWh representing an average increase of 0.82%. The predicted mean BSFC for B20, B40 and B100 was 1.65%, 3.33% and 8.53% respectively. The increase in the BSFC is anticipated as the contribution of biodiesel in the blends of B20, B40 and the neat RME will result to a less LHV of these fuels. As a result more fuel is required to develop the same brake power produced by the MDO during the experiment. However, since the LGO-10 has a higher LHV, this predicted result may not be realistic.

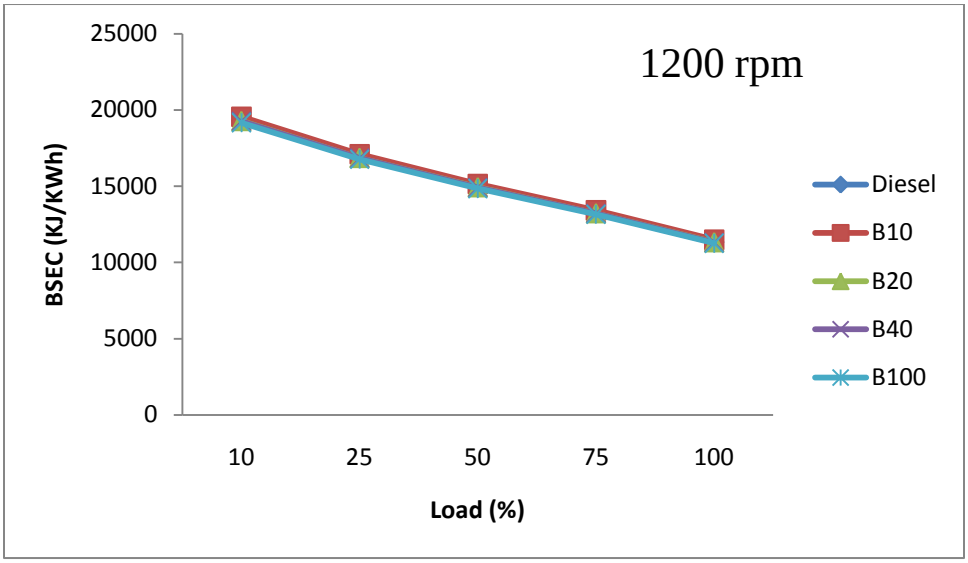


**Figure 88: Brake specific energy consumption of diesel fuel and predicted values for biodiesel and its blends**

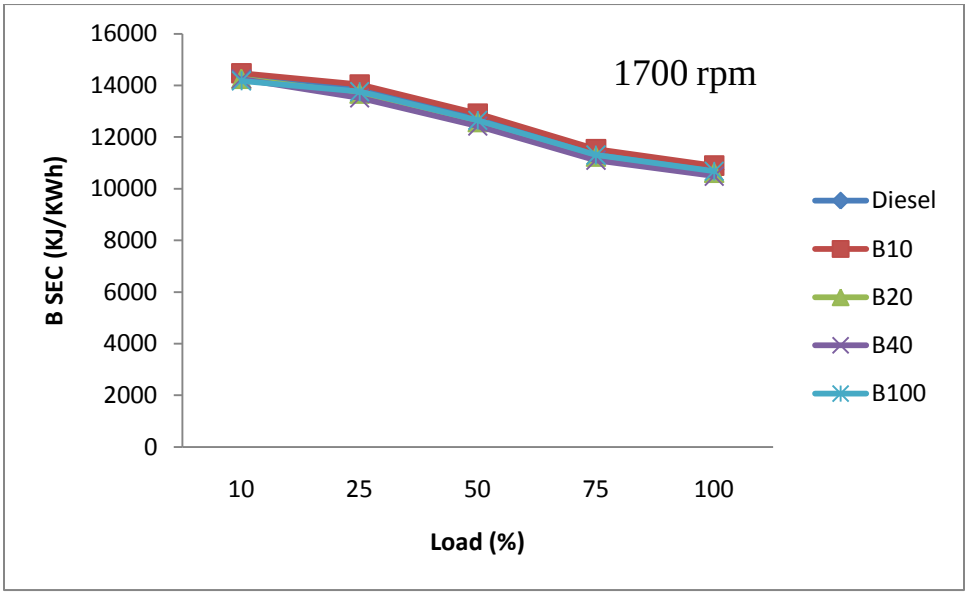


**Figure 89: Brake specific energy consumption of diesel fuel and predicted values for biodiesel and its blends**

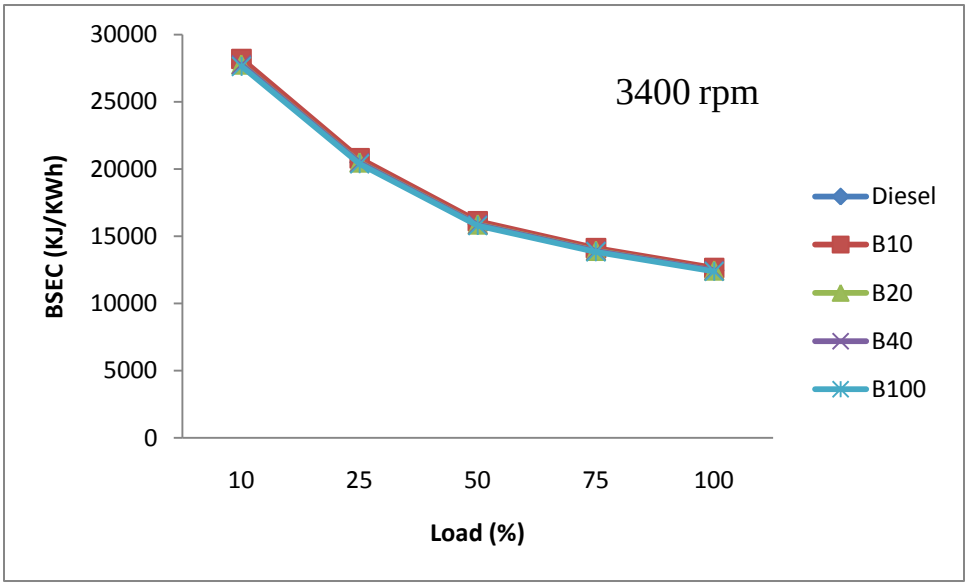


**Figure 90: Brake specific energy consumption of diesel fuel and predicted values of various blends of biodiesel**

However, given the LHV of the MDO and the biodiesel blends, a more realistic comparison will be the brake specific energy consumption (BSEC). Examining the percentage changes in BSFC and BSEC of the experimental MDO and the blends of biodiesel, the difference in the comparison of the two performance parameter is apparent. The predicted BSEC of LGO-10 has increased by 1.39% as against the prediction of 0.82% in the BSFC it can be concluded that this contribution is as a result of the differences in the LHV of the two fuels and the importance of the energy content of the fuel and not necessarily pulse width alone. However, the predicted values of BSEC for the blends of biodiesel B20 and B40 have decreased by 1.16% and 2.34% respectively. This is as a result of the increasing amount of the rapeseed methyl ester (RME) present in the blend which exhibit less LHV.

## 6.3. *Effect on power and torque*

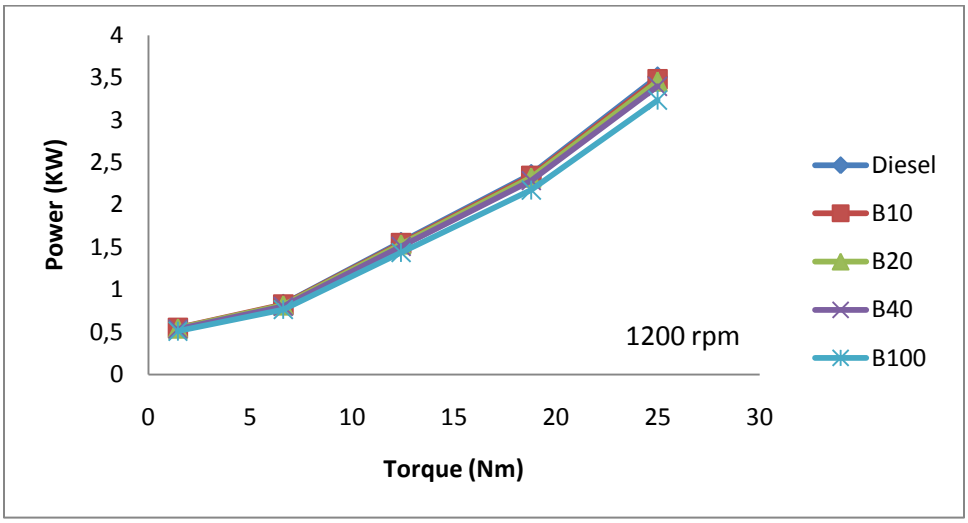


**Figure 91: Actual and predicted power as a function of torque with various renewable fuels and its blends**

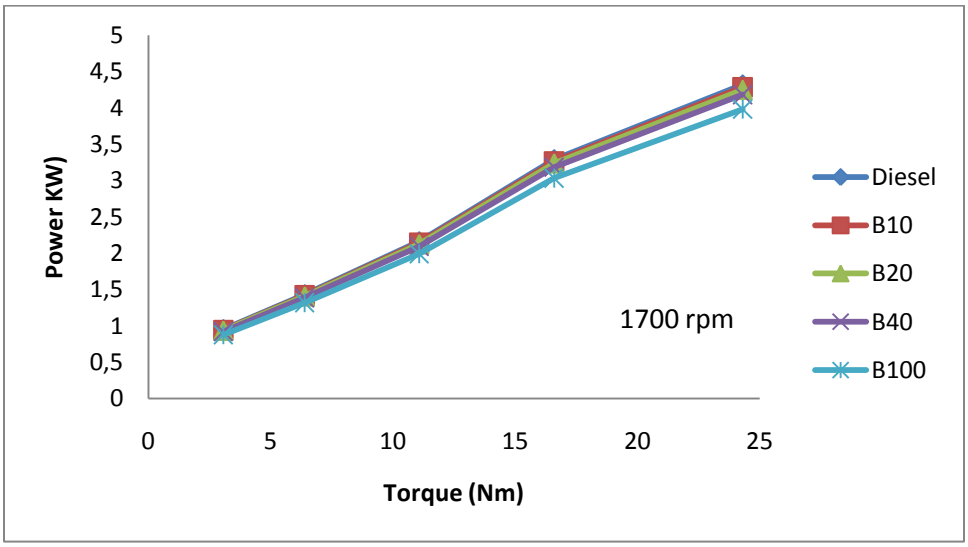


**Figure 92: Actual and predicted power as a function of torque with various renewable fuels and its blends**

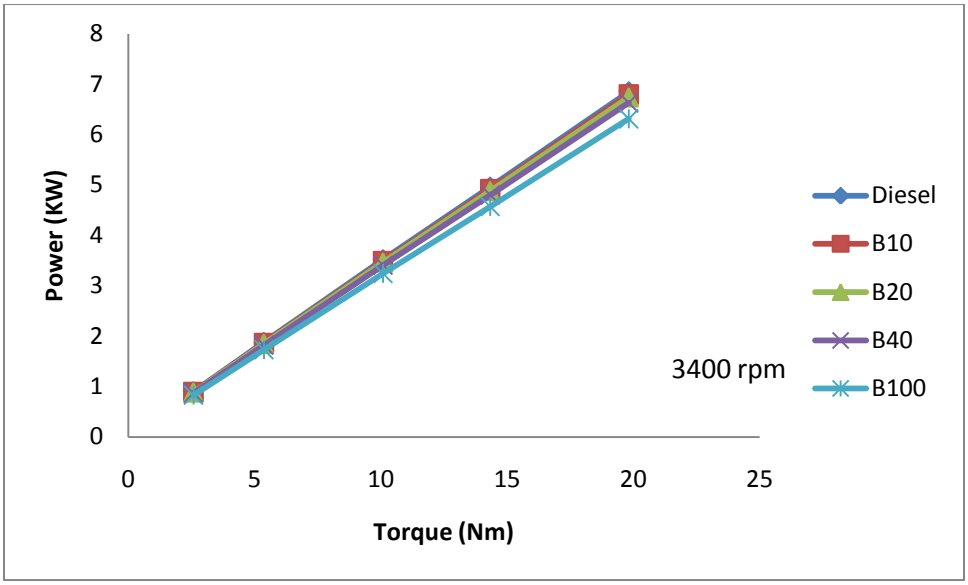


Figure 93: Actual and predicted power as a function of torque with various renewable fuels blends

Figures 91-93 show the variation of brake power as a function of torque for MDO and biodiesel (LGO-10), a blend of 10% by volume of biodiesel and 90% by volume of diesel fuel (B20) and a blend of 60% diesel fuel with 40% biodiesel (B40). From the three graphical presentations it is observed that the brake power and the predicted values increases for all fuels as the brake torque increases.

| Fuel type | Max brake power at max speed | %change in brake power | Max brake power at mid speed | %change in brake power | Max brake power at low speed | %change in brake power |
|---|---|---|---|---|---|---|
| Diesel | 6,85 | - | 4,32 | - | 3,51 | - |
| LGO-10 | 6,79 | -0,88 | 4,28 | -0,93 | 3,48 | -0,85 |
| B20 | 6,74 | -1,61 | 4,25 | -1,62 | 3,45 | -1,71 |
| B40 | 6,63 | -3,21 | 4,18 | -3,24 | 3,4 | -3,13 |
| B100 | 6,31 | -7,86 | 3,98 | -7,86 | 3,23 | -7,86 |

Figure 94: change in maximum brake power at various speeds

At maximum load a reduction in power of 0.85% at low speed and 0.88% at high speed has been observed in the graphical presentation between diesel fuel and the predicted values of LGO-10. The lost in power at maximum load when using B20 is only 1.71% at low speed and 1.61% at high speed. The B100 seems to be affect more in terms of power reduction, exhibiting power lost of as high as 7.86% at maximum power for all three speed levels.

## *6.1. Exhaust emission characeristics*

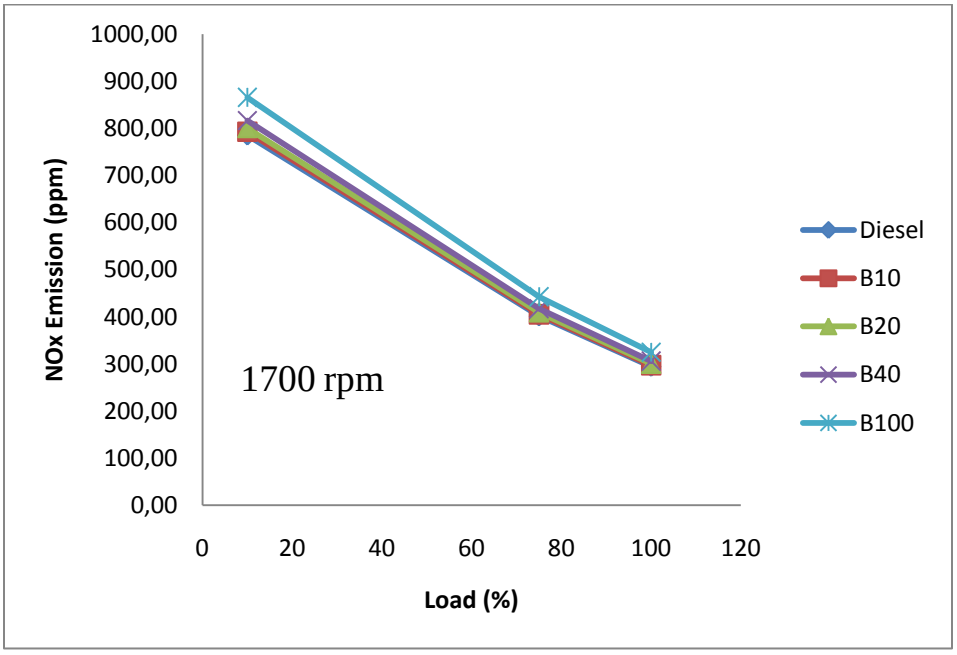


**Figure 95: Actual $NO_x$ emission from diesel and predicted emission from blends of biodiesel**

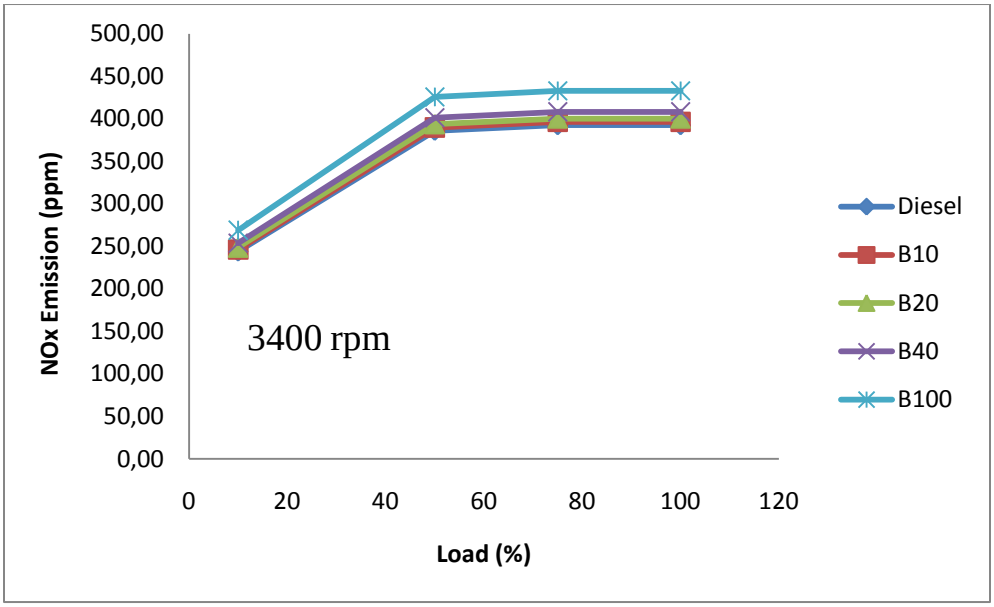


**Figure 96: Actual $NO_x$ emission from diesel and predicted emission from biodiesel and its blends at 3400 rpm**

Figures 95 and 96 showed the comparison of actual nitrogen oxide ($NO_x$) emissions from MDO and predicted $NO_x$ emission from various blends of biodiesel with torque. The graphs show that there is an increase in $NO_x$ emission as the content of biodiesel fuel content in the blend increases. Table 22 shows the mean values of measured and predicted emissions. The mean increase between the measured mean $NO_x$ emission from MDO and the predicted emission from the LGO-10 was 0.98%. This is as a result of a higher amount of oxygen content in biodiesel which supports a fairly complete combustion thus resulting in high combustion temperature inside the cylinder which supports the production of $NO_x$. Thus the formation of $NO_x$ is supported both by properties of the biodiesel content in the blend and thermal processes.

| fuel type | Mean Nox | % change | Mean CO | % change | Mean CO2 | % change | Mean HC | % change |
|---|---|---|---|---|---|---|---|---|
| Diesel | 414 | - | 658 | - | 2,9 | - | 30,27 | - |
| LGO-10 | 418 | 0,98 | 616 | -6,35 | 2,7 | -6,35 | 27,06 | -10,59 |
| B20 | 422 | 1,98 | 577 | -12,30 | 2,6 | -12,30 | 24,20 | -20,06 |
| B40 | 430 | 4,00 | 506 | -23,08 | 2,3 | -23,08 | 19,34 | -36,10 |
| B100 | 456 | 10,29 | 341 | -48,11 | 1,5 | -48,11 | 9,88 | -67,36 |

Table 22: Mean and predicted values of emissions

It is known that $NO_x$ emissions are influenced atomization of the injected fuel in the cylinder and the adiabatic flame temperature. The spray formation depends on the fuel droplet size, its momentum, the degree of mixing with air, the level of penetration inside the cylinder, the evaporation rate and the radiant heat transfer (Sakumar Puhan et al, 2004). The predicted $NO_x$ emissions are higher for the blends of the renewable fuels than the MDO. This is because RME has a higher density than the MDO and this affects the spray formation, fuel penetration, level of mixing with air and the droplet size. Invariably higher combustion temperatures are expected which in turn increase the $NO_x$ emission. The injection timing is also expected to be advanced with the use of the blends resulting to higher combustion temperatures. The trend from the graph suggests that $NO_x$ emission maybe stagnated irrespective of increases in engine load. We can observe sharp increases in $NO_x$ production from 10% load to 50% load but appears to be relatively constant at higher loads.

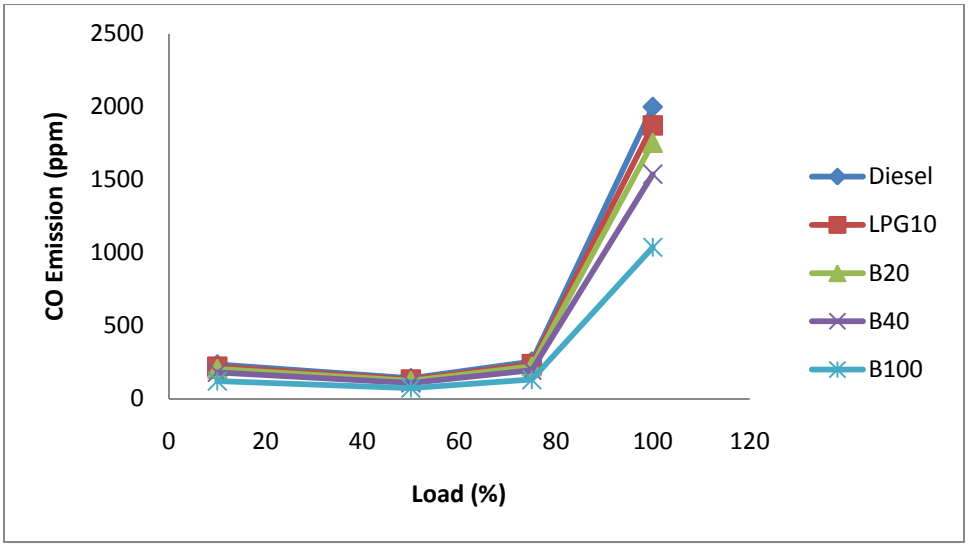


**Figure 97: Carbon monoxide emission of marine diesel fuel with predicted values of renewable diesel blends**

Figure 97 shows the variation of carbon monoxide (CO) emissions as a function of load of different fuel combinations at 3400 rpm. The predicted values showed in the graphical presentation shows that the CO emission decreases with increasing proportion of biodiesel content in the fuel. At low load the difference between the CO emission of the MDO and all the blends are low but significant increase at high load. This is can be attributed to the fact that biodiesel contain oxygen atoms which help in attaining complete combustion at high load where combust is most efficient and as a result produce less CO emission.

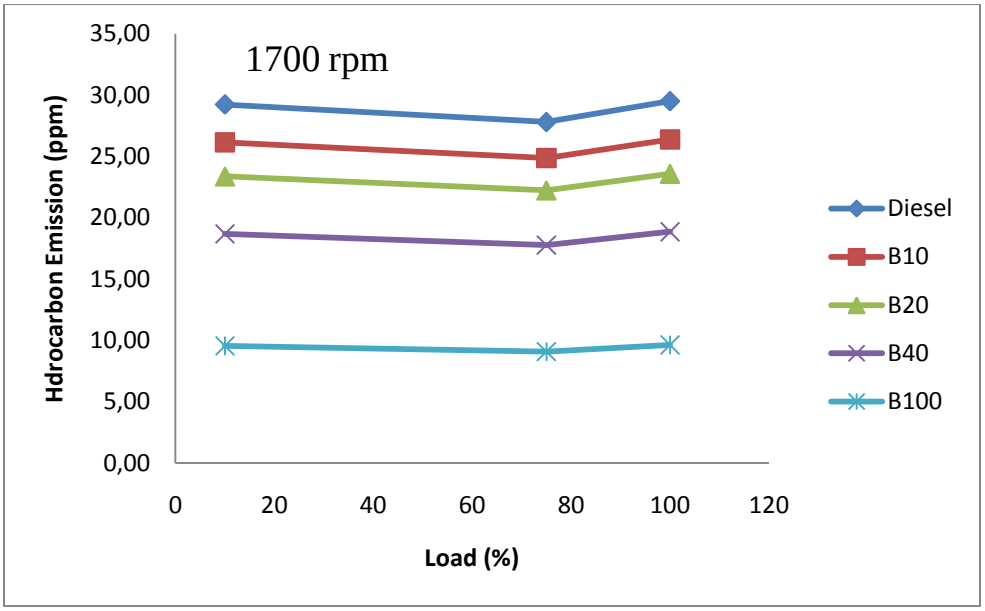


Figure 98: Hydrocarbon emission of diesel fuel and predicted values for biodiesel and its blends

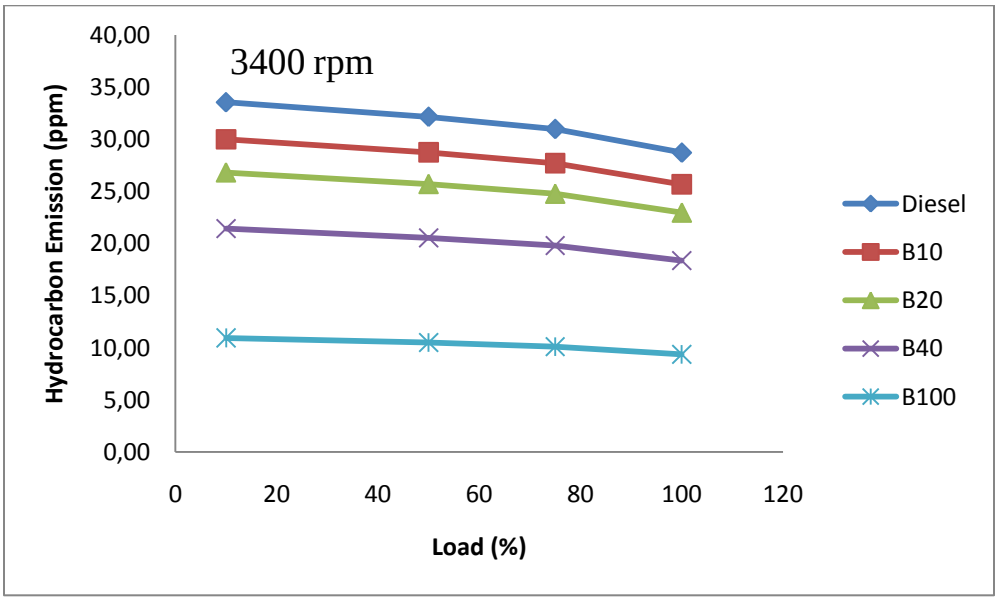


Figure 99: Hydrocarbon emission of diesel fuel and predicted values for various blends of biodiesel

Figure 98 and 99 shows the variation of marine (HC) emission of different fuel combinations with brake torque is shown. It is evident from the graphical representation that the HC emission is reduced with the increase of biodiesel content in the fuel. The mean reduction between the measured mean HC emission from MDO and the predicted HC emission from the LGO-10 was 10.59%. As explained earlier, HC emission depends on the combustion efficiency and the physical properties of the fuel. The presence of oxygen atom contributed by the biodiesel may have also led to a complete combustion of the fuel. Biodiesel have a high CN than diesel fuel, since the CN has an influence on the ignition delay period, HC and CO emissions are also affected by the CN of the fuel. Fuels with higher CN seem to exhibit lower HC and CO emissions. From table 19 it can be established that the CN for LGO-10 and RME are higher by 23.2% and 16.4% respectively. These results are consistent with the results shown by several authors (Canakci, 2005), (Sakumar Puhan et al, 2004) and (Jai-houng Leu, 2009).

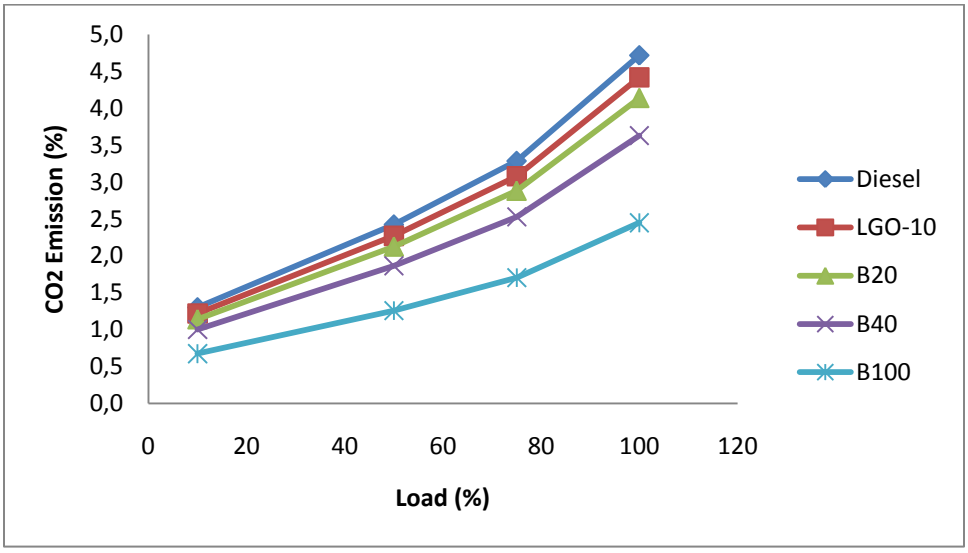


Figure 100: actual and prediction values of $CO_2$ emission as a function of load

Figure 100 shows $CO_2$ emission from experimental results of MDO and the predicted results of RME and its blends. It can be observed that the $CO_2$ emission decreases as the amount of biodiesel in the blend increase. This can also be attributed to the oxygen atoms present in the biodiesel which supports complete combustion and thus less $CO_2$ emission.

# Chapter Seven: Conclusion

Experimental investigation has been done with the Ricardo hydra research engine using MDO to investigate the effect of the fuel on the performance and emission characteristic of the engine. Preliminary results have been used to analyze the stability of the engine and it measurement systems using ANOVA. The analysis of the results showed that the stability of the engine and its measurement system are within acceptable limits. The assessment of the RSD of the measured data showed that the qualities of most of the measurement are within the permissible deviations set by table 4 of ISO 15550:2002(E) within a confidence level of 0.95.

However, the BSFC, Exhaust temperature and $NO_x$ emission at some load points are beyond the permissible deviations. The ANOVA results showed that there is a good repeatability of measurement with minor deviations due mainly to variations in the atmospheric pressure and the presence of few outliers which existence are not well defined. This is evident in the analysis of the Boxplots and the individual value plots shown in chapter 4.

The correlation between the experimental results of the MDO and the predicted results of biodiesel showed that from a technical viewpoint the suitability of biodiesel as an alternative fuel for compression ignition engines is not subjected to controversy. Its performance and emission characteristics are very much comparable with those of the MDO. This has been demonstrated through the analysis of the performance and emission data collected during the experiment and its correlation with the predicted values. Close comparison of the experimental BSFC and the predicted values of the various renewable blends showed a good

correlation with a penalty in BSFC of only 0.82% increase when using PGO10. As the content of the biodiesel in the renewable fuel increases, the predicted values for B20 and B40 further increased by 1.65% and 3.33% respectively.

The increase of biodiesel content in the renewable blend mainly resulted to reduction in power. The reason for this was mainly as a result of less LHV of biodiesel in the content. Lost in power was however, minimal with only 0.85% at low speed and 0.88% at high speed observed in the predicted results of LGO-10 at maximum load. The predicted lost in power at maximum load when using B20 is only 1.71% at low speed and 1.61% at high speed. However, considering increase in LHV of 0.6% for LGO-10 and a reduction of 8.5% for RME. There results therefore may not only be attributed to differences in LHV. The lost in power of only 1.71 and 1.61% as compare to a reduction of almost 8.5% in LHV of the RME can be attributed to the synergistic effect of the combination of the two blends. Example the contribution of oxygen atoms from the RME for a more efficient combustion and a contribution of a LHV of the diesel fuel in the blend. The B100 seems to be affect more in terms of power reduction, exhibiting power lost of as high as 7.86% at maximum power for all three speed levels. When compared with differences in LHVs of the two fuels, it seems likely that there is no significant difference between the MDO and the RME in terms of energy content.

The average BSFC of the LGO-10 has been predicted to increase by 0.82% as compared to the MDO. However, considering the LHV of the LGO-10, this prediction may not be realistic. The predicted mean BSFC for B20, B40 and B100 was 1.65%, 3.33% and 8.53% respectively. This may be attributed to the contribution of biodiesel in the blends resulting to a less LHV of these fuels. As a

result more fuel is required to develop the same brake power produced by the MDO during the experiment. This predicted result also shows a good correlation in terms of energy content considering the LHV of the RME is about 8.5% less than that of MDO. This result is in agreement to the results reported by (Cafer Kaplan et al, 2006)

The mean increase between the measured mean $NO_x$ emission from MDO and the predicted $NO_x$ emission from the LGO-10 was 0.98%. This may be attributed to higher amount of oxygen content in biodiesel which supports a fairly complete combustion thus resulting in high combustion temperature inside the cylinder which supports the production of $NO_x$. Thus the formation of $NO_x$ is supported both by properties of the biodiesel content in the blend and thermal processes.

The mean reduction between the measured mean HC emission from MDO and the predicted HC emission from the LGO-10 was 10.59%. This was expected as HC emission depends on the combustion efficiency and the physical properties of the fuel. The presence of oxygen atom contributed by the biodiesel may thus have also led to a complete combustion of the fuel. Since the CN has an influence on the ignition delay period, HC and CO emissions are also affected by the CN of the fuel. Fuels with higher CN seem to exhibit lower HC and CO emissions. It can be seen from table 19 that the CN for LGO-10 and RME are higher by 23.2% and 16.4% respectively.

From the analysis of the evidences presented in this study it can be concluded the research fuels; RME and its blends can be a viable alternative fuel for DI-CI engines without any significant modification.

## *Future work*

It must be emphasized the predicted results and the analysis are based on the data acquired during the experiment and the information available regarding the test fuels complimented by those found in literature. Every precaution has been taken to ensure accuracy of data. A wide variation of results regarding emission of biodiesel maybe found in literature mainly as a result of several different factors. Possible explanations for these differences maybe the use of varying emission test mode, different engine operating conditions, variant measurement technologies and procedure etc. however, there seems to be a dominant trend among researchers which is to a certain degree consistent with the results presented in this study. However, the results presented by this study are not conclusive and actual experimental work is required on the renewable blends to validate the results presented here.

# Bibliography

(n.d.). Retrieved from US Department of Energy: //www1.eere.energy.gov

15550, I. S. (2002). *ISO 15550: Internal Combustion Engines- Determinationand Method for the measurement of engine power- General requirements.* geneva: ISO.

Andre Valente Bueno et al, J. A. (2009). A new engine indicating neasurement procedure for combustion heat release analysis. *Applied Thermal Engineering* , 1657-1675.

Anyon, P. (2008). Managing diesel particle emissions through engine maintenance -an Australian perspective. Queensland, Autrialia.

Ardito et al, D. L. (1995). Biodiesel fuelled IDI Engines: Performance, Emission and Heat release Investigation. *Bioresource Technology* , 53-59.

Bai-Fu Lin et al, J.-H. H.-Y. (2008). Effect of Biodiesel from Palm Kernel Oil on the Engine Performance, Exhaust Emissions and Combustion Characteristicsof a Direct Injection Diesel Engine.

Bell, S. (1999). *A Beginner's Guide to Uncertainty of Measurement.* Middlesex: National Physical Laboratory.

Cafer Kaplan et al, R. A. (2006). Performance Characteristics of Sunflower Methyl Ester as Biodiesel. *Energy Sources, Part A* , 751-755.

Canakci, M. (2005). Performance and emission charactriastics of biodiesel from soybean oil. *Proceedings of the Institute of Mechanical Engineers, Part D: Journal of Automobile Engineering* , 915- 922.

D.E. Winterbone, D. Y. (1994). *Quantitative Analysis of Combustion in High-speed Direct Injection Diesel Engines.* Manchester: International Symposium COMODIA 94.

David B. Kittelson, W. F. (1999). *Review of Particle Matter Sampling Methods.* Minneapolis, MN: University of Minnesota.

DJ Timoney et al, J. D. (2005). The development of a semi-empirical model for rapid NOx concentration evaluation in diesel engines. *Proceedings of Institute of Mechanical Engineers, Part D: Journal of Automobil engineering* , 215-621.

Dunn, R. O. (2002). Low- Temperature flow properties of vegetable oil/ Cosolvent blend diesel fuels. *Journal of American Chemists' Society* , 709-715.

EPA, U. E. (2002). *A Comprehensive Analysis of Biodiesel Impacts on Exhaust Emission.* Washington D.C: Office of Transport and Air Quality.

Evans, R. (2009). Extending the Lean Limit of Natural-Gas Engines. *Journal of Engineering for Gas Turbines and Power* , Vol. 131 / 032803-3.

F Halek et al, A. K. (2009). Biodiesel as an Alternative Fuel for Diesel Engines.

H. Raheman et al, S. G. (2008). Performance of diesel engine with biodiesel at varying compression ratio and ignition timing.

H. Raheman et al, S. G. (2009). Performance of diesel engine with biodiesel at varying compression ratio and ignition timing. *FUEL* , 2659-2666.

Henein, N. A. (2006). *Army Research Office and Air Force Office of Scientific Research Contractors' Meeting in Chemical Propulsion Held in Arlington, Virginia on June 12-14, 2006: Advance control of diesel engines.* Virginia.

Heywood, J. B. (1998). *Internal Combustion Engines Foundamentals.* New York: McGraw-Hill, New York.

J. Van Gerpen et al, B. S. (2004). *Biodiesel Production Technology.*

Jai-houng Leu, M.-Y. H. (2009). Aternative Fuel Test Study of an Diesel Engine Fed by Synthetic Fuel Derived from Waste Bilge Oil. *Journal of Marine Science and Technology* , Vol. 17, NO.1 PP 7-12.

Jawara, L. (2010). *Renewable diesel fuels effects on performance of performance of diesel engines.* Trondheim.

Joshua A. Bittle at al, J. K. (2010). Biodiesel Effect on Influencing Parameter of Brake Fuel Conversion Efficiency in a Medium Duty Diesel Engine. *Journal of Engineering for Gas Turbines and Power* , Vol. 131 / 122801-1.

Kittelson, D. B. (2000). *Measurement of Engine Exhaust Particle size.* California.

Knothe, G. (2005). Dependence of biodiesel fuel properties on the structure of fatty acid alkyl esters.

Koji Yamane et al, A. U. (2001). Influence of Physical and Chemical Properties of Biodiesel Fuel on Injection, Combustion and Exhaust Emission Characteristics in a DI-CI Engine. *The Fifth International Symposium on Diagnostic and Modlling of Combustion in Internal Combustion Engines* (pp. 402-409). Nagoya: COMODIA.

Kreyszig, E. (2006). *Advanced Engineering Mathematics.* Columbus, Ohio.

Ltd, H. *Portable Gas Analyzer: HORIBA Manual.* Kyoto: HORIBA Ltd.

M&C. (2011, February 22). *Challenging projects*. Retrieved 03 15, 2011, from Delf University of Technology: http://www.tudelft.nl/live/pagina.jsp?id=c6332c13-dd11-41d7-b21b-961d9377fa4d&lang=en

Magin Lapuerta et al, O. A.-F. (2008). Effect of Biodiesel fuels on diesel engine emissions. *Progress in Energy and Combustion Science* , 198-223.

MAN. (n.d.). Exhaust Gas Emission Today and Tomorrow.

Materials, A. S. (2001). *ASTM D 6751.*

Michael S. Graboski et al, R. L. (1999). *EFFECT OF BIODIESEL COMPOSITION ON NOX AND PM EMISSIONS FROM A DDC SERIES 60 ENGINE.* Colorado.

Mohon, R. M. (2011). Performance and Emission of a Diesel Engine Fuelled by Diesel-bioddiesel Blends with Special Attention to Exhaust Odor. *Canadian Journal of Mechanical Science and Engineering* , Vol 2 1-9.

N.K. Miller Jothia et al, G. N. (2006). xperimental studies on homogeneous charge CI engine fueled with LPG using DEE as an ignition enhancer.

Patro, T. N. (1993). COMBUSTION STUDY OF HYDROGEN FUELED DI DIESEL ENGINE: Simplified Heat Release Analysis. Vol. 18, No. 3, pp. 231-241,.

Rizalman Mamat et al, N. R. (2009). Effect of Air Intake Pressure Drop on Performance and Emissions of a Diesel Engine Operating with Biodiesel and Ultra Low Sulphur Diesel (ULSD). *International Conference on Renewable Energies and Power Quality (ICREPQ'09).* Valencia: European Association for the Development of Renewable Energies, Environment and Power Quality.

Ronald E. Walpole, R. H. (2002). *Propability and Statistics for Engineers and Scienctists.* New Jersey: Pearson Prentice Hall.

Sakumar Puhan et al, N. V. (2004). Performance and emission study of Mahua oil (madhuca indica oil) ethyl ester in a 4-stroke natural aspirated direct injection diesel engine. *Renewable Energy* , 1269-1278.

Sathaporn Chuepeng et al, C. K. (2010). Thermodynamic Properties of Gas Generated by Rapeseed Methyl Ester-Air Combustion Under Fuel-Lean Conditions. *Kasetsart ournal* , 308-317.

Slavinska, G. L. (2006). The effect of rapeseed oil methyl ester on direct injection diesel engine performance and exhaust emission. *Energy Conversion and Management* , 1954-1967.

Standard, I. (2006). *ISO 3046-3- Reciprocating internal combustion engines- Performance- Part 3: Test measurement.* Geneva: ISO.

Standard, I. (2006). *ISO 8178-1-Reciprocating internal combustion engines- Exhaust emission measurement- Part 1: Test-bed measurement of gaseous and particulate exhaust emission.* Geneva: ISO.

Standard, I. (2007). *ISO 8178-4: 2006, 2007-Reciprocating Internal Combustion Engines- Exhaust Emission Measurements- Part 4: Steady -state test cycle for different engine applications.* Geneva: ISO.

T. H Gouw, J. C. (1966). Physical Properties of Fatty Acid Methyl Esters. VI. Viscosity. *Journal of American Society of Chemists* .

Takai, M. (2005). Stroke by Stroke Measurement and Analysis of Cylinder Pressure on Board . *Proceedings of the 7th International Symposium on Marine Engineering* . Tokyo.

Thomas R. Karl et al, K. E. (2003). Modern Global Climate Change. *Science* , 1719-1723.

Tiegang Fang, Yuan-Chung Lin, Tien Mun Foong andd Chia-fon Lee. (2008). *Effect of Biodiesel on the Performance and Combustion Parameters of a Turbocharged Compression Ignition Engine .*

UKAS, U. k. (2007). *M3003 The Expression of Uncertainty and Confidence in Measurement.* Middlesex: UKAS.

Unknown. *MINITAB User's Guide 2.*

V. Nagaraju et al, N. H. (2008). Effect of Biodiesel B-20 on Performance and Emission in a Single Cylinde rHSDI Diesel Engine. *CI ENgine Performance for use with Alternative Fuels, 2008 (SP-2176).* Detroit: SAE International.

Valland, H. (2010). Dynamic Cylinder Pressure and rate of heat release . In *TMR9 Internal combustion engines, Advance course* (pp. 1-20). Trondheim.

Valland, H. (February 2010). *Dynamic State Equations for Air Cycles.* Trondheim.

Wikipedia. (n.d.). *wikipedia.com*. Retrieved from http://en.wikipedia.org/wiki/Thorntons#Notable_products

Yadav et al, P. K. (2010). Performance test of palm fatty acid biodiesel on compression ignition engine.

Yinnan YUAN et al, D. M. (2008). Combustion and Emission of the Diesel Engine using Biodiesel Fuel.

Yusuf Ali, Milford A. Hanna and Joseph E. Borg. *Effect of Alternative Diesel Fuels on Heat Release Curves for Cummins N14-410 Diesel Engines.*

This page is blank

Appendix A

# Statistical data for performance measurement

Statistical data for exhaust measurements at high load

| Time | Trial 1 | Trial 2 | Trial 3 | Trial 4 | Trial 5 | Trial 6 | Trial 7 | Trial 8 | Trial 9 | Sum | Mean | Variance | Standard deviation |
|---|---|---|---|---|---|---|---|---|---|---|---|---|---|
| Sec | Deg C | Deg C | Deg C | Deg C | Deg C | Deg C | Deg C | Deg C | Deg C | $\sum Y$ | $\bar{Y}$ | $\sigma^2$ | $\sigma$ |
| 3 | 627,52 | 647,81 | 662,12 | 641,70 | 654,13 | 663,50 | 521,88 | 543,31 | 556,40 | 5518,37 | 613,15 | 3157,74 | **56,19** |
| 7 | 629,17 | 648,93 | 662,74 | 642,34 | 655,25 | 663,47 | 523,35 | 544,03 | 556,87 | 5526,15 | 614,02 | 3144,47 | 56,08 |
| 11 | 630,54 | 649,87 | 663,51 | 642,87 | 656,68 | 664,01 | 524,76 | 544,75 | 557,27 | 5534,26 | 614,92 | 3142,29 | 56,06 |
| 15 | 632,07 | 650,85 | 664,08 | 643,77 | 657,38 | 664,44 | 526,01 | 545,52 | 557,80 | 5541,91 | 615,77 | 3133,16 | 55,97 |
| 19 | 633,26 | 651,52 | 664,38 | 644,33 | 657,99 | 664,84 | 527,15 | 546,28 | 558,31 | 5548,07 | 616,45 | 3116,67 | 55,83 |
| 23 | 634,19 | 652,38 | 664,57 | 644,86 | 658,49 | 665,07 | 528,29 | 546,97 | 558,80 | 5553,61 | 617,07 | 3097,56 | 55,66 |
| 27 | 635,54 | 653,00 | 664,36 | 645,42 | 658,81 | 665,15 | 529,30 | 547,60 | 559,28 | 5558,47 | 617,61 | 3074,01 | 55,44 |
| 31 | 636,52 | 653,43 | 664,23 | 646,14 | 659,20 | 665,78 | 530,32 | 548,26 | 559,77 | 5563,66 | 618,18 | 3056,16 | 55,28 |
| 35 | 637,30 | 654,26 | 664,03 | 646,77 | 659,59 | 666,29 | 531,38 | 548,98 | 560,14 | 5568,74 | 618,75 | 3038,19 | 55,12 |
| 39 | 638,58 | 654,93 | 664,13 | 647,59 | 660,02 | 666,65 | 532,41 | 549,57 | 560,57 | 5574,45 | 619,38 | 3026,55 | 55,01 |
| 43 | 639,59 | 655,46 | 664,23 | 648,13 | 660,29 | 666,78 | 533,40 | 550,15 | 561,00 | 5579,02 | 619,89 | 3007,36 | 54,84 |
| 47 | 640,17 | 655,82 | 663,96 | 648,66 | 660,42 | 666,56 | 534,38 | 550,69 | 561,47 | 5582,13 | 620,24 | 2975,52 | 54,55 |
| 51 | 640,44 | 656,42 | 664,43 | 649,22 | 660,82 | 666,48 | 535,36 | 551,18 | 561,97 | 5586,31 | 620,70 | 2957,81 | 54,39 |
| 55 | 641,16 | 657,01 | 664,67 | 649,61 | 661,19 | 666,50 | 536,26 | 551,76 | 562,37 | 5590,52 | 621,17 | 2941,01 | 54,23 |
| 59 | 641,86 | 657,68 | 664,74 | 649,96 | 661,55 | 666,80 | 537,16 | 552,37 | 562,85 | 5594,96 | 621,66 | 2923,92 | 54,07 |
| 63 | 642,49 | 658,60 | 664,97 | 650,34 | 662,16 | 666,97 | 538,12 | 552,93 | 563,33 | 5599,91 | 622,21 | 2911,60 | 53,96 |
| 67 | 643,30 | 659,17 | 664,94 | 650,87 | 662,52 | 667,36 | 539,20 | 553,55 | 563,76 | 5604,65 | 622,74 | 2892,70 | 53,78 |
| 71 | 644,35 | 659,69 | 665,39 | 651,49 | 662,94 | 667,40 | 540,04 | 554,23 | 564,14 | 5609,67 | 623,30 | 2881,33 | 53,68 |
| 75 | 645,26 | 660,36 | 665,80 | 652,18 | 663,33 | 667,60 | 540,86 | 554,91 | 564,71 | 5615,01 | 623,89 | 2870,49 | 53,58 |
| 79 | 645,82 | 660,71 | 666,53 | 652,86 | 663,13 | 667,91 | 541,82 | 555,48 | 565,25 | 5619,52 | 624,39 | 2853,09 | 53,41 |
| 83 | 646,75 | 661,40 | 667,02 | 653,59 | 663,17 | 668,44 | 542,54 | 555,96 | 565,75 | 5624,61 | 624,96 | 2850,04 | 53,39 |
| | | | | | | | | | | | **619,54** | **3002,46** | **54,79** |

Statistical data for specific fuel consumption at high load

| Time | Trial 1 | Trial 2 | Trial 3 | Trial 4 | Trial 5 | Trial 6 | Trial 7 | Trial 8 | Trial 9 | Sum | Mean | Variance | Standard deviation |
|---|---|---|---|---|---|---|---|---|---|---|---|---|---|
| Sec | g/Kwh | g/Kwh | g/Kwh | g/Kwh | g/Kwh | g/Kwh | g/Kwh | g/Kwh | g/Kwh | $\sum Y$ | $\bar{Y}$ | $\sigma^2$ | $\sigma$ |
| 3 | 292,43 | 294,81 | 287,09 | 283,63 | 286,46 | 285,13 | 276,33 | 278,79 | 279,75 | 2564,41 | 284,93 | 37,64 | 6,14 |
| 7 | 296,15 | 296,04 | 287,72 | 284,59 | 292,29 | 283,30 | 278,10 | 278,49 | 279,46 | 2576,13 | 286,24 | 52,10 | 7,22 |
| 11 | 297,51 | 295,76 | 291,54 | 285,63 | 292,40 | 285,95 | 276,54 | 278,62 | 278,37 | 2582,32 | 286,92 | 61,76 | **7,86** |
| 15 | 296,24 | 289,92 | 292,50 | 286,13 | 289,22 | 286,05 | 277,98 | 278,50 | 276,98 | 2573,51 | 285,95 | 46,82 | 6,84 |
| 19 | 293,47 | 286,04 | 289,38 | 285,20 | 289,06 | 284,63 | 278,69 | 278,77 | 279,05 | 2564,29 | 284,92 | 27,83 | 5,28 |
| 23 | 289,06 | 288,74 | 290,87 | 286,15 | 289,04 | 287,56 | 278,14 | 278,24 | 279,35 | 2567,14 | 285,24 | 26,64 | 5,16 |
| 27 | 289,56 | 292,35 | 289,34 | 287,72 | 286,54 | 288,40 | 278,55 | 276,92 | 278,85 | 2568,24 | 285,36 | 32,32 | 5,68 |
| 31 | 291,73 | 296,53 | 287,60 | 287,19 | 288,32 | 284,97 | 280,26 | 278,28 | 277,49 | 2572,38 | 285,82 | 39,87 | 6,31 |
| 35 | 293,10 | 294,00 | 289,78 | 284,80 | 285,38 | 286,34 | 279,93 | 278,73 | 277,85 | 2569,92 | 285,55 | 35,60 | 5,97 |
| 39 | 291,76 | 286,57 | 286,83 | 284,56 | 287,58 | 285,32 | 277,73 | 278,78 | 278,39 | 2557,53 | 284,17 | 23,43 | 4,84 |
| 43 | 292,43 | 292,91 | 286,47 | 285,15 | 284,81 | 287,97 | 278,63 | 277,45 | 277,86 | 2563,67 | 284,85 | 34,67 | 5,89 |
| 47 | 290,34 | 294,41 | 288,06 | 289,33 | 289,83 | 287,81 | 278,30 | 279,28 | 277,24 | 2574,59 | 286,07 | 37,99 | 6,16 |
| 51 | 292,34 | 294,94 | 285,61 | 286,17 | 288,85 | 287,34 | 276,76 | 278,71 | 278,50 | 2569,23 | 285,47 | 40,32 | 6,35 |
| 55 | 290,54 | 298,76 | 284,31 | 284,97 | 285,87 | 287,04 | 279,22 | 277,13 | 277,47 | 2565,32 | 285,04 | 47,19 | 6,87 |
| 59 | 289,32 | 294,16 | 288,82 | 285,23 | 288,16 | 286,82 | 278,44 | 279,99 | 278,29 | 2569,24 | 285,47 | 30,22 | 5,50 |
| 63 | 292,68 | 291,34 | 288,59 | 285,68 | 288,16 | 285,46 | 277,16 | 278,74 | 279,34 | 2567,15 | 285,24 | 31,87 | 5,65 |
| 67 | 292,60 | 291,16 | 287,42 | 290,68 | 285,06 | 284,16 | 277,87 | 279,95 | 277,33 | 2566,24 | 285,14 | 33,69 | 5,80 |
| 71 | 291,00 | 291,05 | 290,26 | 290,93 | 287,29 | 281,84 | 277,04 | 279,32 | 278,06 | 2566,79 | 285,20 | 36,79 | 6,07 |
| 75 | 295,28 | 290,35 | 290,66 | 286,24 | 287,79 | 288,60 | 279,16 | 279,14 | 277,42 | 2574,64 | 286,07 | 38,01 | 6,17 |
| 79 | 295,12 | 288,13 | 289,44 | 286,51 | 285,76 | 288,38 | 278,05 | 278,95 | 276,99 | 2567,32 | 285,26 | 36,82 | 6,07 |
| 83 | 295,01 | 290,20 | 291,89 | 285,72 | 285,44 | 286,83 | 278,80 | 277,89 | 278,11 | 2569,89 | 285,54 | 39,08 | 6,25 |
| | | | | | | | | | | | **285,45** | **37,65** | **6,10** |

Statistical data for maximum brake power

| Time | Trial 1 | Trial 2 | Trial 3 | Trial 4 | Trial 5 | Trial 6 | Trial 7 | Trial 8 | Trial 9 | Sum | Mean | Variance | Standard deviation |
|---|---|---|---|---|---|---|---|---|---|---|---|---|---|
| Sec | KW | KW | KW | KW | KW | KW | KW | KW | KW | $\sum Y$ | $\bar{Y}$ | $\sigma^2$ | $\sigma$ |
| 3 | 8,05 | 8,03 | 8,02 | 7,89 | 7,86 | 7,87 | 7,89 | 7,88 | 7,88 | 71,36 | 7,93 | 0,01 | 0,08 |
| 7 | 8,07 | 8,03 | 8,05 | 7,87 | 7,87 | 7,89 | 7,89 | 7,89 | 7,88 | 71,43 | 7,94 | 0,01 | 0,08 |
| 11 | 8,04 | 8,03 | 8,02 | 7,89 | 7,87 | 7,86 | 7,89 | 7,87 | 7,88 | 71,34 | 7,93 | 0,01 | 0,08 |
| 15 | 8,02 | 8,04 | 7,96 | 7,86 | 7,89 | 7,86 | 7,86 | 7,88 | 7,90 | 71,26 | 7,92 | 0,01 | 0,07 |
| 19 | 8,05 | 8,05 | 8,07 | 7,87 | 7,87 | 7,85 | 7,89 | 7,87 | 7,87 | 71,39 | 7,93 | 0,01 | **0,09** |
| 23 | 8,07 | 8,03 | 8,03 | 7,89 | 7,88 | 7,87 | 7,88 | 7,89 | 7,87 | 71,42 | 7,94 | 0,01 | 0,08 |
| 27 | 8,06 | 8,04 | 8,01 | 7,87 | 7,88 | 7,82 | 7,89 | 7,91 | 7,88 | 71,36 | 7,93 | 0,01 | 0,08 |
| 31 | 8,07 | 8,02 | 7,99 | 7,88 | 7,87 | 7,85 | 7,89 | 7,88 | 7,86 | 71,33 | 7,93 | 0,01 | 0,08 |
| 35 | 8,05 | 8,02 | 7,99 | 7,87 | 7,90 | 7,85 | 7,87 | 7,90 | 7,89 | 71,33 | 7,93 | 0,01 | 0,07 |
| 39 | 8,05 | 8,08 | 7,97 | 7,87 | 7,88 | 7,88 | 7,88 | 7,91 | 7,87 | 71,40 | 7,93 | 0,01 | 0,08 |
| 43 | 8,02 | 8,01 | 7,99 | 7,85 | 7,96 | 7,85 | 7,90 | 7,89 | 7,90 | 71,36 | 7,93 | 0,00 | 0,07 |
| 47 | 8,06 | 8,00 | 7,91 | 7,83 | 7,86 | 7,85 | 7,90 | 7,88 | 7,89 | 71,18 | 7,91 | 0,01 | 0,07 |
| 51 | 8,02 | 8,01 | 8,02 | 7,86 | 7,83 | 7,86 | 7,90 | 7,89 | 7,88 | 71,27 | 7,92 | 0,01 | 0,08 |
| 55 | 8,03 | 7,98 | 8,02 | 7,86 | 7,87 | 7,84 | 7,89 | 7,86 | 7,89 | 71,23 | 7,91 | 0,01 | 0,07 |
| 59 | 8,00 | 8,03 | 7,99 | 7,87 | 7,86 | 7,85 | 7,90 | 7,87 | 7,89 | 71,25 | 7,92 | 0,00 | 0,07 |
| 63 | 7,98 | 8,06 | 7,98 | 7,87 | 7,83 | 7,82 | 7,92 | 7,87 | 7,88 | 71,21 | 7,91 | 0,01 | 0,08 |
| 67 | 8,00 | 8,03 | 8,01 | 7,88 | 7,87 | 7,84 | 7,91 | 7,85 | 7,89 | 71,29 | 7,92 | 0,01 | 0,07 |
| 71 | 7,98 | 8,03 | 7,99 | 7,86 | 7,84 | 7,83 | 7,89 | 7,88 | 7,89 | 71,20 | 7,91 | 0,01 | 0,07 |
| 75 | 8,00 | 8,03 | 7,99 | 7,88 | 7,85 | 7,84 | 7,88 | 7,87 | 7,88 | 71,22 | 7,91 | 0,00 | 0,07 |
| 79 | 8,00 | 8,04 | 8,01 | 7,86 | 7,85 | 7,85 | 7,91 | 7,90 | 7,89 | 71,31 | 7,92 | 0,01 | 0,07 |
| 83 | 8,02 | 8,00 | 7,99 | 7,84 | 7,87 | 7,83 | 7,88 | 7,89 | 7,90 | 71,21 | 7,91 | 0,01 | 0,07 |
| | | | | | | | | | | | **7,92** | **0,01** | **0,08** |

Statistical data for speed trials

| Time | Trial 1 | Trial 2 | Trial 3 | Trial 4 | Trial 5 | Trial 6 | Trial 7 | Trial 8 | Trial 9 | Trial 10 | Trial 11 | Trial 12 | Sum | Mean | Variance | Standard deviation |
|---|---|---|---|---|---|---|---|---|---|---|---|---|---|---|---|---|
| Sec | RPS | RPS | RPS | RPS | RPS | RPS | RPS | RPS | RPS | RPS | RPS | RPS | $\sum Y$ | $\bar{Y}$ | $\sigma^2$ | $\sigma$ |
| 3 | 49,90 | 49,89 | 49,93 | 49,96 | 50,00 | 49,96 | 50,02 | 50,01 | 50,09 | 49,89 | 49,87 | 50,13 | 599,65 | 49,97 | 0,01 | 0,08 |
| 7 | 49,90 | 49,88 | 49,90 | 49,97 | 50,01 | 49,95 | 50,02 | 50,01 | 50,08 | 49,98 | 50,02 | 50,13 | 599,85 | 49,99 | 0,01 | 0,07 |
| 11 | 49,89 | 49,88 | 49,90 | 49,96 | 50,05 | 49,95 | 50,02 | 50,01 | 50,10 | 50,00 | 50,00 | 50,13 | 599,91 | 49,99 | 0,01 | 0,08 |
| 15 | 49,91 | 49,88 | 49,90 | 49,96 | 50,06 | 49,95 | 50,01 | 50,01 | 50,09 | 50,02 | 50,01 | 50,12 | 599,95 | 50,00 | 0,01 | 0,08 |
| 19 | 49,91 | 49,89 | 49,89 | 49,96 | 50,08 | 49,94 | 50,01 | 50,01 | 50,00 | 50,02 | 50,00 | 50,13 | 599,85 | 49,99 | 0,01 | 0,07 |
| 23 | 49,91 | 49,92 | 49,91 | 49,94 | 50,07 | 49,95 | 50,02 | 50,00 | 49,96 | 50,02 | 50,01 | 50,13 | 599,83 | 49,99 | 0,00 | 0,07 |
| 27 | 49,88 | 49,90 | 49,90 | 49,93 | 50,08 | 49,95 | 50,01 | 50,00 | 49,96 | 50,01 | 50,02 | 50,13 | 599,77 | 49,98 | 0,01 | 0,08 |
| 31 | 49,89 | 49,91 | 49,91 | 49,94 | 50,08 | 50,00 | 50,01 | 50,10 | 49,95 | 50,01 | 50,03 | 50,13 | 599,96 | 50,00 | 0,01 | 0,08 |
| 35 | 49,90 | 49,92 | 49,92 | 49,95 | 50,06 | 49,94 | 50,02 | 50,07 | 49,94 | 50,01 | 50,02 | 50,13 | 599,87 | 49,99 | 0,01 | 0,07 |
| 39 | 49,91 | 49,91 | 49,91 | 49,95 | 50,06 | 49,95 | 50,02 | 49,93 | 49,96 | 50,01 | 50,02 | 50,13 | 599,75 | 49,98 | 0,00 | 0,07 |
| 43 | 49,91 | 49,92 | 49,91 | 49,95 | 50,00 | 49,94 | 50,02 | 49,95 | 49,97 | 50,02 | 50,02 | 50,13 | 599,73 | 49,98 | 0,00 | 0,06 |
| 47 | 49,91 | 49,95 | 49,91 | 49,96 | 50,03 | 49,95 | 50,01 | 50,03 | 50,00 | 50,02 | 50,02 | 50,13 | 599,91 | 49,99 | 0,00 | 0,06 |
| 51 | 49,90 | 49,91 | 49,92 | 49,96 | 50,08 | 49,94 | 50,01 | 49,96 | 50,02 | 50,01 | 50,00 | 50,13 | 599,85 | 49,99 | 0,00 | 0,07 |
| 55 | 49,91 | 49,91 | 49,96 | 49,95 | 50,08 | 49,96 | 50,01 | 49,94 | 49,99 | 50,01 | 49,86 | 50,12 | 599,72 | 49,98 | 0,01 | 0,07 |
| 59 | 49,90 | 49,88 | 50,01 | 49,94 | 50,09 | 49,97 | 50,02 | 49,96 | 49,96 | 50,01 | 49,96 | 50,12 | 599,82 | 49,98 | 0,00 | 0,07 |
| 63 | 49,88 | 49,89 | 50,02 | 49,96 | 50,08 | 50,08 | 50,03 | 49,94 | 49,92 | 50,01 | 50,00 | 50,12 | 599,94 | 49,99 | 0,01 | 0,08 |
| 67 | 49,91 | 49,88 | 50,02 | 49,96 | 50,08 | 49,98 | 50,02 | 49,99 | 49,92 | 50,00 | 50,00 | 50,11 | 599,88 | 49,99 | 0,00 | 0,07 |
| 71 | 49,90 | 49,89 | 50,02 | 49,96 | 50,11 | 50,03 | 50,02 | 50,02 | 49,93 | 50,02 | 50,00 | 50,11 | 600,00 | 50,00 | 0,01 | 0,07 |
| 75 | 49,89 | 49,89 | 49,91 | 49,97 | 50,11 | 50,03 | 50,01 | 50,08 | 49,93 | 50,02 | 49,87 | 50,11 | 599,82 | 49,99 | 0,01 | **0,09** |
| 79 | 49,90 | 49,91 | 49,91 | 50,04 | 50,01 | 49,98 | 49,99 | 50,07 | 49,93 | 50,01 | 49,87 | 50,12 | 599,75 | 49,98 | 0,01 | 0,08 |
| 83 | 49,93 | 49,93 | 49,91 | 50,05 | 49,97 | 50,01 | 50,01 | 49,96 | 49,99 | 50,00 | 49,90 | 50,11 | 599,78 | 49,98 | 0,00 | 0,06 |
| | | | | | | | | | | | | | | **2999,18** | **0,01** | **0,07** |

Statistical data for torque measurements

| Time | Trial 1 | Trial 2 | Trial 3 | Trial 4 | Trial 5 | Trial 6 | Trial 7 | Trial 8 | Trial 9 | Sum | Mean | Variance | Standard deviation |
|---|---|---|---|---|---|---|---|---|---|---|---|---|---|
| Sec | Nm | Nm | Nm | Nm | Nm | Nm | Nm | Nm | Nm | $\sum Y$ | $\bar{Y}$ | $\sigma^2$ | $\sigma$ |
| 3 | 25,65 | 25,64 | 25,54 | 25,01 | 25,00 | 24,97 | 25,12 | 25,19 | 25,08 | 227,21 | 25,25 | 0,08 | 0,28 |
| 7 | 25,73 | 25,52 | 25,52 | 24,95 | 24,97 | 24,89 | 25,10 | 25,10 | 25,13 | 226,91 | 25,21 | 0,09 | 0,30 |
| 11 | 25,65 | 25,55 | 25,45 | 25,01 | 25,05 | 24,94 | 25,11 | 25,14 | 25,11 | 227,01 | 25,22 | 0,07 | 0,26 |
| 15 | 25,60 | 25,76 | 25,44 | 24,93 | 24,98 | 24,85 | 25,02 | 25,20 | 25,08 | 226,86 | 25,21 | 0,10 | **0,32** |
| 19 | 25,69 | 25,53 | 25,50 | 24,96 | 25,25 | 24,92 | 25,11 | 25,14 | 25,14 | 227,23 | 25,25 | 0,07 | 0,27 |
| 23 | 25,74 | 25,49 | 25,45 | 25,02 | 24,97 | 24,88 | 25,10 | 25,09 | 25,11 | 226,84 | 25,20 | 0,08 | 0,29 |
| 27 | 25,70 | 25,53 | 25,44 | 24,97 | 24,88 | 24,91 | 25,11 | 25,12 | 25,09 | 226,76 | 25,20 | 0,09 | 0,29 |
| 31 | 25,75 | 25,44 | 25,54 | 25,01 | 24,99 | 24,94 | 25,13 | 25,04 | 25,13 | 226,96 | 25,22 | 0,08 | 0,29 |
| 35 | 25,67 | 25,54 | 25,47 | 24,96 | 24,97 | 24,86 | 25,07 | 25,05 | 25,14 | 226,74 | 25,19 | 0,09 | 0,29 |
| 39 | 25,68 | 25,68 | 25,42 | 24,98 | 24,89 | 24,88 | 25,10 | 25,07 | 25,06 | 226,75 | 25,19 | 0,10 | 0,32 |
| 43 | 25,58 | 25,59 | 25,19 | 24,91 | 24,99 | 24,85 | 25,15 | 25,01 | 25,16 | 226,44 | 25,16 | 0,07 | 0,27 |
| 47 | 25,71 | 25,61 | 25,44 | 24,85 | 24,91 | 24,93 | 25,15 | 25,11 | 25,10 | 226,80 | 25,20 | 0,10 | 0,31 |
| 51 | 25,59 | 25,59 | 25,56 | 24,95 | 24,93 | 24,91 | 25,13 | 25,07 | 25,15 | 226,89 | 25,21 | 0,08 | 0,29 |
| 55 | 25,63 | 25,64 | 25,62 | 24,93 | 24,92 | 24,92 | 25,12 | 25,14 | 25,10 | 227,04 | 25,23 | 0,10 | 0,31 |
| 59 | 25,52 | 25,50 | 25,56 | 24,98 | 24,98 | 24,96 | 25,16 | 25,13 | 25,05 | 226,83 | 25,20 | 0,06 | 0,25 |
| 63 | 25,47 | 25,57 | 25,56 | 24,96 | 24,98 | 24,94 | 25,20 | 25,09 | 25,13 | 226,91 | 25,21 | 0,07 | 0,26 |
| 67 | 25,52 | 25,65 | 25,59 | 25,02 | 25,04 | 24,88 | 25,18 | 25,08 | 25,12 | 227,08 | 25,23 | 0,08 | 0,28 |
| 71 | 25,47 | 25,57 | 25,56 | 24,94 | 24,96 | 24,92 | 25,12 | 25,08 | 25,09 | 226,70 | 25,19 | 0,07 | 0,27 |
| 75 | 25,52 | 25,35 | 25,53 | 25,00 | 24,95 | 24,86 | 25,09 | 25,17 | 25,12 | 226,59 | 25,18 | 0,06 | 0,24 |
| 79 | 25,54 | 25,67 | 25,47 | 24,94 | 24,92 | 24,86 | 25,17 | 25,06 | 25,02 | 226,65 | 25,18 | 0,09 | 0,30 |
| 83 | 25,58 | 25,58 | 25,39 | 24,87 | 24,99 | 24,80 | 25,09 | 25,08 | 25,08 | 226,46 | 25,16 | 0,08 | 0,29 |
| | | | | | | | | | | | **25,20** | **0,08** | **0,28** |

| Emission data at mode 1 | | | | |
|---|---|---|---|---|
| Nox | CO | $CO_2$ | $O_2$ | HC |
| 347,56 | 2000,00 | 4,82 | 14,09 | 28,45 |
| 347,58 | 2000,00 | 4,81 | 14,10 | 28,59 |
| 347,48 | 2000,00 | 4,81 | 14,10 | 28,66 |
| 346,32 | 2000,00 | 4,80 | 14,10 | 28,59 |
| 345,43 | 2000,00 | 4,80 | 14,12 | 28,52 |
| 345,05 | 2000,00 | 4,79 | 14,13 | 28,57 |
| 345,05 | 2000,00 | 4,78 | 14,14 | 28,60 |
| 345,05 | 2000,00 | 4,78 | 14,15 | 28,61 |
| 345,06 | 2000,00 | 4,77 | 14,16 | 28,64 |
| 344,95 | 2000,00 | 4,75 | 14,18 | 28,64 |
| 343,79 | 2000,00 | 4,74 | 14,20 | 28,66 |
| 343,79 | 2000,00 | 4,73 | 14,22 | 28,68 |
| 342,61 | 2000,00 | 4,72 | 14,24 | 28,66 |
| 342,55 | 2000,00 | 4,72 | 14,25 | 28,65 |
| 342,58 | 2000,00 | 4,71 | 14,27 | 28,75 |
| 341,37 | 2000,00 | 4,71 | 14,28 | 28,84 |
| 341,46 | 2000,00 | 4,72 | 14,28 | 28,79 |
| 341,31 | 2000,00 | 4,71 | 14,28 | 28,66 |
| 341,31 | 2000,00 | 4,70 | 14,28 | 28,71 |
| 340,12 | 2000,00 | 4,69 | 14,29 | 28,77 |
| 339,17 | 2000,00 | 4,69 | 14,30 | 28,77 |
| 338,23 | 2000,00 | 4,68 | 14,31 | 28,79 |
| 337,56 | 2000,00 | 4,67 | 14,31 | 28,76 |
| 336,86 | 2000,00 | 4,66 | 14,33 | 28,91 |
| 336,22 | 2000,00 | 4,66 | 14,34 | 28,91 |
| 335,08 | 2000,00 | 4,66 | 14,35 | 28,73 |
| 335,09 | 2000,00 | 4,66 | 14,35 | 28,86 |
| 335,08 | 2000,00 | 4,66 | 14,35 | 28,88 |
| 335,08 | 2000,00 | 4,67 | 14,34 | 28,77 |
| 333,85 | 2000,00 | 4,67 | 14,34 | 28,76 |
| 333,39 | 2000,00 | 4,66 | 14,34 | 28,80 |
| 332,30 | 2000,00 | 4,65 | 14,34 | 28,79 |
| 330,90 | 2000,00 | 4,65 | 14,35 | 28,80 |

| Emission data at mode 2 | | | | |
|---|---|---|---|---|
| Nox | CO | $CO_2$ | $O_2$ | HC |
| 387,76 | 293,52 | 3,33 | 16,43 | 31,02 |
| 387,75 | 289,06 | 3,32 | 16,44 | 30,89 |
| 388,02 | 284,72 | 3,32 | 16,44 | 30,86 |
| 389,00 | 279,98 | 3,32 | 16,44 | 30,89 |
| 388,99 | 275,93 | 3,32 | 16,45 | 31,01 |
| 389,01 | 271,77 | 3,32 | 16,45 | 31,01 |
| 389,25 | 268,94 | 3,31 | 16,45 | 30,98 |
| 390,26 | 265,02 | 3,31 | 16,45 | 30,90 |
| 390,26 | 262,02 | 3,30 | 16,46 | 30,93 |
| 390,25 | 259,27 | 3,30 | 16,47 | 30,90 |
| 390,24 | 256,47 | 3,30 | 16,47 | 30,94 |
| 390,25 | 253,83 | 3,29 | 16,47 | 31,00 |
| 390,25 | 250,48 | 3,29 | 16,48 | 31,07 |
| 391,43 | 247,42 | 3,28 | 16,49 | 30,94 |
| 391,50 | 245,29 | 3,28 | 16,50 | 30,93 |
| 392,55 | 242,85 | 3,27 | 16,50 | 31,10 |
| 393,32 | 240,37 | 3,27 | 16,51 | 30,95 |
| 394,74 | 238,16 | 3,26 | 16,52 | 30,92 |
| 396,02 | 237,29 | 3,26 | 16,52 | 31,09 |
| 397,27 | 235,19 | 3,25 | 16,53 | 31,10 |
| 398,82 | 234,26 | 3,25 | 16,54 | 30,94 |
| 400,24 | 231,98 | 3,24 | 16,54 | 30,97 |
| 401,31 | 230,71 | 3,24 | 16,55 | 31,05 |
| 401,53 | 229,56 | 3,23 | 16,57 | 31,06 |

| Emission data at mode 3 | | | | |
|---|---|---|---|---|
| Nox | CO | $CO_2$ | $O_2$ | HC |
| 371,13 | 147,20 | 2,39 | 17,72 | 32,14 |
| 372,64 | 146,18 | 2,39 | 17,73 | 32,16 |
| 374,56 | 145,64 | 2,39 | 17,72 | 32,25 |
| 376,01 | 145,65 | 2,39 | 17,72 | 32,26 |
| 377,57 | 145,05 | 2,40 | 17,72 | 32,20 |
| 379,06 | 144,65 | 2,41 | 17,72 | 32,13 |
| 380,51 | 144,64 | 2,41 | 17,71 | 32,10 |
| 382,06 | 143,94 | 2,41 | 17,69 | 32,24 |
| 383,48 | 142,83 | 2,42 | 17,69 | 32,23 |
| 384,89 | 142,65 | 2,42 | 17,69 | 32,04 |
| 385,99 | 142,64 | 2,42 | 17,68 | 32,22 |
| 387,09 | 142,21 | 2,42 | 17,68 | 32,20 |
| 388,35 | 141,68 | 2,42 | 17,68 | 32,04 |
| 389,02 | 141,67 | 2,42 | 17,68 | 32,14 |
| 389,91 | 141,65 | 2,41 | 17,68 | 32,24 |
| 390,29 | 140,73 | 2,41 | 17,69 | 32,14 |
| 390,85 | 140,68 | 2,41 | 17,69 | 32,09 |
| 391,52 | 140,67 | 2,41 | 17,69 | 32,13 |
| 391,53 | 140,67 | 2,41 | 17,69 | 32,20 |
| 391,44 | 140,66 | 2,42 | 17,69 | 32,16 |
| 390,29 | 140,68 | 2,42 | 17,69 | 32,19 |
| 390,02 | 140,67 | 2,43 | 17,67 | 32,21 |
| 389,03 | 140,45 | 2,44 | 17,67 | 32,09 |
| 388,16 | 139,66 | 2,44 | 17,67 | 32,07 |
| 387,68 | 139,66 | 2,45 | 17,65 | 32,08 |
| 386,51 | 139,66 | 2,45 | 17,64 | 32,12 |
| 386,53 | 139,67 | 2,46 | 17,63 | 32,15 |
| 386,51 | 139,34 | 2,46 | 17,64 | 32,18 |
| 387,73 | 138,67 | 2,46 | 17,63 | 32,11 |
| 388,98 | 138,65 | 2,45 | 17,63 | 32,05 |
| 390,33 | 138,20 | 2,45 | 17,62 | 32,06 |
| 392,11 | 137,67 | 2,46 | 17,62 | 32,07 |
| 394,08 | 137,69 | 2,46 | 17,63 | 32,05 |

| Emission data at mode 4 | | | | |
|---|---|---|---|---|
| Nox | CO | $CO_2$ | $O_2$ | HC |
| 246,42 | 235,75 | 1,33 | 19,09 | 33,41 |
| 245,37 | 235,74 | 1,33 | 19,09 | 33,59 |
| 245,27 | 235,76 | 1,32 | 19,10 | 33,53 |
| 246,40 | 235,52 | 1,32 | 19,11 | 33,41 |
| 246,97 | 234,77 | 1,33 | 19,11 | 33,49 |
| 247,66 | 233,53 | 1,33 | 19,10 | 33,54 |
| 248,53 | 232,73 | 1,33 | 19,11 | 33,54 |
| 248,90 | 232,03 | 1,33 | 19,10 | 33,55 |
| 248,99 | 231,74 | 1,33 | 19,09 | 33,54 |
| 249,57 | 231,73 | 1,32 | 19,09 | 33,50 |
| 248,88 | 231,74 | 1,32 | 19,10 | 33,44 |
| 248,90 | 231,72 | 1,32 | 19,11 | 33,49 |
| 248,78 | 231,73 | 1,32 | 19,11 | 33,64 |
| 247,65 | 231,73 | 1,31 | 19,11 | 33,49 |
| 247,66 | 231,72 | 1,31 | 19,12 | 33,42 |
| 247,24 | 231,83 | 1,31 | 19,12 | 33,46 |
| 246,40 | 232,72 | 1,31 | 19,12 | 33,52 |
| 246,40 | 232,74 | 1,31 | 19,12 | 33,53 |
| 246,00 | 232,72 | 1,31 | 19,13 | 33,61 |
| 245,16 | 233,20 | 1,30 | 19,13 | 33,54 |
| 244,57 | 233,72 | 1,30 | 19,13 | 33,58 |
| 243,88 | 234,57 | 1,29 | 19,13 | 33,51 |
| 243,02 | 234,82 | 1,29 | 19,13 | 33,51 |
| 242,23 | 235,95 | 1,29 | 19,14 | 33,49 |
| 241,14 | 237,21 | 1,28 | 19,14 | 33,60 |
| 239,73 | 238,46 | 1,28 | 19,15 | 33,65 |
| 238,49 | 239,21 | 1,28 | 19,16 | 33,53 |
| 237,09 | 240,32 | 1,27 | 19,16 | 33,52 |
| 235,99 | 241,44 | 1,27 | 19,17 | 33,73 |
| 235,13 | 242,70 | 1,26 | 19,17 | 33,47 |
| 233,93 | 243,07 | 1,26 | 19,18 | 33,55 |
| 233,00 | 243,75 | 1,26 | 19,18 | 33,70 |
| 232,63 | 244,20 | 1,26 | 19,18 | 33,52 |

| Emission data at mode 5 | | | | |
|---|---|---|---|---|
| Nox | CO | $CO_2$ | $O_2$ | HC |
| 315,10 | 2000,00 | 4,07 | 15,06 | 29,57 |
| 315,08 | 2000,00 | 4,07 | 15,06 | 29,50 |
| 315,09 | 2000,00 | 4,07 | 15,06 | 29,50 |
| 315,08 | 2000,00 | 4,07 | 15,06 | 29,53 |
| 315,10 | 2000,00 | 4,07 | 15,06 | 29,61 |
| 315,09 | 2000,00 | 4,07 | 15,06 | 29,63 |
| 315,09 | 2000,00 | 4,06 | 15,06 | 29,46 |
| 315,09 | 2000,00 | 4,06 | 15,08 | 29,57 |
| 313,88 | 2000,00 | 4,06 | 15,08 | 29,69 |
| 312,93 | 2000,00 | 4,06 | 15,08 | 29,59 |
| 312,58 | 2000,00 | 4,06 | 15,08 | 29,50 |
| 312,31 | 2000,00 | 4,06 | 15,08 | 29,59 |
| 311,30 | 2000,00 | 4,06 | 15,08 | 29,69 |
| 310,40 | 2000,00 | 4,07 | 15,07 | 29,56 |
| 309,17 | 2000,00 | 4,07 | 15,06 | 29,59 |
| 307,65 | 2000,00 | 4,07 | 15,05 | 29,64 |
| 305,30 | 2000,00 | 4,07 | 15,03 | 29,47 |
| 302,49 | 2000,00 | 4,07 | 15,02 | 29,64 |
| 299,83 | 2000,00 | 4,07 | 15,01 | 29,43 |
| 296,64 | 2000,00 | 4,07 | 15,00 | 29,45 |
| 293,32 | 2000,00 | 4,07 | 14,98 | 29,58 |
| 289,70 | 2000,00 | 4,07 | 14,96 | 29,56 |
| 286,12 | 2000,00 | 4,07 | 14,94 | 29,43 |
| 282,36 | 2000,00 | 4,06 | 14,93 | 29,37 |
| 278,47 | 2000,00 | 4,06 | 14,92 | 29,40 |
| 274,55 | 2000,00 | 4,05 | 14,90 | 29,43 |
| 270,63 | 2000,00 | 4,04 | 14,88 | 29,36 |
| 266,44 | 2000,00 | 4,03 | 14,87 | 29,40 |
| 261,45 | 2000,00 | 4,01 | 14,86 | 29,39 |
| 256,13 | 2000,00 | 3,99 | 14,84 | 29,37 |
| 250,40 | 2000,00 | 3,97 | 14,83 | 29,38 |
| 245,04 | 2000,00 | 3,94 | 14,81 | 29,30 |
| 239,16 | 2000,00 | 3,92 | 14,80 | 29,22 |

| Emission data at mode 6 | | | | |
|---|---|---|---|---|
| Nox | CO | $CO_2$ | $O_2$ | HC |
| 410,18 | 2000,00 | 5,24 | 13,32 | 27,70 |
| 410,14 | 2000,00 | 5,23 | 13,33 | 27,76 |
| 409,10 | 2000,00 | 5,23 | 13,33 | 27,73 |
| 408,88 | 2000,00 | 5,23 | 13,33 | 27,72 |
| 408,64 | 2000,00 | 5,22 | 13,34 | 27,73 |
| 407,66 | 2000,00 | 5,21 | 13,35 | 27,74 |
| 407,24 | 2000,00 | 5,21 | 13,36 | 27,75 |
| 405,98 | 2000,00 | 5,20 | 13,37 | 27,78 |
| 404,58 | 2000,00 | 5,19 | 13,38 | 27,89 |
| 403,89 | 2000,00 | 5,19 | 13,39 | 27,90 |
| 402,70 | 2000,00 | 5,18 | 13,40 | 27,79 |
| 402,07 | 2000,00 | 5,19 | 13,41 | 27,75 |
| 401,30 | 2000,00 | 5,18 | 13,40 | 27,77 |
| 400,14 | 2000,00 | 5,18 | 13,41 | 27,82 |
| 399,25 | 2000,00 | 5,17 | 13,42 | 27,84 |
| 398,88 | 2000,00 | 5,17 | 13,43 | 27,88 |
| 398,90 | 2000,00 | 5,16 | 13,43 | 27,91 |
| 397,71 | 2000,00 | 5,16 | 13,43 | 27,86 |
| 397,64 | 2000,00 | 5,17 | 13,43 | 27,84 |
| 397,64 | 2000,00 | 5,18 | 13,44 | 27,88 |
| 398,05 | 2000,00 | 5,19 | 13,44 | 27,87 |
| 398,87 | 2000,00 | 5,20 | 13,42 | 27,88 |
| 399,93 | 2000,00 | 5,20 | 13,40 | 27,82 |
| 400,12 | 2000,00 | 5,21 | 13,38 | 27,75 |
| 399,26 | 2000,00 | 5,22 | 13,36 | 27,72 |
| 398,89 | 2000,00 | 5,23 | 13,36 | 27,74 |
| 398,01 | 2000,00 | 5,23 | 13,35 | 27,86 |
| 397,09 | 2000,00 | 5,22 | 13,34 | 27,87 |
| 395,83 | 2000,00 | 5,22 | 13,34 | 27,73 |
| 394,57 | 2000,00 | 5,22 | 13,34 | 27,69 |
| 393,15 | 2000,00 | 5,21 | 13,34 | 27,75 |
| 391,01 | 2000,00 | 5,19 | 13,34 | 27,86 |

| Emission data at mode 7 | | | | |
|---|---|---|---|---|
| Nox | CO | $CO_2$ | $O_2$ | HC |
| 789,18 | 162,69 | 4,55 | 14,71 | 29,17 |
| 789,76 | 162,69 | 4,55 | 14,71 | 29,19 |
| 790,46 | 162,68 | 4,56 | 14,71 | 29,22 |
| 790,44 | 162,69 | 4,56 | 14,70 | 29,24 |
| 790,46 | 162,68 | 4,57 | 14,69 | 29,28 |
| 791,63 | 162,68 | 4,58 | 14,69 | 29,26 |
| 791,14 | 162,68 | 4,58 | 14,69 | 29,14 |
| 790,45 | 162,68 | 4,59 | 14,68 | 29,14 |
| 790,44 | 162,67 | 4,60 | 14,66 | 29,14 |
| 789,74 | 162,69 | 4,60 | 14,66 | 29,12 |
| 789,20 | 162,67 | 4,61 | 14,65 | 29,11 |
| 789,21 | 162,69 | 4,62 | 14,64 | 29,13 |
| 788,94 | 162,68 | 4,62 | 14,63 | 29,10 |
| 787,95 | 161,85 | 4,61 | 14,62 | 29,12 |
| 787,71 | 161,70 | 4,59 | 14,63 | 29,11 |
| 786,71 | 161,71 | 4,58 | 14,64 | 29,12 |
| 786,71 | 161,70 | 4,58 | 14,66 | 29,15 |
| 785,50 | 161,71 | 4,57 | 14,68 | 29,23 |
| 785,44 | 161,69 | 4,56 | 14,69 | 29,26 |
| 786,63 | 161,68 | 4,55 | 14,70 | 29,29 |
| 787,74 | 161,67 | 4,53 | 14,71 | 29,17 |
| 787,96 | 161,68 | 4,52 | 14,73 | 29,16 |
| 787,95 | 161,69 | 4,52 | 14,74 | 29,18 |
| 787,85 | 161,70 | 4,51 | 14,74 | 29,31 |
| 786,07 | 161,69 | 4,49 | 14,76 | 29,33 |
| 782,66 | 161,62 | 4,47 | 14,78 | 29,32 |
| 777,75 | 160,40 | 4,44 | 14,80 | 29,26 |
| 772,90 | 159,71 | 4,43 | 14,83 | 29,28 |
| 769,73 | 160,39 | 4,41 | 14,87 | 29,36 |
| 768,32 | 160,71 | 4,42 | 14,90 | 29,48 |
| 768,80 | 160,70 | 4,43 | 14,90 | 29,44 |
| 769,98 | 160,71 | 4,45 | 14,89 | 29,42 |
| 772,48 | 160,68 | 4,47 | 14,88 | 29,38 |

| Emission data at mode 7 | | | | |
|---|---|---|---|---|
| Nox | CO | $CO_2$ | $O_2$ | HC |
| 253,92 | 448,87 | 1,39 | 18,92 | 33,34 |
| 253,99 | 448,87 | 1,39 | 18,91 | 33,39 |
| 253,99 | 448,68 | 1,39 | 18,91 | 33,39 |
| 253,91 | 447,88 | 1,39 | 18,91 | 33,39 |
| 252,75 | 447,88 | 1,39 | 18,92 | 33,33 |
| 252,35 | 447,88 | 1,38 | 18,91 | 33,33 |
| 250,93 | 447,87 | 1,38 | 18,92 | 33,34 |
| 249,99 | 447,86 | 1,38 | 18,93 | 33,40 |
| 249,00 | 447,87 | 1,37 | 18,93 | 33,39 |
| 248,99 | 448,31 | 1,37 | 18,94 | 33,47 |
| 247,82 | 448,87 | 1,37 | 18,94 | 33,42 |
| 247,06 | 448,88 | 1,36 | 18,96 | 33,36 |
| 246,51 | 448,94 | 1,36 | 18,95 | 33,37 |
| 245,33 | 449,86 | 1,36 | 18,94 | 33,38 |
| 245,00 | 449,86 | 1,36 | 18,95 | 33,42 |
| 244,00 | 449,88 | 1,35 | 18,96 | 33,49 |
| 243,59 | 449,99 | 1,35 | 18,96 | 33,39 |
| 242,75 | 450,81 | 1,35 | 18,96 | 33,28 |
| 241,56 | 450,87 | 1,35 | 18,96 | 33,37 |
| 240,96 | 451,05 | 1,35 | 18,97 | 33,48 |
| 240,27 | 451,86 | 1,35 | 18,98 | 33,47 |
| 240,17 | 452,18 | 1,35 | 18,98 | 33,36 |
| 239,02 | 452,86 | 1,34 | 18,98 | 33,37 |
| 239,01 | 453,43 | 1,35 | 18,98 | 33,43 |
| 239,72 | 453,86 | 1,35 | 18,98 | 33,49 |
| 240,25 | 453,87 | 1,35 | 18,98 | 33,46 |
| 240,25 | 454,42 | 1,35 | 18,98 | 33,42 |
| 240,25 | 454,85 | 1,35 | 18,98 | 33,29 |
| 240,95 | 455,17 | 1,36 | 18,97 | 33,40 |
| 241,49 | 455,86 | 1,36 | 18,96 | 33,31 |
| 241,49 | 455,83 | 1,36 | 18,96 | 33,34 |
| 242,66 | 456,03 | 1,36 | 18,95 | 33,40 |
| 242,72 | 456,87 | 1,36 | 18,95 | 33,43 |

This page is blank

## Appendix B

# Cylinder pressure trace and derivatives

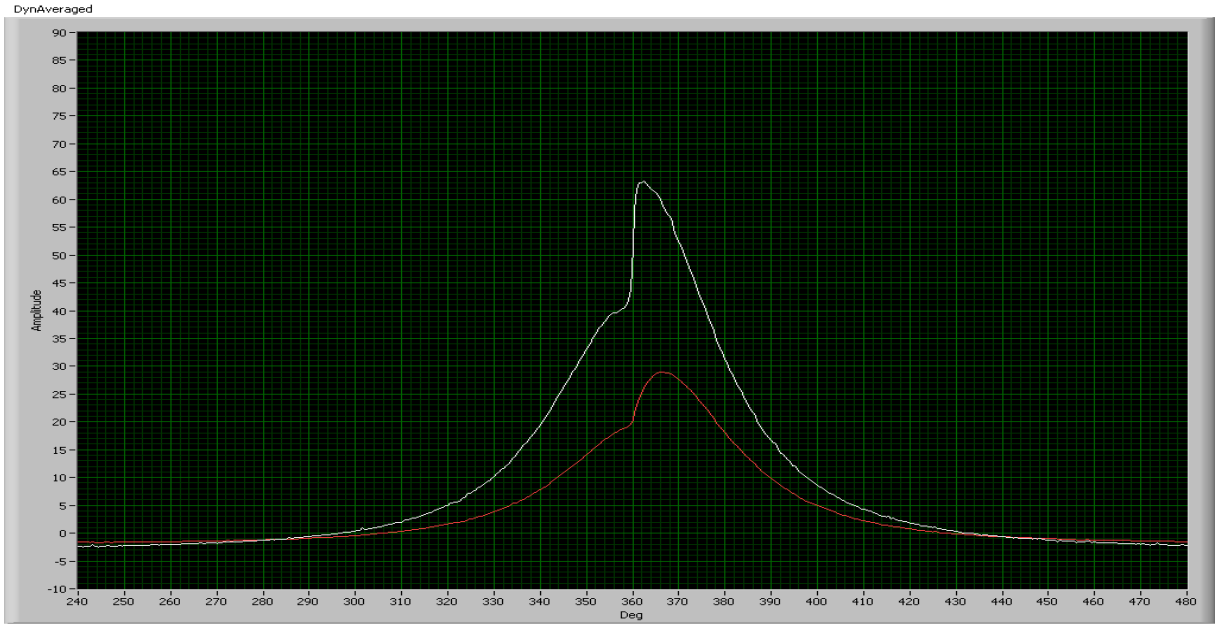


**Figure 101: Mode 8- Dynamic cylinder pressure as a function of crank angle for marine diesel fuel at idle speed**

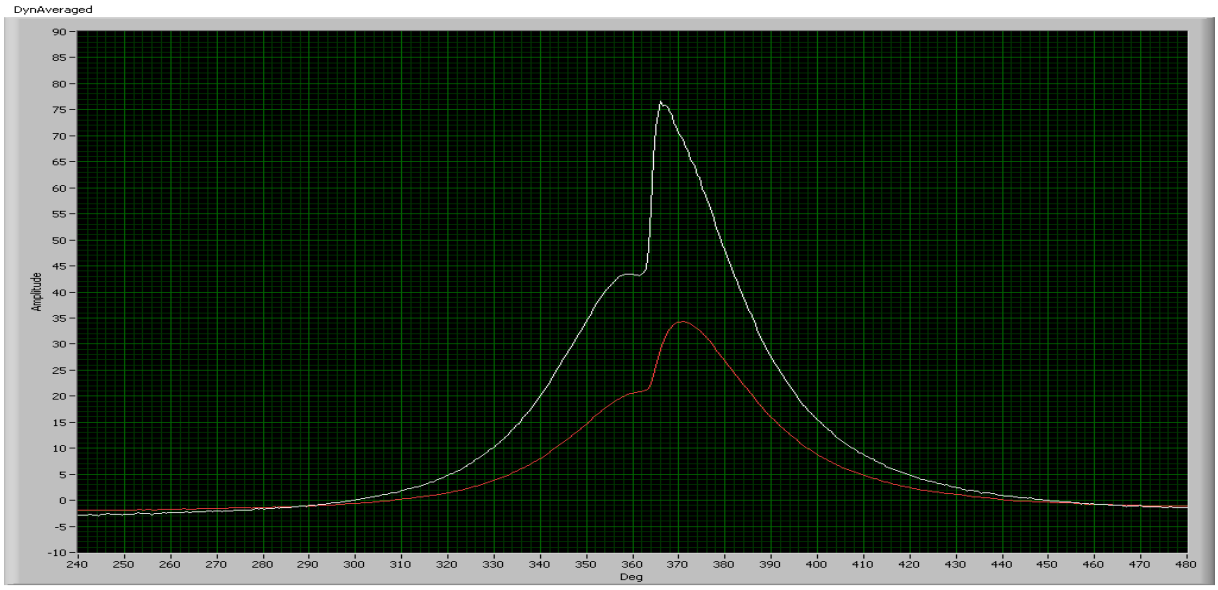


**Figure 102: Mode 7- Dynamic cylinder pressure as a function of crank angle for marine diesel fuel at 50% load and 2250 rpm**

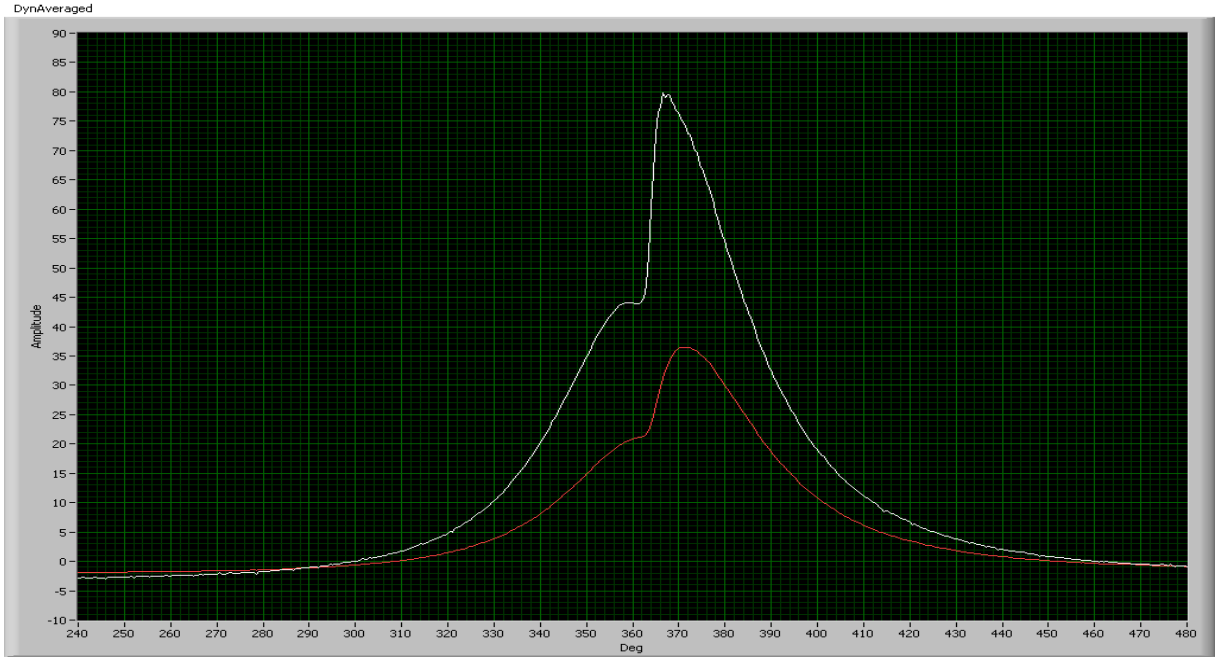


**Figure 103: Mode 6- Dynamic cylinder pressure as a function of crank angle for marine diesel fuel at 75% load and 2250 rpm**

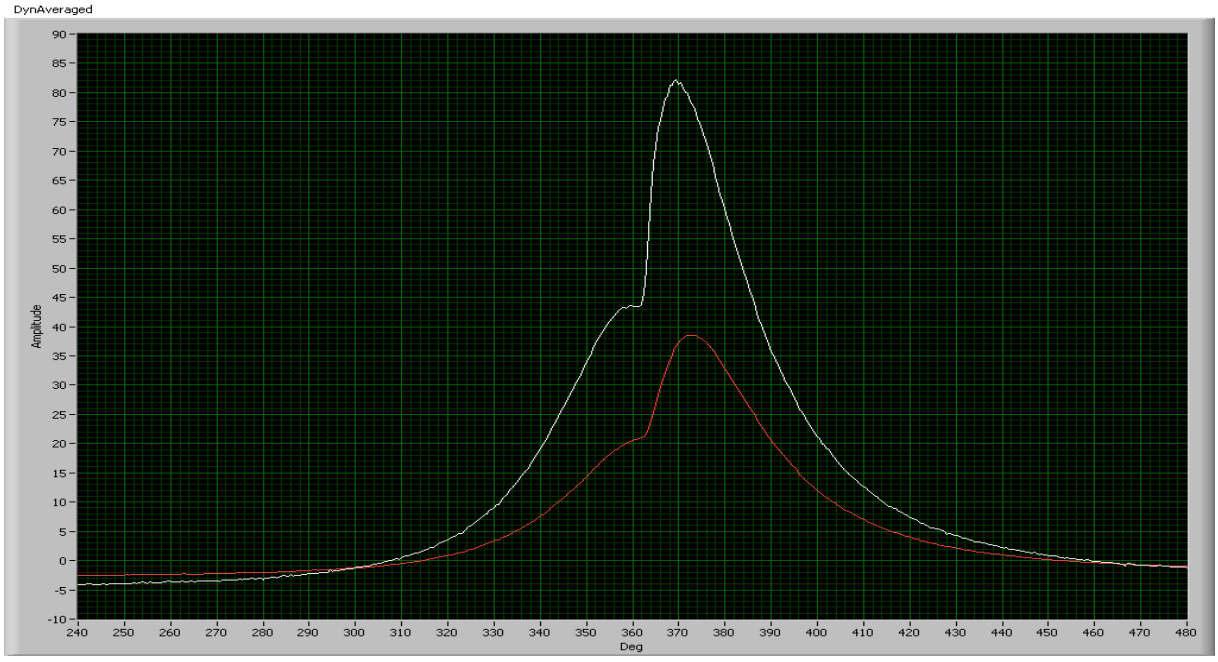


**Figure 104: Mode 5- Dynamic cylinder pressure as a function of crank angle for marine diesel fuel at 100% load and 2250 rpm**

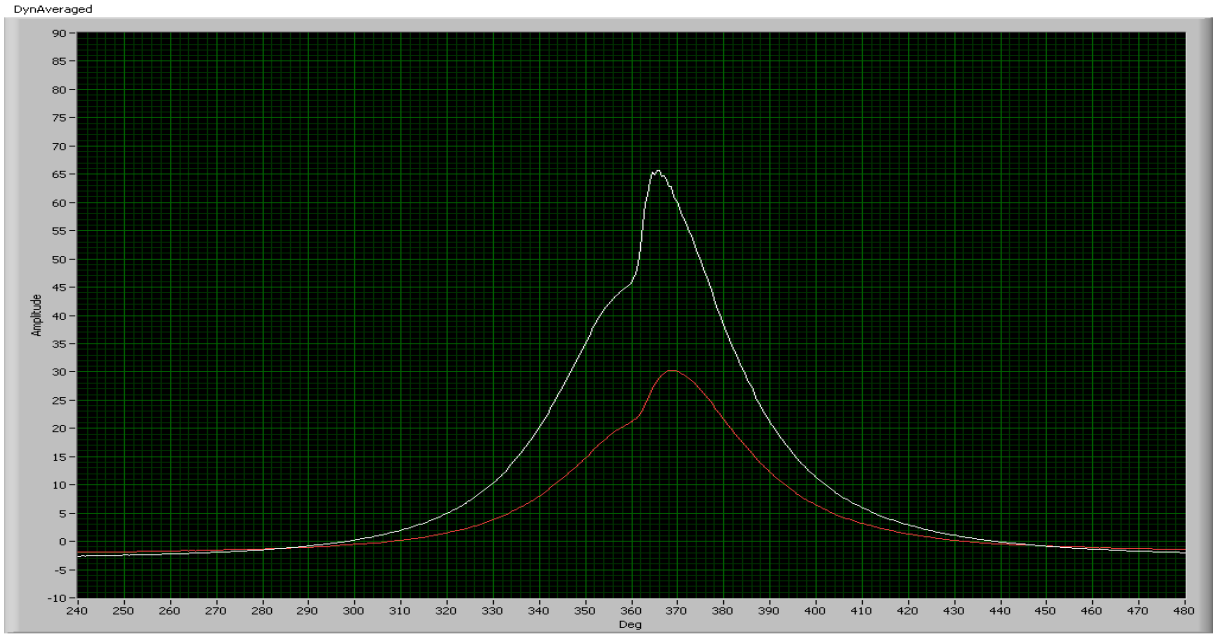


**Figure 105: Mode 4- Dynamic cylinder pressure as a function of crank angle for marine diesel fuel at 10% load and 3000 rpm**

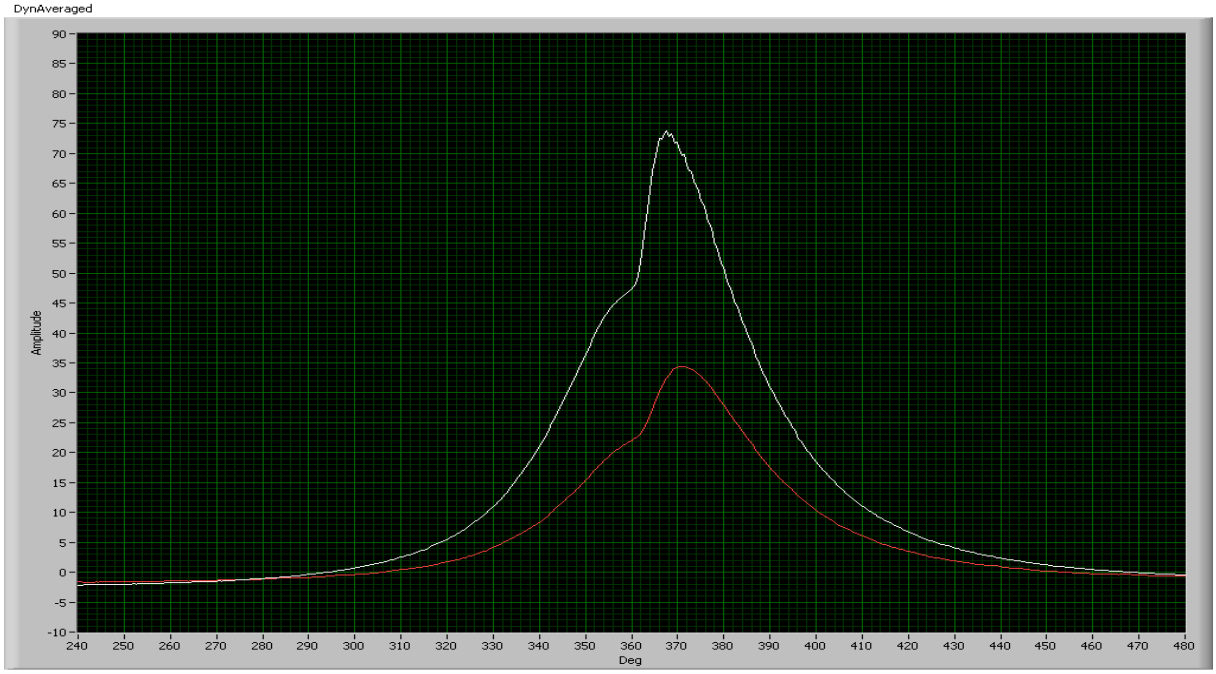


**Figure 106: Mode 3- Dynamic cylinder pressure as a function of crank angle for marine diesel fuel at 50% load and 3000 rpm**

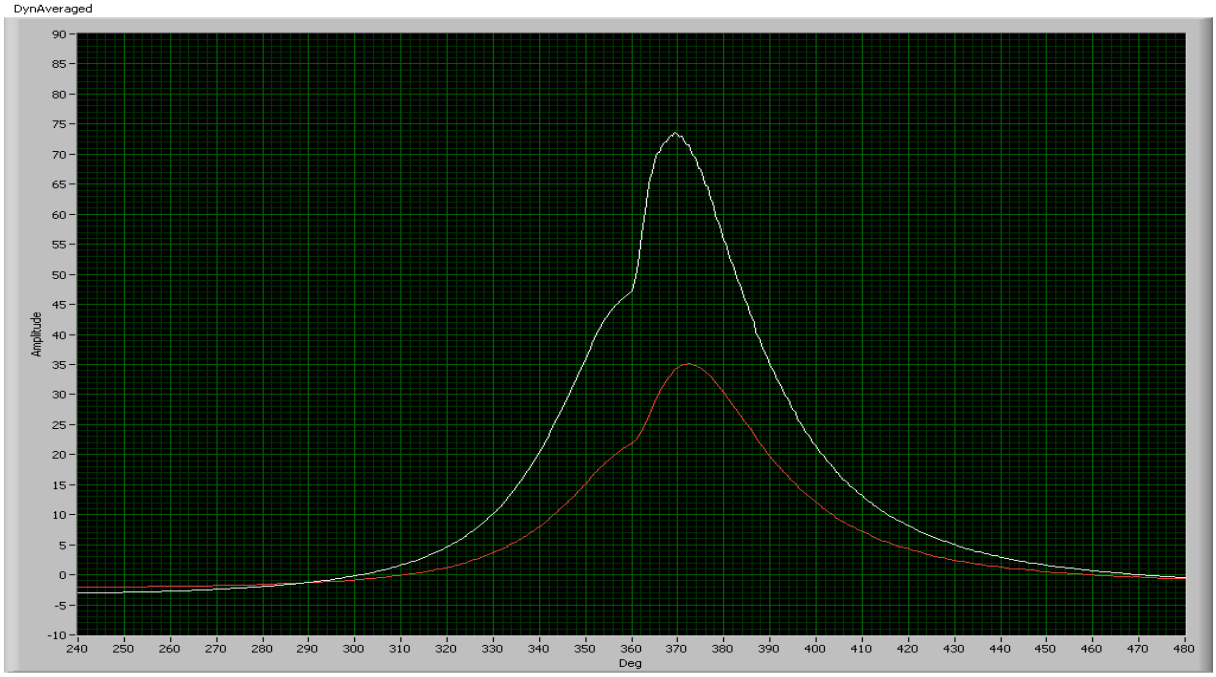


Figure 107: Mode 2- Dynamic cylinder pressure as a function of crank angle for marine diesel fuel at 75% load and 3000 rpm

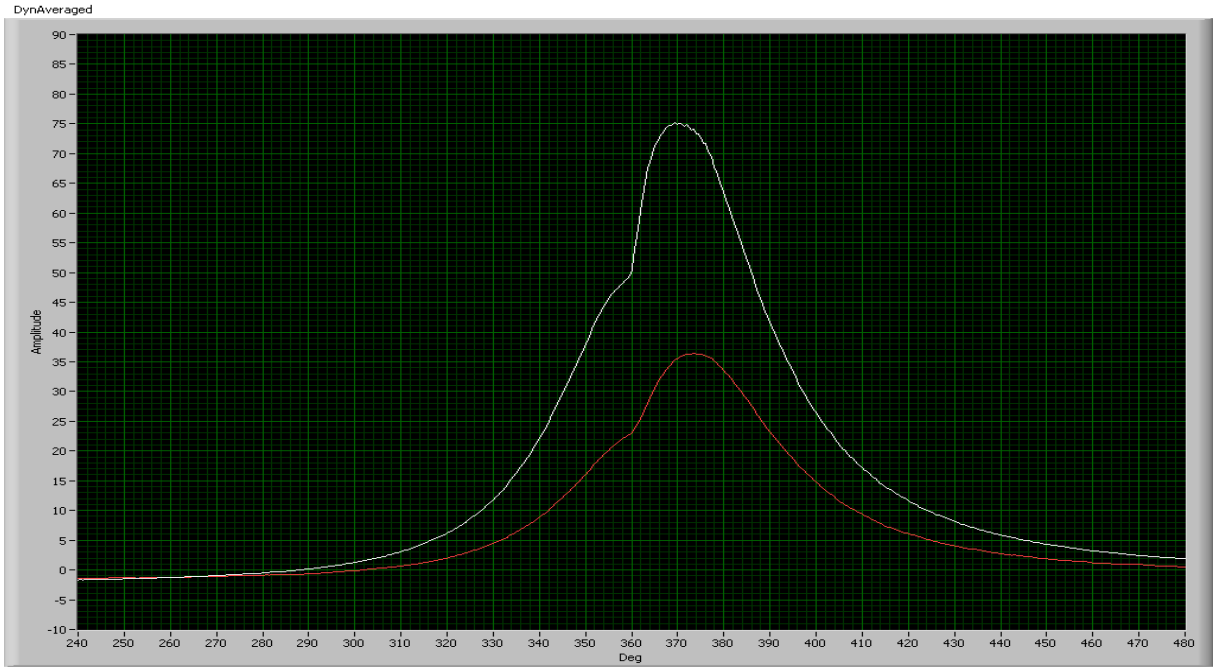


Figure 108: Mode 1- Dynamic cylinder pressure as a function of crank angle for marine diesel fuel at 100% load and 3000 rpm

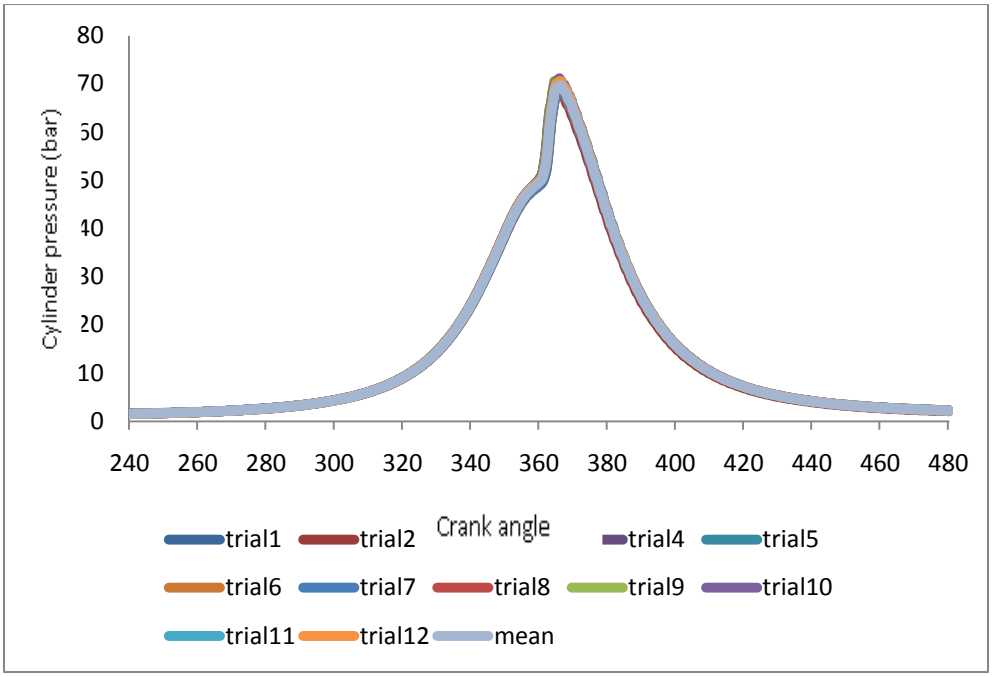
Cylinder pressure (bar)
0
10
20
30
40
50
60
70
80
240
260
280
300
320
340
360
380
400
420
440
460
480
Crank angle
trial1
trial2
trial4
trial5
trial6
trial7
trial8
trial9
trial10
trial11
trial12
mean

a) Low load

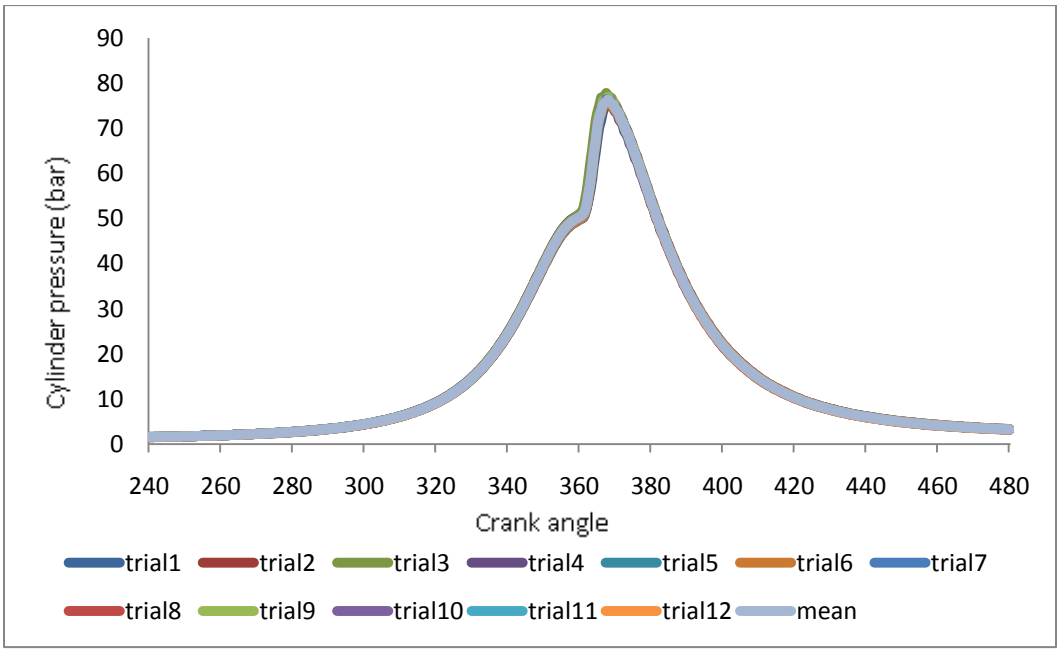
Cylinder pressure (bar)
0
10
20
30
40
50
60
70
80
90
240
260
280
300
320
340
360
380
400
420
440
460
480
Crank angle
trial1
trial2
trial3
trial4
trial5
trial6
trial7
trial8
trial9
trial10
trial11
trial12
mean

b) Part load

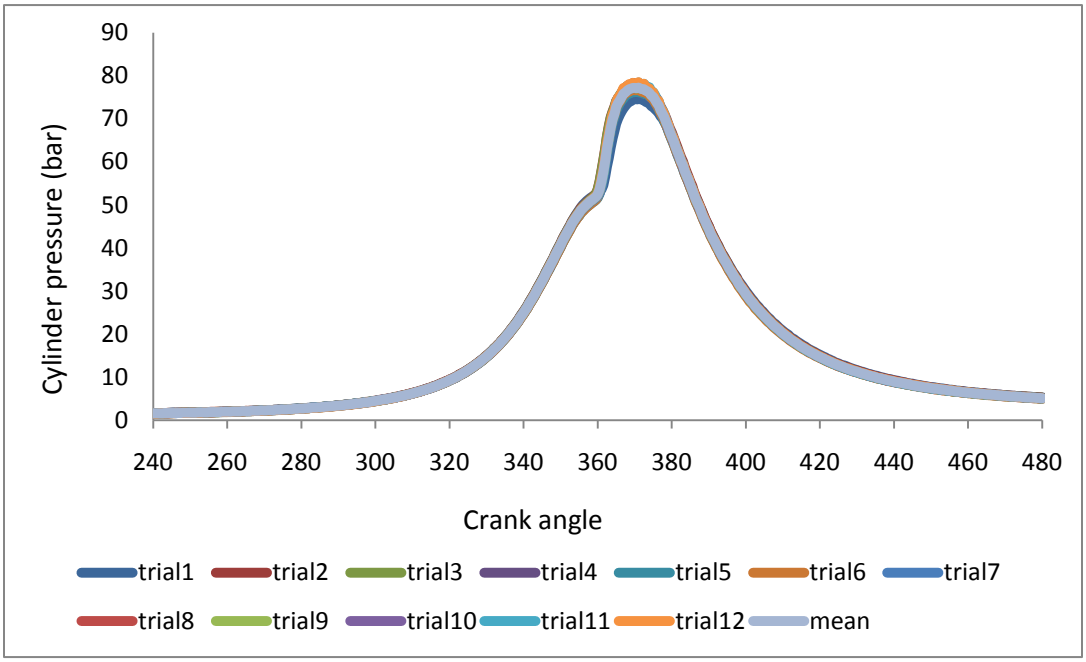


c) Full load

**Figure 109: Dynamic cylinder pressure vs. crank angle at (a) low load (b) medium load and (c) full load at 3000rpm for 12 different trials**

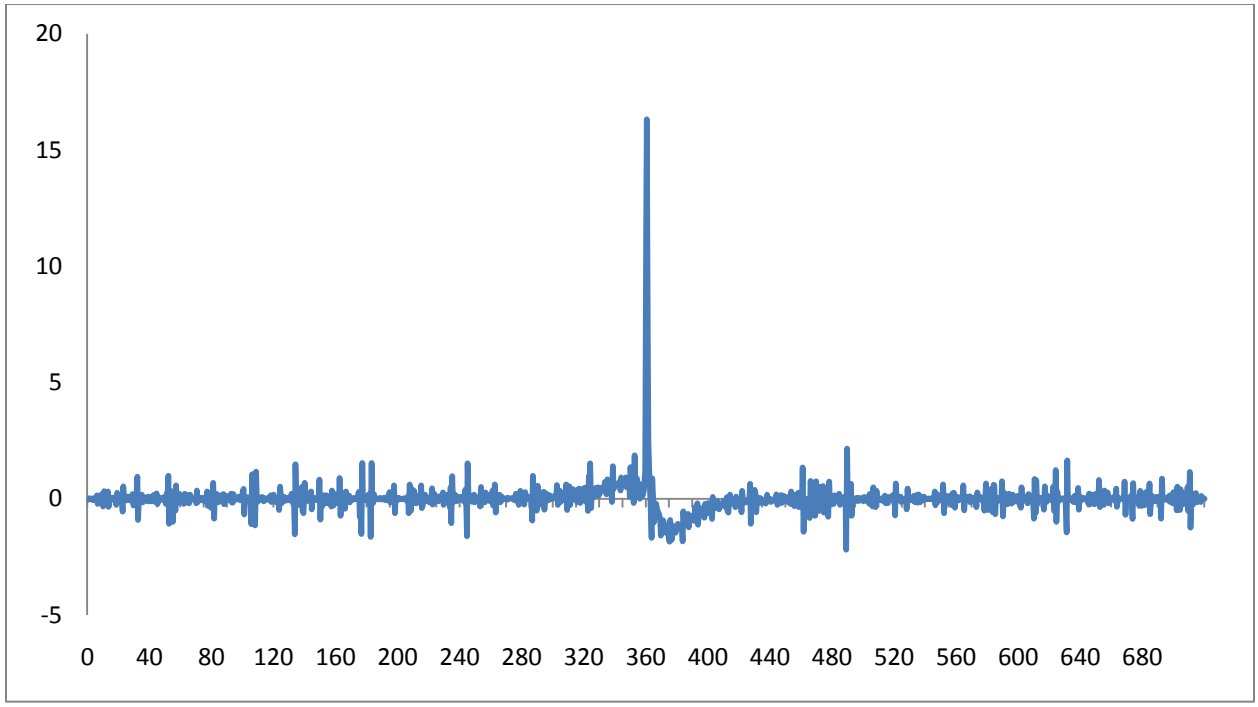
20
15
10
5
0
-5
0 40 80 120 160 200 240 280 320 360 400 440 480 520 560 600 640 680

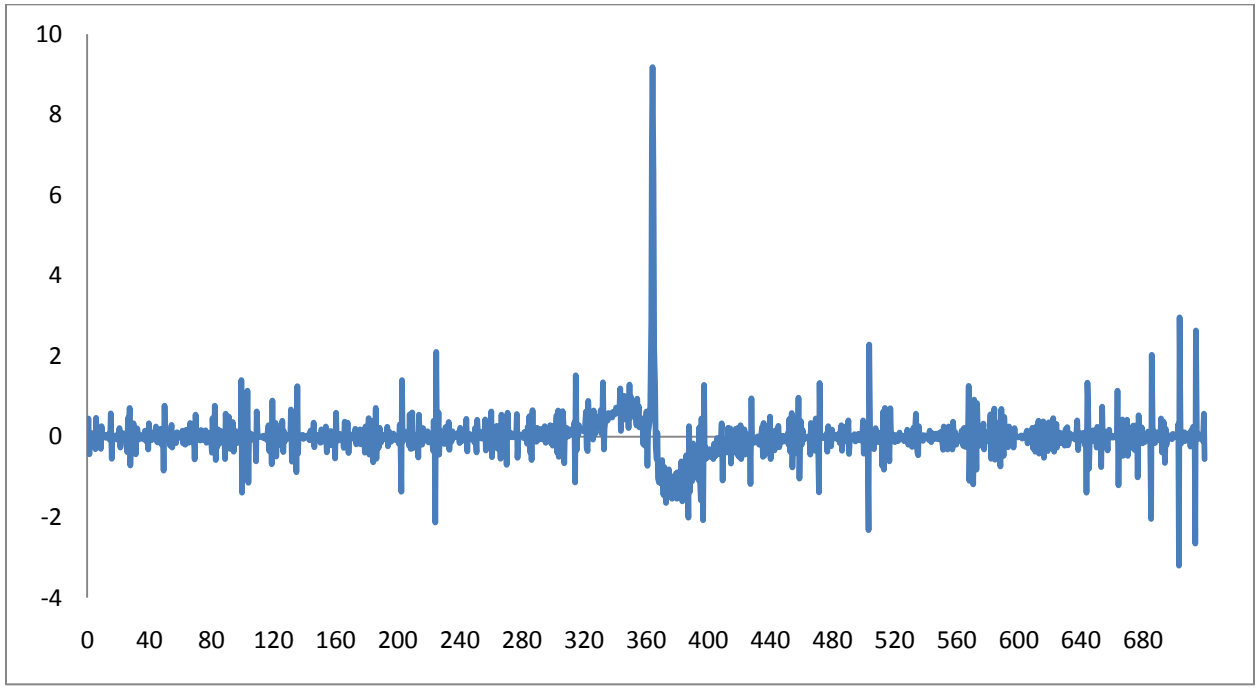
10
8
6
4
2
0
-2
-4
0 40 80 120 160 200 240 280 320 360 400 440 480 520 560 600 640 680

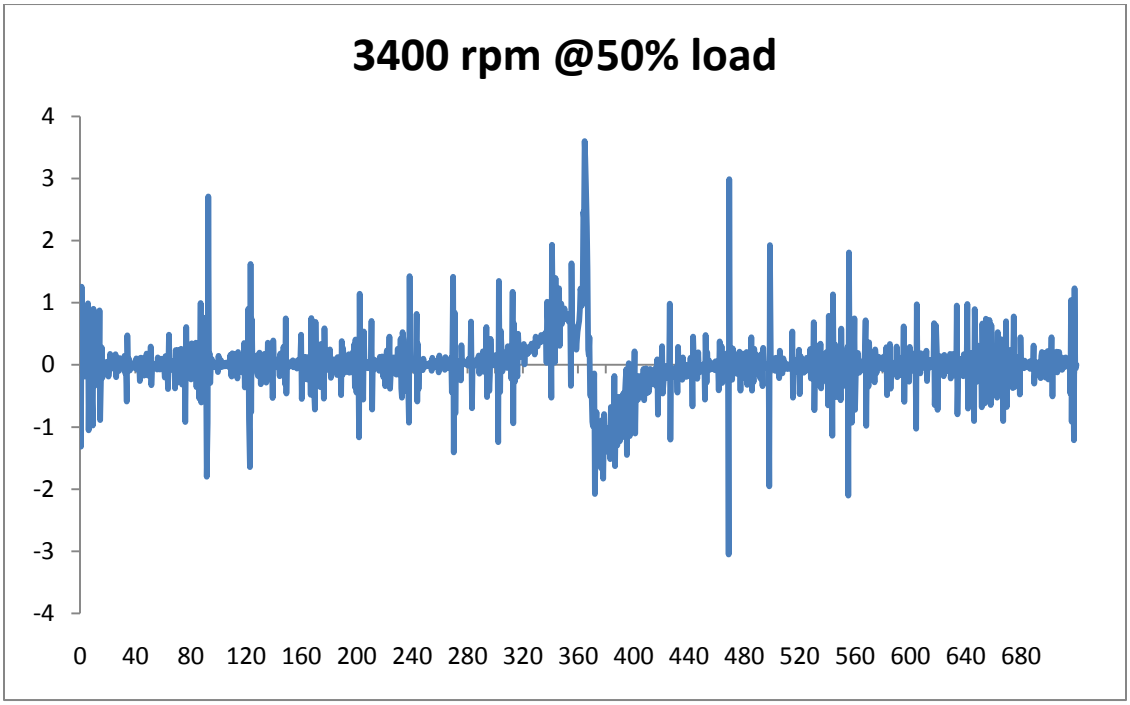
3400 rpm @50% load
4
3
2
1
0
-1
-2
-3
-4
0 40 80 120 160 200 240 280 320 360 400 440 480 520 560 600 640 680

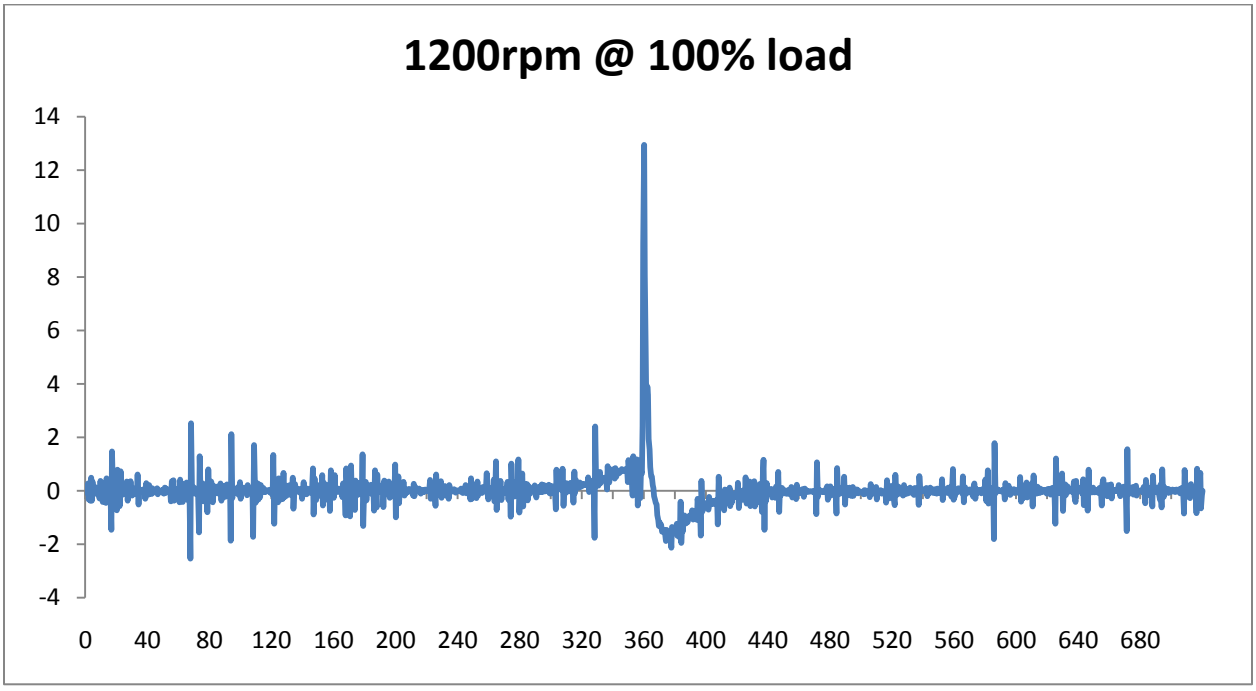
1200rpm @ 100% load
14
12
10
8
6
4
2
0
-2
-4
0 40 80 120 160 200 240 280 320 360 400 440 480 520 560 600 640 680

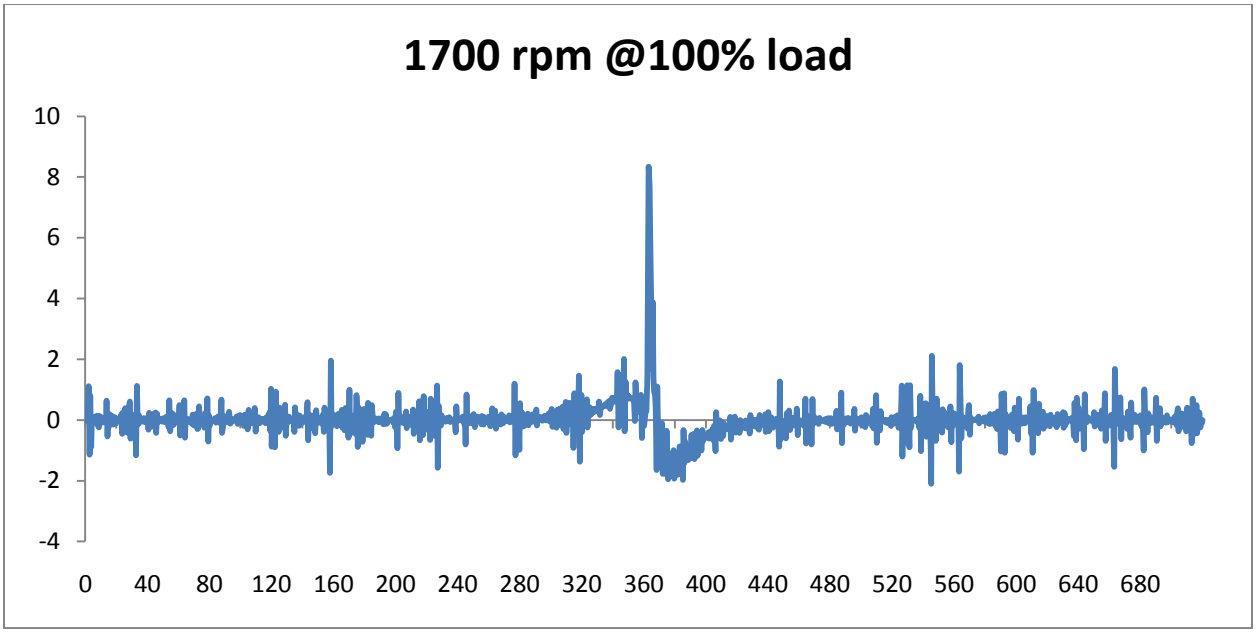


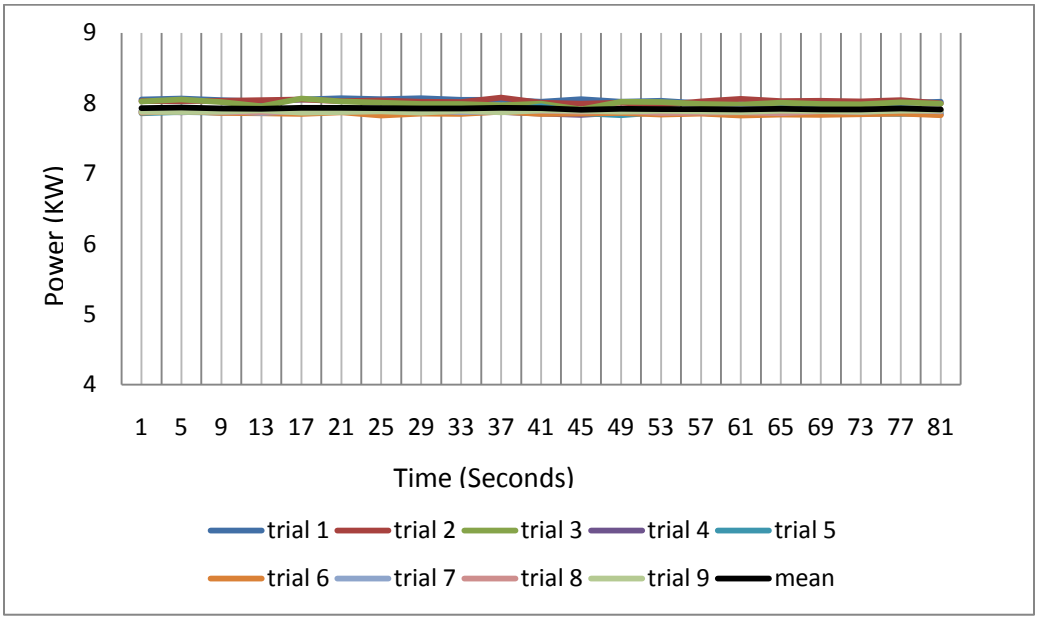


Time series of power measurements for nine trials

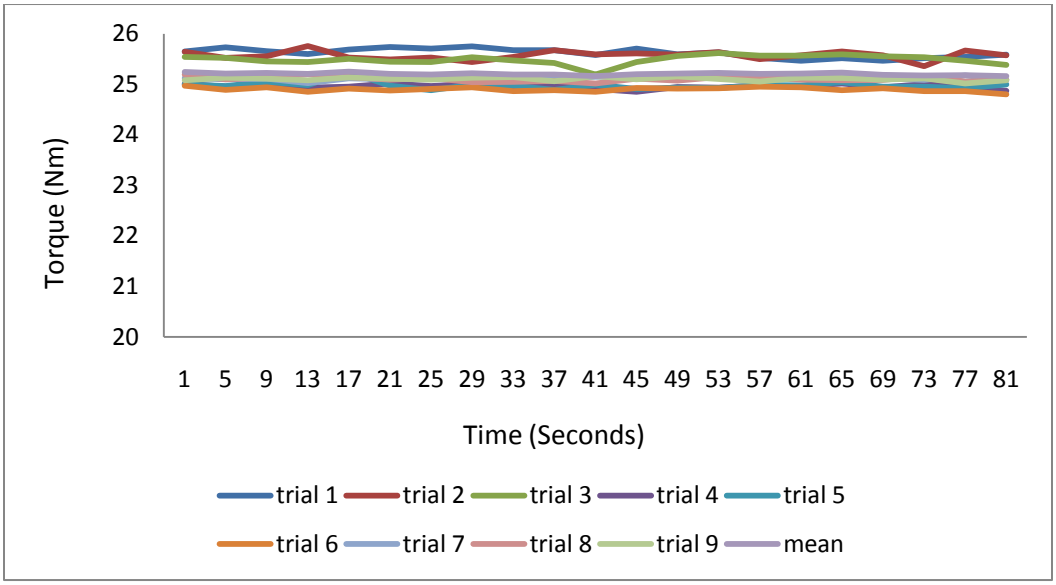


**Time series of torque measurements for nine trials**

## Appendix C

# Fuel System

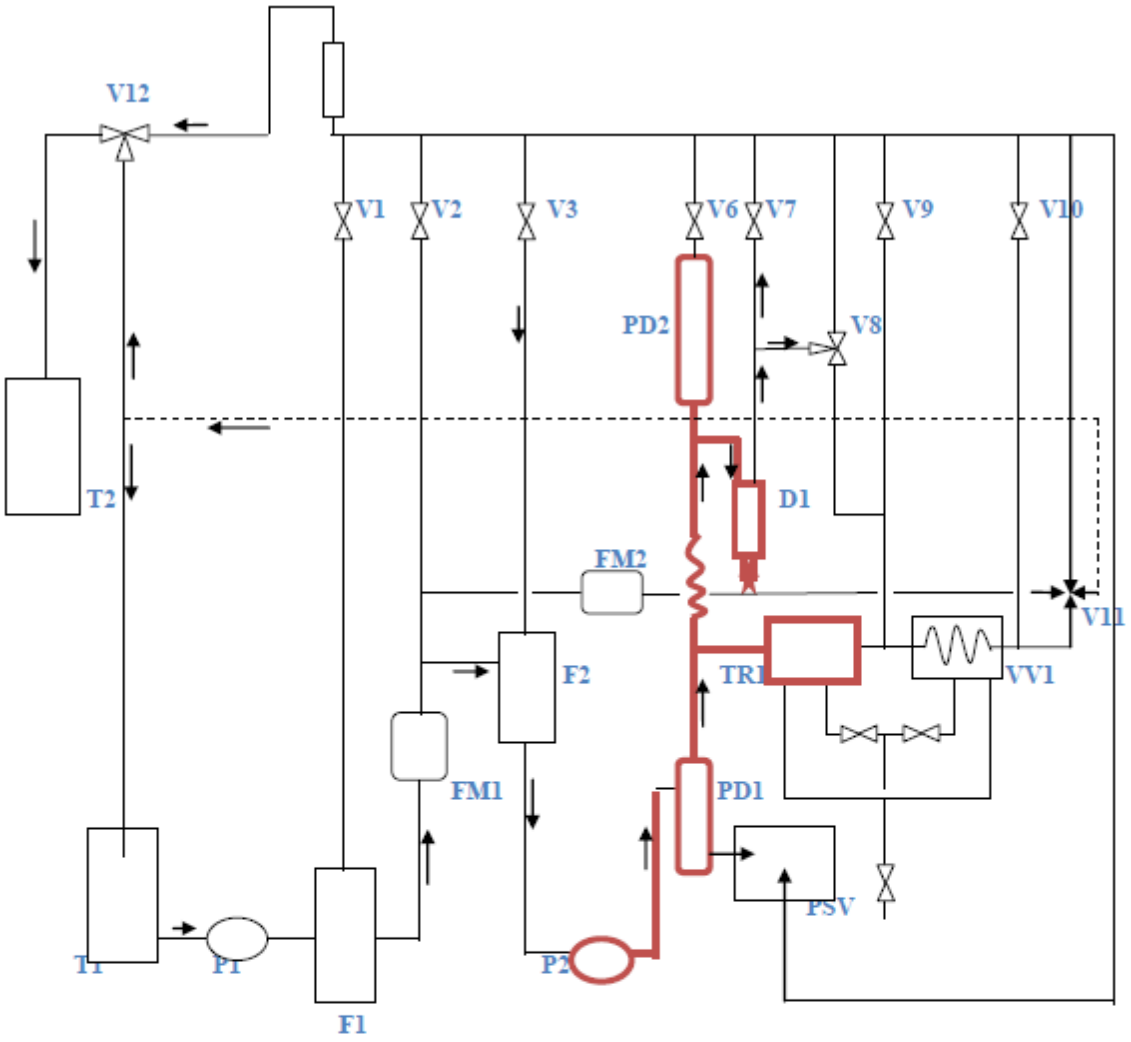


| | | | |
|---|---|---|---|
| D1 - | Fuel Injector | V1 | Valve for filter |
| F1 - | Filter | V2 | Flow meter valve |
| FM1 | Flow meter from tank | V3 | Valve for F2 |
| FM2 | Flow meter fuel return from high pressure side | V6 | Pulsation damper PD valve |
| P1 | Low pressure pump | V7 | Injector return valve |
| P2 | High pressure pump | V8 | Select fuel injector return |
| PD1 | Pulsation damper on rack | V9 | Valve before cooler |
| PD2 | Pulsation damper on engine | V10 | Valve after cooler |
| PSV | High pressure safety valve | V11 | Select fuel return |
| T1 | Fuel tank | V12 | 3-way fuel return valve |
| T2 | Fuel slope tank | VV1 | Cooler for diesel return |
| TR1 | Pressure regulator- high pressure side | | |

**Figure 6: Schematic diagram of fuel injection system**

## Appendix D

# Engine specification data

Test engine specification before modification

| | |
|---|---|
| Type | Single cylinder, liquid cooled, 4-stroke |
| Bore (mm) | 80.26 |
| Stroke (mm) | 88.90 |
| Displacement volume ($dm^3$) | 0.45 |
| Maximum speed (rps) | 75 |
| Maximum power (KW) | 8 |
| Maximum cylinder pressure (bar) | 120 |
| Compression ratio | 20:1 |
| Valve arrangement | Overhead camshaft, two vertical valves |
| Valve timing | |
| • Inlet opens<br>• Inlet closes<br>• Exhaust opens<br>• Exhaust closes | $10^0$ Before TDC<br>$42^0$ After TDC<br>$58^0$ Before BDC<br>$10^0$ After TDC |
| Tappet clearance<br>• Inlet<br>• Exhaust | <br>0.3 – 0.4 mm<br>0.3 – 0.4 mm |

Audi A6 V-engine specification

| | |
|---|---|
| Engine type | AFB, V6 |
| Capacity ($dm^3$) | 2.496 |
| Bore (mm) | 78.35 |
| Stroke (mm) | 86.4 |
| Compression ratio | 19.5 : 1 |
| Cold start | Glowplug |
| Valve timing<br>• Inlet opens<br>• Inlet closes<br>• Exhaust opens<br>• Exhaust closes | <br>$12^0$ Before TDC<br>$8^0$ After TDC<br>$34^0$ Before BDC<br>$12^0$ After TDC |
| Valve clearance | n/a (hydraulic) |
| Ignition pump timing | $2^0$After TDC $\pm 2^0$ at idle |
| Ignition pressure (bar) | 180 – 190 |
| thermostat | $87^0$C |

Screen flow chart with relevant key operations for emission measurement

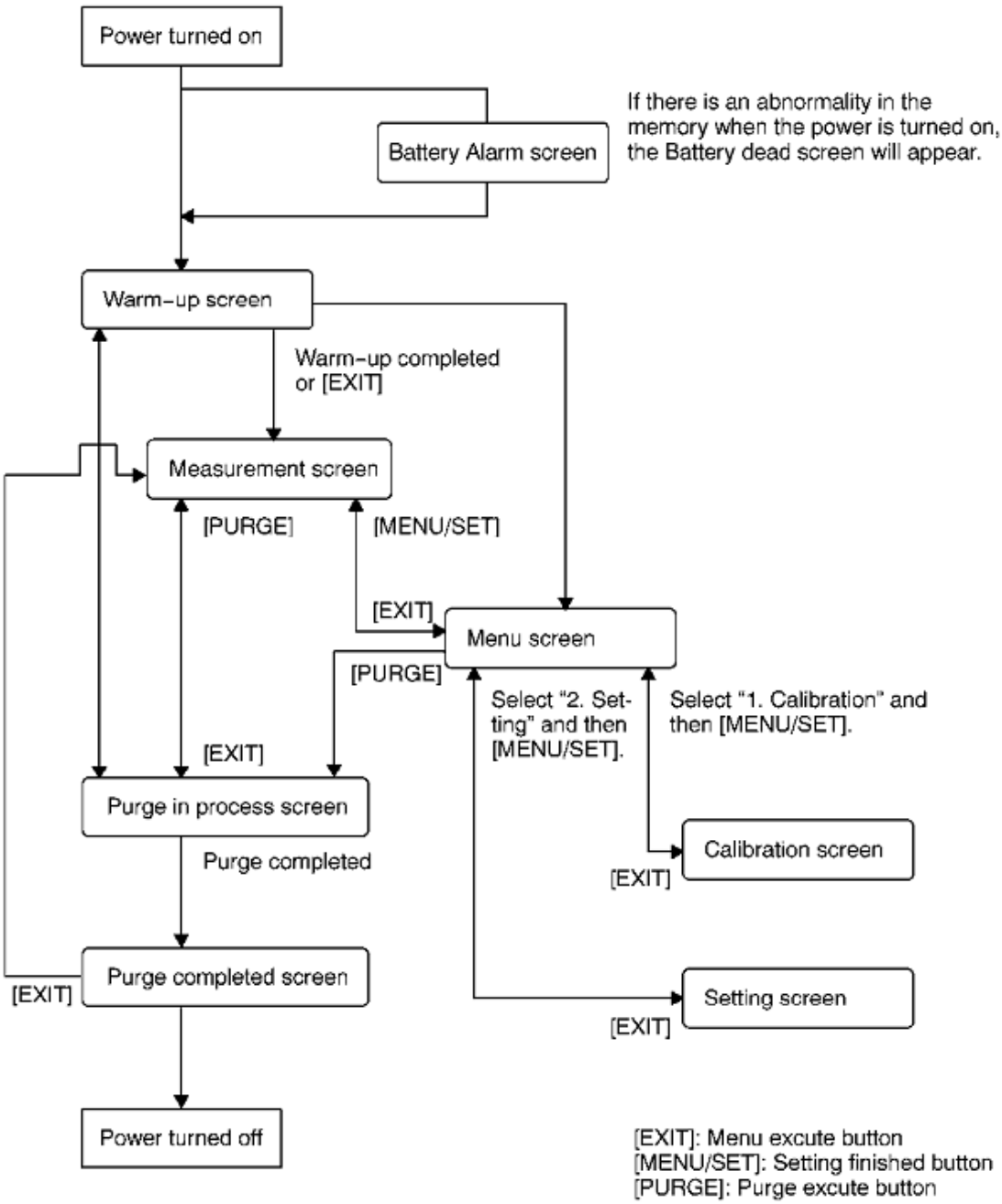

# Appendix E

## Heat Release Calculations

$$PV = mRT$$

$$\frac{dP}{d\theta}\cdot\frac{dV}{d\theta} = mR\frac{dT}{d\theta}$$

$$\frac{dT}{d\theta} = \frac{1}{mR}\frac{dP}{d\theta}\cdot\frac{dV}{d\theta}$$

$$mC_v\left(\frac{dP}{P}+\frac{dV}{V}\right)T = dQ - PdV$$

$$U = mC_vT \qquad T = \frac{U}{mC_v}$$

$$mC_v\frac{dP}{P}T + mC_v\frac{dV}{V}T = dQ - PdV$$

$$mC_v\cdot V\frac{dP}{P}\cdot T + mC_v\,dV\,T = dQ\cdot V - V\cdot P\,dV$$

$$dQ\cdot V = mC_v\cdot V\frac{dP}{P}T + mC_v\cdot dV\cdot T + VP\,dV$$

$$dQ\,V\cdot P = mC_vV\cdot\frac{dP}{P}T + P\cdot mC_v\,dV\,T + PV\,dV$$

$$dQ\,mRT = mC_vV\cdot dP\,T + PmC_v\,dV\,T + P\cdot mRT\,dV$$

$$dQR = C_vV\,dP + C_v\,dV + mR\,dV$$

$$dQ(C_p - C_v) = C_v V dP + m C_v dV + m(C_p - C_v) dV$$

$$dQ(C_p - C_v) = C_v V dP + m C_v dV + m C_p dV - m C_v dV$$

$$dQ(C_p - C_v) = C_v V dP + m C_p dV$$

$$dQ = \left(\frac{C_v}{C_p - C_v}\right) V dP + \frac{C_p}{C_p - C_v} P dV$$

$$dQ = \frac{1}{K - 1} V dP + \frac{K}{K - 1} P dV$$

$$dQ = \frac{1}{K - 1}\left[V dP + K P dV\right]$$